Thermal stability criteria embedded in advanced control systems for batch process intensification

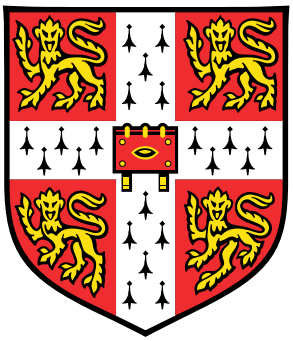

Walter Kähm

Department of Chemical Engineering and Biotechnology

University of Cambridge

This dissertation is submitted for the degree of

Doctor of Philosophy

Sidney Sussex College August 2019

I would like to dedicate this thesis to my loving parents and brother for their constant support over all these years. Without them I would have never gotten to this point on a professional, but more importantly on a personal level.

Declaration

I hereby declare that except where specific reference is made to the work of others, the contents of this dissertation are original and have not been submitted in whole or in part for consideration for any other degree or qualification in this, or any other University. This dissertation is the result of my own work and includes nothing which is the outcome of work done in collaboration, except where specifically indicated in the text. This dissertation contains less than 65,000 words including appendices, bibliography, footnotes, tables and equations and has less than 150 figures.

Walter Kähm
August 2019

Acknowledgements

Since my undergraduate years my supervisor Vassilios Vassiliadis has been a source of support and inspiration in research, as well as life. I learned a lot under his guidance, including how to work effectively with different types of people, and how to deal with unexpected results. For these lessons I am extremely grateful.

Most of my ideas developed during discussions in the Process Systems Engineering (PSE) group under the supervision of Vassilios Vassiliadis. Therefore I would like to thank Eduardo Nolasco, Dongda Zhang, Antonio del-Rio Chanona, Fabio Fiorelli, Sai Darshan Adloor and Hyunil Park, past and present PhD students within the group, and Masters students Andrei Kanavalau and Riaz Masers, for these discussions.

My close friends helped me stay in a healthy state of mind throughout the course of my undergraduate and PhD studies. For this I thank them deeply. Without this support I would have never gotten to where I am today. In particular I would like to thank my better half Onusa Charuwana, and close friends from undergraduate studies Peter Birch, Kieran Chambers, Helen Sheehan, and Heather White.

Within the department of Chemical Engineering and Biotechnology there are many people who contributed to this work. Creating an extensive list is doomed to fail, but it will be attempted nevertheless: Eric Bringley, Angiras Menon, Dushanth Severatnam, Joseph Wong, Gustavo León, Fernando León, Luca Banetta, Chung Lao, Laura Pascazio, Maurin Salamanca, Kaitlin Cunningham, Kimberley Bowal, Ana Morgado, Luís Rocha, Eugenia Biral, Maria Zacharopoulo, Apoorv Jain, Elise Siouve, Jana Weber, Selina Zhuang, Aurelia Li, Danilo Russo and Drew Baker. I thank them for their support and making the PhD more than just work.

Abstract

Thermal stability criteria embedded in avanced control systems for batch process intensification

Thermal stability of batch processes is a major factor for the safe and efficient production of polymers and pharmaceutical chemicals. The prediction of thermal stability for such nonlinear, non steady-state processes is unreliable when using most stability criteria found in literature.

A new stability criterion $\mathscr{K}$ is proposed. This is derived for complex reaction networks based on the divergence criterion. Lyapunov exponents are an alternative method to predict thermal runaway behaviour.

Embedding thermal stability criteria within Model Predictive Control (MPC) frameworks results in advanced control systems capable of intensifying batch processes safely, hence resulting in shorter processing times.

It is shown that embedding criterion $\mathscr{K}$ within MPC results in more efficient computational times than embedding Lyapunov exponents. Lyapunov exponents potentially can be applied to systems different from chemical exothermic batch reactors due to the general mathematical form.

The effect of parametric uncertainty for process control is of utmost importance for industrial application. It is shown that the use of scenario-based MPC and worst case MPC, together with criterion $\mathscr{K}$ and Lyapunov exponents, results in a robust control scheme capable of intensifying batch processes whilst keeping them under control subject to parametric uncertainty. Both, scenario-based and worst case MPC with these two criteria resulted in safe control capable of intensifying batch processes. It is found that worst case MPC embedded with criterion $\mathscr{K}$ results in the most computationally efficient robust control scheme for the intensification of processes considered in this work.

Walter Kähm

This work has resulted in the following peer-reviewed publications:

Kähm, W. and Vassiliadis, V. S. (2018). Lyapunov exponents with model predictive control for exothermic batch reactors. In IFAC-PapersOnLine, 51:423-428. doi: 10.1016/j.ifacol.2018.09.337

Kähm, W. and Vassiliadis, V. S. (2018). Optimal Laypunov exponent parameters for stability analysis of batch reactors with model predictive control. Computers and Chemical Engineering, 119:270–292. doi: 10.1016/j.compchemeng.2018.08.038

Kähm, W. and Vassiliadis, V. S. (2018). Stability criterion for the intensification of batch processes with model predictive control. Chemical Engineering Research and Design, 138:292–313. doi: 10.1016/j.cherd.2018.08.017

Kähm, W. and Vassiliadis, V. S. (2018). Thermal stability criterion integrated in model predictive control for batch reactors. Chemical Engineering Science, 188:192–207. doi: 10.1016/j.ces.2018.05.032

Kähm, W. and Vassiliadis, V. S. (2019). Thermal stability criterion of complex reactions for batch processes. Chemical Engineering Research and Design, 150:187-205. doi: 10.1016/j.cherd.2019.07.028.

Kanavalau, A., Masters, R., Kähm, W. and Vassiliadis, V. S. (2019). Robust thermal stability for model predictive control of batch processes. Computers and Chemical Engineering, 130. doi: 10.1016/j.compchemeng.2019.106574

The following publications are currently under review:

Nolasco, E., Kähm, W., Adloor, S.D., Al-Ismaili, R., Katritsis, N.M., Mappas, V., Zhang, Q. and Vassiliadis, V.S (2019). Optimal Control on Chemical Processes: Past, Present and Future. Computers and Chemical Engineering, UNDER REVIEW.

Table of contents

List of Figures

List of Tables

Nomenclature

Abbreviations

MPC	Model Predictive Control
OCP	Optimal Control Problem
PI/PID	Proportional Integral / Proportional-Integral-Differential

Roman Symbols

A	heat transfer area between reactor and cooling jacket $\left[\mathrm{m}^2\right]$
a	constraint counter $[-]$
B	Barkelew number $[-]$
A, B, C, D, E, F, G	components for each reaction $[-]$
$[\mathrm{A}]$	concentration of component A $\left[\mathrm{kmol\,m}^{-3}\right]$
C_p	heat capacity of reacting mixture $\left[\mathrm{kJ\,mol}^{-1}\,\mathrm{K}^{-1}\right]$
D	diameter $[\mathrm{m}]$
Da, $\mathrm{Da}_{\mathrm{res}}$	Damköhler number and resultant Damköhler number, respectively $[-]$
ΔH_r	heat of reaction $\left[\mathrm{J\,kmol}^{-1}\right]$
$\mathrm{div}\,[\mathbf{J}]$	divergence of the Jacobian $\left[\mathrm{s}^{-1}\right]$
E_a	activation energy $\left[\mathrm{J\,kmol}^{-1}\right]$
f	generic function $[-]$
g	differential equation $[-]$
h	algebraic equation $[-]$
i	reaction index $[-]$

$\mathbf{J}$	Jacobian matrix $[-]$
k_0	pre-exponential Arrhenius coefficient $[-]$
K_P	proportional constant for PI controller $\left[\mathrm{m^3\,K^{-1}\,s^{-1}}\right]$
L	characteristic length $[\mathrm{m}]$
M	number of reactions within a reaction network $[-]$
m_B, $m_{\mathrm{Da_{res}}}$, m_γ, m_{St}	Gradient coefficients with respect to B, $\mathrm{Da_{res}}$, γ and St $[-]$
N	number of reagents $[-]$
n	reaction order $[-]$
P	power input by impeller $[\mathrm{W}]$
p	search direction of optimisation algorithm $[-]$
Pr	Prandtl number $[-]$
Q	heat flow $[\mathrm{W}]$
q	volumetric flow rate $\left[\mathrm{m^3\,s^{-1}}\right]$
R	universal molar gas constant $\left[\mathrm{J\,kmol^{-1}K^{-1}}\right]$
r	reaction rate $\left[\mathrm{kmol\,m^{-3}\,s^{-1}}\right]$
Re	Reynolds number $[-]$
s	slack variables $[-]$
St	Stanton number $[-]$
T	temperature $[\mathrm{K}]$
t	time of simulation $[\mathrm{s}]$
$\bar{t}_{\mathrm{comp}}$	average computational time per MPC step $[\mathrm{s}]$
RTol, ATol, Tol	relative, absolute, and generic tolerance $[-]$
t_{ref}	reference time for dimensionless groups $[\mathrm{s}]$
U	heat transfer coefficient between reactor and cooling jacket $\left[\mathrm{W\,m^{-2}\,K^{-1}}\right]$
u	control input $[-]$

V	volume $\left[\mathrm{m}^3\right]$
v	flow velocity $\left[\mathrm{m\,s}^{-1}\right]$
X	conversion $[-]$
x	differential variable $[-]$
y	general variable $[-]$

Greek Symbols

ξ	Lagrange multiplier $[-]$
ε	error of trajectory for PI controller [K]
γ	Arrhenius number $[-]$
Λ	Lyapunov exponent $\left[\mathrm{s}^{-1}\right]$
λ	thermal conductivity $\left[\mathrm{W\,m}^{-1}\mathrm{K}^{-1}\right]$
μ	viscosity [Pa s]
ν	stoichiometric coefficient $[-]$
Ω	rotational speed of the impeller $\left[\mathrm{s}^{-1}\right]$
Φ	objective function for MPC $[-]$
Π	power number of stirrer $[-]$
ρ	density $\left[\mathrm{kg\,m}^{-3}\right]$
σ	standard deviation $[-]$
τ_I	integral constant for PI controller $\left[\mathrm{K\,s}^2\mathrm{m}^{-3}\right]$
$\theta, \bar{\theta}, \hat{\theta}$	mass, molar and volume fraction, respectively $[-]$
ζ	penalty parameter for optimisation $[-]$

Subscripts

0	initial point of simulation $[-]$
C	coolant property $[-]$
c	control horizon $[-]$

chem	chemical stability properties $[-]$
A, B, C, D, E, F, G	components for each reaction $[-]$
f	final point of simulation $[-]$
g	inequality constraint $[-]$
gen	generation $[-]$
h	equality constraint $[-]$
i	reaction index $[-]$
impeller	impeller property $[-]$
in	inlet conditions $[-]$
j	reaction component index $[-]$
p	prediction horizon $[-]$
peak	properties at the peak temperature during the process $[-]$
R	reacting mixture property $[-]$
reac	properties at the end of the reaction $[-]$
ref	reference $[-]$
rem	removal $[-]$
sp	set-point $[-]$

Superscripts

(s)	time step for simulations $[-]$

Other Symbols

$\mathscr{D}$	divergence of the Jacobian due to single reaction $\left[\mathrm{s}^{-1}\right]$
$\mathscr{E}$	estimate of the divergence at boundary of stability $\left[\mathrm{s}^{-1}\right]$
$\mathscr{K}$	thermal stability criterion $\left[\mathrm{s}^{-1}\right]$
$\mathscr{L}$	Lagrangian function $[-]$

Chapter 1

Introduction and literature review

Batch processes with exothermic chemical reactions are a major part of the chemical processing industry. Of profound importance is the correct setting for the set-point temperature to ensure thermal stability for such processes. The loss of thermal stability in exothermic batch processes leads to an uncontrolled increase in reaction temperature called a *thermal runaway*. Thermal runaways have significant economic and environmental impacts due to interruption of normal operation and the potential release of chemicals. Furthermore, thermal runaways can cause an uncontrolled increase in the pressure within batch reactors, presenting a serious safety hazard. Due to these reasons the reaction temperature for exothermic batch processes has to be evaluated by considering the thermal stability of such systems.

The chemical stability of reaction systems determines the upper temperature limit T_{chem} beyond which unwanted side products would be produced. The thermal stability of batch processes is considered from a dynamic standpoint, considering the heat generated by the reaction and the cooling capacity available. Most batch processes in industry employ Proportional-Integral-Derivative (PID) control, keeping a constant temperature during the process. This is achieved by providing the PID controller with a set-point temperature, which defines the target temperature of the control. As reagents are consumed during the reaction, the heat generated by the reaction decreases. This reduction in heat generation leads to reduced coolant flow rate by the PID controller in order to keep the reactor at the set-point temperature.

A flexible increase in reaction set-point temperature during batch processes leads to an intensification of the chemical reaction, shortening the process time and hence making batch processes more efficient. This is schematically shown in Figure 1.1.

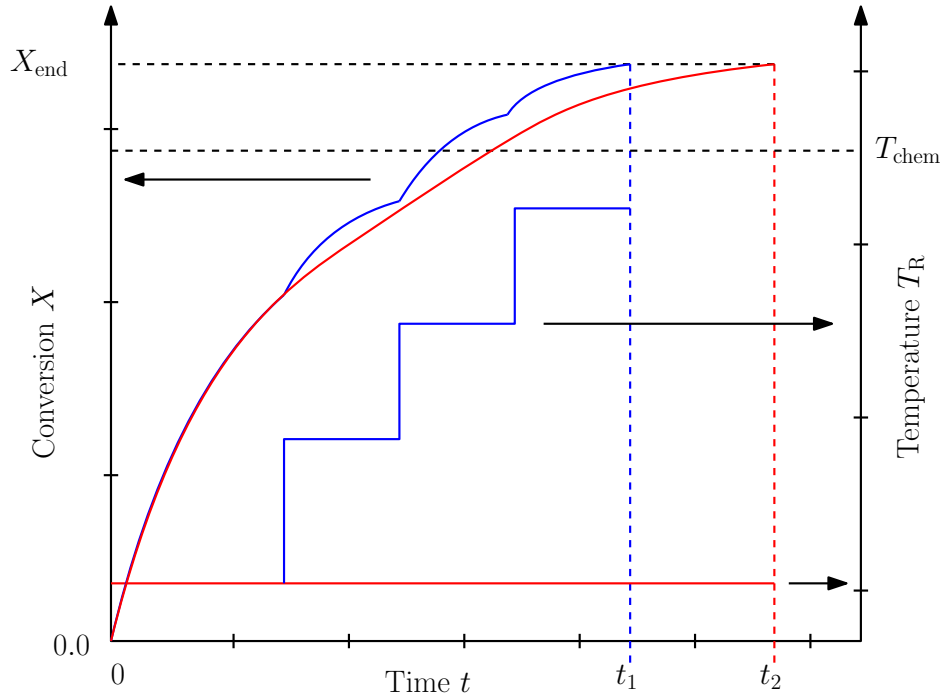

Fig. 1.1 Schematic representation of batch process intensification with (blue lines) and without (red lines) step increases in set-point temperature.

The process with step increases in set-point temperature, given by the blue lines, reaches the target conversion X_{end} in a shorter time t_1 than the constant set-point temperature process, given by the red lines. The lines shown in Figure 1.1 are for illustration purposes and have no relation to the processes considered in the following chapters.

The implementation of Model Predictive Control (MPC) enables the continuous analysis of the thermal stability during the process, which can be used to flexibly change the reaction conditions. To avoid thermal runaways in batch processes, a reliable measure of thermal stability that can be embedded within MPC is essential.

The fundamental goal of this work is to improve the efficiency of exothermic batch processes by a flexible increase in reaction temperature during the process using MPC with an embedded stability analysis.

To achieve this goal the first step involves a detailed analysis of literature on batch reactor models, current thermal stability criteria, and how such stability measures can be embedded in an MPC framework.

1.1 Batch reactor process model

1.1.1 Batch reactors

Batch reactors are an essential part of industry, with products ranging from pharmaceuticals (Štampar *et al.*, 2011) to polymers (Chang and Hung, 2002). Many processes carried out in batch reactors are exothermic, *i.e.* releasing heat during the reaction (Theis, 2014). The release of heat hence requires cooling in order to keep the reactor under control and not exceeding the upper temperature limit T_{chem}. Hence, understanding the heat transfer for the temperature control by cooling in batch reactor systems is essential. Several ways of cooling batch reactors exist. Different cooling arrangements include cooling jackets, internal cooling coils, and external heat exchangers (Salmi *et al.*, 2011), as shown in Figure 1.2.

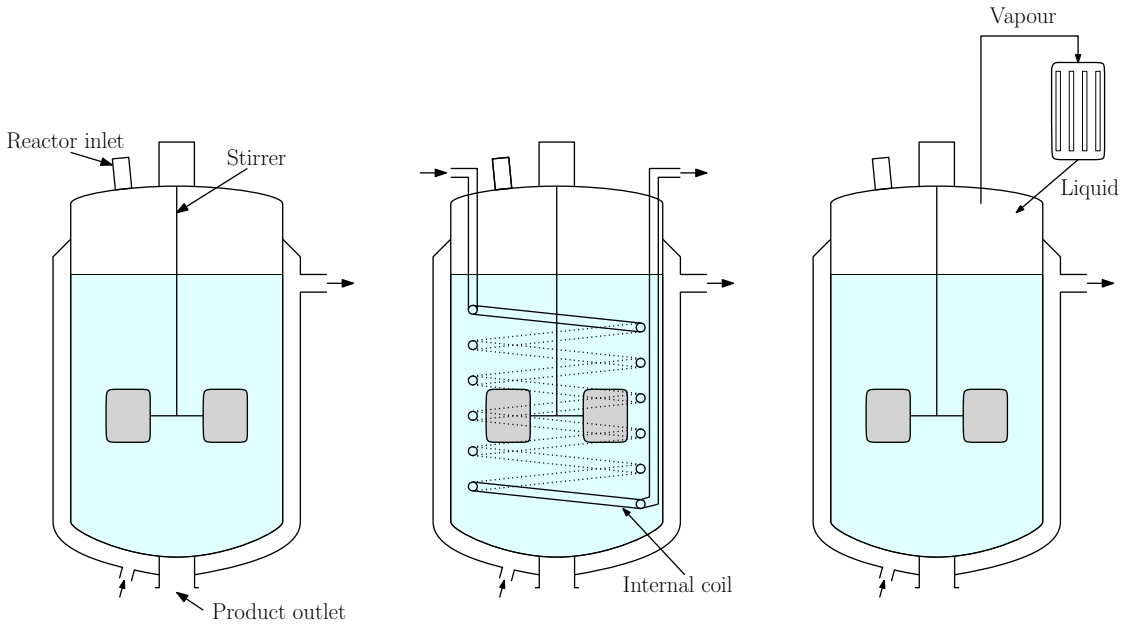

(a) Cooling jacket only (b) Internal cooling coil (c) External heat exchanger

Fig. 1.2 Cooling arrangements of batch reactors.

The dimensions of the pipes running through the cooling jacket, internal coil or heat exchanger are often chosen such that the Reynolds number Re is in the turbulent regime, $\text{Re} \approx 10^5$ (Schlichting and Gersten, 2017), when the maximum coolant flow rate is applied. The Reynolds number within the cooling jacket is given by (Bird *et al.*, 2007):

$$\text{Re} = \frac{\rho_{\text{C}} v_{\text{C}} D_{\text{C}}}{\mu_{\text{C}}} \tag{1.1}$$

where ρ_C is the coolant density, v_C is the flow velocity within the cooling jacket, D_C is the internal diameter of the cooling jacket pipe, and μ_C is the viscosity of the coolant. The Reynolds number describes the ratio of inertial to viscous forces in the fluid.

A stirrer is present in the reactor to mix the contents such that uniform properties are present. Uniform properties are desirable for several reasons: inhomogeneous conditions lead to local concentration differences with varying reaction rates and hence variations in heat generation. Furthermore, homogeneous conditions result in a simplified system model description. Different stirrers exist for batch reactors with different flow profiles (Torotwa and Ji, 2018). Several different types of impellers are used in industry. A sample of common impellers is shown in Figure 1.3. Rushton impellers are used due their wide range of applicability in terms of viscosity (Paul *et al.*, 2004). Furthermore, Rushton impellers are commonly used to achieve turbulent mixing within the reactor. Propellers are often used for mixtures with low viscosity, whilst anchor impellers are usually operated at a low rotational speed, but can achieve thorough mixing for a wide range of viscosities (Paul *et al.*, 2004). Helical screws are most often used for highly viscous mixtures (Ameur *et al.*, 2018).

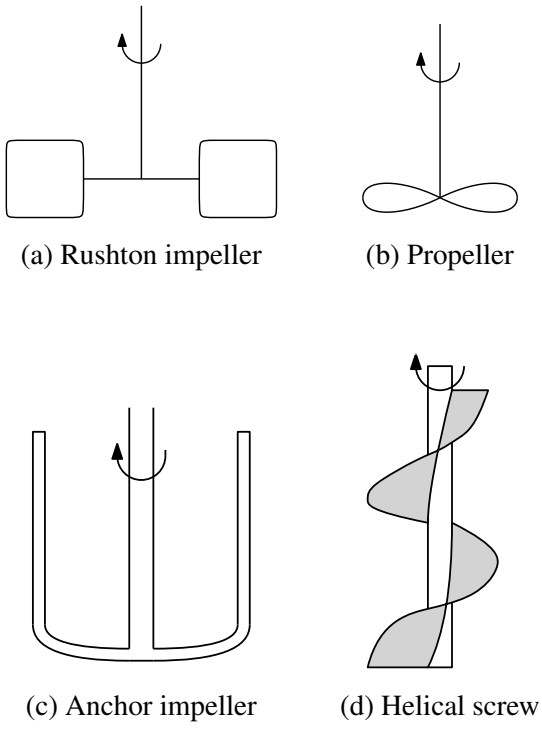

(a) Rushton impeller (b) Propeller

(c) Anchor impeller (d) Helical screw

Fig. 1.3 Diagrams of various impeller types present in industry.

The contents within batch reactors are usually filled up to 80% of the total volume to leave space for stirred contents and possible foam formation.

The heat transfer coefficient for the heat transfer between the cooling jacket and the reactor contents, U, depends on the physical properties of the coolant and the reacting mixture, as well as the flow intensity on both sides (Sinnot, 2005). If turbulent flow is present within the reactor, the major influence on U is due to physical properties of the reacting mixture and the coolant flow rate.

As the flow rate of coolant is reduced, the Reynolds number Re decreases significantly. Hence the heat transfer coefficient between the reacting mixture and the cooling jacket are estimated depending on the Reynolds and Prandtl number Pr within the cooling jacket and the Reynolds and Prandtl number of the reacting mixture. The Prandtl number is given by the following (Bird *et al.*, 2007):

$$\mathrm{Pr} = \frac{C_p \mu}{\lambda} \tag{1.2}$$

where λ is the thermal conductivity and C_p is the heat capacity of the fluid considered. The Prandtl number represents a ratio of momentum diffusivity to thermal diffusivity.

For Reynolds numbers of $\mathrm{Re} \geq 10^4$ within the cooling jacket pipes, *i.e.* turbulent flow, if $0.7 \leq \mathrm{Pr} \leq 100$, and if the length to diameter ratio of the pipes exceeds a value of 60, the Dittus-Boelter equation can be used to find a relation between the heat transfer coefficient and water flow rate (Bird *et al.*, 2007):

$$\mathrm{Nu} = 0.23\,\mathrm{Re}^{0.8}\,\mathrm{Pr}^{0.4} \tag{1.3}$$

where Nu is the Nusselt number, given by:

$$\mathrm{Nu} = \frac{UL}{\lambda} \tag{1.4}$$

where L is a characteristic length. Effectively, the Nusselt number describes the ratio of convective to conductive heat transfer.

If laminar flow is present in the tubes, a different correlation is required. Sieder and Tate came up with such a correlation (Çengel, 2002) which is valid in the entrance region of the pipe. For long pipes, which are usually present in cooling jackets, a constant value of $\mathrm{Nu} \approx 3.66$ if the wall is at a constant temperature, or $\mathrm{Nu} \approx 4.36$ if there is a constant heat flux through the wall can be assumed (Hagedorn, 1965).

On the reactor side the boundary layer giving rise to changes in heat transfer resistance has to be considered, too. For agitated batch reactors the Chilton, Drew and Jebens correlation

(Green and Perry, 2008*b*; Hagedorn, 1965) is used:

$$\mathrm{Nu} = 0.87\,\mathrm{Re}^{2/3}\,\mathrm{Pr}^{1/3}\left(\frac{\mu}{\mu_{\mathrm{wall}}}\right)^{0.14} \tag{1.5}$$

where μ_{wall} is the viscosity of the reacting mixture calculated at the wall conditions of the reactor, and the Reynolds and Prandtl numbers are evaluated for the bulk properties. The correlation shown in Equation (1.5) is valid for Reynolds numbers within the reactor of $300 \leq \mathrm{Re} \leq 3 \times 10^5$.

1.1.2 Chemical reactions

All chemical reactions in this work occur in a homogeneous liquid phase. The analysed reactions proceed mainly in one direction and are therefore considered irreversible. The nature of each reaction varies with respect to the following parameters:

- number of reagents and products
- reaction order
- stoichiometric coefficients
- activation energy
- enthalpy of reaction
- model of reaction kinetics

In this work it is assumed that the kinetics of every reaction follow Arrhenius type behaviour (Davis and Davis, 2003). Furthermore, single reactions can be combined to result in reaction networks. Chemical reactions with increasing complexity, varying from a single reaction with one reagent to six simultaneous reactions, are analysed in this thesis.

In industrial applications single reactions rarely occur, hence reaction networks are considered in detail. The increase in complexity for chemical reactions allows to apply the theory derived in this work to complex industrial case studies. One industrial reaction system examined in this work is the nitration of toluene.

For the analysis in the next sections a single chemical reaction of the following form is assumed:

$$\mathrm{A} + \mathrm{B} \rightarrow \mathrm{C} \tag{1.6}$$

It is noted that this is an exothermic reaction with enthalpy of reaction ΔH_r. In the next section the mass and energy balances for such a reaction occurring in a batch reactor are considered.

1.1.3 Mass and energy balances

Modelling a batch reactor requires mathematical equations which describe the current state and the evolution of all states with time. For this work the conversion of reagents into products and the change in temperature due to the nature of each chemical reaction have to be taken into account. Hence, mass and energy balances have to be formulated.

The overall mass balance of the batch reactor (assuming constant density with time) with respect to time t is given by:

$$\rho_{\mathrm{R}} \frac{\mathrm{d}V_{\mathrm{R}}}{\mathrm{d}t} = 0 \tag{1.7}$$

where V_{R} is the reactor volume, and ρ_{R} is the reacting mixture density. Equation (1.7) states that no reagents and products are added or removed during the reaction.

The reaction rates considered in this work are given by Arrhenius expressions (Davis and Davis, 2003). For the reaction given in Equation (1.6) the reaction rate is hence given by:

$$r = k_0 \exp\left(-\frac{E_a}{R T_{\mathrm{R}}}\right) [\mathrm{A}]^{n_{\mathrm{A}}} \tag{1.8}$$

where k_0 is the Arrhenius factor, E_a is the activation energy, R is the universal molar gas constant, $[\mathrm{A}]$ is the concentration of component A, n_{A} is the order of reaction, and T_{R} is the reactor temperature. As a batch reactor is present, no in- or outflows are present, hence reducing the mass balances to reaction rates only. For component A, the mass balance is therefore given by:

$$\frac{\mathrm{d}[\mathrm{A}]}{\mathrm{d}t} = -r \tag{1.9}$$

In the reaction considered in this example only components A and B are present. In general there can be any number of components.

For batch reactors two sets of energy balances have to be considered: the reaction mixture and the cooling jacket. The energy balance of the reaction mixture, including the heat generated by the reaction, is given by the following expression:

$$\frac{\mathrm{d}}{\mathrm{d}t}\left(\rho_{\mathrm{R}} C_{p,\mathrm{R}} T_{\mathrm{R}} V_{\mathrm{R}}\right) = k_0 \exp\left(-\frac{E_a}{R T_{\mathrm{R}}}\right) [\mathrm{A}]^{n_{\mathrm{A}}} \left(-\Delta H_r\right) V_{\mathrm{R}} - UA\left(T_{\mathrm{R}} - T_{\mathrm{C}}\right) + Q_{\mathrm{stirrer}} \tag{1.10}$$

where ΔH_r is the enthalpy of reaction, A is the heat transfer area to the cooling jacket, T_{C} is the cooling jacket temperature, and Q_{stirrer} is the heat generated by the stirring action. From Equation (1.10) several dimensionless variables can be obtained which will become useful in

later analyses:

$$B = \frac{-\Delta H_r \left[\mathrm{A}\right]}{\rho_{\mathrm{R}} C_{p,\mathrm{R}} T_{\mathrm{R}}} \tag{1.11a}$$

$$\gamma = \frac{E_a}{R T_{\mathrm{R}}} \tag{1.11b}$$

$$\mathrm{Da} = k_0 \left[\mathrm{A}\right]^{n_{\mathrm{A}-1}} t_{\mathrm{ref}} \tag{1.11c}$$

$$\mathrm{St} = \frac{U A}{\rho_{\mathrm{R}} C_{p,\mathrm{R}} V_{\mathrm{R}}} t_{\mathrm{ref}} \tag{1.11d}$$

where B is the Barkelew number, γ is the Arrhenius number, Da is the Damköhler number, and St is the Stanton number. A variable for unit of time, t_{ref}, is included to make the Damköhler and Stanton numbers dimensionless. The value of t_{ref} does not matter, as it cancels out in further derivations.

The Barkelew number is the ratio of heat generation by a chemical reaction and the enthalpy of the reacting mixture. The Arrhenius number is the ratio of activation energy to thermal energy. The Damköhler number is the ratio of reaction rate to mass transport rate. The Stanton number is the ratio of heat transfer to the reacting mixture to its thermal capacity.

The energy balance of the cooling jacket is given by the following expression:

$$\frac{\mathrm{d}}{\mathrm{d}t}\left(\rho_{\mathrm{C}} C_{p,\mathrm{C}} T_{\mathrm{C}} V_{\mathrm{C}}\right) = q_{\mathrm{C}} \rho_{\mathrm{C}} C_{p,\mathrm{C}} \left(T_{\mathrm{C,in}} - T_{\mathrm{C}}\right) + UA \left(T_{\mathrm{R}} - T_{\mathrm{C}}\right) \tag{1.12}$$

where ρ_{C} is the density of the coolant, $C_{p,\mathrm{C}}$ is the heat capacity of the coolant, q_{C} is the coolant flow through the cooling jacket, V_{C} is the cooling jacket volume, and $T_{\mathrm{C,in}}$ is the coolant inlet temperature.

The cooling jacket in Equation (1.12) is assumed to behave as an ideally stirred tank itself. Ideally the cooling jacket should be assumed to behave as a pipe wrapped around the reactor vessel, but this would require an additional differential equation with respect to the length along the pipe (Russel *et al.*, 2008). Such a model would significantly increase the complexity and hence increase the computational time to evaluate the system dynamics.

1.1.4 Model of ideal mixing

If strong mixing is present in a reactor vessel, the properties of the reacting mixture can be assumed to be uniform (Padron, 2003). In this case the mixture properties can be assumed not to change throughout the reactor up until the boundary layer at the wall.

As mentioned in Section 1.1.1, the heat transfer coefficient is strongly affected by the Reynolds and Prandtl numbers, as well as the viscosity of the reacting mixture and coolant at their respective walls (Bird *et al.*, 2007; Green and Perry, 2008*b*; Hagedorn, 1965).

The change in concentrations within the boundary layer on the reactor side, on the other hand, will have little influence on the overall heat transfer. The only effect on the thermal properties of the reactor system due to internal changes in concentration are caused by changes in the rates of reaction. Compared to the reactor size, changes in heat generation by the reaction within the boundary layer are typically very small.

If turbulent mixing is achieved within the reactor, it can therefore be assumed that there is no spatial variation in concentration (Rajavathsavai *et al.*, 2014). The effect of temperature changes inside the reactor still has to be considered to evaluate heat transfer coefficients, because this is one of the main factors influencing thermal stability (Till *et al.*, 2019).

1.1.5 Physical properties of fluids

The changes in density, viscosity and heat capacity of the reaction mixture with changing temperature and composition are approximated in the simulation. Depending on the composition the physical properties of the reaction mixture are estimated by the following equations:

$$\frac{1}{\rho} = \sum_j \theta_j / \rho_j \tag{1.13a}$$

$$\ln \mu = \sum_j \bar{\theta}_j \ln \mu_j \tag{1.13b}$$

$$C_p = \sum_j \theta_j C_{pj} \tag{1.13c}$$

$$\lambda = \sum_j \hat{\theta}_j \lambda_j \tag{1.13d}$$

where ρ is the density, μ is the viscosity, C_p is the heat capacity, λ is the thermal conductivity, θ_j is the mass fraction, $\bar{\theta}_j$ is the molar fraction, and $\hat{\theta}_j$ is the volume fraction of component j. These equations are obtained from Hirschfelder *et al.* (1955), Teja (1983) and Green and Perry (2008*a*). The accurate description of the temperature and composition relationships for liquid mixtures is very difficult. Hence, for the change in temperature linear interpolation of tabulated physical properties for each reagent is used.

1.2 Thermal stability of non steady-state reactors

Several thermal stability criteria exist in literature. The criteria found generally apply to two different types of systems: continuous stirred tank reactors (CSTRs) and batch reactors. Common criteria for both these systems are derived in detail below and examined further in Chapter 2. Once it is found which criteria reliably predict the thermal stability of batch processes, further analyses can be carried out.

1.2.1 Thermal stability criteria for CSTRs

For CSTRs stability criteria found in literature work well, *e.g.* the theory of heat explosion (Semënov, 1940), the Barkelew criterion (Barkelew, 1959), the Balakotaiah criterion (Balakotaiah, 1989), the Baerns criterion (Baerns and Renken, 2004), the Frank Kaminetskiĭ criterion (Frank-Kamenetskiĭ, 1969), and the Routh-Hurwitz criterion (Anagnost and Desoer, 1991; Hurwitz, 1895; Routh, 1877; Stephanopoulos, 1984). All of the above criteria, except the Routh-Hurwitz criterion, are based on the Semënov theory of heat explosions (Rupp, 2015). Hence, if it is shown that the Semënov criterion does not predict the thermal stability correctly, the Barkelew, Balakotaiah, Baerns and Frank-Kaminetskiĭ criteria are not valid for batch processes, either. It is emphasised at this point that the applicability of these criteria for CSTRs is not challenged in any way.

Semënov criterion

The first quantification of stability occurred in 1940, when the theory of thermal explosions by Semënov was introduced (Semënov, 1940). In this work the heat generation of the reaction system was compared to the available cooling capacity in order to formulate a criterion of stability beyond which a thermal runaway would occur.

Consider the batch reactor system shown in Section 1.1, where heat is generated by exothermic reactions, denoted by Q_{gen}, and heat is removed by the cooling jacket, denoted by Q_{rem}. The conditions of stability according to Semënov are given by the following expressions:

$$Q_{\text{gen}} \leq Q_{\text{rem}} \tag{1.14a}$$

$$\frac{\mathrm{d}Q_{\text{gen}}}{\mathrm{d}t} \leq \frac{\mathrm{d}Q_{\text{rem}}}{\mathrm{d}t} \tag{1.14b}$$

These conditions can be represented graphically: consider a single reaction generating heat according to Equation (1.10), subject to cooling according to Equation (1.12). The equations used to analyse how Q_{gen} and Q_{rem} change with reactor temperature are:

$$Q_{\text{gen}} = r\,(-\Delta H_r)\,V_{\text{R}} \tag{1.15a}$$

$$Q_{\text{rem}} = U\,A\,(T_{\text{R}} - T_{\text{C}}) \tag{1.15b}$$

The resulting energy generation and removal rates for different coolant temperatures with respect to reactor temperature, as given in Equation (1.15), are shown in Figure 1.4.

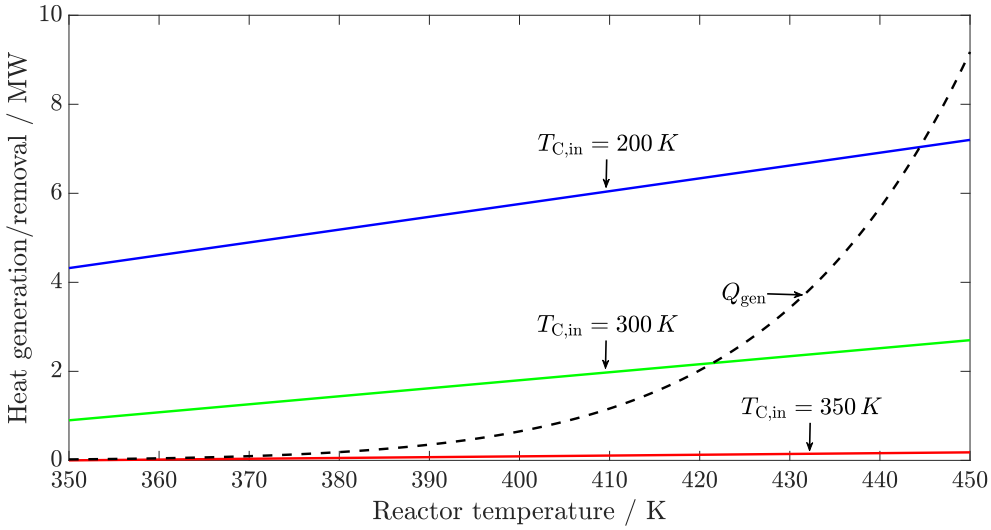

Fig. 1.4 Heat generation (black, dashed line) and heat removal for different coolant inlet temperatures. For the coolant inlet temperatures of 200 K, 300 K, and 350 K, heat transfer coefficient values of 800 $\text{W m}^{-2}\text{K}^{-1}$, 500 $\text{W m}^{-2}\text{K}^{-1}$, and 50 $\text{W m}^{-2}\text{K}^{-1}$, respectively, were used for illustrative purposes.

The region to the left of the intersection for each line gives the stable temperature range for the batch reactor at a single point in time. The analysis of stability according to Semënov only gives steady-state results of stability, which is a major limitation.

In Figure 1.4 several interesting features can be seen: if the coolant inlet temperature is too high, in this case 350 K, then only if no heat is generated is the system stable. As the coolant inlet temperature decreases, the feasible temperature range of operation increases. As the coolant inlet temperature is decreased from 350 K to 300 K and 200 K, the heat transfer coefficient values are increased from 50 $\text{W m}^{-2}\text{K}^{-1}$ to 500 $\text{W m}^{-2}\text{K}^{-1}$ to 800 $\text{W m}^{-2}\text{K}^{-1}$.

These values for the heat transfer coefficients are constant and do not vary with reactor temperature. This can be seen by the increase in gradient of the heat removal lines, hence again increasing the range in feasible reactor temperature. Once the solid lines in Figure 1.4 cross the dashed line, the value for Q_{gen} will always be larger than that of Q_{rem} due to the exponential nature of the heat generation. Therefore, once the solid lines and the dashed line cross the stable region of a stationary process can be identified according to Equation (1.14a). No discussion on the dynamic nature of the process is possible according to Equation (1.14b) with the results given in Figure 1.4.

Routh-Hurwitz Criterion

The Routh-Hurwitz criterion quantifies the stability of Differential Algebraic Equation (DAE) systems with the use of the Jacobian matrix. For nonlinear systems, a linear approximation can be made by using a Taylor expansion. Consider a set of differential equations:

$$\dot{x}_1 = f_1(x,t) \tag{1.16a}$$
$$\dot{x}_2 = f_2(x,t) \tag{1.16b}$$
$$\vdots \quad \vdots$$
$$\dot{x}_N = f_N(x,t) \tag{1.16c}$$

where $\dot{x}$ represents the derivative of variable x with time, N is the number of differential variables $\dot{x}$, and $x \in \mathbb{R}^N$. The set of nonlinear equations can be approximated by a Taylor series expansion close to a steady-state operating point in the following manner:

$$\dot{x} = \mathbf{J}x \tag{1.17}$$

where $\mathbf{J}$ is the Jacobian matrix including all first order derivatives. The entry at row j and column l, J_{jl}, is evaluated by the following expression:

$$J_{jl} = \frac{\partial f_j}{\partial x_l} \tag{1.18}$$

The eigenvalues of the Jacobian matrix are then found (Anagnost and Desoer, 1991), giving rise to the stability of the system. If any of the real parts of all eigenvalues are positive, then according to Routh and Hurwitz the system is unstable (Hurwitz, 1895; Routh, 1877). Hence,

a stable system is present when the following expression is given:

$$\mathrm{re}\left(\mathrm{eig}\left[\mathbf{J}\right]\right) \leq 0 \tag{1.19}$$

where the output of operator $\mathrm{re}(x)$ is the real part of x.

1.2.2 Lyapunov exponent method

The Lyapunov exponents describe how state variables "drift off" after a large amount of time for an initial small perturbation δx_0. The deviation of the state variables is assumed to follow an exponential profile, which enables to quantify if a stable system is present. A diagram showing the possible evolution of this deviation is shown in Figure 1.5.

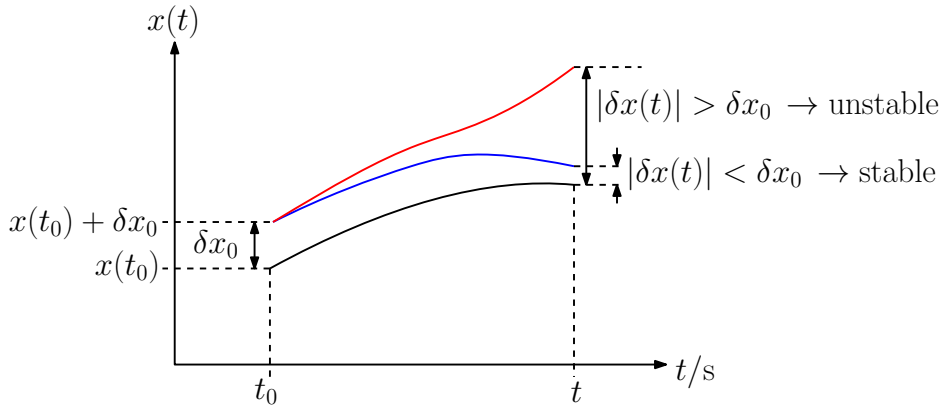

Fig. 1.5 Deviation of an initially perturbed state variable for a stable system and an unstable system.

The following expression quantifies the deviation of an initially perturbed state variable after time t:

$$\delta x_0 \exp\left(\Lambda\left(x\left(t_0\right)\right)t\right) = \left|x\left(t, x\left(t_0\right)\right) - x\left(t, x\left(t_0\right) + \delta x_0\right)\right| \tag{1.20}$$

$$\Lambda\left(x\left(t_0\right)\right) = \frac{1}{t}\ln\left(\frac{\left|x\left(t, x\left(t_0\right)\right) - x\left(t, x\left(t_0\right) + \delta x_0\right)\right|}{\delta x_0}\right) \tag{1.21}$$

At the limit of a very small perturbation and infinite time:

$$\Lambda\left(x\left(t_0\right)\right) = \lim_{t\to\infty}\left\{\frac{1}{t}\ln\left(\left|\frac{\delta x\left(t, x\left(t_0\right)\right)}{\delta x_0}\right|\right)\right\} \tag{1.22}$$

where Λ is known as the *Lyapunov exponent* (Strozzi and Zaldívar, 1994). Numerically, Lyapunov exponents can be evaluated by simulating several systems in parallel, for which each state variable is perturbed initially by an amount δx_0. The values of each perturbed state at final time t are then compared to the unperturbed states. If the distance between the states has increased compared to the initial perturbation δx_0, an unstable system is present, as illustrated in Figure 1.5. If the system is unstable, the Lyapunov exponent Λ becomes positive since the distance of the perturbed and unperturbed states has increased with time.

Simulating the systems for an infinite amount of time is of course infeasible for practical purposes. Therefore, a large time horizon is chosen instead, which is supposed to give a good approximation of the final value, known as the *local Lyapunov exponent*. This means that at each point in time, a long simulation is carried out in order to find the local Lyapunov exponent, Λ_l, given by:

$$\Lambda_\mathrm{l}\left(x\left(t_0\right), t\right) = \frac{1}{t_\mathrm{Lyap}} \ln\left(\left|\frac{\delta x\left(t + t_\mathrm{Lyap}, x\left(t_0\right)\right)}{\delta x_0}\right|\right) \tag{1.23}$$

where t_Lyap is the time frame for the Lyapunov exponent evaluation. Other methods for evaluating the Lyapunov exponents are available (Melcher, 2003).

The choice of the Lyapunov horizon t_Lyap in Equation (1.23) is made based on a detailed sensitivity analysis due to the issue shown in Figure 1.6.

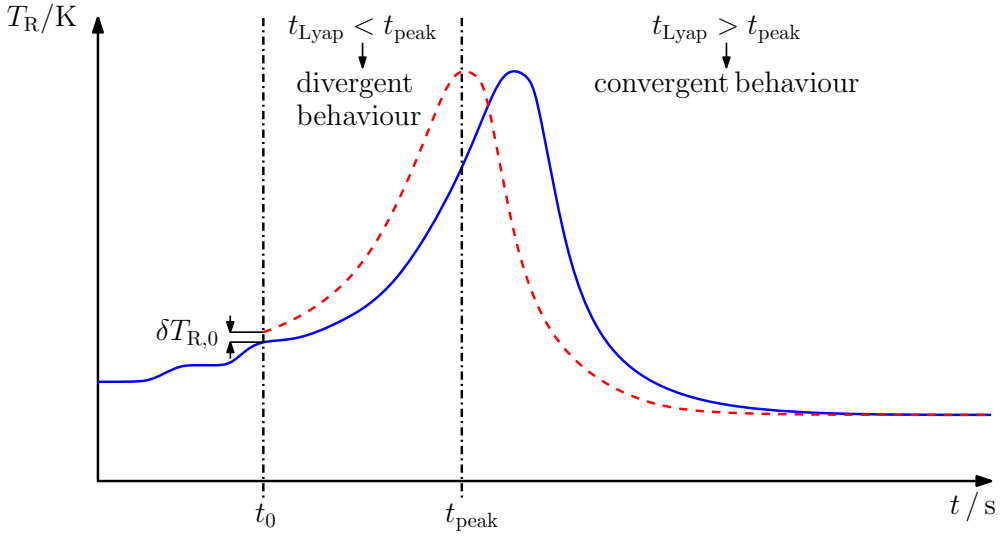

Fig. 1.6 Schematic of the temperature profile for a thermal runaway reaction (blue solid line), including the resulting temperature profile with perturbation δT_R occurring at time t_0 (red dashed line). Time t_peak shows the time at which the peak temperature is reached for the perturbed temperature profile.

An interesting property of batch processes, as opposed to steady-state processes, is the convergent nature after a long time frame. If all reagents have been consumed during the reaction, the reactor temperature will decrease to that of the coolant after long enough time. Hence, as is seen in Figure 1.6, the value of t_{Lyap} must not be chosen too large for Lyapunov exponents to give reliable stability predictions. The value of t_{Lyap} should not be much larger than the time required until the peak temperature is observed for thermal runaway reactions, because after this time the temperature, as well as concentration profiles start to converge as no more reaction occurs. It is therefore essential to understand the dynamic behaviour of the underlying batch process before choosing a value for t_{Lyap}.

1.2.3 Divergence criterion

The divergence criterion, which is based on Liouville's theorem (Arnold, 1973), can be used for the analysis of stability for linear systems. Consider the linear differential equation according to Equation (1.17). For this system the divergence criterion identifies a stable process if the following is given:

$$\operatorname{div}[\mathbf{J}] = \operatorname{tr}[\mathbf{J}] < 0 \tag{1.24}$$

where $\operatorname{tr}[\mathbf{J}]$ is the trace of matrix $\mathbf{J}$, which is the sum of all diagonal elements in $\mathbf{J}$. The system present is stable when the divergence of matrix $\mathbf{J}$ is negative (Strozzi and Zaldívar, 1999). According to Strozzi and Zaldívar (1999) the change from a stable to an unstable system occurs at a sign change of the divergence. This criterion does not require as many evaluations as Lyapunov exponents and therefore promises to be a more computationally efficient measure of stability.

According to Copelli *et al.* (2014) and Bosch *et al.* (2004), the main contributing factors for a thermal runaway are only those variables which influence the heat generation Q_{gen} in the reactor energy balance. In this case study, according to the reaction in Equation (1.6), this is represented by the following expressions:

$$Q_{\text{gen}} = r\,(\Delta H_r)\,V_{\text{R}} \tag{1.25}$$

Therefore, the state variables of interest are the reagents within each reaction rate r and the temperature of the reactor T_{R}, as these are the contributors for the heat generated by the exothermic reaction. The coolant temperature, as well as the concentrations of products which are not reactants for other reactions do not appear in Equation (1.25). Therefore the

diagonal elements of the Jacobian **J** with respect to the coolant temperature and the products of the reactions are neglected when evaluating the *modified divergence*, as shown in Copelli *et al.* (2014).

1.3 Control theory: PI/PID and MPC

1.3.1 PI/PID control

The temperature within batch reactors can be controlled in several different ways. Proportional Integral (PI) control is most commonly found in industry for this purpose (Winde, 2009; Zhang, 2017). Proportional Integral Derivative (PID) control can also be used, but this type of control is known to cause instabilities in the process, if tuned incorrectly (Stephanopoulos, 1984). For temperature control of reactor systems the PI/PID controller regulates the coolant flow to keep a given set-point temperature. As the reaction proceeds, more reactants are consumed and therefore the heat generation decreases. Therefore, there is an opportunity of continuously increasing the reactor temperature which cannot be implemented using PI/PID control only, because PI/PID control does not determine but only follows set-points.

For the purpose of this work, PI control is used to examine how well each stability criterion predicts the thermal runaway nature of several reaction schemes. A PI controller is mathematically described by the following equation:

$$u(t) = K_P \varepsilon(t) + \frac{1}{\tau_I} \int_{t_0}^{t_f} \varepsilon(t)\, \mathrm{d}t \tag{1.26}$$

where $u(t)$ is the control variable given by the coolant flow rate, $\varepsilon(t)$ is the error at time t in this case given by the temperature deviation, K_P is the proportional constant of the PI controller, and τ_I is the integral constant of the PI controller. K_P and τ_I define how the PI controller behaves for the process, and are set to $K_P = 10$ m^3 K^{-1} s^{-1} and $\tau_I = 1000$ K s^2 m^{-3}. The purpose of the PI controller used in this work is to examine when each batch process becomes unstable if the set-point temperature is set too high. As such no rigorous tuning methods such as Ziegler-Nichols (Yucelen *et al.*, 2006) or Cohen-Coon (Joseph and Olaiya, 2018) are applied in this work. Hence, these values are not general PI controller settings to be used in batch processes, but are specifically set up for the systems considered in this thesis.

1.3.2 Structure of MPC

Model Predictive Control (MPC) started to be vastly implemented in industry in the 1980s as an alternative to the commonly used PID control (Lee, 1994, 2011). The advantage of MPC over PID controllers is the capability of optimising a system during operation, whilst considering system constraints and nonlinear system dynamics (Anucha *et al.*, 2015; Chuong La *et al.*, 2017; Mayne, 2014). Constraints cannot be included in PID control which may lead to saturation of control valves or exceeding certain criteria for the process, *e.g.* maximum allowable temperatures.

MPC is capable of using a process model to continuously carry out a specified optimisation of control variables, also called inputs, in order to achieve that particular goal (Haber *et al.*, 2011). For this purpose a method called "receding horizon" control is employed, which is described in detail in Rawlings and Mayne (2015) and Christofides *et al.* (2011). The implementation of a receding horizon method is schematically shown in Figure 1.7.

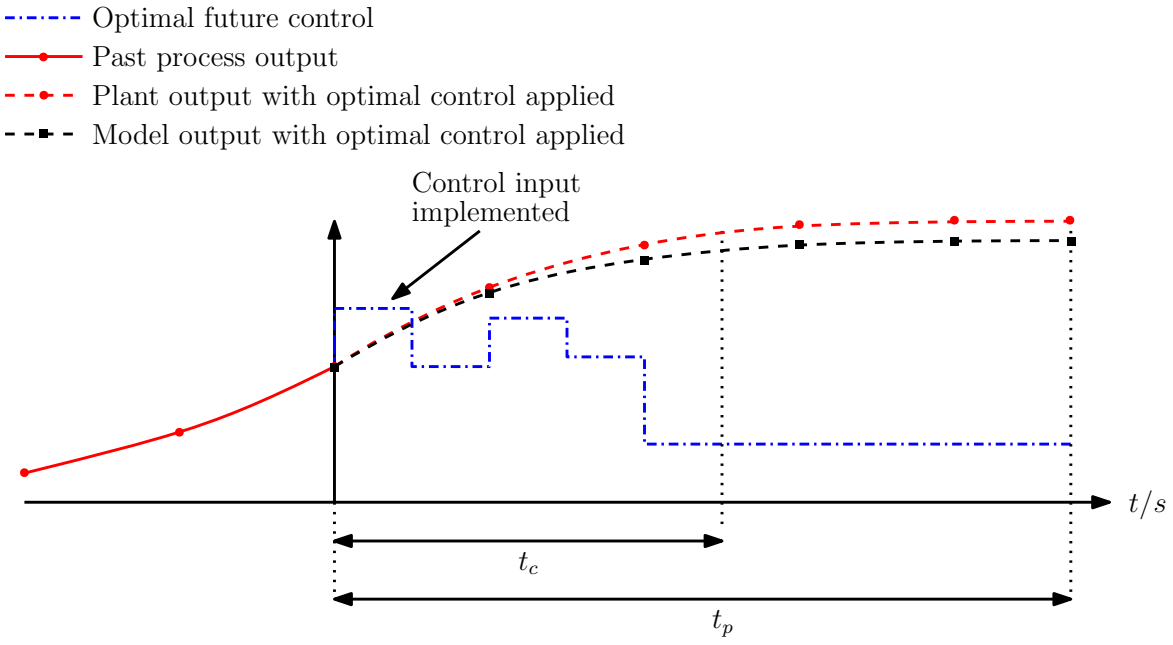

Fig. 1.7 Schematic showing the principles of the receding horizon Model Predictive Control algorithm, including control horizon t_c and prediction horizon t_p. Only the first control input found is implemented in a moving horizon manner (Rawlings and Mayne, 2015).

In this approach of process control the process model is used to predict how the system will behave to certain input values. It is desired to find the sequence of input variables that optimises the objective of the problem. The inputs are split into several piecewise constant control steps which are allowed to vary over a control horizon t_c (Akpan and Hassapis, 2011).

To make sure a solution is obtained which converges to a desired reference trajectory, a prediction horizon t_p is included, for which the system is simulated with the control inputs found from the optimisation (Rawlings and Mayne, 2015). The control value assumed for the prediction horizon is equal to the last control step of the control horizon, as shown in Figure 1.7.

In general, the larger the number of control steps and the longer the prediction horizon, the more stable the system controlled MPC will be. The drawback of increasing the control and prediction horizon is the exponential increase in computational time required for the evaluation of the MPC algorithm. Hence, careful consideration of the control and prediction horizon lengths is required when using MPC.

Different MPC techniques have been developed in literature for different purposes. Robust MPC tackles the issue of uncertainty in the process model and tries to ensure constraint satisfaction (Lucia *et al.*, 2012; Martí *et al.*, 2015). Economic MPC (EMPC) has found wide applications for supervisory control of whole plant sections: by using a common objective given in monetary units, the most efficient process conditions are implemented for each process under control (Griffith *et al.*, 2017; Jäschke *et al.*, 2014; Wu *et al.*, 2018). This requires detailed information about costs, but once such data are available, is very useful for industrial application. The general structure of all MPC algorithms developed is still similar in that an objective has to be optimised to find the control inputs to be implemented.

1.3.3 Optimisation methods for MPC

At the heart of MPC is the optimisation problem which has to be solved at every sampling time. Many optimisation methods are present in literature which can be used for this purpose.

Due to process constraints a *constrained* optimisation problem is present. This rules out all unconstrained optimisation algorithms such as pure line-search (Goldfarb, 1980) or pure trust-region (Byrd *et al.*, 1988; Schultz *et al.*, 1985) methods. Furthermore, the equations present in MPC formulations are, in general, nonlinear. Algorithms that solve linear constrained systems, *e.g.* the Simplex method (Dantzig, 1963; Vanderbei, 2001), can therefore not be used in this work.

The most common optimisation algorithms that solve nonlinear constrained optimisation problems are augmented Lagrangian methods, the interior point method (IPM), and the sequential quadratic programming (SQP) method.

For each optimisation algorithm the following general formulation is assumed:

$$\min_x f(x) \tag{1.27a}$$

subject to:

$$h_a(x) = 0,\ a = 1, 2, \ldots, a_h \tag{1.27b}$$

$$g_a(x) \leq 0,\ a = 1, 2, \ldots, a_g \tag{1.27c}$$

where a_h and a_g are the number of equality and inequality constraints, respectively, $h_a(x)$ are equality constraints, and $g_a(x)$ are inequality constraints including bounds. The advantages and disadvantages of each method mentioned above are outlined below.

Augmented Lagrangian and penalty methods

Augmented Lagrangian and penalty methods both transform the initially constrained optimisation problem into an unconstrained problem by introducing the constraints into the objective function (Bertsekas, 1982). After this transformation unconstrained solution algorithms such as Newton's method (Osborne, 1976) can be used to find a solution. The method by which the constraints are included in the objective function differs between the augmented Lagrangian and the penalty method.

Penalty methods can use different functions to include the constraints in the objective. The most common penalty function is the *square penalty* function. To use square penalty functions the problem in Equation (1.27) is reformulated in the following manner (Courant, 1943):

$$\min_x f(x) + \zeta_{\text{SP}} \sum_{a=1}^{a_h} h(x)^2 + \zeta_{\text{SP}} \sum_{a=1}^{a_g} \max\{g_a(x), 0\}^2 \tag{1.28}$$

where ζ_{SP} is the penalty parameter for the square penalty function.

Initially the value of ζ_{SP} is close to zero, resulting in the unconstrained optimiser of the problem in Equation (1.27), *i.e.* the constraints are not taken into account. This solution is then used as the initial guess for a larger value of ζ_{SP}. This procedure is repeated until the value of ζ_{SP} is very large, in which case a violation in the constraints would have significant contributions to the objective function in Equation (1.28).

Augmented Lagrangian methods use the following reformulation of the problem shown in Equation (1.27) (Hestens, 1969):

$$\min_x f(x) \tag{1.29a}$$

subject to:

$$h_a(x) = 0, a = 1, 2, \ldots, a_h \tag{1.29b}$$

$$g_a(x) + s_a = 0, a = 1, 2, \ldots, a_g \tag{1.29c}$$

$$s_a > 0 \tag{1.29d}$$

where s_a are slack variables which transform the inequality constraints into equality constraints.

This allows the following reformulation of the problem in Equation (1.29):

$$\min_x f(x) + \sum_{a=1}^{a_h} \xi_{h,a} h_a + \sum_{a=1}^{a_g} \xi_{g,a} (g_a + s_a) + \zeta_{\text{AL}} \left[\sum_{a=1}^{a_h} h_a^2 + \sum_{a=1}^{a_h} (g_a + s_a)^2 \right] \tag{1.30}$$

where ζ_{AL} is the penalty parameter for the augmented Lagrangian method, and $\xi_{h,a}$ and $\xi_{g,a}$ are the Lagrange multipliers with respect to equality constraints $h_a(x) = 0$ and $g_a(x) + s_a = 0$, respectively.

Similar to the penalty parameter in Equation (1.28), the value of ζ_{AL} is increased with each iteration. The values of $\xi_{h,a}$ and $\xi_{g,a}$ at each iteration are obtained by the solution of the Karush-Kuhn-Tucker (KKT) conditions (Bryson and Ho, 1975).

As long as good values for the penalty parameters ζ are chosen, these optimisation methods result in numerically stable solutions. The inherent problem with these methods is the potential stiffness: a large value of ζ_{AL} or ζ_{SP} imposes a large value on the objective function. The derivatives of the objective function therefore become very large, which can cause issues during the solution procedure.

For the application to MPC the optimisation method has to give a solution in order for the process to be controlled. The penalty parameters ζ would have to be adjusted depending on the system dynamics to make sure results are obtained. This is not necessary with the two optimisation methods shown below. Therefore augmented Lagrangian and penalty methods are not used for the MPC implementation.

Interior point methods

Interior point methods (IPMs) have found great application in literature (Wächter and Biegler, 2006) when dealing with nonlinear constrained optimisation problems. The problem

in Equation (1.27) is reformulated to give the following:

$$\min_x f(x) - \zeta_{\text{IPM}} \sum_{a=1}^{a_g} \ln s_a \tag{1.31a}$$

subject to:

$$h_a(x) = 0, a = 1, 2, \ldots, a_h \tag{1.31b}$$

$$g_a(x) + s_a = 0, a = 1, 2, \ldots, a_g \tag{1.31c}$$

where ζ_{IPM} is the penalty parameter for the IPM.

The minimisation of the objective in Equation (1.31a) ensures the value of the slack variables s_a stays positive. Therefore, the separate constraint $s_a \geq 0$ is not necessary.

From Equation (1.31) the KKT conditions are solved to find a search direction for x. Then either line-search or trust-region methods can be used to advance the optimisation procedure. Since feasibility is guaranteed with IPMs, line-search methods are more efficient when used for IPMs. At every step of the IPM it is ensured that $s_a \geq 0$ and therefore $g_a(x) \leq 0$, hence staying in the feasible region. A more detailed discussion on IPMs can be found in (Wächter and Biegler, 2006).

Even though IPMs find many applications in literature due to their ability of solving large scale optimisation problems, issues arise: the choice of the starting point for the optimisation procedure needs to be within the feasible region. Furthermore, the scaling of the problem and the updating of the penalty parameter ζ_{IPM} can cause convergence issues. Lastly, as IPMs approach the boundary of the feasible region the algorithm slows down significantly due to the increased stiffness of the natural logarithm in the objective function. For process intensification with MPC it is required to be close to the boundary of stability, included as a bounded constraint. If the MPC algorithm slows down significantly when reaching the stability boundary, it is expected that longer computational times are obtained.

Sequential quadratic programming (SQP) method

The main idea of the sequential quadratic programming (SQP) method is the following: approximate the optimisation problem at the current point to be quadratic. This gives a locally convex problem for which a search direction for the next iteration can be found (Nocedal and Wright, 2006). The optimisation problem in Equation (1.27) is reformulated to

give the following:

$$\min_{p} f + \nabla f^{\mathrm{T}} p + \frac{1}{2} p^{\mathrm{T}} \nabla^2_{xx} \mathscr{L} p \tag{1.32a}$$

subject to:

$$\nabla h_a^{\mathrm{T}} p + h_a(x) = 0, l = 1, 2, \ldots, l_h \tag{1.32b}$$

$$\nabla g_a^{\mathrm{T}} p + g_a(x) \leq 0, l = 1, 2, \ldots, l_g \tag{1.32c}$$

where p is the search direction to be found, and $\mathscr{L}$ is the Lagrangian function.

The Lagrangian function $\mathscr{L}$ in Equation (1.32) is given by the following:

$$\mathscr{L} = f + \sum_{a=1}^{a_h} \xi_{h,a} h_a + \sum_{a=1}^{a_h} \xi_{g,a} (g_a + s_a) \tag{1.33}$$

with the optimisation problem given by Equation (1.29).

Once it is known which constraints in Equation (1.32c) are active a line-search method, *e.g.* Newton's method, can be used to find the optimal search direction p. Since SQPs do not guarantee constraint satisfaction, trust-region methods are more efficient than line-search methods in this case.

For a small number of free variables SQP methods are very efficient (Nocedal and Wright, 2006). Unlike IPMs or penalty function methods, the SQP method does not suffer from scaling issues with respect to penalty parameters.

The MPC problems considered in this work focus on controlling the coolant flow rate, which constitutes a single free variable. Furthermore it is required to obtain solutions reliably and operating close to the boundary of stability to achieve process intensification. Due to the small problem size, the SQP optimisation method is used in this work. Furthermore, stiffness problems as for IPMs when approaching the bounds of feasibility are avoided by using SQP.

1.3.4 Process uncertainty and robust control

MPC requires the use of a process model, according to which the optimal sequence of control inputs are evaluated. In industry it is rarely possible to find process models which are 100% accurate for such purposes. Parameters within the model can be uncertain (Kalmuk *et al.*, 2017; Sirohi and Choi, 1996) or the model might have the wrong structure, often called

model-plant mismatch (Badwe *et al.*, 2010; Hong *et al.*, 2012). Uncertainty in the process model can have significant effects on process control if not taken into account.

The ability to keep a process under control whilst experiencing uncertainties is called *robust control*. A significant amount of work was carried out for robust control using PID controllers and MPC.

PID controllers have a pre-defined structure which defines their behaviour with respect to process errors. To achieve robust control due to process disturbances a general controller is found for which the process stays close to its desired operating point (Zhou and Doyle, 1998). Once the mathematical description of such a controller is found, PID controllers are arranged to achieve the desired behaviour (Ge *et al.*, 2002). This type of robust control works well for systems with a clearly defined steady-state operating point. This is the case as the system can be described linearly close to the operating point, which cannot be done for batch processes which are highly nonlinear with time.

The structure of models for chemical reactor systems can often be found from first principles techniques. The biggest issue becomes the estimation of the parameters within the model (Dochain, 2003). From plant measurements the parameters can be estimated as the process proceeds, but uncertainty will still be present.

For chemical reactor systems the effect of each parameter can often be identified, *e.g.* an increase in enthalpy of reaction ΔH_r will increase the amount of heat released. This property enables the identification of the *worst* set of parameters for the system model, *i.e.* the set of parameters that makes the process as unstable as possible. In the case of thermal stability the worst set of parameters is the one resulting in the largest heat generation. This idea led to the development of the open-loop min-max MPC approach (Campo and Morari, 1987). This approach assumes the most unstable set of parameters for which a stable system is obtained. If the most unstable process can be kept under control, the real process will be kept stable as well. This results in overly conservative control since feedback of the MPC throughout the process is not taken into account (Lucia *et al.*, 2014; Martí *et al.*, 2015).

One approach to deal with uncertainty is the continuous estimation of the process model with the use of Gaussian processes (Jones *et al.*, 1998; Kocijan *et al.*, 2004). This method uses the maximum likelihood estimator with samples from the process to find the most likely process model. Several case studies in literature were considered using this approach (Bradford *et al.*, 2018; Likar and Kocijan, 2007; Maciejowski and Yang, 2013). Using Gaussian processes results in black box models which work well to control certain processes,

but offer no physical insight. Similar results are obtained when using models generated by artificial neural nets (Ghaffar *et al.*, 2014; Hosen *et al.*, 2011).

Other approaches to overcome the limitation of the open-loop control are closed-loop min-max MPC (Mayne *et al.*, 2005; Rakovic *et al.*, 2011; Rawlings and Animit, 2009) and tube-based MPC (Muñoz-Carpintero *et al.*, 2016). These methods take into account that new information will be available as the process occurs, but issues with respect to overly conservative control and computational costs arise.

To avoid the overly conservative nature of closed-loop min-max MPC, a multistage MPC framework was developed (Bernadini and Bemporad, 2009; Lucia *et al.*, 2013; Martí *et al.*, 2015; Scokaert and Mayne, 1998). This method assumes that the uncertainty within the system can be represented by multiple scenarios with state variables x, each representing a possible set of parameters in the model. This is shown diagrammatically in Figure 1.8, where the subscript denotes the stage, and the superscript denotes the scenario within each stage.

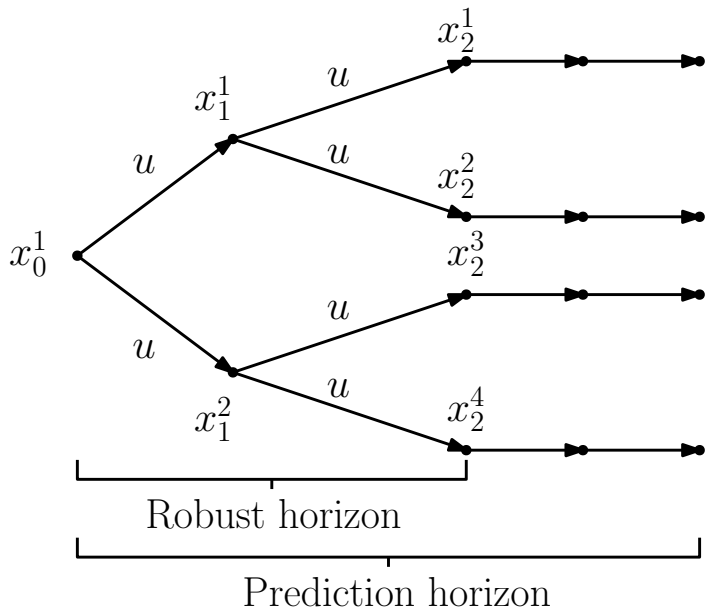

Fig. 1.8 Scenario-based multi-stage MPC framework. Within the robust horizon different scenarios of state variable x are assumed at each stage. Beyond the robust horizon and within the prediction horizon no new scenarios are added. The same control input u is used for each stage.

In Figure 1.8 it is seen that the control value implemented for each scenario is identical. This is the case because the MPC algorithm cannot predict which scenario will occur. Within the robust horizon it is assumed that several scenarios can occur, where each scenario is

equivalent to a particular set of values for all uncertain parameters in the system. Beyond the robust horizon, the behaviour of each scenario is simulated within the prediction horizon, similar to the standard MPC framework outlined in Section 1.3.2. For parametric uncertainty only one stage within the robust horizon is required, because a value for each uncertain parameter can be sampled independently. Each set of parameter values can then be used as a single scenario.

The number of evaluations required for this method grows exponentially with the number of scenarios simulated, but each scenario is independent of each other. Hence, the optimisation problem does not increase in size, but the size of the simulation model does. This method is considered extensively in literature (Krishnamoorthy *et al.*, 2018; Lucia and Paulen, 2014; Thangavel *et al.*, 2018).

1.4 Research aims and objectives

To improve the efficiency of batch processes by a flexible increase of the reactor temperature the following steps for the further analysis are necessary:

1. develop a concept to embed thermal stability criteria within MPC for batch processes
2. verify the reliability of using the above stability criteria to identify unstable behaviour in exothermic batch processes
3. embed these stability criteria within MPC and examine the behaviour and efficiency of batch processes
4. implement robust MPC techniques to ensure safe operation with respect to model-plant mismatch

The validation of the stability criteria to identify unstable behaviour in batch processes is done on the basis of the model of batch processes with all relevant parameters presented in Chapter 2.

Chapter 2

Batch reactor model

In this chapter the detailed model used for all simulations in this thesis is outlined. The basis for the processes is the model of ideal mixing, which requires the evaluation of heat transfer coefficients depending on coolant and reacting mixture properties. The concept of MPC with embedded stability analysis, as well as the frameworks used for the intensification of batch processes are explained in detail. Furthermore, all example reaction processes are introduced and thermal runaway behaviour for each process is demonstrated with the use of PI control. The examples of thermal runaway behaviour are used in following chapters to examine the reliability of thermal stability prediction.

2.1 Basis of simulation model

Batch reactors represent one unit operation in industry, linked to several other parts which determine how the batch process can be operated. In this section a simplified flow chart of a batch reactor, together with all relevant dimensions are shown.

2.1.1 Batch reactor model and flowsheet

Due to its common and flexible use in industry, a simple cooling jacket is assumed for the batch reactor model, as shown in Figure 1.2 (a). To achieve turbulent mixing for a large variation in viscosities, a Rushton impeller is used for the batch reactor model, as is common in industry (Padron, 2003).

The batch reactor model uses a Reynolds number of $\mathrm{Re} \geq 10^5$ for the reacting mixture. Therefore, the assumption of ideal mixing for the concentration of all reagents, as outlined in

Section 1.1.4, is valid. This is due to the fact that the volume of reactants within the boundary layer at the reactor wall is negligible with respect to the overall volume. Hence, uniform concentrations throughout the reactor can be assumed.

This is not the case for the reactor temperature: as outlined in Section 1.1.1 the boundary layer has significant effects on heat transfer from the reacting mixture to the cooling jacket. Therefore the boundary layer will strongly affect the thermal stability properties of the batch reactor model. To incorporate this effect the Chilton, Drew and Jebens correlation in Equation (1.5) is used to calculate the heat transfer coefficient between the reactor contents and the cooling jacket. This correlation requires the evaluation of composition, viscosity, density, and thermal conductivity at every point in time, which give rise to the Nusselt and Prandtl numbers. For the model in this thesis the wall conditions are assumed to be equal to those in the reacting mixture, *i.e.* $\mu_{\text{wall}} = \mu_{\text{R}}$. The stirrer is assumed to keep the reacting mixture in the turbulent regime at all times, such that $\text{Re}_{\text{impeller}} = 10^5$.

Changes in the heat transfer coefficient on the coolant side are taken into account by a constant Nusselt number of $\text{Nu} \approx 3.66$ in the laminar regime, when $\text{Re} \leq 10^4$, and by the Dittus-Boelter correlation in Equation (1.3) in the turbulent regime, when $\text{Re} \geq 10^4$. At the maximum coolant flow rate the Reynolds number is assumed to be $\text{Re} = 10^5$. Since only water flows through the cooling jacket, no changes in composition occur. Therefore, only changes in density, viscosity and thermal conductivity with respect to temperature have to be taken into account.

To identify the important parts which lead to the reactor model, a flow sheet of the batch reactor used in the simulations is shown in Figure 2.1.

After the reactor is filled up with the reagents, the contents are heated up such that the reaction starts generating heat and the process starts. The heating is provided by steam running through the cooling jacket controlled by flow-indicating-controller FIC-301. Once the reaction starts, no more heating is necessary. Hence the steam flow is stopped and cooling water is now supplied at a temperature of 300 K, controlled by FIC-201. The set-point for FIC-201 is set from the computer system, depending on the current state of the reactor. In the simulations carried out in this work, it is assumed that the reactor contents start at the temperature after heating by steam has been applied. As such the time required to heat up the reactor contents is not taken into consideration.

During the process no more reactants are added to the reactor, hence a batch process is present. This is ensured by control valve FIC-101, which is only open when the reactor is charged with reagents. Furthermore, no products are removed during the process meaning control valve

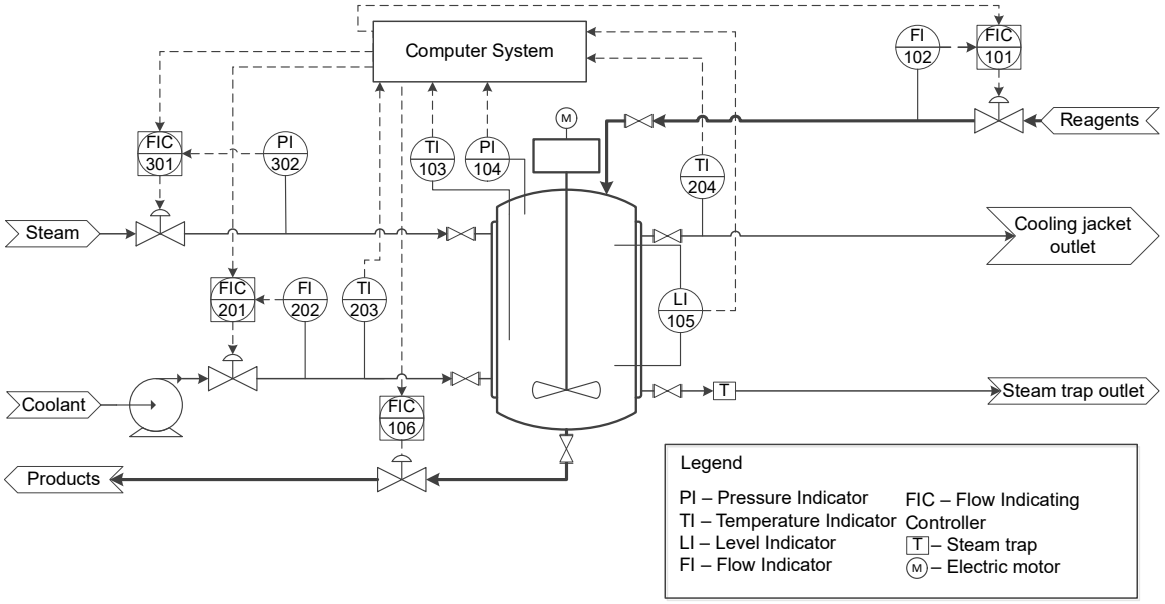

Fig. 2.1 Batch reactor diagram for simulated systems. For the temperature integrated control (TIC) either a PI controller or MPC can be used.

FIC-106 is shut until the process finished. The inlet and outlet lines are only active whilst removing the final product or adding reagents. The liquid level indicator LI-105 measures the amount of reagents added, which is compared to the respective flow rate indicator FI-102. In case of a discrepancy between these two measurements, one of the indicators is faulty and the wrong amounts of reagents were added.

During the process the temperatures and pressures are measured with TI-103 and PI-104 to check the current state of the reactor. Furthermore, the heat generation within the reactor is obtained by a mass balance of the coolant, using temperature and flow measurements from FI-202, TI-203 and TI-204. Since the coolant used is water, the physical properties are known to an acceptable degree in order to carry out this calculation.

Within each FIC and TIC in Figure 2.1 a PI/PID controller is present. The set-point of each of these controllers is set by the computer system.This computer system can be a pre-programmed set of set-points, or an MPC optimising the set-points for each PI/PID controller

at each time step. Therefore, the MPC structure developed in this work, incorporating a stability criterion, is within the computer system shown in Figure 2.1.

The system dynamics were simulated using *ode15s* (Shampine *et al.*, 1999) within MATLAB^{TM}, which uses an adjusted time step Runge-Kutta method (Cellier and Kofman, 2006). MATLAB^{TM} was used due to its simplicity of developing code. All simulations shown in this thesis were carried out on an HP EliteDesk 800 G2 Desktop Mini PC with an Intel® Core i5-65000 processor with 3.20 GHz and 16.0 GB RAM, running on Windows 7 Enterprise.

2.1.2 Process parameters for simulation models

To cover a variety of dynamic behaviours, different reactor parameters are used for different processes. 4 different reaction schemes are used in this thesis, each with up to 20 process parameter sets. The processes within each reaction scheme use different parameter values. To distinguish between each process the following notation is introduced: as an example, process 3 within reaction scheme 2 is denoted by P_3^2. All remaining processes within the 4 reaction schemes are denoted in a similar manner. The data of the different reactor settings are shown in Table 2.1.

Table 2.1 Batch reactor parameters for the processes considered, where V_R and V_C are the reactor and cooling jacket volumes, repectively, A is the heat transfer area and $q_{C,in}$ is the maximum coolant flow rate.

Process	V_R $[m^3]$	V_C $[m^3]$	A $[m^2]$	$q_{C,in}$ $[m^3\,s^{-1}]$
$P_1^1 - P_{15}^1$	16	1.2	30.7	0.037
$P_1^2 - P_5^2$	32	2.0	36.0	0.060
$P_6^2 - P_{10}^2$	20	1.4	35.8	0.043
$P_{11}^2 - P_{15}^2$	8.0	0.50	20.0	0.023
$P_{16}^2 - P_{20}^2$	0.80	0.17	4.2	0.0050
$P_1^3 - P_4^3$	32	2.0	49.1	0.060
$P_5^3 - P_6^3$	25	1.7	42.2	0.051
$P_1^4 - P_4^4$	20	1.4	35.8	0.043
$P_5^4 - P_6^4$	16	1.1	30.7	0.037
Nitration of toluene	8	0.5	20.0	0.023

The values of V_R shown in Table 2.1 represent the volume of the reagents and not the volume of the whole reactor. As mentioned in Section 1.1.1, the reactor is only filled up to 80% of the total volume.

Turbulent mixing is achieved for a Reynolds number of $\mathrm{Re}_\mathrm{impeller} = 10^5$ within the reactor (Padron, 2003), which is used for all simulation models in this work. Highly turbulent flow within the reactor leads to the assumption of uniform physical properties in the radial and axial direction of the batch reactor vessel. The power input by the stirrer is calculated according to Padron (2003). The Reynolds number for fluid flow within a vessel is given by:

$$\mathrm{Re}_\mathrm{impeller} = \frac{\rho \Omega D_\mathrm{impeller}^2}{\mu_R} \tag{2.1}$$

where μ_R is the viscosity of the reagents, Ω is the rotational speed of the impeller, and D_impeller is the diameter of the impeller.

The power number Π is a dimensionless number representing the power input into the reacting mixture by the stirrer:

$$\Pi = \frac{P}{\rho \Omega^3 D_\mathrm{impeller}^5} \tag{2.2}$$

where P is the power transferred to the liquid by the stirrer (Padron, 2003). Representative physical properties for the processes considered are a viscosity of $\mu_\mathrm{R} = 10^{-3}$ Pa s and a density of $\rho = 10^3\,\mathrm{kg\,m^{-3}}$. Hence, Equation (2.1) can be rearranged, given a value of $\mathrm{Re}_\mathrm{impeller} = 10^5$:

$$\Omega D_\mathrm{impeller} = \frac{10^5 \times 10^{-3}}{10^3 \times D_\mathrm{impeller}} \tag{2.3a}$$

$$\Omega D_\mathrm{impeller} = \frac{1}{10 D_\mathrm{impeller}} \tag{2.3b}$$

If turbulent flow is present, uniform physical properties are present within the reactor. In Padron (2003) it is shown that for Rushton impellers a Reynolds number of 10^4 yields a power number of $\Pi \approx 3$. Rearranging Equation (2.2) and using the result from Equation (2.3b), the required power input can be found:

$$3 = \frac{P}{10^3 \times \left(\frac{1}{10 D_\mathrm{impeller}}\right)^3 D_\mathrm{impeller}^2} \tag{2.4a}$$

$$3 = P D_\mathrm{impeller} \tag{2.4b}$$

For an industrial reactor with a volume of $V_\mathrm{R} = 20\,\mathrm{m}^3$ and aspect ratio of height to diameter of $H/D = 3$, and ratio of reactor diameter to impeller diameter of $D/D_\mathrm{impeller} = 3$, it is found that:

$$V_\mathrm{R} = \frac{\pi D_\mathrm{impeller}^2}{4} \times H \tag{2.5a}$$

$$V_R = \frac{3\pi D_\mathrm{impeller}^3}{4} \tag{2.5b}$$

$$D_\mathrm{impeller} = \left(\frac{4V_R}{3\pi}\right)^{1/3} \tag{2.5c}$$

$$D_\mathrm{impeller} = \frac{1}{3}\left(\frac{4\times 20}{3\pi}\right)^{1/3} \tag{2.5d}$$

$$D_\mathrm{impeller} = 0.68\,\mathrm{m} \tag{2.5e}$$

Using Equation (2.4) and Equation (2.5), the following power input into the reactor is found:

$$P = \frac{3}{0.68} \tag{2.6a}$$

$$P = 4.4\,\mathrm{W} \tag{2.6b}$$

This value for the power input is compared to the heat generated by the exothermic reactions in Section 2.3. If the power input by the stirrer is much less than the heat generation by the reaction, this can be neglected in further analyses.

2.2 Example set of reaction processes

The reaction kinetics presented in the following sections are ordered in terms of complexity: first a single reaction whose rate of reaction is dependent on a single reagent, denoted by *reaction scheme 1*, is shown. *Reaction scheme 2* still considers a single reaction, but the reaction rate depends on two components. *Reaction scheme 3* consists of 4 reactions occurring simultaneously, whereas *reaction scheme 4* consists of 6 simultaneous reactions.

This section is concluded by presenting the industrially relevant *nitration of toluene*, which presents a challenge due to its exothermic nature.

The physical properties of all components presented below are evaluated based on Equation (1.13), as well as the data given in Tables A.6−A.9 in Appendix A.5. For different temperatures the data given in Tables A.6−A.9 are interpolated to obtain the respective physical property values. If the temperature of the reacting mixture exceeds 500 K, the maximum values given in Tables A.6−A.9 are used.

2.2.1 Reaction scheme 1

Reaction scheme 1 consists of a single reaction. The reaction occurring is given by:

$$\mathrm{A} + \mathrm{B} \rightarrow \mathrm{C} \tag{2.7}$$

Examples of reactions with this kinetic scheme are polycondensation reactions, *e.g.* of dicarboxylic acid and diols, or the addition reaction for the synthesis of ethylene glycol from ethylene oxide and water.

The reaction rate is given by an Arrhenius expression (Davis and Davis, 2003):

$$r = k_0 \exp\left(-\frac{E_a}{R T_\mathrm{R}}\right) [\mathrm{A}]^{n_\mathrm{A}} \tag{2.8}$$

15 different sets of parameters are used for reaction scheme 1, hence resulting in 15 different processes. The order of reaction with respect to reagent A, n_A, is varied between values of 1.0 to 3.0. The reaction data for these processes are given in Table A.1 in Appendix A.1.

2.2.2 Reaction scheme 2

Reaction scheme 2 consists of a single reaction whose reaction rate depends on two reagents. The following reaction is considered to occur within the batch reactor:

$$\nu_\mathrm{A}\mathrm{A} + \nu_\mathrm{B}\mathrm{B} \rightarrow \mathrm{C} \tag{2.9}$$

where ν_A and ν_B are the stoichiometric coefficients with respect to reagents A and B, respectively.

The rate of reaction for this reaction scheme now depends on reagents A and B, the orders of which are given by n_A and n_B. The Arrhenius rate expression is given by:

$$r = k_0 \exp\left(-\frac{E_a}{R T_\mathrm{R}}\right) [\mathrm{A}]^{n_\mathrm{A}} [\mathrm{B}]^{n_\mathrm{B}} \tag{2.10}$$

A total of 20 reactions are considered within reaction scheme 2. The process parameters are summarised in Table A.2 in Appendix A.2. The initial concentration of reagent B is set to $[\mathrm{B}] = 8$ kmol m^{-3} for each process within reaction scheme 2.

2.2.3 Reaction scheme 3

In reaction scheme 3, there are 4 reactions occurring simultaneously. The reaction network is given by:

$$\nu_{\mathrm{A},1}\mathrm{A} + \nu_{\mathrm{B},1}\mathrm{B} \rightarrow \mathrm{C} \tag{2.11a}$$
$$\nu_{\mathrm{A},2}\mathrm{A} + \nu_{\mathrm{C},2}\mathrm{C} \rightarrow \mathrm{D} \tag{2.11b}$$
$$\nu_{\mathrm{A},3}\mathrm{A} + \nu_{\mathrm{B},3}\mathrm{B} \rightarrow \mathrm{E} \tag{2.11c}$$
$$\nu_{\mathrm{A},4}\mathrm{A} + \nu_{\mathrm{E},4}\mathrm{E} \rightarrow \mathrm{F} \tag{2.11d}$$

The reactions rates for each reaction given in Equation (2.11) are given by:

$$r_1 = k_{0,1}\exp\left(-\frac{E_{a,1}}{RT_{\mathrm{R}}}\right) \times [\mathrm{A}]^{n_{\mathrm{A},1}}[\mathrm{B}]^{n_{\mathrm{B},1}} \tag{2.12a}$$
$$r_2 = k_{0,2}\exp\left(-\frac{E_{a,2}}{RT_{\mathrm{R}}}\right) \times [\mathrm{A}]^{n_{\mathrm{A},2}}[\mathrm{C}]^{n_{\mathrm{C},2}} \tag{2.12b}$$
$$r_3 = k_{0,3}\exp\left(-\frac{E_{a,3}}{RT_{\mathrm{R}}}\right) \times [\mathrm{A}]^{n_{\mathrm{A},3}}[\mathrm{B}]^{n_{\mathrm{B},3}} \tag{2.12c}$$
$$r_4 = k_{0,4}\exp\left(-\frac{E_{a,4}}{RT_{\mathrm{R}}}\right) \times [\mathrm{A}]^{n_{\mathrm{A},4}}[\mathrm{E}]^{n_{\mathrm{E},4}} \tag{2.12d}$$

The reaction rate giving rise to r_i is called reaction i hereafter. Hence reactions 1 and 2 are described by the rate equations given for r_1 and r_2 within Equation (2.12). Similarly, reactions 3 and 4 are described by the expressions for r_3 and r_4 in Equation (2.12).

The processes are denoted by $\mathrm{P}_1^3 - \mathrm{P}_6^3$ for processes 1 through 6 within reaction scheme 3. For reactions 1 and 2, the data used for processes $\mathrm{P}_1^3 - \mathrm{P}_6^3$ are summarised in Table A.3 in Appendix A.3. The reaction data for reactions 3 and 4 for processes $\mathrm{P}_1^3 - \mathrm{P}_6^3$ are given in Table A.4 in Appendix A.3.

The initial concentrations of reagents A and B are given by the following:

$$[\mathrm{A}]_0 = 15.0\,\mathrm{kmol\,m^{-3}} \tag{2.13a}$$

$$[\mathrm{B}]_0 = 17.0\,\mathrm{kmol\,m^{-3}} \tag{2.13b}$$

Components C, D and E are products of the initial reactions between reagents A and B. Hence their initial concentrations are set to $0.0\,\mathrm{kmol\,m^{-3}}$.

2.2.4 Reaction scheme 4

Reaction scheme 4 is composed of the parallel reactions shown in reaction scheme 3, given in Equation (2.11), as well as an additional set of reactions occurring in parallel. These additional reactions are given by:

$$\nu_{\mathrm{A},5}\mathrm{A} + \nu_{\mathrm{B},5}\mathrm{B} \rightarrow \mathrm{G} \tag{2.14a}$$

$$\nu_{\mathrm{A},6}\mathrm{A} + \nu_{\mathrm{G},6}\mathrm{G} \rightarrow \mathrm{H} \tag{2.14b}$$

Reaction scheme 3 is the basis for reaction scheme 4. This means that the data for reactions 1 to 4 given in Tables A.3 and A.4 are the same for reaction scheme 4. Furthermore, the initial concentrations in Equation (2.13) and for components C, D and E of $0.0\,\mathrm{kmol\,m^{-3}}$ are used also for reaction scheme 4. As for reaction scheme 3, the reaction rates are dependent on the concentration of the respective reagents and their respective reaction orders, hence given by:

$$r_5 = k_{0,5} \exp\left(-\frac{E_{a,5}}{R T_\mathrm{R}}\right) \times [\mathrm{A}]^{n_{\mathrm{A},5}} [\mathrm{B}]^{n_{\mathrm{B},5}} \tag{2.15a}$$

$$r_6 = k_{0,6} \exp\left(-\frac{E_{a,6}}{R T_\mathrm{R}}\right) \times [\mathrm{A}]^{n_{\mathrm{A},6}} [\mathrm{G}]^{n_{\mathrm{G},6}} \tag{2.15b}$$

The reaction rates given in Equation (2.15) are again expressed as Arrhenius relations (Davis and Davis, 2003). The reaction rates r_5 and r_6 given in Equation (2.15) correspond to reactions 5 and 6 within reaction scheme 4. The data of the additional reactions is given in Table A.5 in Appendix A.4. The data given in Tables A.3, A.4 and A.5 are the basis for all reactions occurring in reaction scheme 4.

2.2.5 Industrial case study: nitration of toluene

The nitration of toluene is an industrially relevant reaction which consists of both endothermic and exothermic reactions (Halder *et al.*, 2008). Overall, a net exothermic process is present which is why thermal runaways can occur for this reaction system. The reaction is initiated by the formation of a nitronium ion $\left(NO_2^+\right)$, followed by 3 parallel reactions with toluene:

$$HNO_3 + H_2SO_4 \rightarrow NO_2^+ + HSO_4^- + H_2O \qquad \text{Reaction } (1) \tag{2.16a}$$

$$NO_2^+ + C_7H_8 + H_2O \rightarrow \text{o-}C_7H_7NO_2 + H_3O^+ \qquad \text{Reaction } (2) \tag{2.16b}$$

$$NO_2^+ + C_7H_8 + H_2O \rightarrow \text{p-}C_7H_7NO_2 + H_3O^+ \qquad \text{Reaction } (3) \tag{2.16c}$$

$$NO_2^+ + C_7H_8 + H_2O \rightarrow \text{m-}C_7H_7NO_2 + H_3O^+ \qquad \text{Reaction } (4) \tag{2.16d}$$

where the letters o-, p- and m- stand for ortho, para and meta positions, respectively, of the nitronium ion on toluene (Mawardi, 1982). The reactions in Equations (2.16) are referred to as reactions $(1)-(4)$ hereafter. The concentration of the nitronium ion and toluene influence each of reactions $(2)-(4)$. From an engineering standpoint the heat release of reactions $(2)-(4)$ is similar, which is why the reaction enthalpies for these reactions are assumed to be equal. This simplification is not possible for the reaction kinetics: as described in Mawardi (1982) the product of such a reaction will form a molar mixture of 60% ortho-, 37% para-, and 3% meta-nitrotoluene.

Each individual reaction can be described by Arrhenius rate expressions. The reaction rates are given by the following expressions:

$$r_1 = k_{0,1} \exp\left(\frac{-E_{a,1}}{RT_R}\right) \times [HNO_3]^{n_{1,1}} \times [H_2SO_4]^{n_{2,1}} \tag{2.17a}$$

$$r_2 = k_{0,2} \exp\left(\frac{-E_{a,2}}{RT_R}\right) \times \left[NO_2^+\right]^{n_{1,2}} \times [C_7H_8]^{n_{2,2}} \tag{2.17b}$$

$$r_3 = k_{0,3} \exp\left(\frac{-E_{a,3}}{RT_R}\right) \times \left[NO_2^+\right]^{n_{1,3}} \times [C_7H_8]^{n_{2,3}} \tag{2.17c}$$

$$r_4 = k_{0,4} \exp\left(\frac{-E_{a,4}}{RT_R}\right) \times \left[NO_2^+\right]^{n_{1,4}} \times [C_7H_8]^{n_{2,4}} \tag{2.17d}$$

where $n_{1,i}$ and $n_{2,i}$ are orders of reaction with respect to each reagent for reaction i. Important to note is that each of reactions $(2)-(4)$ produces a H_3O^+ ion, which will combine with

Table 2.2 Process parameters for the nitration of toluene reaction network (Chen *et al.*, 2008; Luo and Chang, 1998; Mawardi, 1982; Sheats and Strachan, 1978).

Reaction i	$k_{0,i}$ $\left[\mathrm{m^3\,mol^{-1}\,s^{-1}}\right]$	$E_{a,i}$ $\left[\mathrm{kJ\,mol^{-1}}\right]$	$\Delta H_{r,i}$ $\left[\mathrm{kJ\,mol^{-1}}\right]$	$n_{1,i}$ $[-]$	$n_{2,i}$ $[-]$
(1)	2.00×10^3	76.5	+30.0	1.00	1.00
(2)	109	12.5	-122	2.27	0.293
(3)	67.3	12.5	-122	2.27	0.293
(4)	5.46	12.5	-122	2.27	0.293

HSO_4^- to form H_2SO_4. Hence the sulphuric acid in this reaction network acts as a catalyst. The data used for this reaction network are given in Table 2.2.

This reaction network includes both an endothermic dissociation reaction (1) and the highly exothermic electrophilic substitution reactions $(2)-(4)$. Hence, this reaction system presents a challenge in order to keep the process under control. The initial concentrations of each reagent are given by:

$$[HNO_3]_0 = 6.0\,\mathrm{kmol\,m^{-3}} \tag{2.18a}$$

$$[H_2SO_4]_0 = 1.0\,\mathrm{kmol\,m^{-3}} \tag{2.18b}$$

$$[C_7H_8]_0 = 5.5\,\mathrm{kmol\,m^{-3}} \tag{2.18c}$$

These initial concentrations are used throughout all case studies for the nitration of toluene. The reactor dimensions for this system are given in Table 2.1.

2.3 Mass and energy balances for example models

The reaction schemes analysed in this work constitute both single reactions and multiple reaction networks. Hence, general equations for the mass and energy balances are derived in this section. The reaction network considered for the general mass and energy balances is

given by the following expressions:

$$\nu_{\mathrm{A},1}\mathrm{A} + \nu_{\mathrm{B},1}\mathrm{B} \rightarrow \mathrm{C} \tag{2.19a}$$

$$\vdots$$

$$\nu_{\mathrm{A},i}\mathrm{A} + \nu_{\mathrm{D},i}\mathrm{D} \rightarrow \mathrm{E} \tag{2.19b}$$

$$\vdots$$

$$\nu_{\mathrm{A},M}\mathrm{A} + \nu_{\mathrm{G},M}\mathrm{G} \rightarrow \mathrm{H} \tag{2.19c}$$

$$i = 1, 2, ..., M \tag{2.19d}$$

where the reactions follow an Arrhenius expression according to Equation (1.8). The reaction rates are given by:

$$r_1 = k_{0,1} \exp\left(\frac{-E_{a,1}}{R T_{\mathrm{R}}}\right) [\mathrm{A}]^{n_{\mathrm{A},1}} [\mathrm{B}]^{n_{\mathrm{B},1}} \tag{2.20a}$$

$$\vdots$$

$$r_i = k_{0,i} \exp\left(\frac{-E_{a,i}}{R T_{\mathrm{R}}}\right) [\mathrm{A}]^{n_{\mathrm{A},i}} [\mathrm{D}]^{n_{\mathrm{D},i}} \tag{2.20b}$$

$$\vdots$$

$$r_M = k_{0,M} \exp\left(\frac{-E_{a,M}}{R T_{\mathrm{R}}}\right) [\mathrm{A}]^{n_{\mathrm{A},M}} [\mathrm{G}]^{n_{\mathrm{G},M}} \tag{2.20c}$$

$$i = 1, 2, ..., M \tag{2.20d}$$

where as for Equation (2.19) index i represents the i^{th} reaction within the M reactions present.

To examine if the stirrer energy input is significant for the processes in this work, the heat initially generated by process P_1^1 is considered. According to the data given in Table A.1, the heat generated initially at a temperature of 300 K, which is very low, is given by:

$$Q_{\mathrm{gen}} = 2.76 \times 10^6 \times \exp\left(-\frac{9525}{300}\right) \left(13.0 \times 10^3\right)^{1.0} \times 75.0 \times 10^3 \tag{2.21a}$$

$$Q_{\mathrm{gen}} = 43.8\,\mathrm{W} \tag{2.21b}$$

For an extremely low temperature of 300 K the heat generated by the reaction is 10 times larger than that put in by the stirrer, as shown in Equation (2.6b). The heat input by the

stirrer is assumed to be approximately constant for all remaining reaction processes. The heat generation due to exothermic reactions, on the other hand, is expeted to vary significantly with each reaction process and with temperature. The analysis on thermal instability therefore needs to consider how the rate of heat generation changes during each reaction. The constant heat input by the stirrer is therefore neglected in the following analyses. Hence, the stirrer heat input is neglected in the energy balance derivation.

The energy balance of the reactor contents, given the M simultaneous reactions, is hence evaluated by the following:

$$\frac{\mathrm{d}}{\mathrm{d}t}\left(\rho_{\mathrm{R}} C_{p,\mathrm{R}} T_{\mathrm{R}} V_{\mathrm{R}}\right) = \sum_{i=1}^{M}\left[r_i\left(\Delta H_{r,i}\right) V_{\mathrm{R}}\right] - UA\left(T_{\mathrm{R}} - T_{\mathrm{C}}\right) \tag{2.22}$$

The energy balance for the cooling jacket does not change due to several chemical reactions occurring. Therefore this energy balance is still given by Equation (1.12).

2.4 Thermal instability of batch process examples

The verification of the different stability criteria considered requires a method for examining the reliability of each. For the reaction schemes presented in the previous section the following simulations are performed for each respective process: an initially stable process is kept at constant temperature with a PI controller. Increases in the set-point temperature bring each process closer to the boundary of instability until thermal runaway behaviour occurs.

The times at which thermal runaway starts are identified in the following manner: for each process shown in the following sections the same simulation is carried out with a smaller second increase in set-point temperature. The maximum second increase in set-point temperature still resulting in a stable process is found. Up until the times indicated by vertical dash-dotted lines the two simulations are identical. The times indicated are hence the first points in time at which thermal runaway behaviour is unavoidable. The timing and quantity of each temperature set-point increase in the following section is determined manually for each process to obtain the above behaviour.

From the temperature plots the points in time where thermal instability occurs are identified. Finally, the predictions of each thermal stability criterion are compared to the actual loss of stability. This procedure sets the basis for analysing the reliability of each stability criterion. If a criterion results in unreliable thermal stability predictions, this criterion is not considered

further. The temperature profiles shown below are used throughout this thesis to verify which stability criteria work for batch processes and which do not.

2.4.1 Batch processes with reaction scheme 1

Reaction scheme 1 consists of a single reaction, the rate of which depends on a single reagent as outlined in the previous section.

The temperature profiles for processes $P_1^1 - P_5^1$ are shown in Figure 2.2. After some time the first increase in set-point temperature occurs. This increase in temperature is caused by a reduction of cooling water controlled by a PI controller. After this increase in intensification of the reaction, more coolant is required by the PI controller to keep the reaction temperature constant. At this point processes $P_1^1 - P_5^1$ are still stable. A further increase in set-point temperature leads to an uncontrollable increase in reactor temperature. The cooling capacity is not enough to remove the heat generated by each reaction. Therefore processes $P_1^1 - P_5^1$ are now unstable.

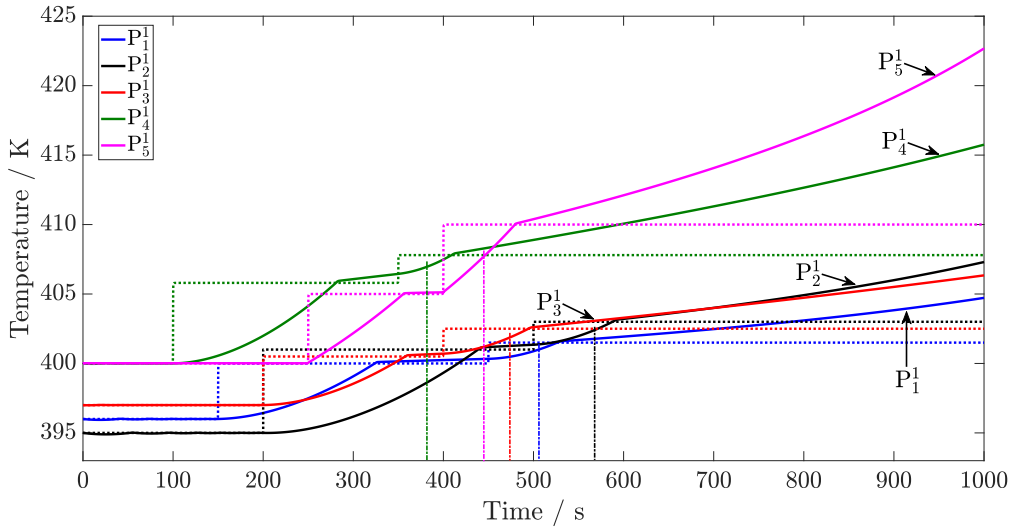

Fig. 2.2 Temperature profiles of processes $P_1^1 - P_5^1$. The dotted lines indicate the set-point temperatures. The dash-dotted lines parallel to the y-axis indicate the time where each process becomes unstable.

Similar results are obtained for processes $P_6^1 - P_{10}^1$, the temperature profiles of which are shown in Figure 2.3.

In Figures 2.2 and 2.3 it can be seen that the PI controller is not able to keep each process under control after the second set-point temperature increase. This is the case because the

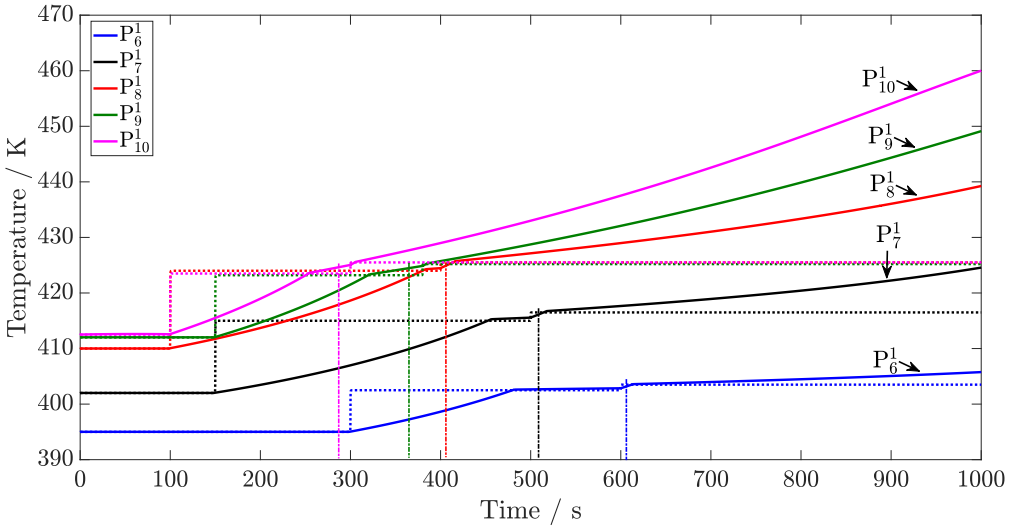

Fig. 2.3 Temperature profiles of processes $P_6^1 - P_{10}^1$. The dotted lines indicate the set-point temperatures. The dash-dotted lines parallel to the y-axis indicate the time where each process becomes unstable.

cooling capacity is not sufficient to remove the heat generated by the exothermic reaction. Before the second increase in set-point temperature these processes could still be controlled without thermal runaway behaviour occurring.

For processes $P_{11}^1 - P_{15}^1$ the same features are observed as for processes $P_1^1 - P_{10}^1$. For conciseness the temperature profiles for processes $P_{11}^1 - P_{15}^1$ are not shown.

2.4.2 Batch processes with reaction scheme 2

As described in the previous section, reaction scheme 2 consists of a single reaction, the rate of which depends on two reagents. The temperature profiles for processes $P_1^2 - P_5^2$ are shown in Figure 2.4, while the temperature profiles for processes $P_6^2 - P_{10}^2$ are shown in Figures 2.5. The temperature set point is increased in similar fashion to the PI controlled processes $P_1^1 - P_{15}^1$ in the previous section.

Processes $P_1^2 - P_{10}^2$ are made unstable with increases in the set-point temperature, hence giving a clear transition from stable to unstable operation. As was observed for reaction scheme 1, the PI controller is not capable of identifying that thermal runaway is occurring. Hence maximum cooling is applied too late, resulting in thermal runaway behaviour. It is emphasised that the PI controller used for this analysis is not required to result in good control. A clear transition from thermally stable to thermally unstable operation is necessary, such that the reliability of potential thermal stability criteria can be examined.

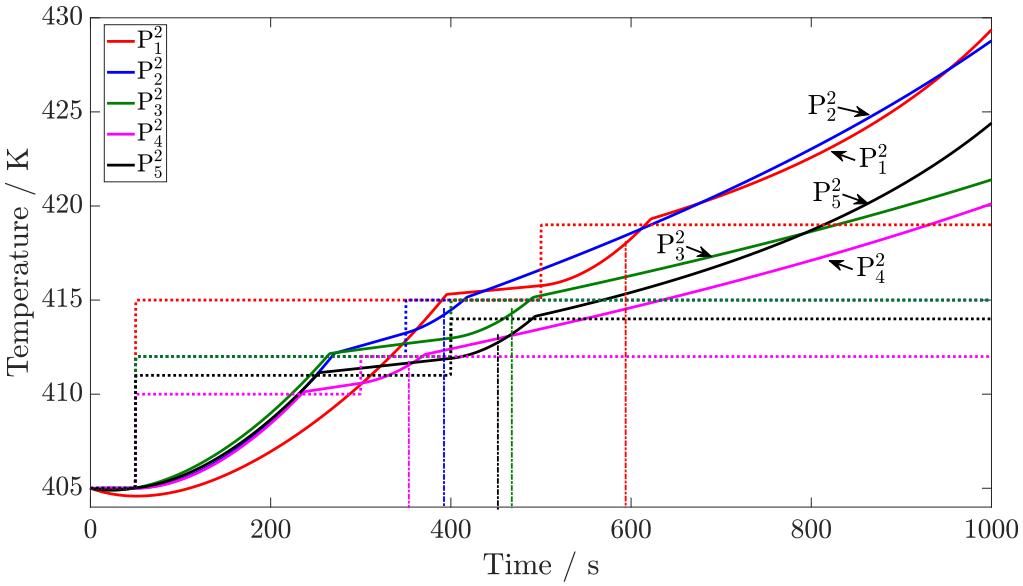

Fig. 2.4 Temperature profiles for processes $P_1^2 - P_5^2$. The dotted lines indicate the set-point temperatures. The dash-dotted lines parallel to the y-axis indicate the time where each process becomes unstable.

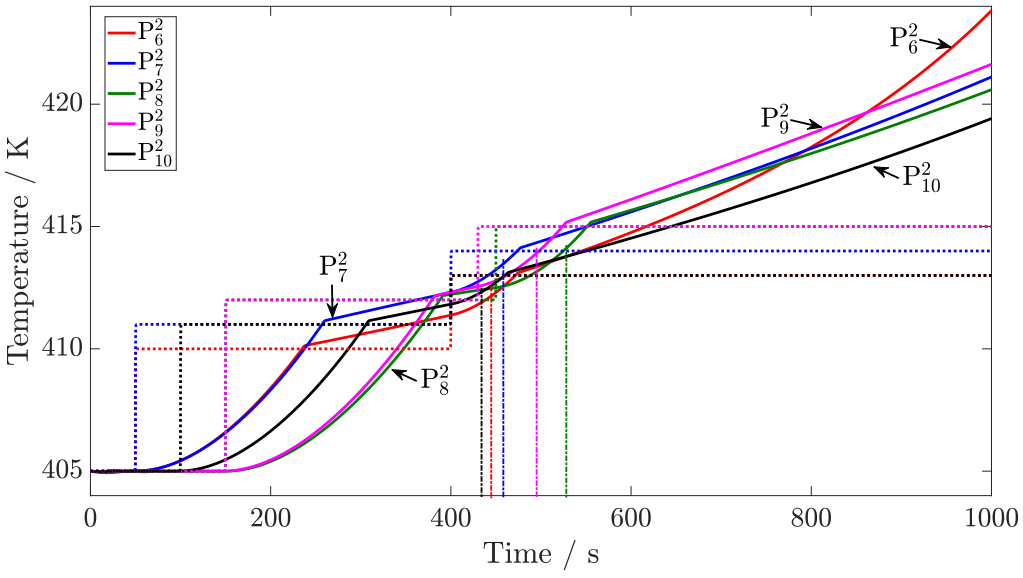

Fig. 2.5 Temperature profiles for processes $P_6^2 - P_{10}^2$. The dotted lines indicate the set-point temperatures. The dash-dotted lines parallel to the y-axis indicate the time where each process becomes unstable.

Similar temperature profiles are obtained for processes $P_{11}^2 - P_{20}^2$. Hence, for clarity, these graphs are not explicitly shown here.

2.4.3 Batch processes with reaction scheme 3

In reaction scheme 3 a total of 4 reactions are present which overall are exothermic. The resulting temperature profiles from increasing the set-point temperature of the PI controller for processes $P_1^3 - P_3^3$ are shown in Figure 2.6.

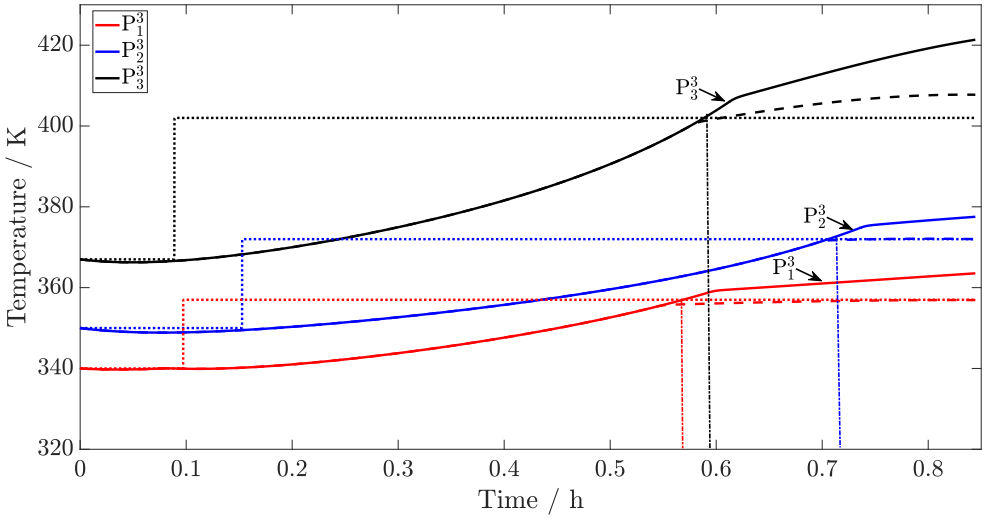

Fig. 2.6 Temperature profiles for processes $P_1^3 - P_3^3$. The dotted lines indicate the set-point temperatures for the PI controller. The dashed lines represent stable processes with lower increased set-point temperatures. The dash-dotted lines parallel to the y-axis indicate when stability is lost in the system.

In Figure 2.6 two simulations per process are shown. The solid lines indicate the simulations where each process becomes unstable after the increase in set-point temperature. As can be seen, the temperature continues to increase after reaching the dotted set-point temperature line, ultimately resulting in a thermal runaway. This is the case because the maximum coolant flow rate the PI controller can use is not enough to cool the system sufficiently.

The dashed lines represent the same processes, with a marginally lower set-point increase in the temperature. As can be seen, the dashed lines do not continue to increase, because the respective processes can be controlled by the PI controller. Up to the point where the dashed line becomes visible, both simulations follow the same trajectory. With these two simulations it can be identified when the system stability is actually lost. The loss of stability must occur

between the point in time where each dashed line becomes visible and where the solid line reaches the set-point temperature. The point of loss of stability for processes $P_1^3 - P_3^3$ are indicated by dash-dotted lines parallel to the y-axis in Figure 2.6. For processes P_1^3, P_2^3, and P_3^3 the loss of stability occurs at a time of 0.57 h, 0.71 h and 0.60 h respectively.

The same analysis as for processes $P_1^3 - P_3^3$ is carried out for processes $P_4^3 - P_6^3$, the temperature profiles of which are shown in Figure 2.7.

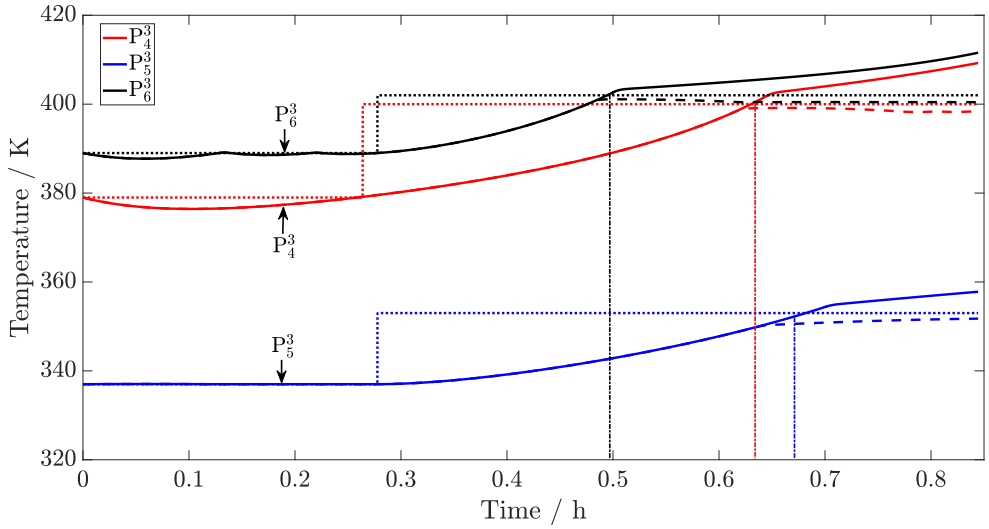

Fig. 2.7 Temperature profiles for processes $P_4^3 - P_6^3$. The dotted lines indicate the set-point temperatures for the PI controller. The dashed lines represent stable processes with lower increased set-point temperatures. The dash-dotted lines parallel to the y-axis indicate when stability is lost in the system.

As was observed for processes $P_1^3 - P_3^3$, the temperature profiles for processes P_4^3, P_5^3, and P_6^3 are initially controllable at a temperature of 337 K, 379 K and 389 K, respectively. Each process becomes unstable once the new set-point temperature, given by the dotted lines, is reached. This is the case as each temperature profile, given by the solid lines, increases at an accelerated rate after the new set-point temperature is reached. The PI controller is not able to keep the system under control, because the cooling capacity at this point is not large enough to deal with the heat generated by the exothermic reactions.

The dashed lines in Figure 2.7 again represent the same process with a lower set-point temperature. It can be seen that the profiles given by the dashed lines do not increase after the set-point temperature is reached. Therefore the point at which the stability of the system is lost can be identified between the stable profiles, given as dashed lines, and the unstable

profiles, given by the solid lines. The times when each system becomes unstable are given by 0.63 h, 0.68 h, and 0.50 h for processes P_4^3, P_5^3 and P_6^3, respectively.

2.4.4 Batch processes with reaction scheme 4

The analysis for reaction scheme 4 is similar to that carried out for reaction scheme 3: two simulations are carried out per process, one showing an initially stable system becoming unstable after an increase in set-point temperature. The second simulation of the same process involves a smaller increase in set-point temperature, resulting in a stable system after this set-point increase. The temperature profiles for processes $P_1^4 - P_3^4$ are shown in Figure 2.8.

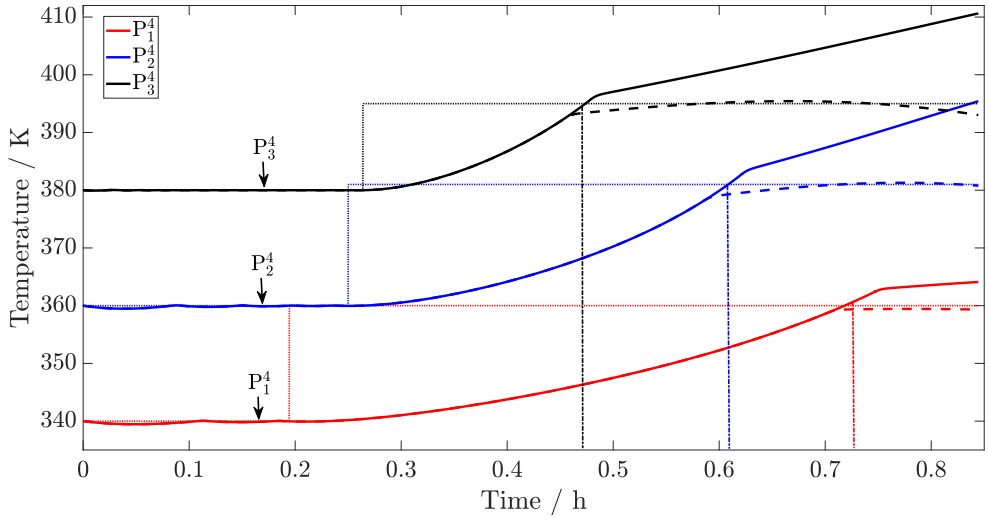

Fig. 2.8 Temperature profiles for processes $P_1^4 - P_3^4$. The dashed lines indicate the set-point temperatures for the PI controller. The dash-dotted lines parallel to the y-axis indicate when stability is lost in the system.

In Figure 2.8 it can be seen that the solid lines representing temperatures increase further than the set-point temperatures. This is the case because thermally unstable systems are obtained for the set-point temperature given by the dotted lines. The PI controller cannot cool the systems enough to avoid thermal runaway behaviour, even when opening the cooling valve completely. The dashed lines representing the temperature profiles of the system with a smaller increase in set-point temperature show that stable systems can be achieved. Initially stable processes are present. As was done for the processes in reaction scheme 3, the point at which thermal stability is lost can be identified by comparing the stable and unstable systems, between which stability is lost. The point at which stability is lost is indicated by vertical

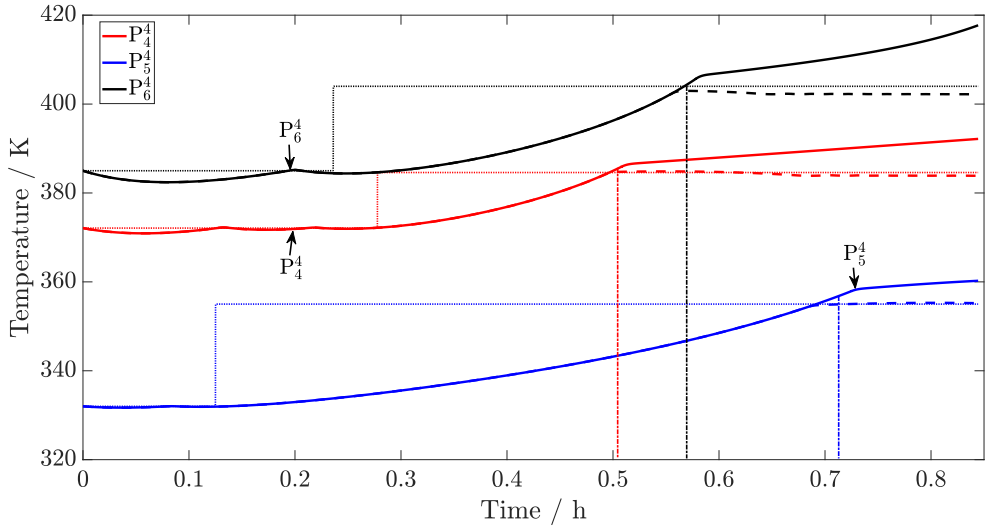

Fig. 2.9 Temperature profiles for processes $P_4^4 - P_6^4$. The dashed lines indicate the set-point temperatures for the PI controller. The dash-dotted lines parallel to the y-axis indicate when stability is lost in the system.

dash-dotted lines given in Figure 2.8. Similar temperature profiles are obtained for processes $P_4^4 - P_6^4$, which are shown in Figure 2.9.

The temperature profiles in Figure 2.9 show how the initially stable processes become unstable as the set-point temperature is increased. Initially the temperature set-points are at 332 K, 374 K and 385 K for processes P_4^4, P_5^4, and P_6^4, respectively. After each respective set-point temperature is reached, the solid lines increase further leading to a thermal runaway. The dashed lines show the same process with a lower temperature set-point, hence only becoming visible once this stable set-point is reached. As was done for processes $P_1^4 - P_3^4$, the time where stability is lost is given between the points in time where stability can still be achieved and where thermal stability is lost. The dash-dotted lines show at which times this loss of system stability occurs.

2.5 MPC framework with embedded stability analysis

The intensification of batch processes requires the full nonlinear model as there is no steady-state operating point. This condition presents issues with respect to defining stable operating points, which is why a different approach is required. For this reason a modified MPC framework is employed: the analysis of stability of batch processes is incorporated into the classical MPC flow sheet, which is shown in Figure 2.10.

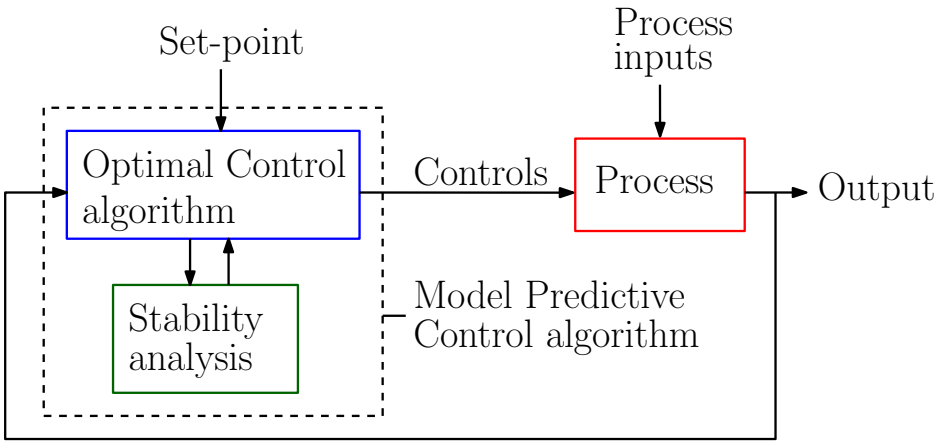

Fig. 2.10 Model Predictive Control scheme with integrated stability analysis.

Stability criteria based on Lyapunov functions were implemented in systems operating at steady state before, for which a good review is given by Albalawi *et al.* (2018). For continuous systems in industry good results were obtained with such an approach (Albalawi *et al.*, 2016, 2017; Zhang *et al.*, 2018). This work cannot be easily transferred to batch reactors, which is why further investigation is required.

The structure of embedding stability criteria as additional system constraints within an MPC framework is present in literature (Zhang *et al.*, 2018). This method found in literature is limited to systems where steady-state operating points exist, because for such systems a single linearisation describes the system dynamics reasonably well. This thesis tackles the same issue but for batch processes, which are inherently non-steady state.

To intensify batch processes, the set-point temperature can be set to the maximum allowable temperature of the system, as the stability constraint will restrict the system to increase in temperature too fast and enter an unstable regime. Furthermore there is the option to maximise yield of a certain chemical, which lets the control system decide on its own by how much the temperature can be increased. For certain reactions, the highest possible reaction temperature, without causing thermal runaways, is the target (Rupp *et al.*, 2013).

The optimisation problem solved at every MPC step for tracking a certain set-point temperature is hence given by:

$$\min_{u} \Phi = \int_{t_0}^{t_0+t_p} \left(T_\mathrm{R} - T_\mathrm{sp}\right)^2 \mathrm{d}t \tag{2.23a}$$

subject to:

$$f(x,y,u,t) = \dot{x} \tag{2.23b}$$
$$h(x,y,u,t) = 0 \tag{2.23c}$$
$$g(x,y,u,t) \leq 0 \tag{2.23d}$$
$$t_0 \leq t^{(s)} \leq t_0 + t_p \tag{2.23e}$$

where Φ is the objective function of the MPC algorithm, $g(x,y,u,t)$ incorporates the stability criterion and maximum temperature limit, t_0 and $t_0 + t_p$ are the initial and final times of the current MPC step, respectively.

The formulation in Equation (2.23) is used for each stability criterion considered in this work. In the case of standard MPC formulations no stability criterion is used within $g(x,y,u,t)$.

2.5.1 MPC frameworks

In this work three different MPC frameworks are used. Each is applied to every batch process introduced in Section 2.2. The control horizon t_c and prediction horizon t_p, introduced in Section 2.10 are defined as given in Figure 1.7. The maximum allowable temperature T_{chem} must not be exceeded during each process due to material property specifications and potential by-product formation. The target conversions and concentrations are given in the sections for the intensification of batch processes for each specific reaction scheme.

The length and number of control steps implemented for MPC algorithms are tuning parameters dependent on each process. A clear trade-off can be observed: the more control steps are used, the higher the computational time to find the optimal values. The longer the control steps, the longer the time during which no change in control occurs which can potentially lead to oscillations or unstable control. The shorter the control step length, the more frequent the evaluation of control inputs and hence the faster the optimisation has to be carried out.

MPC framework 1

MPC framework 1 uses a suitable stability criterion as an additional constraint in the MPC optimisation formulation. This MPC framework is the newly developed control scheme for batch processes which has to be compared to currently available control schemes in the literature, as well as industry.

The control horizon is set to $t_c = 60$ s, with 6 control steps of 10 s, while the prediction horizon is set to $t_p = 100$ s, according to Figure 1.7. How well this control framework can intensify batch processes safely is examined in the next chapter.

MPC framework 2

MPC framework 2 uses a constant temperature set-point for which the processes are thermally stable. This control scheme serves as the baseline to compare the batch duration and computational times of the other MPC frameworks. A constant set-point temperature close to the boundary of instability is used, as is commonly done in industry for batch processes. No information about system stability is included, because the process is initially stable and no further increases in set-point temperature are carried out.

The control horizon is set to 30 s, with 3 control steps of 10 s, and a prediction horizon of 40 s. The prediction horizon is shorter than for the other MPC frameworks, since no change in set-point temperature is applied. This also means that an overall longer reaction time is expected in order to reach the target conversion for the reaction.

MPC framework 3

MPC framework 3 consists of a standard nonlinear MPC, as is commonly found in the literature. This MPC framework is used throughout the thesis to show if the omission of stability information can still result in stable process control. Furthermore, the computational time requried per MPC step is of importance when compared to MPC framework 1. Therefore, it is verified if MPC framework 1 results in improved process control at lower computational cost compared to MPC frameworks in the current literature, given by MPC framework 3.

An extended control horizon of 100 s, with 10 control steps of 10 s, and a prediction horizon of 300 s. This is to ensure that stable control is obtained as the set-point temperature is increased. No additional information about the system stability is present in this MPC framework. Hence, the extended horizon is required to capture the potentially unstable system behaviour.

2.6 Chapter summary

In this chapter the batch reactor model used for all simulations is introduced including:

- the batch reactor flow sheet with all important components
- reactor parameters
- concept of MPC with stability criteria
- MPC frameworks
- reaction kinetics
- mass and energy balances

All parameters and control frameworks introduced in this chapter are used throughout this work. 4 different reaction schemes are used in order of increasing complexity, such that the stability criteria in the next section can be examined for the simple reaction schemes first. As a narrower selection of thermal stability criteria is found, the performance and reliability for more complex reaction schemes is investigated. If reliable thermal stability prediction for all reaction schemes in this thesis is achieved, these criteria will likely work for any exothermic reaction within batch reactors. This would allow the important extension to industrial systems.

Temperature profiles of example thermal runaway reactions for each reaction scheme are presented in this chapter. Each process is subject to two increases in set-point temperature. The second increase in set-point temperature results in thermal runaway behaviour, allowing to identify the time at which each process becomes unstable. This sets the basis for examining the validity of each stability criterion considered in the next chapter.

Chapter 3

Analysis of thermal stability criteria for non steady-state reactors

In this chapter common stability criteria for CSTRs, specifically the Semënov and Routh-Hurwitz criteria, and for batch processes, namely Lyapunov exponents and the divergence criterion, are examined in terms of their:

1. reliability of predicting thermal runaway behaviour
2. applicability for batch process intensification

The temperature profiles of example thermal runaway reactions, shown in Section 2.4, are used to determine the reliability of each stability criterion.

The applicability of stability criteria for process intensification is examined by embedding each stability criterion within an MPC framework, as discussed in Section 2.5. If stable operation is obtained, the times to reach the target conversion, and the computational times for each MPC step are the key values for this comparison.

3.1 Verification of Semënov and Routh-Hurwitz criteria

In this section common stability criteria for CSTRs, namely the Semënov and the Routh-Hurwitz criterion, are applied to batch processes. Batch processes from reaction scheme 1 are used to examine how reliable the prediction of thermal instability is for these criteria.

3.1.1 Semënov criterion for reaction scheme 1

The reliability of the Semënov criterion is tested by considering processes $P_1^1 - P_4^1$, for which the temperature profiles are shown in Figure 2.2. The dash-dotted lines in Figure 2.2 indicate at which points in time each process becomes unstable. Ideally, at these times the Semënov criterion, as described in Section 1.2.1, becomes greater than one.

As can be seen in Figure 2.2 the temperature profiles initially follow the set-point temperatures. As the set-point temperature increases, each process becomes unstable, resulting in a thermal runaway. In order to see how well the Semënov criterion describes this transition from stable to unstable operation, the corresponding profiles of the ratio Q_{gen}/Q_{rem} are plotted in Figure 3.1.

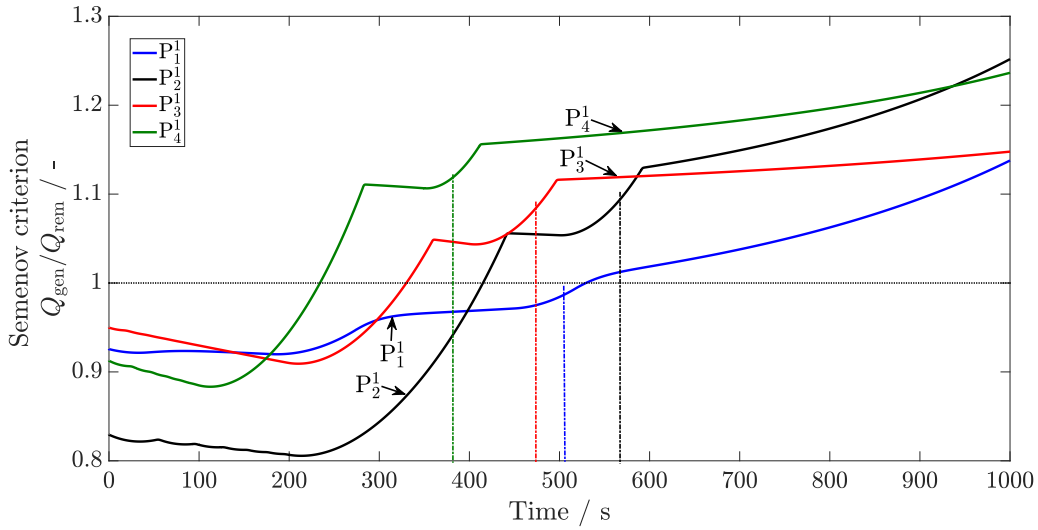

Fig. 3.1 Ratio of heat generation to heat removal, Q_{gen}/Q_{rem}, for processes $P_1^1 - P_4^1$. The temperature profiles for these processes are shown in Figure 2.2. The dash-dotted lines parallel to the y-axis indicate when each of processes $P_1^1 - P_4^1$ becomes unstable.

As can be seen in Figure 3.1, the criterion $Q_{gen}/Q_{rem} \leq 1$ does not give very good predictions of system stability for batch processes. The value of Q_{gen}/Q_{rem} is greater than one after the first increase in set-point temperature. At this point each process is still stable, whilst the Semënov criterion indicates an unstable process. This is a wrong prediction of thermal stability for batch processes, therefore this criterion is not used further. For process P_1^1 a different behaviour is observed. The first Semënov criterion indicates stable operation up to 550 s, even when thermal runaway behaviour starts before. Hence, unreliable prediction of thermal stability according to the first Semënov criterion is obtained.

The second condition of the Semënov criterion in Equation (1.14) with respect to heat generation and removal rates, $\frac{\mathrm{d}Q_{\mathrm{gen}}}{\mathrm{d}t} / \frac{\mathrm{d}Q_{\mathrm{rem}}}{\mathrm{d}t}$, is shown for processes $\mathrm{P}_1^1 - \mathrm{P}_4^1$ in Figure 3.2.

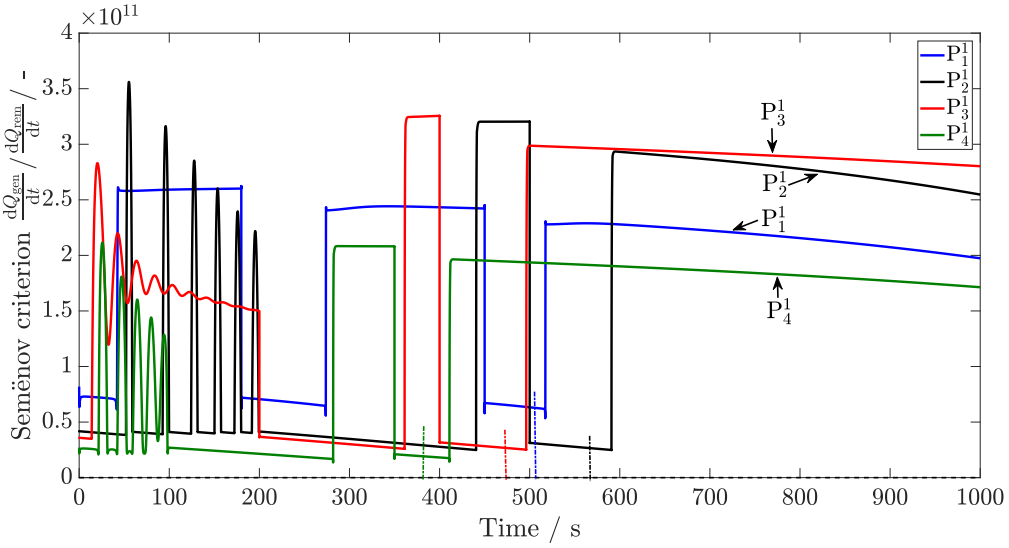

Fig. 3.2 Ratio of heat generation to heat removal rate, $\frac{\mathrm{d}Q_{\mathrm{gen}}}{\mathrm{d}t} / \frac{\mathrm{d}Q_{\mathrm{rem}}}{\mathrm{d}t}$, for processes $\mathrm{P}_1^1 - \mathrm{P}_4^1$. The vertical dash-dotted lines indicate the points in time when each respective process becomes unstable. The horizontal dashed line, very close to zero, indicates where the second Semënov criterion equals 1.

According to Equation (1.14) an unstable system is present once the system reaches $\frac{Q_{\mathrm{gen}}}{Q_{\mathrm{rem,max}}} > 1$ and/or $\frac{\mathrm{d}Q_{\mathrm{gen}}}{\mathrm{d}t} / \frac{\mathrm{d}Q_{\mathrm{rem}}}{\mathrm{d}t} > 1$. This means that as long as $\frac{Q_{\mathrm{gen}}}{Q_{\mathrm{rem,max}}} \leq 1$ and $\frac{\mathrm{d}Q_{\mathrm{gen}}}{\mathrm{d}t} / \frac{\mathrm{d}Q_{\mathrm{rem}}}{\mathrm{d}t} \leq 1$ a stable system is present.

The second condition of the Semënov criterion $\frac{\mathrm{d}Q_{\mathrm{gen}}}{\mathrm{d}t} / \frac{\mathrm{d}Q_{\mathrm{rem}}}{\mathrm{d}t}$ for processes $\mathrm{P}_1^1 - \mathrm{P}_4^1$, given in Figure 3.2, is always larger than 1 hence predicting unstable operation throughout. Clearly, the profiles for the second Semënov criterion given in Figure 3.2 do not give a reliable prediction of thermal stability according to Equation (1.14b).

The Semënov criterion was formulated for steady state processes. Since batch processes are inherently non-steady, this criterion does not work well for such processes.

3.1.2 Routh-Hurwitz criterion for reaction scheme 1

As was done for the Semënov criterion, the Routh-Hurwitz criterion is applied to processes $\mathrm{P}_1^1 - \mathrm{P}_4^1$ the temperature profiles of which are shown in Figure 2.2.

The system simulated contains 19 variables. The Routh-Hurwitz criterion requires the real parts of all eigenvalues of the Jacobian to be negative for the system to be stable, as discussed in Section 1.2.1. Therefore it is of interest if any real part of all eigenvalues is positive, as shown in Equation 1.19. If the maximum value is below zero, a stable system is indicated. The transition from stable to unstable operation has to be identified with this criterion to make it useful for batch processes.

To visualise the criterion on a single figure, the maximum real part of all eigenvalues of the Jacobian matrix is plotted for processes $P_1^1 - P_4^1$ in Figure 3.3.

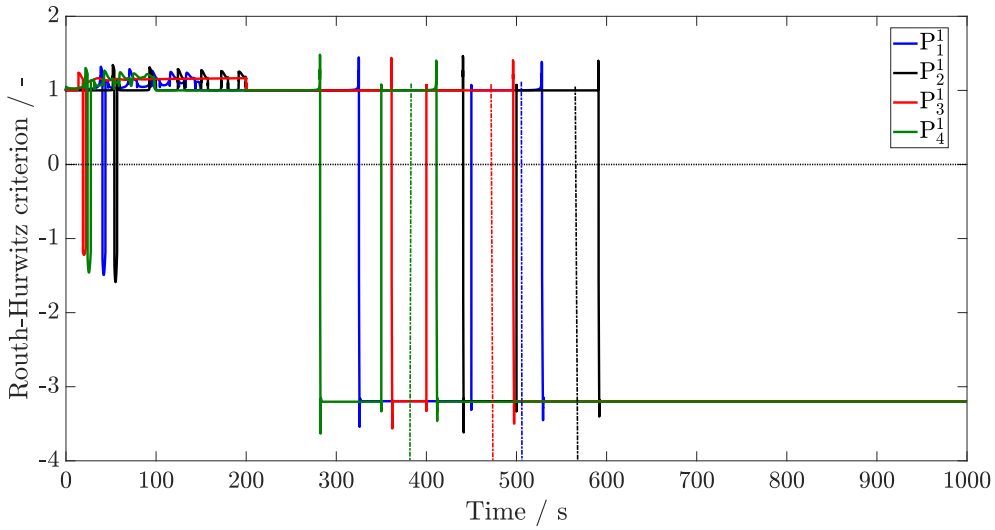

Fig. 3.3 Routh-Hurwitz criterion for processes $P_1^1 - P_4^1$. The temperature profiles for these processes are shown in Figure 2.2. The horizontal dotted line indicates where the Routh-Hurwitz criterion equals zero. The dash-dotted lines parallel to the y-axis indicate when each of processes $P_1^1 - P_4^1$ becomes unstable.

As can be seen in Figure 3.3 the Routh-Hurwitz criterion predicts unstable behaviour from the beginning of the process. The large fluctuations occur due to the fact that the maximum real eigenvalue out of 19 eigenvalues from the Jacobian is plotted. For each of the processes $P_1^1 - P_4^1$ a maximum eigenvalue of approximately one is present for most of the process. Interestingly, after thermal runaway starts, the maximum eigenvalues becomes negative. As was the case for the Semënov criterion, the Routh-Hurwitz criterion does not seem to work reliably for batch processes, which are inherently non-steady state. Therefore a different stability criterion is required for this purpose.

3.2 Optimisation and verification of Lyapunov exponent method

The variables contributing towards thermal runaway behaviour are those that influence the heat generation in the batch reactor. The heat generation for general batch processes is effected by the reaction rates:

$$Q_{\text{gen}} = \sum_{i=1}^{M} \left[r_i \left(\Delta H_{r,i} \right) V_{\text{R}} \right] \tag{3.1}$$

The reaction rates in this work follow Arrhenius type behaviour (Davis and Davis, 2003). Hence, the concentrations of the reagents and the reactor temperature influence the heat generation. Therefore, the Lyapunov exponents for only these variables are evaluated in order to quantify the thermal stability of batch processes. Variables that have no influence on the heat generation are thus neglected.

For reaction scheme 2, shown in Section 2.2, the variables of interest are [A], [B], and T_R. Hence, the local Lyapunov exponents at time t for each variable are evaluated with the following expressions:

$$\Lambda_{\text{l},1}\left([\text{A}]_0, t \right) = \frac{1}{t_{\text{Lyap}}} \ln \left(\left| \frac{[\text{A}]\left(t + t_{\text{Lyap}}, [\text{A}]_0 \right) - [\text{A}]\left(t + t_{\text{Lyap}}, [\text{A}]_0 + \delta x_0 \right)}{\delta x_0} \right| \right) \tag{3.2}$$

$$\Lambda_{\text{l},2}\left([\text{B}]_0, t \right) = \frac{1}{t_{\text{Lyap}}} \ln \left(\left| \frac{[\text{B}]\left(t + t_{\text{Lyap}}, [\text{B}]_0 \right) - [\text{B}]\left(t + t_{\text{Lyap}}, [\text{B}]_0 + \delta x_0 \right)}{\delta x_0} \right| \right) \tag{3.3}$$

$$\Lambda_{\text{l},3}\left(T_{\text{R},0}, t \right) = \frac{1}{t_{\text{Lyap}}} \ln \left(\left| \frac{T_{\text{R}}\left(t + t_{\text{Lyap}}, T_{\text{R},0} \right) - T_{\text{R}}\left(t + t_{\text{Lyap}}, T_{\text{R},0} + \delta x_0 \right)}{\delta x_0} \right| \right) \tag{3.4}$$

where $\Lambda_{\text{l},1}$, $\Lambda_{\text{l},2}$, and $\Lambda_{\text{l},3}$ are the local Lyapunov exponents for concentrations of reagents A and B, and the reactor temperature, respectively. All other variables are defined as outlined in Section 1.2.2.

The evaluation of the Lyapunov exponents requires a particular value of the control variable. In this work it is assumed that the cooling valve is opened 95% in order to evaluate the Lyapunov exponents.

As mentioned in Section 1.2.2, to apply Lyapunov exponents as a measure of thermal stability, detailed sensitivity analyses on choosing values for the initial perturbation, δx_0 and the Lyapunov time frame, t_{Lyap}, are carried out.

3.2.1 Sensitivity analysis for initial perturbation δx_0

To show the effect of δx_0 on the results obtained for the Lyapunov exponents, a sensitivity analysis on δx_0 is carried out. For values of $\delta x_0 = 10^0, 10^{-1}, 10^{-2}, 10^{-3}, 10^{-4}$ the Lyapunov exponent profiles are evaluated for process P_5^2 as a sample. The units of the deviations are equal to those of each individual state variable, which in this case are $\mathrm{kmol\,m^{-3}}$ for concentration and K for temperature. Similar results are obtained for all remaining processes within reaction scheme 2. The temperature profile for this process is shown in Figure 2.4. The absolute errors, denoted by ε_Λ, for each Lyapunov exponent with respect to the values obtained when setting $\delta x_0 = 10^{-5}$ and $t_{\mathrm{Lyap}} = 5000$ s as a reference are computed and shown in Figures 3.4−3.6. The equation for the error ε_Λ is given by:

$$\varepsilon_\Lambda = \left|\Lambda\left(x, t_{\mathrm{Lyap}}, \delta x_0\right) - \Lambda\left(x, t_{\mathrm{Lyap}}, \delta x_{0,\mathrm{ref}}\right)\right| \tag{3.5}$$

where $\Lambda\left(x, t_{\mathrm{Lyap}}, \delta x_0\right)$ is the Lyapunov exponent evaluated with the initial perturbation to be tested, and $\Lambda\left(x, t_{\mathrm{Lyap}}, \delta x_{0,\mathrm{ref}}\right)$ is the Lyapunov exponent evaluated using the reference value for the initial perturbation. The reference value $t_{\mathrm{Lyap}} = 5000$ s is chosen, since this is the value of the Lyapunov time frame found in the following section. The initial perturbation $\delta x_0 = 10^{-5}$ is used for the reference, because this is the smallest value of δx_0 not suffering from excessive numerical inaccuracies.

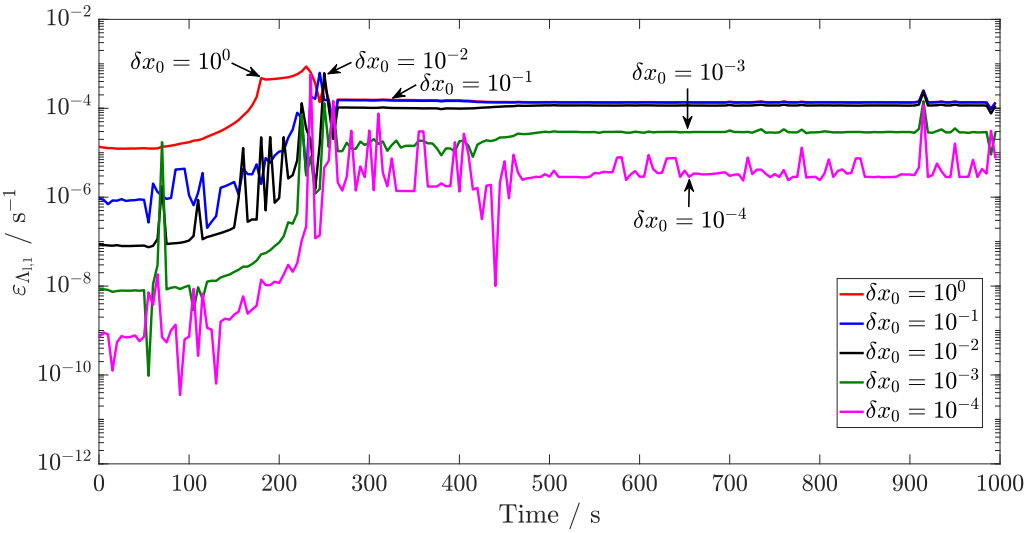

Fig. 3.4 Errors ε obtained for the Lyapunov exponents with respect to state variable [A], $\Lambda_{\mathrm{l},1}$, with changes in the initial perturbation δx_0 for process P_5^2.

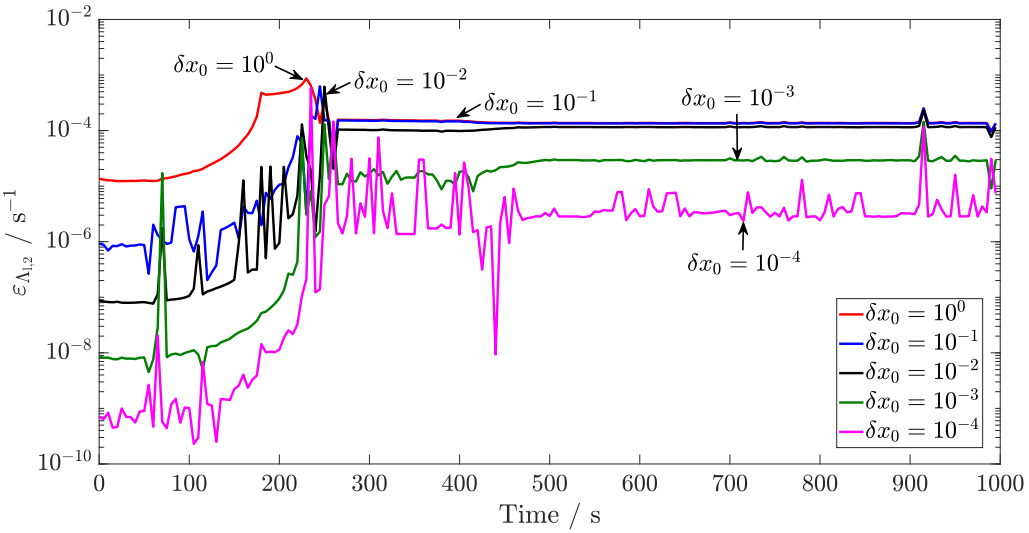

Fig. 3.5 Errors ε obtained for the Lyapunov exponents with respect to state variable [B], $\Lambda_{1,2}$, with changes in the initial perturbation δx_0 for process P_5^2.

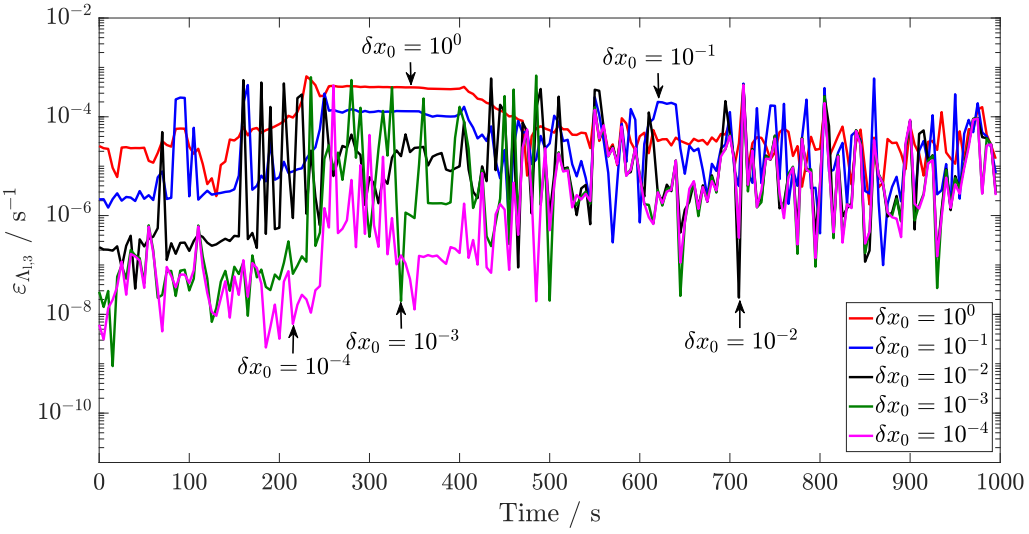

Fig. 3.6 Errors ε obtained for the Lyapunov exponents with respect to state variable T_R, $\Lambda_{1,3}$, with changes in the initial perturbation δx_0 for process P_5^2.

The errors obtained for the Lyapunov exponents when using various initial perturbations are similar, and have a maximum value of 10^{-3}. This is a relatively large error, but the relative size compared to the magnitude of the Lyapunov exponents is of greater importance. For the first and second Lyapunov exponents, $\Lambda_{l,1}$ and $\Lambda_{l,2}$, similar profiles are obtained. This is the case because these two Lyapunov exponents correspond to the concentrations of reactants A and B, respectively. Both reagents have a first order of reaction, the same stoichiometric coefficients and initial concentrations, hence expected to result in similar Lyapunov exponent profiles. The parameters for process P_5^2 can be seen in Table A.2 in the Appendix.

The Lyapunov exponent corresponding to reactor temperature, $\Lambda_{l,3}$, is shown in Figure 3.6. The maximum error for the Lyapunov exponent $\Lambda_{l,3}$ is obtained for the largest value of the initial perturbation δx_0, but never exceeding 10^{-3}.

The smaller the initial perturbation, the more prone the stability detection is to fluctuations in the final values obtained. By visual inspection the smallest initial perturbation δx_0 not resulting in excessive oscillations is given by $\delta x_0 = 10^{-3}$, as shown by the sensitivity analysis above.

3.2.2 Determination of reliable time horizon t_{Lyap}

As was done for δx_0 in the section above, a sensitivity analysis on t_{Lyap} is carried out. For values of $t_{\text{Lyap}} = 1000, 2500, 5000, 10^4$, and 5×10^4 s the Lyapunov exponent profiles are evaluated for process P_5^2, the temperature profile of which is shown in Figure 2.4. For clarity, only the analysis of process P_5^2 is presented here, as for all other processes similar results are obtained. The respective profiles for each Lyapunov exponent with respect to the values obtained when $\delta x_0 = 10^{-3}$ are computed and shown in Figures 3.7−3.9.

In Figures 3.7−3.9 it can be seen that different Lyapunov horizons t_{Lyap} lead to different predictions of thermal stability. Furthermore it can be seen that the most useful Lyapunov exponent relates to the temperature of the system. The Lyapunov exponent with respect to the temperature gives the best indication of system stability. The Lyapunov exponents with respect to concentrations [A] and [B] are initially negative, only becoming positive in a sharp manner after the first increase in set-point temperature at $t \approx 250$ s. Directly after the sharp increase, the values for $\Lambda_{l,1}$ become negative again, although the thermal runaway is occurring at $t \approx 450$ s. Therefore, using $\Lambda_{l,1}$ and $\Lambda_{l,2}$ as the main indicator of instability is unreliable. Nevertheless valuable information can be obtained from the Lyapunov exponents with respect to reagents A and B at the point where the system becomes unstable.

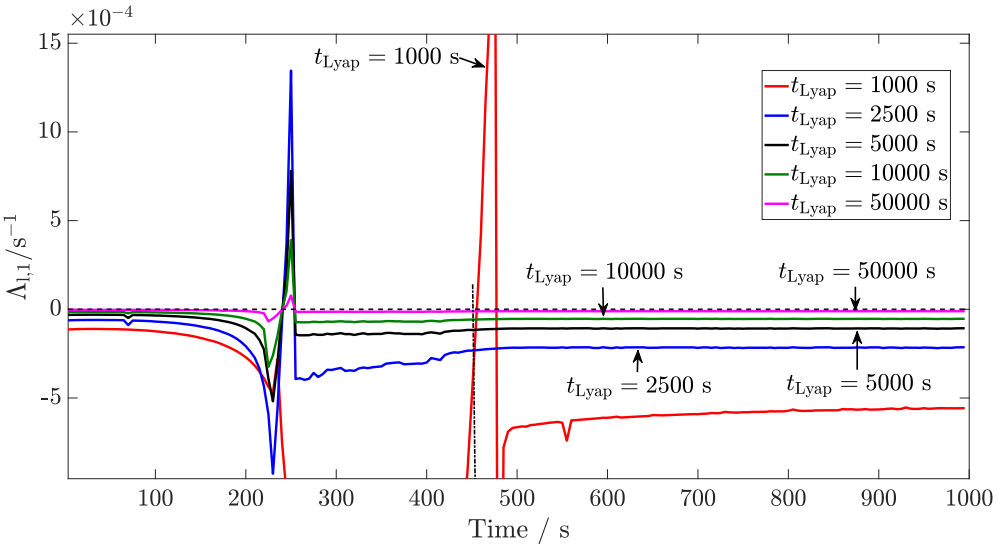

Fig. 3.7 Lyapunov exponent profiles with respect to state variable [A], $\Lambda_{1,1}$, with various settings for the Lyapunov time frame t_{Lyap} for process P_5^2. The dash-dotted line parallel to the y-axis shows the point in time where process P_5^2 becomes unstable according to Figure 2.4.

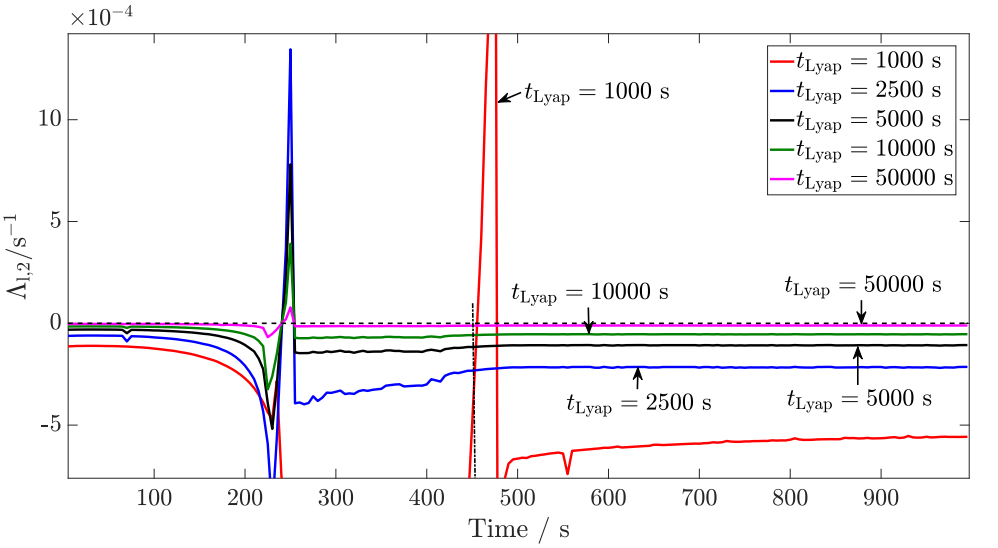

Fig. 3.8 Lyapunov exponent profiles with respect to state variable [B], $\Lambda_{1,2}$, with various settings for the Lyapunov time frame t_{Lyap} for process P_5^2. The dash-dotted line parallel to the y-axis shows the point in time where process P_5^2 becomes unstable according to Figure 2.4.

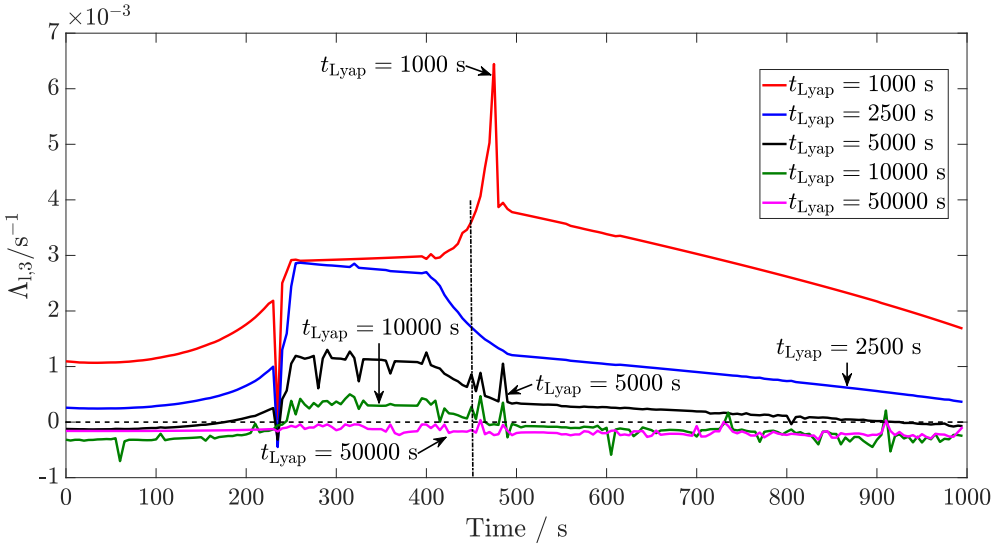

Fig. 3.9 Lyapunov exponent profiles with respect to state variable T_R, $\Lambda_{l,3}$, with various settings for the Lyapunov time frame t_{Lyap} for process P_5^2. The dash-dotted line parallel to the y-axis shows the point in time where process P_5^2 becomes unstable according to Figure 2.4.

The Lyapunov exponent with respect to the system temperature, $\Lambda_{l,3}$, gives a good estimate of the thermal stability when using a Lyapunov time frame of $t_{Lyap} = 5000\,s$. At time $t = 150\,s$ a thermal runaway is predicted. The thermal runaway for process P_5^2 occurs at time $t = 450\,s$. Hence, when using a time frame of $t_{Lyap} = 5000\,s$, the thermal runaway is predicted 5 minutes ahead of time. Using a Lyapunov time frame of $t_{Lyap} = 10^4\,s$ correctly classifies the system at $t = 450\,s$ as being unstable and predicts the thermal runaway at $t = 250\,s$. This time frame is twice the size of $t_{Lyap} = 5000\,s$ and as such will result in higher computational time. As it is required to have a stability criterion with low computational cost, the time frame of $t_{Lyap} = 5000\,s$ is chosen for further applications. The conservative nature of the stability estimate is in the best interest for control schemes, as therefore the boundary of stability is never crossed, giving stable operation.

Lyapunov exponents due to the concentrations do not give a clear indication of when the system becomes unstable. This is to be expected, since the effect of increasing the concentration of a reagent does not have one universal effect on heat generation. Examples of such cases are endothermic reactions and reactants acting as catalysts, hence not influencing the reaction kinetics. Nevertheless, for more complex systems, the effect due to concentration should not be ignored outright. Useful information could still be present within Lyapunov exponents with respect to concentrations. It is noted, however, that most important is the inclusion of the Lyapunov exponent with respect to reactor temperature to quantify thermal stability of the processes considered in this thesis.

As is seen in Figure 3.7, there is a spike in the Lyapunov exponent with respect to the concentration of A at approximately 450 s, which suggests that valuable information is still present. Therefore, for the PI control case studies following this section, only $\Lambda_{l,3}$ corresponding to the reactor temperature is plotted. In the Model Predictive Control (MPC) case studies Lyapunov exponents with respect to concentrations as well as reactor temperature are included as constraints in the MPC frameworks.

3.2.3 Compatibility of Lyapunov exponents: reaction schemes 1 and 2

The parameters defining the local Lyapunov exponents, δx_0 and t_{Lyap}, are now applied to several processes. This analysis is carried out to test the reliability of the stability prediction with Lyapunov exponents for batch processes.

First, processes $P_1^1 - P_5^1$ are tested, the temperature profiles of which are shown in Figure 2.2. In reaction scheme 1 only a single reaction is present with product C. As discussed in the section above, only the local Lyapunov exponent with respect to reactor temperature is shown. This is done because the profiles of $\Lambda_{l,3}$ indicate most clearly if thermal runaway behaviour is predicted. The profiles for $\Lambda_{l,3}$ for processes $P_1^1 - P_5^1$ are shown in Figure 3.10.

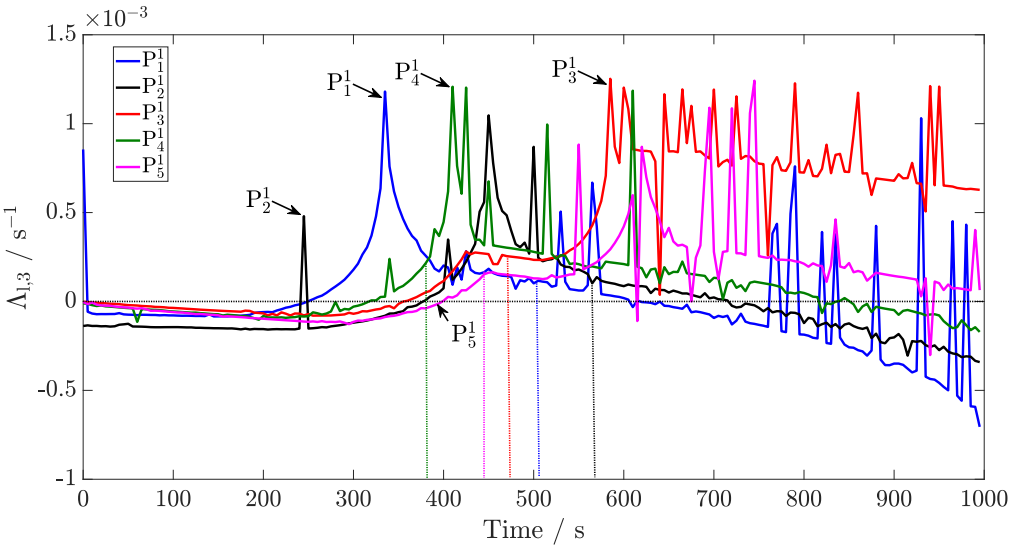

Fig. 3.10 Local Lyapunov exponent profiles with respect to state variable T_R, denoted by $\Lambda_{l,3}$, for processes $P_1^1 - P_5^1$. The dash-dotted lines parallel to the y-axis show the point in time when each process becomes unstable according to Figure 2.2.

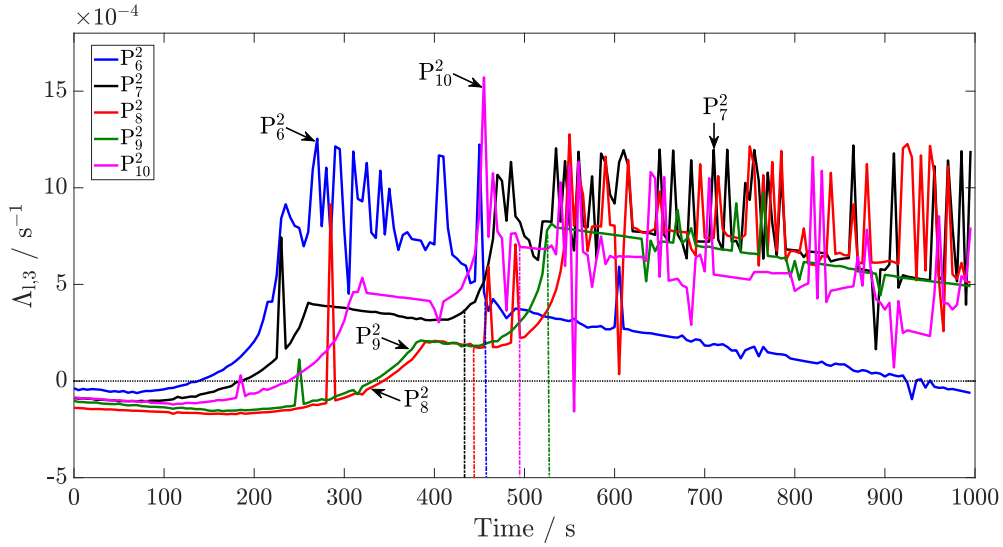

Fig. 3.11 Local Lyapunov exponent profiles with respect to state variable T_R, denoted by $\Lambda_{l,3}$, for processes $P_6^2 - P_{10}^2$. The dash-dotted lines parallel to the y-axis show the point in time when each process becomes unstable according to Figure 2.5.

In Figure 3.10 a transition from stable to unstable operation is clearly indicated by the Lyapunov exponents with respect to reactor temperature, $\Lambda_{l,3}$. This transition occurs when $\Lambda_{l,3} \geq 0$. The dash-dotted lines in Figure 3.10 show when each process becomes unstable. For each process the value of $\Lambda_{l,3}$ is greater than zero at these points in time. Hence reliable prediction of thermal stability is achieved for kinetics according to reaction scheme 1. For all remaining processes of reaction scheme 1 the same key features are observed.

The same analysis is now carried out for processes $P_6^2 - P_{10}^2$, where a single reaction depends on the concentration of reagents A and B. The temperature profiles for these processes are shown in Figure 2.5. The local Lyapunov exponents for processes $P_6^2 - P_{10}^2$, again denoted by $\Lambda_{l,3}$, are shown in Figure 3.11.

In Figure 3.11 a clear transition from stable to unstable operation is clearly indicated according to the Lyapunov exponents with respect to reactor temperature. This transition occurs when $\Lambda_{l,3} \geq 0$. The dash-dotted lines in Figure 3.11 show when each process becomes unstable. For each process the value of $\Lambda_{l,3}$ is greater than zero at these points in time. Hence reliable prediction of thermal stability is achieved for kinetics according to reaction scheme 2. For all remaining processes of reaction scheme 2 the same key features are observed.

With the parameter values of δx_0 and t_{Lyap} derived in Sections 3.2.1 and 3.2.2, respectively, it is hence shown that the thermal stability of batch processes can be predicted reliably for the systems considered here. It has to be noted that only the Lyapunov exponents for the

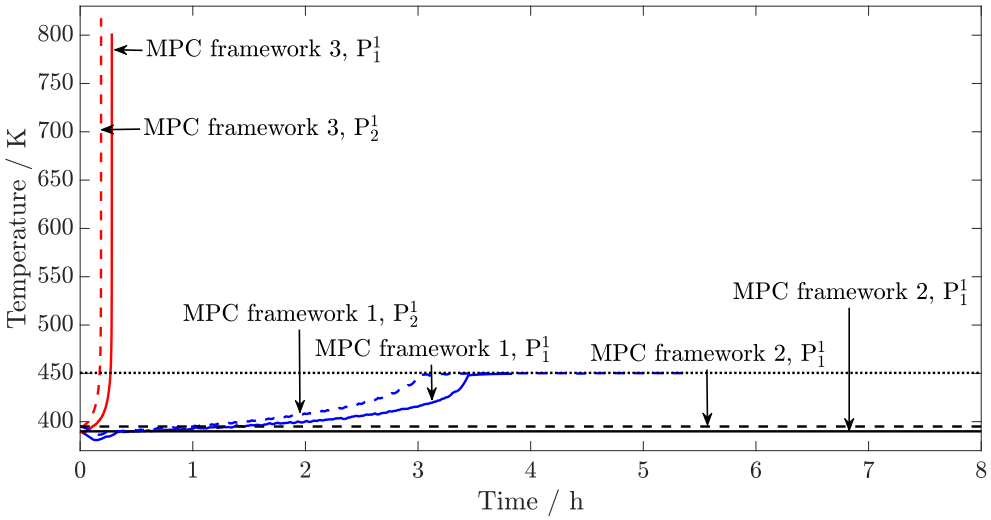

Fig. 3.12 Temperature profiles of processes $P_1^1 - P_2^1$, controlled with three different MPC frameworks. The horizontal dotted line indicates the maximum allowable temperature of $T_{\text{chem}} = 450\,\text{K}$.

reactor temperature were shown in this section. The concentrations of each reagent will have to be considered as well to get an overall picture of the thermal stability of the system when embedded within an MPC framework.

3.2.4 Intensification and computational times: reaction scheme 1

To examine if Lyapunov exponents can be used for process intensification of batch processes, the MPC structure and frameworks outlined in Section 2.5 are used.

Reaction scheme 1 is a single reaction dependent on one component, as introduced in Section 2.2.1. In this section batch processes $P_1^1 - P_2^1$ are carried out to examine if Lyapunov exponents embedded within MPC can be used for batch process intensification. The maximum allowable temperature for these processes is set to $T_{\text{chem}} = 450$ K. The temperature profiles for processes $P_1^1 - P_2^1$ controlled with the three different MPC frameworks introduced in Section 2.5 are shown in Figure 3.12.

From Figure 3.12 it is seen that MPC framework 3 results in thermal runaway behaviour: the temperature profiles increase sharply after 0.1 h until a maximum temperature of approximately 820 K is reached. This exceeds the maximum allowable temperature of $T_{\text{chem}} = 450\,\text{K}$ and therefore MPC framework 3 does not result in satisfactory control. This is attributed to the lack of a stability criterion. It is demonstrated (not shown) that an increase in the

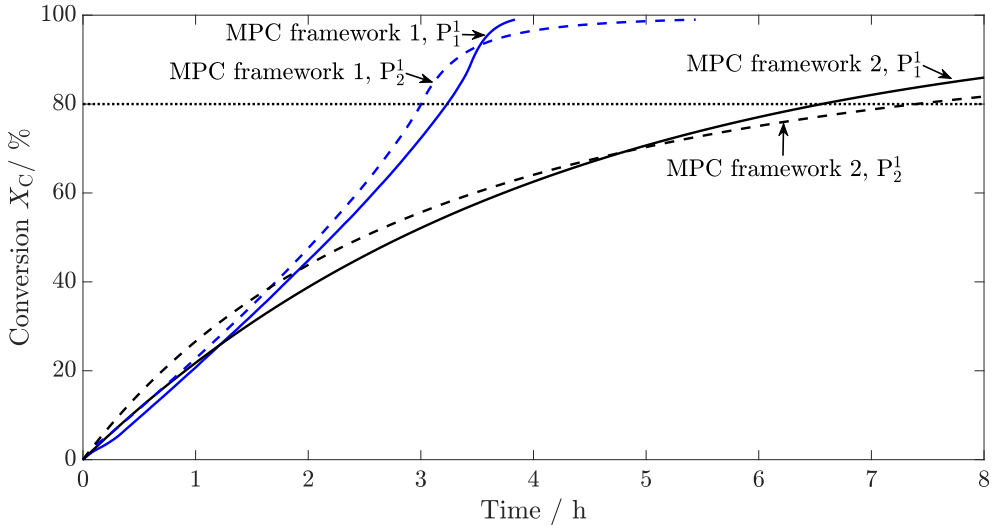

Fig. 3.13 Conversion profiles with respect to product C for processes $P_1^1 - P_2^1$. Only MPC framework 1 and 2 are applied to these processes. The dotted line indicates the target conversion of $X_C = 80\%$.

prediction horizon of the MPC scheme can result in stable control with significant drawbacks with respect to computational time, as discussed later in this section.

MPC framework 2 results in stable control as expected: the set-point temperature is constant throughout. The reactor temperature follows the set-point throughout and no thermal runaway behaviour occurs. The maximum allowable temperature is not exceeded, hence satisfactory control is achieved without any intensification.

MPC framework 1, as can be seen in Figure 3.12, results in a steady increase in reactor temperature whilst never exceeding the maximum allowable temperature of 450 K. No thermal runaway behaviour occurs, since there are no sudden spikes in temperature. Therefore satisfactory control of the batch processes is obtained. Similar results are obtained for all remaining processes within reaction scheme 1.

The intensification of processes $P_1^1 - P_2^1$ with MPC framework 1 compared to MPC framework 2 is examined using the conversion profiles of component C, X_C. The conversion profiles for these processes are shown in Figure 3.13

In Figure 3.13 it is seen that the target conversion of $X_C = 80\%$ with MPC framework 1 is reached after 3.2 h and 3.0 h for processes P_1^1 and P_2^1, respectively. A constant reactor temperature, as is done with MPC framework 2, achieves the target conversion after approximately

Table 3.1 Summary of results obtained for reaction scheme 1 controlled by each MPC framework, where t_{reac} is the time required to reach the target conversion of $X_{C,target} = 80\%$, T_{peak} is the peak temperature during the process, which is not allowed to exceed 450 K, and $\bar{t}_{comp}$ is the average computational time required to evaluate each MPC step.

	MPC framework 1			MPC framework 2		MPC framework 3	
	t_{reac}/h	T_{peak}/K	$\bar{t}_{comp}$/CPU s	t_{reac}/h	$\bar{t}_{comp}$/CPU s	T_{peak}/K	$\bar{t}_{comp}$/CPU s
P_1^1	3.2	450	2.43	6.5	0.60	807	5.54
P_2^1	3.0	450	1.73	7.4	0.32	821	4.21
P_3^1	2.8	450	1.44	15.7	0.31	814	4.84
P_4^1	2.6	450	1.42	20.3	0.35	810	5.12
P_5^1	2.7	450	1.52	47.3	0.29	789	4.36
P_6^1	3.5	449	1.48	6.6	0.32	845	3.70
P_7^1	2.2	450	1.85	6.1	0.42	746	4.85
P_8^1	1.5	450	1.10	4.9	0.27	702	4.87
P_9^1	2.3	449	1.30	12.5	0.26	630	4.94
P_{10}^1	2.7	449	1.58	35.9	0.29	599	3.86
P_{11}^1	1.3	450	1.47	2.0	0.32	654	4.69
P_{12}^1	1.3	450	2.50	2.0	0.29	689	3.20
P_{13}^1	1.8	450	1.65	2.6	0.30	749	6.55
P_{14}^1	2.3	450	3.35	3.1	0.30	820	4.50
P_{15}^1	2.8	450	1.69	3.8	0.29	883	6.16

5.0 h for both processes. Therefore a significant reduction in processing time is achieved with in MPC framework 1, whilst keeping the batch processes under control.

The last important feature of all these MPC frameworks to note is the computational time required to use each of these MPC frameworks. The smaller the computational time, the more feasible the application to industrial processes. The average computational times per MPC step, $\bar{t}_{comp}$, together with the time to reach the target conversion, t_{reac}, and the peak temperature throughout each process, T_{peak}, are summarised in Table 3.1.

From Table 3.1 it can be seen that MPC framework 3 results in peak temperatures $T_{peak} > T_{chem}$, hence giving unfeasible processes. Furthermore, MPC framework 3 requires the largest computational time per MPC step. This is the case because this MPC framework has the longest control and prediction horizon. Important to note is that this MPC framework is not able to keep the processes under control. A longer prediction horizon would be required

to achieve stable control, leading to even larger computational times. This poses a potential problem for industrial applications.

MPC framework 2 gives close to constant temperature profiles as shown in Figure 3.12. The initial temperatures for each process controlled with MPC framework 2 are close to the boundary of stability initially: a further increase in the initial temperature of 1 K would result in unstable processes. The computational time given in Table 3.1 for MPC framework 2 is the smallest amongst all MPC frameworks: a smaller control horizon with the objective of just keeping a constant temperature is much simpler than for the other MPC frameworks.

MPC framework 1, embedding Lyapunov exponents, results in peak temperatures below the maximum allowable temperature T_{chem}. As is seen in Figure 3.12 the temperature is increased in a controlled manner throughout the process, hence resulting in an intensified reaction. From the times required to reach the target conversion, t_{reac}, given in Table 3.1 it is seen that a significant decrease of reaction time is achieved when implementing MPC framework 1, compared to MPC framework 2. The computational times $\bar{t}_{\text{comp}}$ shown are larger than those for MPC framework 2, but smaller than those for MPC framework 3. With MPC framework 1 an improvement in efficiency of the process is obtained at the cost of larger computational times compared to MPC framework 2, but shorter than those for standard MPC frameworks.

3.2.5 Intensification and computational times: reaction scheme 2

Reaction scheme 2, as introduced in Section 2.2.2, consists of a single reaction. The reaction rate depends on the concentration of both reagents, A and B. This is the next level in complexity with respect to reaction scheme 1. The same MPC frameworks as in the previous section are applied. The maximum allowable temperature for the processes within reaction scheme 2 is set to $T_{\text{chem}} = 470$ K.

As a sample the results for processes $\text{P}_3^2 - \text{P}_4^2$ are shown in detail. Similar behaviours for the temperature and conversion profiles are obtained for all remaining processes within reaction scheme 2. The temperature profiles for processes $\text{P}_3^2 - \text{P}_4^2$ are shown in Figure 3.14.

In Figure 3.14 thermal runaway behaviour is observed with MPC framework 3. The peak temperatures for each process reach approximately 760 K at 0.1 h for processes P_3^2 and P_4^2. The maximum temperature of 470 K is exceeded, which is why this MPC framework results in unsatisfactory control.

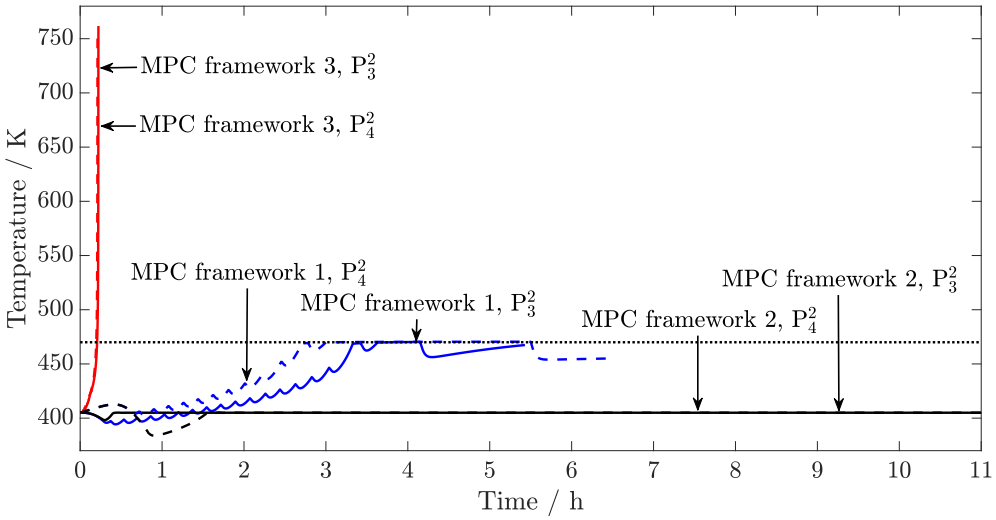

Fig. 3.14 Temperature profiles of processes $P_3^2 - P_4^2$, controlled with three different MPC frameworks. The horizontal dotted line indicates the maximum allowable temperature of $T_{\text{chem}} = 470\,\text{K}$.

No instability occurs for MPC framework 2, because the reactor temperature follows the set-point temperature throughout the process. Stable control is achieved without any process intensification, since no temperature increase is introduced during operation.

The maximum temperature of 470 K is not exceeded with MPC framework 1. Furthermore, the reactor temperature increases continuously during the process in a stable manner. For process P_4^2 the peak temperature reaches 470 K. After 5.5 h the temperature decreases, because most reagents have reacted, reducing the heat generation significantly. For process P_3^2 similar behaviour is observed. During the first 3.5 h of the process sudden drops in reactor temperature can be observed. This is the case because the Lyapunov exponents detect unstable operation and hence more cooling is applied to act against potential thermal runaway behaviour. At approximately 4.2 h a drop in temperature occurs for the same reason, but the effect of cooling is now amplified due to the low concentration of reagents.

The process intensification is examined by looking at the conversion profiles with respect to product C, for MPC frameworks 1 and 2. MPC framework 3 is omitted from this analysis due to the unstable control obtained. The conversion profiles for processes $P_3^2 - P_4^2$ are shown in Figure 3.15.

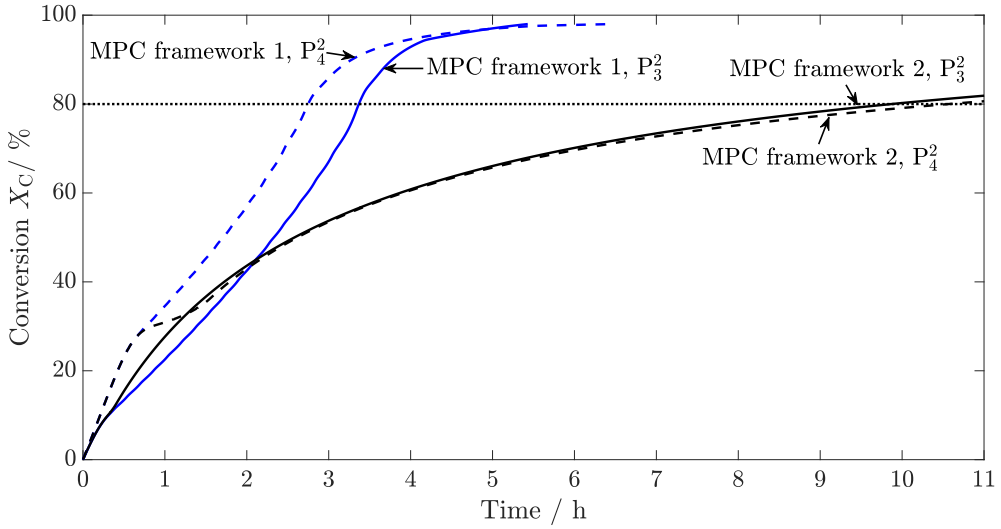

Fig. 3.15 Conversion profiles with respect to product C for processes $P_3^2 - P_4^2$. Only MPC framework 1 and 2 are applied to these processes. The dotted line indicates the target conversion of $X_C = 80\%$.

In Figure 3.15 it is seen that MPC framework 1 achieves the target conversion much faster than MPC framework 2. As expected, increasing the reactor temperature in a stable manner throughout the batch process improves the efficiency of such processes. For processes P_3^2 and P_4^2 the target conversion of 80% is reached after 3.3 h and 2.7 h, respectively, for MPC framework 1. If a constant reactor temperature were to be used, the target conversion is reached after approximately 9.9 h for process P_3^2 and after 10.6 h for process P_4^2.

The computational times required for each process when controlled by each MPC framework are shown in Table 3.2.

Similar to the results for reaction scheme 1, MPC framework 3 results in the largest computational time, although the peak temperatures exceed the maximum allowable temperature of 470 K, hence resulting in unacceptable control. Furthermore, the extended control and prediction horizons t_c and t_p would have to be further extended in order to achieve stable control, hence increasing the computational time even further. Therefore, the computational time per MPC step would potentially exceed the available time of 10 s.

MPC framework 2 results in the shortest computational times, since no intensification is required. The time required to reach the target conversion of 80% with respect to product C are significantly longer than those for MPC framework 1. This is expected, as no temperature increase occurs for processes controlled by MPC framework 2.

Table 3.2 Summary of results obtained for reaction scheme 1 controlled by each MPC framework, where t_{reac} is the time required to reach the target conversion of $X_{C,target} = 80\%$, T_{peak} is the peak temperature during the process, which is not allowed to exceed 470 K, and $\bar{t}_{comp}$ is the average computational time required to evaluate each MPC step.

	MPC framework 1			MPC framework 2		MPC framework 3	
	t_{reac}/h	T_{peak}/K	$\bar{t}_{comp}$/CPU s	t_{reac}/h	$\bar{t}_{comp}$/CPU s	T_{peak}/K	$\bar{t}_{comp}$/CPU s
P_1^2	5.8	470	1.15	13.4	0.81	978	5.45
P_2^2	3.5	470	1.41	40.3	0.93	776	6.25
P_3^2	3.3	470	1.05	9.9	0.65	762	5.11
P_4^2	2.7	470	1.30	10.6	0.72	759	5.73
P_5^2	5.1	470	1.07	13.9	0.53	940	5.60
P_6^2	3.5	469	1.07	20.2	0.61	894	6.35
P_7^2	3.9	469	1.97	31.0	0.84	819	4.42
P_8^2	4.5	470	1.05	35.5	0.36	856	6.11
P_9^2	7.3	469	1.19	>100	0.76	861	5.15
P_{10}^2	2.8	470	1.74	7.2	0.65	727	6.14
P_{11}^2	1.8	470	1.76	6.9	0.75	638	6.31
P_{12}^2	2.0	470	1.84	7.1	0.81	645	7.36
P_{13}^2	1.6	469	2.25	7.9	0.86	629	6.20
P_{14}^2	6.6	470	1.05	>100	0.49	651	5.16
P_{15}^2	6.7	469	1.14	>100	0.54	634	6.18
P_{16}^2	2.8	469	1.68	6.0	0.73	703	6.14
P_{17}^2	1.7	470	1.04	5.4	0.52	716	5.18
P_{18}^2	1.4	470	1.99	5.6	0.63	698	6.30
P_{19}^2	2.1	469	1.88	5.6	0.74	681	5.26
P_{20}^2	2.0	470	1.70	5.4	0.83	680	4.03

MPC framework 1 results in shorter computational times and more stable processes than MPC framework 3. Therefore a safe intensification with improved computational efficiency is achieved when embedding Lyapunov exponents within a standard MPC framework.

3.2.6 Intensification and computational times: nitration of toluene

The aim of this case study is to demonstrate that Lyapunov exponents embedded in standard MPC, as is done with MPC framework 1, can intensify more complex reaction networks safely. For this purpose, the nitration reaction network presented in Section 2.2.5 is simulated for different initial temperatures, while the maximum allowable temperature is set $T_{\text{chem}} = 510\,\text{K}$. The resulting temperature and conversion profiles are presented below, as well as the computational time of using each MPC framework.

The desired product for the nitration of toluene is ortho-nitrotoluene. Hence, the objective of the optimal control problem for this case study is to reach the maximum concentration of o-nitrotoluene during the process:

$$\min_{q_C(t)} \Phi^{(i)}\left(x\left(t\right), q_C\left(t\right)\right) = -\left[\text{o-}C_7H_7NO_2\right]\left(t_f^{(i)}\right) \tag{3.6}$$

where $\left[\text{o-}C_7H_7NO_2\right]\left(t_f^{(i)}\right)$ is the concentration at final time $t_f^{(i)}$ of the product, given by ortho-nitrotoluene, hereafter referred to as o-nitrotoluene. The final time in this case study is given by the final time of the MPC prediction horizon. This optimisation tries to optimise the final concentration of o-nitrotoluene at each step of the MPC algorithm. Hence an optimisation of the product concentration is carried out with respect to constraints forcing the system to stay below the maximum allowable temperature, $T_{\text{chem}} = 510\,\text{K}$, and keeping the system stable.

As there are four reagents and one temperature influencing the rate of heat generation in this system, a total of five Lyapunov exponents have to be evaluated at each step. The influence of increasing the number of relevant system variables on the computational time is analysed below. The resulting computational time will show how close this method is to the limit of applicability in an industrial setting.

The underlying MPC scheme is MPC framework 1, given in detail in Section 2.5.1. Since only the first MPC step is implemented, It is required that the computational time does not exceed 10 s, which is the duration of the first control step. Otherwise this method is not fast enough to be implemented in industry.

The resulting temperature profiles for the addition reaction with MPC and Lyapunov exponents are given in Figure 3.16.

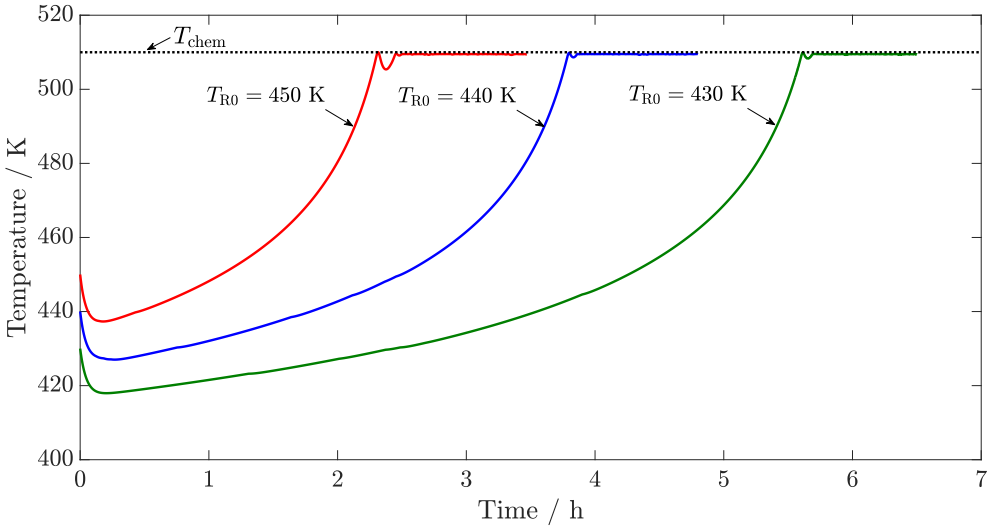

Fig. 3.16 Temperature profiles for the intensification of the nitration of toluene. Three different initial temperatures are used and controlled by MPC framework 1. The horizontal dotted line indicates the maximum allowable temperature of $T_{\text{chem}} = 510$ K.

The concentration profiles for the nitration of toluene with MPC framework 1 are shown below in Figure 3.17.

As the temperature for each process increases, the rate of increase in conversion increases. The target concentration for o-nitro-toluene of 2.5 kmol m^{-3} is reached after at most 6 h for all analysed processes. Furthermore it can be seen that a higher initial temperature leads to faster conversion. Furthermore an initial decrease in reactor temperature is seen: This occurs not due to the Lyapunov exponents wrongly identifying an unstable process, but because of the nature of the chemical reactions and the cooling jacket. The first reaction to occur is endothermic, hence removing heat. Additionally, the cooling jacket removes heat even without any coolant flow. Once the rates of the exothermic reactions increase, enough heat is generated for the system temperature to increase.

To show if using Lyapunov exponents with MPC framework 1 results in process intensification, the concentration profiles for MPC framework 2 are considered next. The concentration profiles for MPC framework 2 with different initial temperatures are shown below in Figure 3.18.

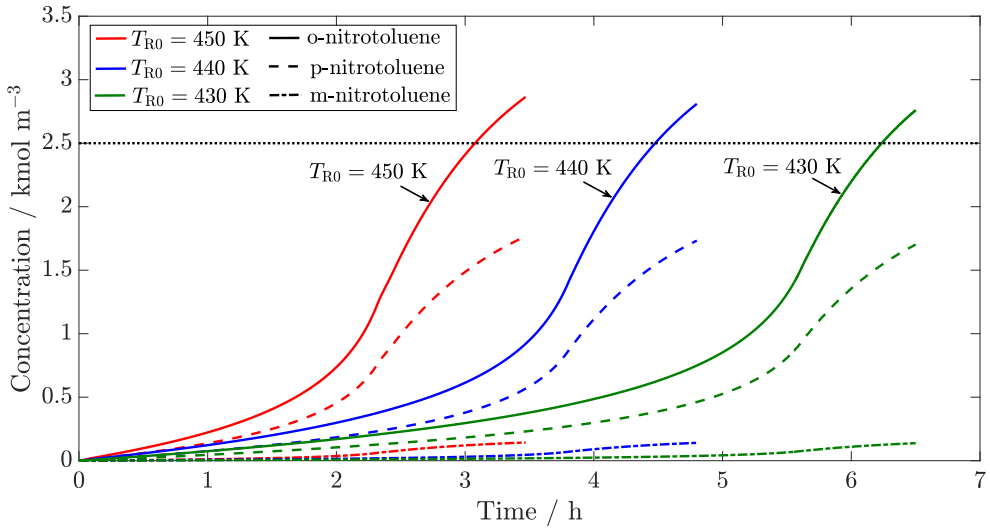

Fig. 3.17 Concentration profiles of nitration reaction using an MPC scheme including Lyapunov exponents with different initial temperatures. The dotted line indicates the target concentration of o-nitrotoluene.

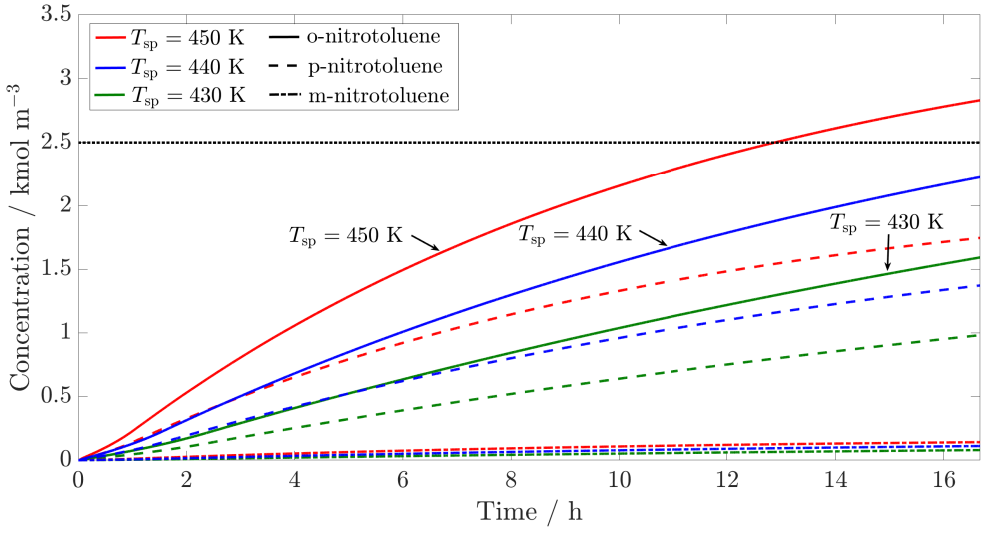

Fig. 3.18 Concentration profiles of nitration reaction using an MPC framework 2 with different initial temperatures. The dotted line indicates the target concentration of o-nitrotoluene.

Comparing Figures 3.18 and 3.17 highlights the intensification achieved by using an MPC scheme with Lyapunov exponents: the concentration for o-nitrotoluene reaches the target concentration of 2.5 kmol m^{-3} after 13 h for a set-point temperature of 450 K. A lower set-point temperature does not reach the target concentration within 16 h. Hence an intensification of at least two-fold is achieved. To show the dynamic behaviour of these processes, the time frame is truncated up to 16.5 h. Figure 3.18 shows that using Lyapunov exponents as a stability measure for complex reaction kinetics works as well as for simple reactions.

As for this complex reaction scheme the computational time at each iteration is of great importance, the average CPU seconds required per iteration for each MPC scheme are shown in Table 3.3.

Table 3.3 Computational time for each MPC framework 1 applied to the nitration of toluene.

Initial temperature of MPC controlled process	Computational time / CPU s
$T_{R0} = 430$ K	8.9
$T_{R0} = 440$ K	8.5
$T_{R0} = 450$ K	9.1

The computational time is just below the upper limit of 10 s, hence showing the feasibility of this method. These results show that the limit of applicability of this method, implemented as outlined above, is reached. Considerable improvements for computational time are necessary in order to implement this in an industrial setting, where continuous parameter estimation before the MPC stage could be necessary, requiring computational time as well. Hence, further improvements with respect to computational time are essential for a successful implementation in industry. Nevertheless, the batch processes of this industrially relevant reaction can be intensified by embedding Lyapunov exponents within standard MPC schemes.

3.3 Divergence criterion for batch processes

The divergence method, as opposed to Lyapunov exponents, results in a single number which determines the system stability. This simplifies the evaluations, because the number of criteria evaluated does not increase with the system size. As described in Section 1.2.3 only the variables contributing towards the heat generation in batch reactors are taken into account.

Therefore, only the entries of the Jacobian with respect to reagent concentrations and the reactor temperature are used to evaluate the divergence of the system.

In the following sections the divergence for reaction scheme 1 is derived in detail. The divergence criterion is then applied to processes $\mathrm{P}_6^1 - \mathrm{P}_{10}^1$ within reaction scheme 1, and processes $\mathrm{P}_1^2 - \mathrm{P}_5^2$ of reaction scheme 2.

3.3.1 Divergence of the Jacobian for batch processes

In this section sample processes from reaction schemes 1 and 2 are used to verify if the divergence criterion gives reliable predictions about thermal stability. As a sample, the form of the divergence criterion for reaction scheme 1 is derived below.

Reaction scheme 1 consists of a single reaction, as shown in Section 2.2. Using the definition of the divergence crterion in Section 1.2.3 the relevant variables for the generation of heat in the system are the concentration of reagent A, [A], and the reactor temperature T_R. The differential equations of interest are given by:

$$r = k_0 \exp\left(-\frac{E_a}{R T_\mathrm{R}}\right) [\mathrm{A}]^{n_\mathrm{A}} \tag{3.7a}$$

$$\frac{\mathrm{d}[\mathrm{A}]}{\mathrm{d}t} = -r \tag{3.7b}$$

$$\frac{\mathrm{d}}{\mathrm{d}t}\left(\rho_\mathrm{R} C_{p,\mathrm{R}} T_\mathrm{R} V_\mathrm{R}\right) = r\,(\Delta H_r)\,V_\mathrm{R} - UA\,(T_\mathrm{R} - T_\mathrm{C}) \tag{3.7c}$$

The diagonal Jacobian entries with respect to [A] and T_R are given by:

$$\frac{\partial}{\partial [\mathrm{A}]}\left(\frac{\mathrm{d}[\mathrm{A}]}{\mathrm{d}t}\right) = -n_\mathrm{A} k_0 \exp\left(-\frac{E_a}{R T_\mathrm{R}}\right) [\mathrm{A}]^{n_\mathrm{A}-1} \tag{3.8a}$$

$$\frac{\partial}{\partial T_\mathrm{R}}\left(\frac{\mathrm{d}}{\mathrm{d}t}\left(\rho_\mathrm{R} C_{p,\mathrm{R}} T_\mathrm{R} V_\mathrm{R}\right)\right) = k_0 \frac{E_a}{R T_\mathrm{R}^2} \exp\left(-\frac{E_a}{R T_\mathrm{R}}\right) [\mathrm{A}]^{n_\mathrm{A}}\,(\Delta H_r)\,V_\mathrm{R} - UA \tag{3.8b}$$

Equations (3.8a) and (3.8b) are added to give the divergence of the batch process with reaction scheme 1:

$$\begin{aligned}\operatorname{div}[\mathbf{J}] = &- n_{\mathrm{A}} k_0 \exp\left(-\frac{E_a}{R T_{\mathrm{R}}}\right)[\mathrm{A}]^{n_{\mathrm{A}}-1} \\ &+ k_0 \frac{E_a}{R T_{\mathrm{R}}^2} \exp\left(-\frac{E_a}{R T_{\mathrm{R}}}\right)[\mathrm{A}]^{n_{\mathrm{A}}} (\Delta H_r) V_{\mathrm{R}} - UA \end{aligned} \tag{3.9}$$

Equation (3.9) is the expression for the divergence of the Jacobian for batch processes with reaction scheme 1. A thermal runaway is detected with the expression in Equation (3.9) if $\operatorname{div}[\mathbf{J}] > 0$.

3.3.2 Verification of divergence method: reaction schemes 1 and 2

The reliability of the divergence criterion is examined using processes $\mathrm{P}_6^1 - \mathrm{P}_{10}^1$ and $\mathrm{P}_1^2 - \mathrm{P}_5^2$ as a sample. The temperature plots of processes $\mathrm{P}_6^1 - \mathrm{P}_{10}^1$ are shown in Figure 2.3. The respective divergence criterion profiles are shown in Figure 3.19.

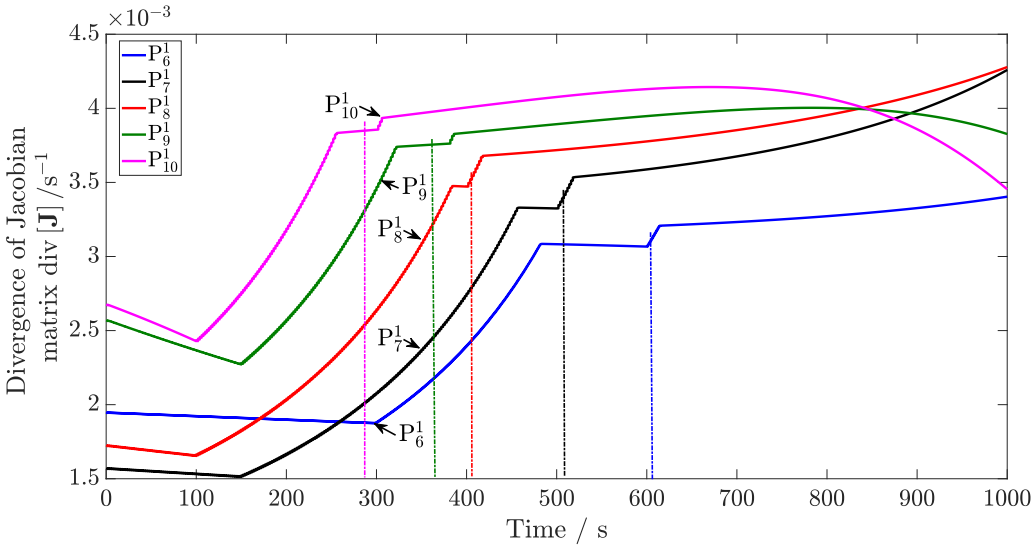

Fig. 3.19 Divergence criterion for processes $\mathrm{P}_6^1 - \mathrm{P}_{10}^1$. The dash-dotted lines parallel to the y-axis show the point in time when each process becomes unstable according to Figure 2.3.

The dash-dotted lines in Figure 3.19 indicate when each process becomes unstable according to the temperature profiles. In Figure 3.19 it is seen that the value of each divergence criterion is positive at all times. This means that an unstable system is predicted at all times which is not true as can be seen from the temperature profiles. Hence, a very conservative prediction

of system stability is obtained. The divergence criterion correspond well to the temperature profiles shown in Figure 2.3, which is one of the main indicators for thermal stability.

The same analysis as for reaction scheme 1 above is carried out for reaction scheme 2. The temperature profiles for processes $P_1^2 - P_5^2$ are shown in Figure 2.8. The respective divergence profiles for these processes are shown in Figure 3.20.

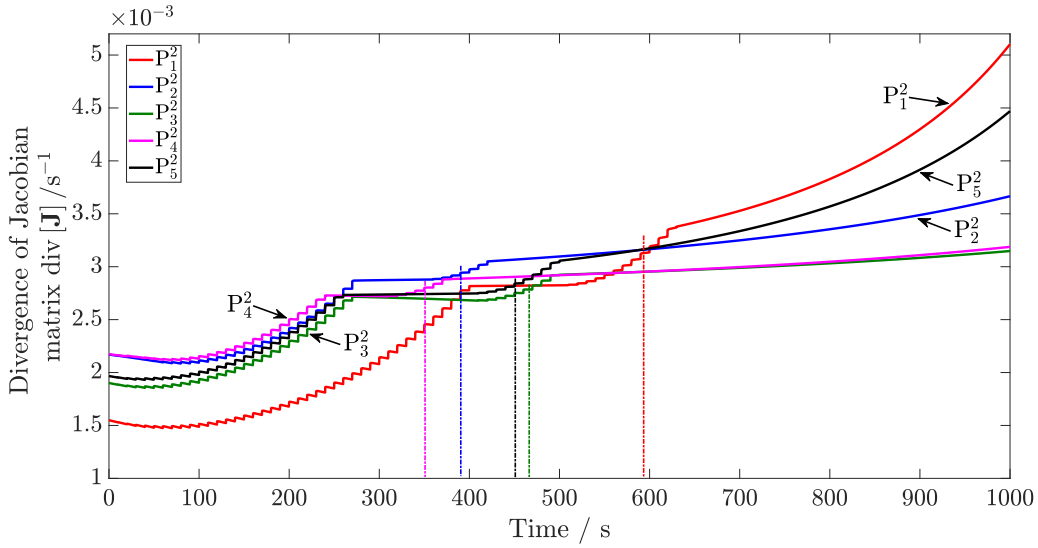

Fig. 3.20 Divergence criterion for processes $P_1^2 - P_5^2$. The dash-dotted lines parallel to the y-axis show the point in time when each process becomes unstable according to Figure 2.8.

In Figure 3.20 it is seen that similar results to that for processes $P_6^1 - P_{10}^1$ are obtained: the values for the divergence criterion are positive at all points in time. This is the case even though initially each process is stable. The profiles of the divergence criteria follow a similar profile to that of the temperature profiles shown in Figure 2.8.

Qualitatively the divergence criteria profiles follow a very similar profile to that of the temperature profiles. Quantitatively the divergence criteria systematically over-predict the thermal instability of the processes. Therefore the divergence criterion on its own does not result in a reliable measure of thermal stability. This is in contrast to results found in literature (Bosch *et al.*, 2004; Strozzi and Zaldívar, 1999), where different batch processes are considered. Nevertheless, the profiles of the divergence criteria can be used. A correction function would be necessary to make the criterion less conservative.

3.3.3 Sensitivity analysis of divergence criterion

The values of the divergence criterion, as shown in Figures 3.19 and 3.20, are of the order of 10^{-3}. This is not due to numerical effects of the ODE solver employed, because a relative and absolute tolerance of 10^{-8} is used. The divergence is evaluated using algebraic expressions, as shown in Equation (3.9), which do not add errors of the order of 10^{-3}.

To prove this point, a sensitivity analysis of process P_5^1 is carried out with varying tolerances for the ODE solver employed. The relative tolerances, RTol, and absolute tolerances, ATol, are set to RTol = ATol = 10^{-6}, 10^{-7}, 10^{-8}, 5×10^{-9}, 4×10^{-9}. Since the values of RTol and ATol are set equal for each simulation, they are hereafter referred to as Tol.

The simulation using the highest accuracy, *i.e.* the smallest value of the tolerance Tol, is used as the reference. The error with respect to the reference trajectory, ε_{div}, is plotted on a logarithmic scale in Figure 3.21.

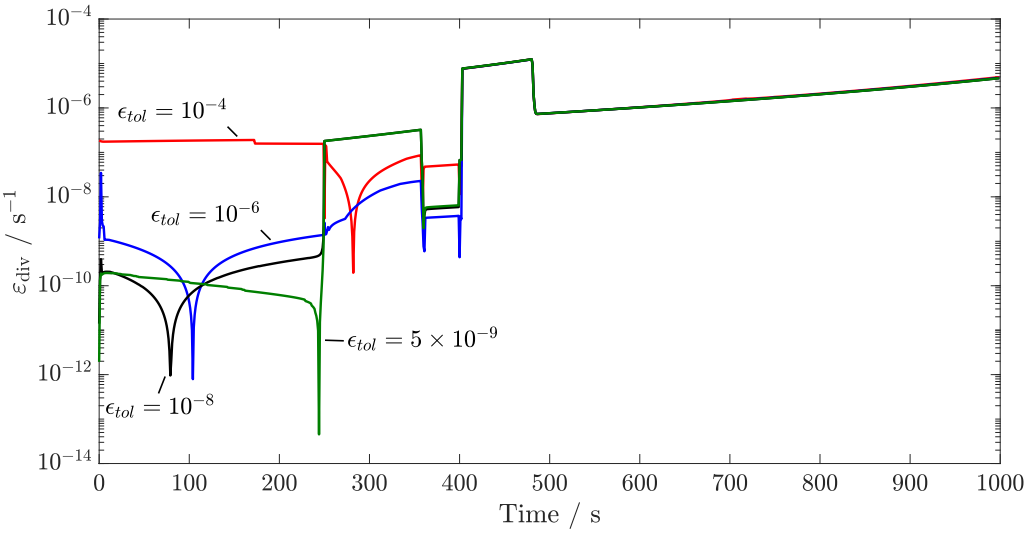

Fig. 3.21 Error profiles for each sensitivity setting with respect to Tol = 4×10^{-9} for process P_5^1 plotted on a logarithmic scale.

As can be seen in Figure 3.21 the errors are below 10^{-6} at all times. The tolerance setting used throughout all simulations is Tol = 10^{-8}. As can be seen from Figure 3.21 the error for the divergence obtained is below 10^{-4} at all times. The numerical effects due to the ODE solver used do not cause the divergence to be positive during stable operation, because the divergence criterion is evaluated by an algebraic equation as shown in Equation (3.9).

3.3.4 Intensification and computational times: reaction scheme 1

In this section it is examined if the conservative nature of the divergence criterion when identifying thermal instability has negative effects on batch processes intensification, if this measure of stability is embedded within an MPC framework. Processes $P^1_{11} - P^1_{15}$ from reaction scheme 1 are used for this purpose.

In Section 3.2.4 it was shown that standard MPC, given by MPC framework 3, results in unstable control if process intensification is attempted. Hence, only MPC framework 1 with the divergence criterion is considered in this section.

The temperature profiles of processes $P^1_{11} - P^1_{15}$ controlled by MPC framework 1 with the divergence criterion are shown in Figure 3.22.

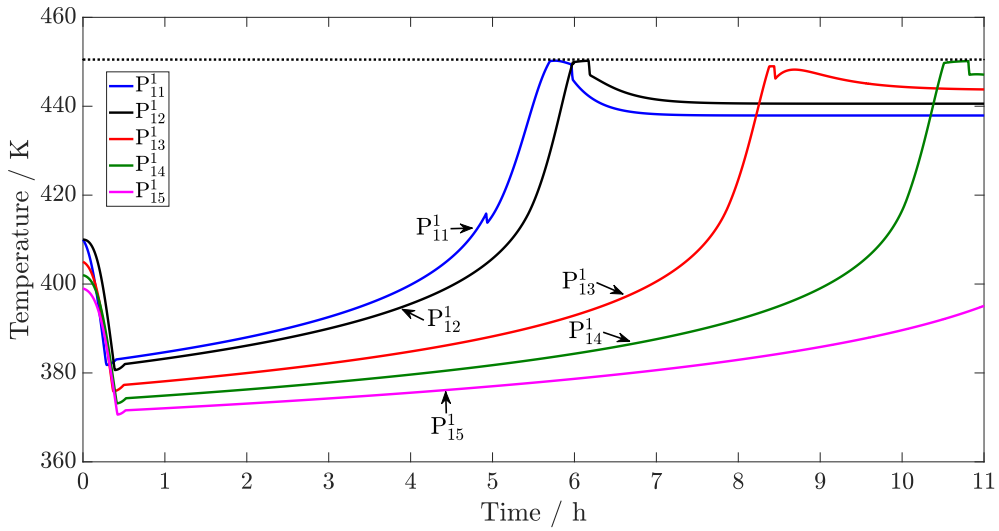

Fig. 3.22 Temperature profiles for processes $P^1_{11} - P^1_{15}$ controlled by MPC framework 1. The horizontal dotted line indicates the maximum allowable temperature of $T_{\text{chem}} = 450\,\text{K}$.

In Figure 3.22 it is seen that for every process the temperature is decreased initially. This is due to the overly conservative nature of the divergence criterion, which identifies each process to be unstable initially. This is the case even though MPC framework 2 was able to keep the initial set-point temperature, as discussed in Section 3.2.4. After the initial decrease in reactor temperature, the temperature is increased gradually without exceeding the maximum allowable temperature of $T_{\text{chem}} = 450\,\text{K}$.

The intensification achieved by using the divergence criterion within MPC framework 1 is examined by considering the conversion profiles with respect to product C. The con-

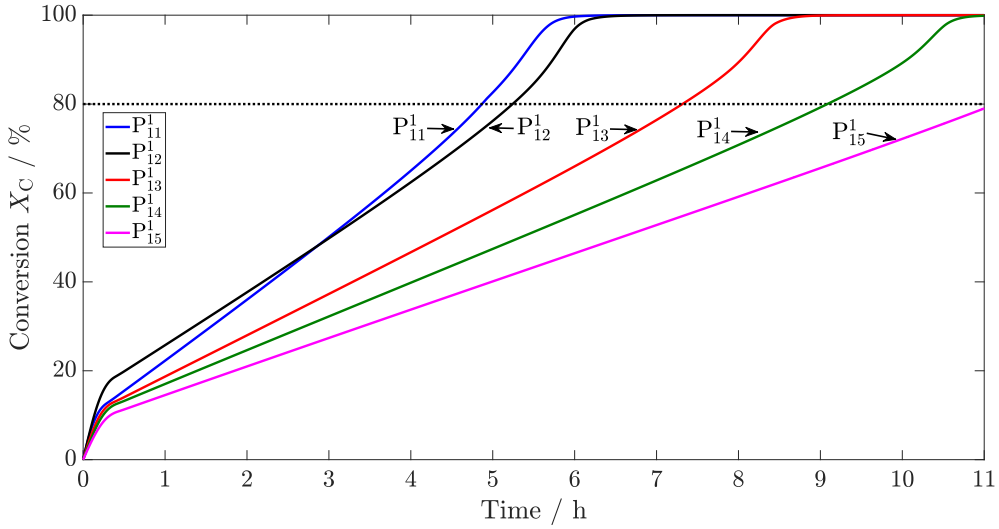

Fig. 3.23 Conversion profiles for processes $P^1_{11} - P^1_{15}$ controlled by MPC framework 1. The dotted line indicates the target conversion of $X_C = 80\%$.

version profiles for processes $P^1_{11} - P^1_{15}$ controlled by MPC framework 1 are shown in Figure 3.23.

In Figure 3.23 it is seen that the target conversion is reached after more than 7 h for each process. The results for all remaining processes are summarised in Table 3.4.

When comparing the values of t_{reac} for MPC framework 1 with the divergence criterion and MPC framework 2 in Table 3.4 it is seen that MPC framework 2 results in shorter processing times for several processes, *e.g.* processes P^1_1 and P^1_2. This means that no intensification is achieved using the divergence criterion due to the large decrease in temperature at the beginning of the process. Therefore, the divergence criterion on its own is too conservative to be useful for process intensification.

The maximum allowable temperatures are not exceeded, which means stable process control is obtained. This is expected, since the divergence criterion gives overly conservative thermal stability predictions.

The computational times per MPC step with the divergence criterion are at least as short as those for MPC framework 1 with Lyapunov exponents. The values for $\bar{t}_{comp}$ are not expected to increase with the system size, because a single value for the divergence is evaluated instead of one Lyapunov exponent per system variable. Using the divergence criterion within MPC framework 1 for large reaction networks hence results in a computationally more efficient control scheme than using Lyapunov exponents.

Table 3.4 Summary of results obtained for reaction scheme 1 controlled by MPC framework 1 with the divergence criterion. The target conversion is $X_{C,target} = 80\%$, and T_{peak} is the peak temperature during the process, which is not allowed to exceed 450 K. The processing times for MPC framework 2 are shown here for reference.

	MPC framework 1			MPC framework 2
	t_{reac}/h	T_{peak}/K	$\bar{t}_{comp}$/CPU s	t_{reac}/h
P_1^1	9.6	449	1.01	6.5
P_2^1	9.3	449	1.00	7.4
P_3^1	8.6	450	1.14	15.7
P_4^1	8.0	450	1.27	20.3
P_5^1	7.5	450	1.27	47.3
P_6^1	10.4	408	0.85	6.6
P_7^1	6.8	449	0.83	6.1
P_8^1	4.6	450	1.50	4.9
P_9^1	4.4	450	1.49	12.5
P_{10}^1	4.8	450	1.87	35.9
P_{11}^1	4.9	450	0.52	2.0
P_{12}^1	5.3	450	0.54	2.0
P_{13}^1	7.3	448	0.69	2.6
P_{14}^1	9.1	450	0.93	3.1
P_{15}^1	11.4	395	0.89	3.8

3.3.5 Intensification and computational times: reaction scheme 2

In the previous section it was shown that using the divergence criterion with MPC framework 1 results in overly conservative process control for reaction scheme 1. To verify that this behaviour is not an artefact of reaction scheme 1, the same MPC framework is applied to reaction scheme 2.

As a sample, the temperature profiles of processes $P_1^2 - P_5^2$ controlled by MPC framework 1 with the divergence criterion embedded are shown in Figure 3.24.

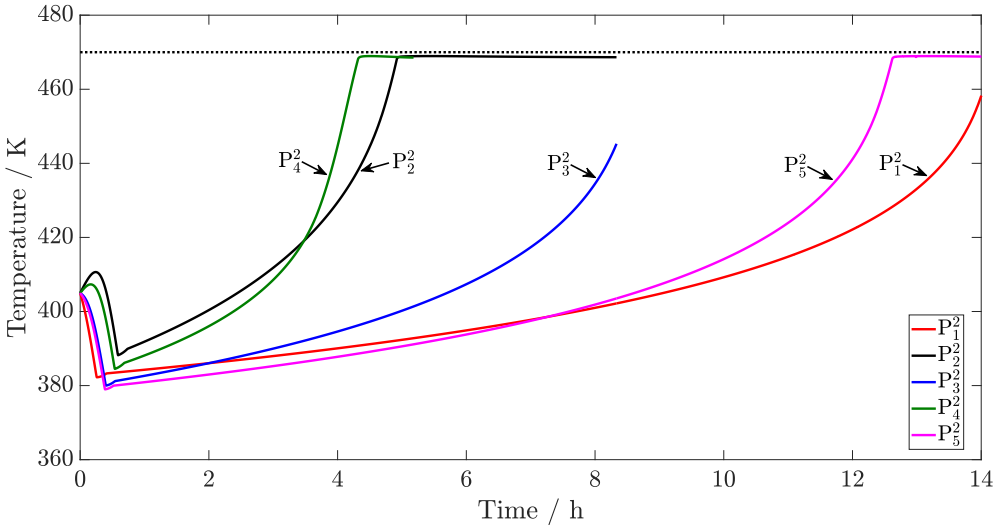

Fig. 3.24 Temperature profiles for processes $P_1^2 - P_5^2$ controlled by MPC framework 1. The horizontal dotted line indicates the maximum allowable temperature of $T_{\text{chem}} = 470\,\text{K}$.

From Figure 3.24 similar results to those for reaction scheme 1 are observed. Due to the overly conservative nature of the divergence criterion the reactor temperature initially is decreased, although stable operation is present. Only after considerable amount of time is the temperature increased towards the maximum allowable temperature T_{chem}.

The process intensification of MPC framework 1, embedded with the divergence criterion, is examined using conversion profiles of reagent A. The conversion profiles for processes $P_1^2 - P_5^2$ controlled by MPC framework 1 are shown in Figure 3.25.

The target conversion of X_C is reached after at least 4 h for processes $P_1^2 - P_5^2$ in Figure 3.25. How the results for processes $P_1^2 - P_5^2$, as well as all remaining processes, compare to MPC framework 2 is shown in Table 3.5.

Similar results as for reaction scheme 1 are obtained in Table 3.5 for reaction scheme 2. For processes P_2^2 and P_9^2, for example, t_{reac} is much smaller if MPC framework 1 with embedded divergence criterion is used instead of MPC framework 2 with constant temperature set-point. For processes such as $P_{16}^2 - P_{20}^2$ on the other hand, t_{reac} is similar for MPC framework 1 with the divergence criterion and MPC framework 2. No consistent intensification of batch processes can be achieved with the divergence criterion as in contrast to when using Lyapunov exponents.

The computational times shown in Table 3.5 are shorter than those obtained for MPC framework 1 with Lyapunov exponents, shown in Table 3.2. Therefore, as was observed for reaction

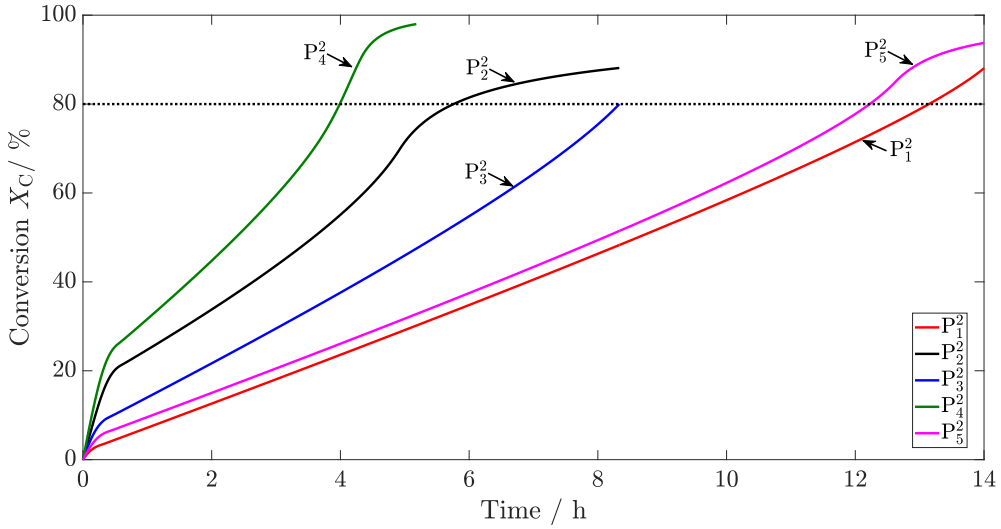

Fig. 3.25 Conversion profiles for processes $P_1^2 - P_5^2$ controlled by MPC framework 1. The dotted line indicates the target conversion of $X_C = 80\%$.

scheme 1, embedding the divergence criterion within MPC results in a computationally more efficient control system.

The maximum temperature of $T_{chem} = 470$ K is not exceeded when using MPC framework 1 with the divergence criterion embedded. This is due to the conservative nature of the divergence criterion, not letting the system enter an unstable operating point at any time. This is in line with the results obtained for reaction scheme 1 in Table 3.4.

Table 3.5 Summary of results obtained for reaction scheme 2 controlled by MPC framework 1 with the divergence criterion. The target conversion is $X_{C,target} = 80\%$, and T_{peak} is the peak temperature during the process, which is not allowed to exceed 470 K. The processing times for MPC framework 2 are shown here for reference.

	MPC framework 1			MPC framework 2
	t_{reac}/h	T_{peak}/K	$\bar{t}_{comp}$/CPU s	t_{reac}/h
P_1^2	13.1	457	1.07	13.4
P_2^2	5.8	469	1.00	40.3
P_3^2	8.3	445	1.07	9.9
P_4^2	4.0	469	1.06	10.6
P_5^2	12.2	469	1.01	13.9
P_6^2	9.6	429	1.09	20.2
P_7^2	7.7	469	1.05	31.0
P_8^2	8.6	470	1.01	35.5
P_9^2	6.7	469	1.01	>100
P_{10}^2	6.3	470	1.00	7.2
P_{11}^2	5.4	469	1.01	6.9
P_{12}^2	7.0	469	0.99	7.1
P_{13}^2	6.0	469	1.09	7.9
P_{14}^2	4.3	469	0.61	>100
P_{15}^2	4.9	469	0.59	>100
P_{16}^2	6.1	469	0.88	6.0
P_{17}^2	6.0	470	0.77	5.4
P_{18}^2	4.1	470	0.87	5.6
P_{19}^2	5.9	469	0.98	5.6
P_{20}^2	5.9	470	1.08	5.4

3.4 Chapter summary

Stability criteria for CSTRs, including the Semënov criterion, are found to give unreliable predictions of thermal stability of batch processes. Other stability criteria used for CSTRs, such as the Barkelew criterion (Barkelew, 1959), the Balakotaiah criterion (Balakotaiah, 1989), the Baerns criterion (Baerns and Renken, 2004), and the Frank Kaminet͡skiĭ criterion (Frank-Kamenet͡skiĭ, 1969), are all strongly based on the Semënov criterion. Since the Semënov criterion does not give reliable predictions of thermal stability in batch processes, these criteria cannot be used for this purpose either.

The Routh-Hurwitz criterion works reliably for CSTRs (Stephanopoulos, 1984), but for inherently non steady-state processes this criterion does not work well. Therefore, this criterion is not considered further in this work.

Lyapunov exponents are shown to work well for batch processes. Advantages of Lyapunov exponents for batch process intensification are:

1. reliable predictions of thermal stability once optimal parameters δx_0 and t_{Lyap} are found
2. easy to implement within an MPC framework for process intensification
3. could be used for different runaway systems due to the general mathematical nature

Disadvantages of Lyapunov exponents for batch process intensification are:

1. exponential increase in computational time with increase in system variables
2. close to exceed available MPC time for relatively small reaction networks
3. may require repeated tuning of optimal parameters for different systems

The divergence criterion has the following advantages for process intensification:

1. short computational times when embedded within MPC frameworks
2. qualitatively the divergence criterion has similar character to that of the thermal runaway potential

Disadvantages of the divergence criterion are:

1. quantitatively the divergence criterion systematically over-predicts thermal instability
2. when embedded within MPC frameworks, overly conservative control is achieved achieving no process intensification

It is important to note that the divergence criterion was applied in literature to analyse the thermal stability of batch processes (Bosch *et al.*, 2004; Strozzi and Zaldívar, 1999), where reliable stability prediction is reported. This is not the case for all batch processes considered in this thesis.

The advantages of the Lyapunov exponents and the divergence criterion are both necessary for potential application in industry. An appropriate function for the divergence criterion could shift, or *correct*, its value to give less conservative predictions. This would make it a reliable, as well as computationally efficient thermal stability criterion when embedded in an MPC framework. Such a correction function is developed in the next chapter.

Chapter 4

Development of a stability criterion for exothermic batch processes

Leading on from the previous chapter, a new thermal stability criterion based on the divergence criterion is derived in this chapter. The reason for choosing the divergence criterion as the basis are fast computational times and the behaviour of the trajectory of the divergence criterion when thermal runaways occur. This new thermal stability criterion will be called criterion $\mathscr{K}$ throughout this work.

4.1 Properties and form of stability criterion $\mathscr{K}$

Stability criterion $\mathscr{K}$ describes the transition from thermally stable to unstable operation in batch reactors. For a thermally stable process, the criterion should give a value of:

$$\mathscr{K} \leq 0 \tag{4.1}$$

The stability criterion $\mathscr{K}$ is based on the difference between the divergence of the Jacobian of the relevant system variables and the correction function $\mathscr{E}$. At each current time step (s) stability criterion $\mathscr{K}^{(s)}$ is given by:

$$\mathscr{K}^{(s)} = \text{div}\left[\mathbf{J}^{(s)}\right] - \left|\mathscr{E}^{(s)}\right| \tag{4.2}$$

The correction function $\mathscr{E}^{(s)}$ is derived as a function of the divergence of the Jacobian at the previous time step $(s-1)$, $\text{div}\left[\mathbf{J}^{(s-1)}\right]$, and the following dimensionless numbers:

Damköhler number Da, Barkelew number B, Arrhenius number γ, and the Stanton number St. The definition of each dimensionless variable for a single reaction system is given in Equation (1.11).

The function for $\mathscr{E}^{(s)}$ represents the linear estimate of the divergence $\operatorname{div}\left[\mathbf{J}^{(s)}\right]$ at the boundary of instability, dependent on the following variables:

$$\mathscr{E}^{(s)} = f\left(\operatorname{div}\left[\mathbf{J}^{(s-1)}\right], B^{(s)}, B^{(s-1)}, \gamma^{(s)}, \gamma^{(s-1)}, \mathrm{Da}^{(s)}, \mathrm{Da}^{(s-1)}, \mathrm{St}^{(s)}, \mathrm{St}^{(s-1)}\right) \tag{4.3}$$

From Equation (4.3) it can be seen that the value of the linear estimate at time step (s), $\mathscr{E}^{(s)}$, uses information from the current time step (s) and the previous time step $(s-1)$. This function is sought after in order to correct for the fact that the value of the divergence $\operatorname{div}\left[\mathbf{J}^{(s)}\right]$ over-predicts the thermal runaway potential of the system. It is worth noting that, since information from the previous step $(s-1)$ is required to evaluate $\mathscr{E}^{(s)}$, no value of $\mathscr{E}$ is evaluated at step $(s=0)$. The whole concept behind criterion $\mathscr{K}$ is shown schematically in Figure 4.1.

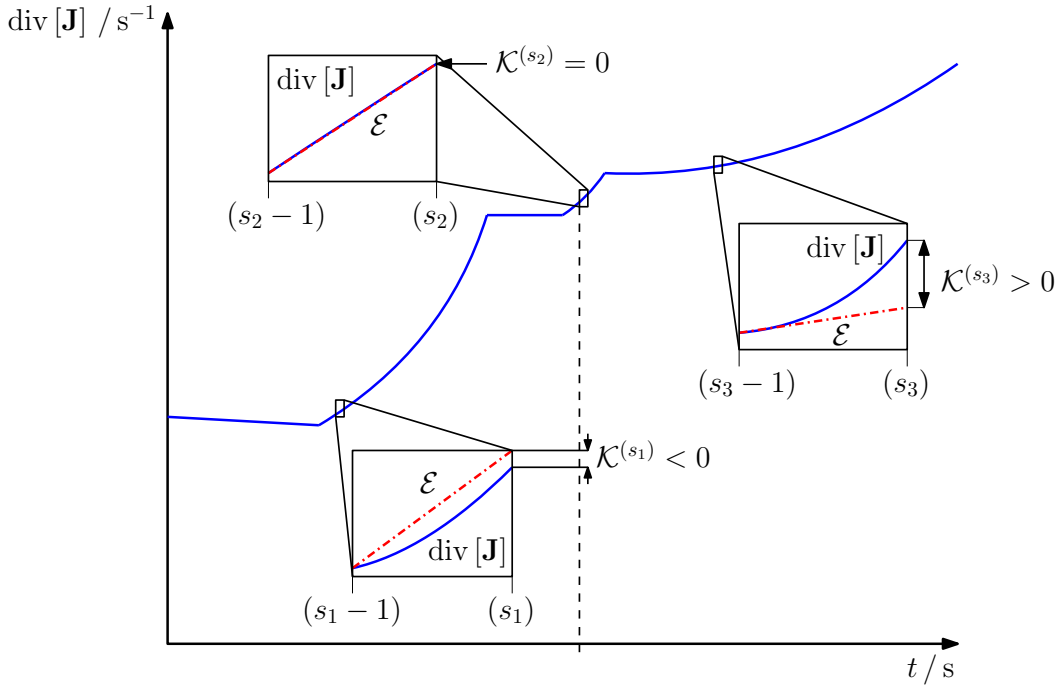

Fig. 4.1 Concept behind evaluation of criterion $\mathscr{K}$ based on correction function $\mathscr{E}$ (red, dash-dotted) and $\operatorname{div}[\mathbf{J}]$ (blue, solid). The vertical dashed line indicates the time at which the process becomes unstable. Steps (s_1), (s_2), and (s_3) represent times at which the process is stable, at the onset of instability, and unstable, respectively. The time between each time step, *i.e.* between $(s-1)$ and (s), is set to 10^{-3} s.

In Figure 4.1 it is seen that correction function $\mathscr{E}$ equals the divergence of the Jacobian matrix in step $(s-1)$. A linear estimate is then carried out to approximate what the value of div $[\mathbf{J}]$ is in step (s). The difference between $\mathscr{E}^{(s)}$ and div $\left[\mathbf{J}^{(s)}\right]$ is equal to criterion $\mathscr{K}$ in time step (s). The form of this linear approximation of the divergence at the boundary of stability is outlined in the following sections.

4.2 Divergence criterion for general reaction network

The divergence of the Jacobian matrix requires to express all variables that are changing due to differential equations. In batch reactor systems, as shown in the previous section, relevant variables are given by concentrations of reagents, as well as the reactor temperature. To derive the divergence, a sample reaction network with M reactions is considered for which the general form of the divergence is derived. The reaction network is given by a set of parallel reactions with two reacting components resulting in a single product. This assumption is used for clarity of the derivation, but does not limit the validity of this derivation for different reaction types. The reaction network considered for the derivation in this work is given by the following expressions:

$$\nu_{\mathrm{A},1}\mathrm{A} + \nu_{\mathrm{B},1}\mathrm{B} \rightarrow \mathrm{C} \tag{4.4a}$$

$$\vdots$$

$$\nu_{\mathrm{A},i}\mathrm{A} + \nu_{\mathrm{D},i}\mathrm{D} \rightarrow \mathrm{E} \tag{4.4b}$$

$$\vdots$$

$$\nu_{\mathrm{A},M}\mathrm{A} + \nu_{\mathrm{G},M}\mathrm{G} \rightarrow \mathrm{H} \tag{4.4c}$$

$$i = 1, 2, ..., M \tag{4.4d}$$

where the reactions follow an Arrhenius expression according to:

$$r_1 = k_{0,1} \exp\left(\frac{-E_{a,1}}{R T_{\mathrm{R}}}\right) [\mathrm{A}]^{n_{\mathrm{A},1}} [\mathrm{B}]^{n_{\mathrm{B},1}} \tag{4.5a}$$

$$\vdots$$

$$r_i = k_{0,i} \exp\left(\frac{-E_{a,i}}{R T_{\mathrm{R}}}\right) [\mathrm{A}]^{n_{\mathrm{A},i}} [\mathrm{D}]^{n_{\mathrm{D},i}} \tag{4.5b}$$

$$\vdots$$

$$r_M = k_{0,M} \exp\left(\frac{-E_{a,M}}{R T_{\mathrm{R}}}\right) [\mathrm{A}]^{n_{\mathrm{A},M}} [\mathrm{G}]^{n_{\mathrm{G},M}} \tag{4.5c}$$

$$i = 1, 2, ..., M \tag{4.5d}$$

where index i represents the i^{th} reaction within the M reactions present.

The divergence of the Jacobian for this reaction network, occurring in a batch reactor with an energy balance according to Equation (1.10), is given by the following equation:

$$\begin{aligned}
\operatorname{div}[\mathbf{J}] = &- \left(\nu_{\mathrm{A},1} n_{\mathrm{A},1} [\mathrm{A}]^{n_{\mathrm{A},1}-1} [\mathrm{B}]^{n_{\mathrm{B},1}} + \nu_{\mathrm{B},1} n_{\mathrm{B},1} [\mathrm{A}]^{n_{\mathrm{A},1}} [\mathrm{B}]^{n_{\mathrm{B},1}-1}\right) k_{0,1} \exp\left(-\frac{E_{a,1}}{R T_{\mathrm{R}}}\right) \\
&\vdots \\
&- \left(\nu_{\mathrm{A},i} n_{\mathrm{A},i} [\mathrm{A}]^{n_{\mathrm{A},i}-1} [\mathrm{D}]^{n_{\mathrm{D},i}} + \nu_{\mathrm{D},i} n_{\mathrm{D},i} [\mathrm{A}]^{n_{\mathrm{A},i}} [\mathrm{D}]^{n_{\mathrm{D},i}-1}\right) k_{0,i} \exp\left(-\frac{E_{a,i}}{R T_{\mathrm{R}}}\right) \\
&\vdots \\
&- \left(\nu_{\mathrm{A},M} n_{\mathrm{A},M} [\mathrm{A}]^{n_{\mathrm{A},M}-1} [\mathrm{G}]^{n_{\mathrm{G},M}} + \nu_{\mathrm{G},M} n_{\mathrm{G},M} [\mathrm{A}]^{n_{\mathrm{A},M}} [\mathrm{G}]^{n_{\mathrm{G},M}-1}\right) k_{0,M} \exp\left(-\frac{E_{a,M}}{R T_{\mathrm{R}}}\right) \\
&+ \frac{1}{\rho C_p V_{\mathrm{R}}} \left[\frac{E_{a,1}}{R T_{\mathrm{R}}^2} k_{0,1} \exp\left(-\frac{E_{a,1}}{R T_{\mathrm{R}}}\right) [\mathrm{A}]^{n_{\mathrm{A},1}} [\mathrm{B}]^{n_{\mathrm{B},1}} (-\Delta H_{r,1}) V_{\mathrm{R}}\right. \\
&\vdots \\
&+ \frac{E_{a,i}}{R T_{\mathrm{R}}^2} k_{0,i} \exp\left(-\frac{E_{a,i}}{R T_{\mathrm{R}}}\right) [\mathrm{A}]^{n_{\mathrm{A},i}} [\mathrm{D}]^{n_{\mathrm{D},i}} (-\Delta H_{r,i}) V_{\mathrm{R}} \\
&\vdots \\
&\left.+ \frac{E_{a,M}}{R T_{\mathrm{R}}^2} k_{0,M} \exp\left(-\frac{E_{a,M}}{R T_{\mathrm{R}}}\right) [\mathrm{A}]^{n_{\mathrm{A},M}} [\mathrm{G}]^{n_{\mathrm{G},M}} (-\Delta H_{r,M}) V_{\mathrm{R}} - UA\right]
\end{aligned} \tag{4.6}$$

The expression given in Equation (4.6) can be further generalised to give the following expression:

$$\begin{aligned}
\operatorname{div}[\mathbf{J}] t_{\mathrm{ref}} = &- (\nu_{\mathrm{A},1} n_{\mathrm{A},1} \mathrm{Da}_{\mathrm{A},1} + \nu_{\mathrm{B},1} n_{\mathrm{B},1} \mathrm{Da}_{\mathrm{B},1}) \exp(-\gamma_1) \\
&\vdots \\
&- (\nu_{\mathrm{A},i} n_{\mathrm{A},i} \mathrm{Da}_{\mathrm{A},i} + \nu_{\mathrm{D},i} n_{\mathrm{D},i} \mathrm{Da}_{\mathrm{D},i}) \exp(-\gamma_i) \\
&\vdots \\
&- (\nu_{\mathrm{A},M} n_{\mathrm{A},M} \mathrm{Da}_{\mathrm{A},M} + \nu_{\mathrm{G},M} n_{\mathrm{G},M} \mathrm{Da}_{\mathrm{G},M}) \exp(-\gamma_M) \\
&+ \sum_{i=1}^{M} (B_i \gamma_i \mathrm{Da}_{\mathrm{A},i} \exp(-\gamma_i)) - \mathrm{St}
\end{aligned} \tag{4.7}$$

where

$$B_i = \frac{[\mathrm{A}]\,(-\Delta H_{r,i})}{\rho_\mathrm{R} C_{p,\mathrm{R}} T_\mathrm{R}} \tag{4.8a}$$

$$\gamma_i = \frac{E_{a,i}}{R T_\mathrm{R}} \tag{4.8b}$$

$$\mathrm{Da}_{\mathrm{A},i} = k_{0,i}\,[\mathrm{A}]^{n_{\mathrm{A},i}-1}\,[\mathrm{D}]^{n_{\mathrm{D},i}}\,t_\mathrm{ref} \tag{4.8c}$$

$$\mathrm{Da}_{\mathrm{D},i} = k_{0,i}\,[\mathrm{A}]^{n_{\mathrm{A},i}}\,[\mathrm{D}]^{n_{\mathrm{D},i}-1}\,t_\mathrm{ref} \tag{4.8d}$$

$$\mathrm{St} = \frac{UA}{\rho_\mathrm{R} C_{p,\mathrm{R}} V_\mathrm{R}} t_\mathrm{ref} \tag{4.8e}$$

where B_i is the Barkelew number of reaction i, γ_i is the Arrhenius number of reaction i, $\mathrm{Da}_{\mathrm{A},i}$ and $\mathrm{Da}_{\mathrm{D},i}$ are the Damköhler numbers for reaction i for reagents A and D, respectively, St is the Stanton number, and t_ref is a reference time ensuring each variable in Equation (4.7) is dimensionless.

In the general case the components so far given as A, B, G and H in Equation (4.4), are denoted by index j. In Equation (4.7) it is seen that one Damköhler number is present for each reagent per reaction, each having the same Arrhenius pre-exponential factor of $k_{0,i}$. A resultant Damköhler number $\mathrm{Da}_{\mathrm{res},i}$ can be introduced to simplify the expression for the divergence by summarising the effect of the single reaction:

$$\mathrm{Da}_{\mathrm{res},i} = \nu_{\mathrm{A},i}\, n_{\mathrm{A},i}\, \mathrm{Da}_{\mathrm{A},i} + \nu_{\mathrm{D},i}\, n_{\mathrm{D},i}\, \mathrm{Da}_{\mathrm{D},i} \tag{4.9}$$

The general expression for the resultant Damköhler number of reaction i is given by:

$$\mathrm{Da}_{\mathrm{res},i} = \sum_{j=1}^{N} \left(\nu_{j,i} n_{j,i} \mathrm{Da}_{j,i}\right), \qquad i = 1,2,...,M \tag{4.10}$$

The resultant Damköhler number for reaction i, $\mathrm{Da}_{\mathrm{res},i}$, is required when analysing the effect of the Arrhenius pre-exponential factor $k_{0,i}$.

The divergence of the Jacobian for a multi-reaction system can be generalised for M reactions with a total of N reagents, each with their respective reaction orders and stoichiometric coefficients. When looking at Equation (4.7), the generalised form of the divergence is given by the following equation:

$$\mathrm{div}\,[\mathbf{J}]\,t_\mathrm{ref} = \sum_{i=1}^{M} \left(\left[\sum_{j=1}^{N} \left(-\nu_{j,i} n_{j,i}\, \mathrm{Da}_{j,i}\right) + B_i\, \gamma_i\, \mathrm{Da}_{l,i} \right] \exp\left(-\gamma_i\right) \right) - \mathrm{St} \tag{4.11}$$

where $\mathrm{Da}_{l,i}$ represents a Damköhler number which is not zero for the i^{th} reaction. Not every reactant present in the system will contribute towards reaction i. Hence it is necessary to choose a reagent l that does not have zero order for reaction i resulting in $\mathrm{Da}_{l,i}$. The expression given in Equation (4.11) is used for the further generalisation of thermal stability criterion $\mathscr{K}$.

From Equation (4.11) it can be seen that every reaction i contributes to the total divergence of the system. Solely the Stanton number, St, appears once as this is representing the cooling of the reactor. The individual part of the divergence of the Jacobian related to each reaction i, denoted $\mathscr{D}_i$, is given by:

$$\mathscr{D}_i = \left[\sum_{j=1}^{N} \left(-\nu_{j,i} n_{j,i} \mathrm{Da}_{j,i} \right) + B_i \gamma_i \mathrm{Da}_{l,i} \right] \exp\left(-\gamma_i\right) \tag{4.12}$$

Using Equations (4.11) and (4.12), the final form of the total divergence of the Jacobian for a multiple reaction system can be summarised by the following:

$$\mathrm{div}\left[\mathbf{J}\right] t_{\mathrm{ref}} = \sum_{i=1}^{M} \mathscr{D}_i t_{\mathrm{ref}} - \mathrm{St} \tag{4.13}$$

Equation (4.13) will be used in the generalisation of thermal stability criterion $\mathscr{K}$.

4.3 Thermal stability criterion $\mathscr{K}$ for reaction scheme 1

In this section the general expression of the divergence of the Jacobian, given in Equation (4.13), is used to formulate the function of the divergence estimate $\mathscr{E}$. The expression for $\mathscr{E}$ is used to find criterion $\mathscr{K}$. The necessary coefficients are found and this form of criterion $\mathscr{K}$ is tested with the example thermal runaway reactions shown in Section 2.4.

4.3.1 Derivation of criterion $\mathscr{K}$

Using Equation (4.13) and Section 3.3.1, the function of the divergence criterion for reaction scheme 1 can be written as:

$$\mathrm{div}\left[\mathbf{J}\right] t_{\mathrm{ref}} = f\left(B, \mathrm{Da}_{\mathrm{res}}, \gamma, \mathrm{St}\right) \tag{4.14}$$

The function for the estimate of the divergence, $\mathscr{E}$, therefore is a function of the variables $\mathrm{Da_{res}}$, B, γ and St, as given in Equation (4.3). In the case of reaction scheme 1 there is only reagent A taking part in the reaction. Therefore the resultant Damköhler number is given by:

$$\mathrm{Da_{res}} = \nu_{\mathrm{A}} n_{\mathrm{A}} \mathrm{Da_A} \tag{4.15}$$

In the following analysis the effect of varying the reaction rate constant k_0, the enthalpy of reaction ΔH_r, the heat transfer coefficient U, and the activation energy E_a are considered. Taking the total derivative of Equation (4.14) gives the following:

$$\begin{aligned}\mathrm{d}\left(\mathrm{div}\left[\mathbf{J}\right]t_{\mathrm{ref}}\right) = &\left(\frac{\partial\left(\mathrm{div}\left[\mathbf{J}\right]t_{\mathrm{ref}}\right)}{\partial\left(B\right)}\right)_{\mathrm{Da_{res}},\gamma,\mathrm{St}}\mathrm{d}\left(B\right) + \left(\frac{\partial\left(\mathrm{div}\left[\mathbf{J}\right]t_{\mathrm{ref}}\right)}{\partial\left(\mathrm{Da_{res}}\right)}\right)_{B,\gamma,\mathrm{St}}\mathrm{d}\left(\mathrm{Da_{res}}\right)\\ &+\left(\frac{\partial\left(\mathrm{div}\left[\mathbf{J}\right]t_{\mathrm{ref}}\right)}{\partial\left(\gamma\right)}\right)_{B,\mathrm{Da_{res}},\mathrm{St}}\mathrm{d}\left(\gamma\right) + \left(\frac{\partial\left(\mathrm{div}\left[\mathbf{J}\right]t_{\mathrm{ref}}\right)}{\partial\left(\mathrm{St}\right)}\right)_{B,\mathrm{Da_{res}},\gamma}\mathrm{d}\left(\mathrm{St}\right)\end{aligned} \tag{4.16}$$

To reformulate the expression given in Equation (4.16) into the required form given by Equation (4.3), the differential of a logarithm has to be introduced:

$$\mathrm{d}\ln x^{(s)} = \frac{\mathrm{d}x^{(s)}}{x^{(s-1)}} = \lim_{\Delta x^{(s)}\to 0}\frac{\Delta x^{(s)}}{x^{(s-1)}} \approx \frac{x^{(s)}-x^{(s-1)}}{x^{(s-1)}} \tag{4.17}$$

Equation (4.16) can hence be re-written in terms of logarithms:

$$\begin{aligned}\mathrm{d}\ln\left(\mathrm{div}\left[\mathbf{J}\right]t_{\mathrm{ref}}\right) = &\left(\frac{\partial\ln\left(\mathrm{div}\left[\mathbf{J}\right]t_{\mathrm{ref}}\right)}{\partial\ln\left(B\right)}\right)_{\mathrm{Da_{res}},\gamma,\mathrm{St}}\mathrm{d}\ln\left(B\right)\\ &+\left(\frac{\partial\ln\left(\mathrm{div}\left[\mathbf{J}\right]t_{\mathrm{ref}}\right)}{\partial\ln\left(\mathrm{Da_{res}}\right)}\right)_{B,\gamma,\mathrm{St}}\mathrm{d}\ln\left(\mathrm{Da_{res}}\right)\\ &+\left(\frac{\partial\ln\left(\mathrm{div}\left[\mathbf{J}\right]t_{\mathrm{ref}}\right)}{\partial\ln\left(\gamma\right)}\right)_{B,\mathrm{Da_{res}},\mathrm{St}}\mathrm{d}\ln\left(\gamma\right)\\ &+\left(\frac{\partial\ln\left(\mathrm{div}\left[\mathbf{J}\right]t_{\mathrm{ref}}\right)}{\partial\ln\left(\mathrm{St}\right)}\right)_{B,\mathrm{Da_{res}},\gamma}\mathrm{d}\ln\left(\mathrm{St}\right)\end{aligned} \tag{4.18}$$

where

$$m_B = \left(\frac{\partial \ln\left(\operatorname{div}\left[\mathbf{J}\right] t_{\mathrm{ref}}\right)}{\partial \ln\left(B\right)} \right)_{\mathrm{Da_{res}},\,\gamma,\,\mathrm{St}} \tag{4.19a}$$

$$m_{\mathrm{Da_{res}}} = \left(\frac{\partial \ln\left(\operatorname{div}\left[\mathbf{J}\right] t_{\mathrm{ref}}\right)}{\partial \ln\left(\mathrm{Da_{res}}\right)} \right)_{B,\,\gamma,\,\mathrm{St}} \tag{4.19b}$$

$$m_\gamma = \left(\frac{\partial \ln\left(\operatorname{div}\left[\mathbf{J}\right] t_{\mathrm{ref}}\right)}{\partial \ln\left(\gamma\right)} \right)_{B,\,\mathrm{Da_{res}},\,\mathrm{St}} \tag{4.19c}$$

$$m_{\mathrm{St}} = \left(\frac{\partial \ln\left(\operatorname{div}\left[\mathbf{J}\right] t_{\mathrm{ref}}\right)}{\partial \ln\left(\mathrm{St}\right)} \right)_{B,\,\mathrm{Da_{res}},\,\gamma} \tag{4.19d}$$

where m_B, $m_{\mathrm{Da_{res}}}$, m_γ, and m_{St} are the gradient coefficients with respect to each dimensionless variable.

The function for $\mathscr{E}^{(s)}$ is an estimate of the divergence at time step (s). This means that, as shown in Figure 4.1, the divergence of the Jacobian matrix in step $(s-1)$ and the gradient information of the divergence are used to calculate the value of $\mathscr{E}$ in time step (s). Using the differential of a logarithm in Equation (4.17) to approximate how the divergence of the Jacobian behaves at the boundary of stability, $\mathscr{E}^{(s)}$ can be written as:

$$\mathrm{d}\ln\left(\operatorname{div}\left[\mathbf{J}^{(s)}\right] t_{\mathrm{ref}}\right) = \frac{\mathscr{E}^{(s)} - \operatorname{div}\left[\mathbf{J}^{(s-1)}\right]}{\operatorname{div}\left[\mathbf{J}^{(s-1)}\right]} \tag{4.20a}$$

$$\mathscr{E}^{(s)} = \operatorname{div}\left[\mathbf{J}^{(s-1)}\right] + \operatorname{div}\left[\mathbf{J}^{(s-1)}\right] \mathrm{d}\ln\left(\operatorname{div}\left[\mathbf{J}^{(s)}\right] t_{\mathrm{ref}}\right) \tag{4.20b}$$

With the expression found for $\mathrm{d}\ln\left(\operatorname{div}\left[\mathbf{J}^{(s)}\right] t_{\mathrm{ref}}\right)$ based on a Taylor series expansion, Equation (4.18) is inserted into Equation (4.20b) to obtain:

$$\begin{aligned}\mathscr{E}^{(s)} = \operatorname{div}\left[\mathbf{J}^{(s-1)}\right] \Bigg(1 + m_B \frac{B^{(s)} - B^{(s-1)}}{B^{(s-1)}} + m_{\mathrm{Da_{res}}} \frac{\mathrm{Da_{res}}^{(s)} - \mathrm{Da_{res}}^{(s-1)}}{\mathrm{Da_{res}}^{(s-1)}} + \\ m_\gamma \frac{\gamma^{(s)} - \gamma^{(s-1)}}{\gamma^{(s-1)}} + m_{\mathrm{St}} \frac{\mathrm{St}^{(s)} - \mathrm{St}^{(s-1)}}{\mathrm{St}^{(s-1)}}\Bigg)\end{aligned} \tag{4.21}$$

The stability criterion $\mathscr{K}$ can now be evaluated as the difference of the actual divergence of the Jacobian and the correction function at time step (s):

$$\mathscr{K}^{(s)} = \operatorname{div}\left[\mathbf{J}^{(s)}\right] - \left|\mathscr{E}^{(s)}\right| \tag{4.22}$$

The values of coefficients m_B, $m_{\mathrm{Da_{res}}}$, m_γ, and m_{St} are evaluated in the next section.

4.3.2 Evaluation of gradient coefficients m_B, m_γ, $m_{\mathrm{Da_{res}}}$, and m_{St}

The coefficients m_B, $m_{\mathrm{Da_{res}}}$, m_γ and m_{St} are evaluated as the gradients of the function $\ln(\mathrm{div}\,[\mathbf{J}]\,t_{\mathrm{ref}})$ with respect to variables B, $\mathrm{Da_{res}}$, γ and St, as given by Equation (4.18). The gradient coefficients are evaluated at the point where the system becomes unstable for processes $\mathrm{P}_1^1 - \mathrm{P}_{15}^1$.

The first coefficient m_B is evaluated at the boundary of stability while keeping the values of $\mathrm{Da_{res}}$, γ and St constant, as shown in Equation (4.19a). The gradients of $\ln(\mathrm{div}\,[\mathbf{J}]\,t_{\mathrm{ref}})$ with respect to $\ln(B)$ for processes $\mathrm{P}_6^1 - \mathrm{P}_{10}^1$ are shown in Figure 4.2.

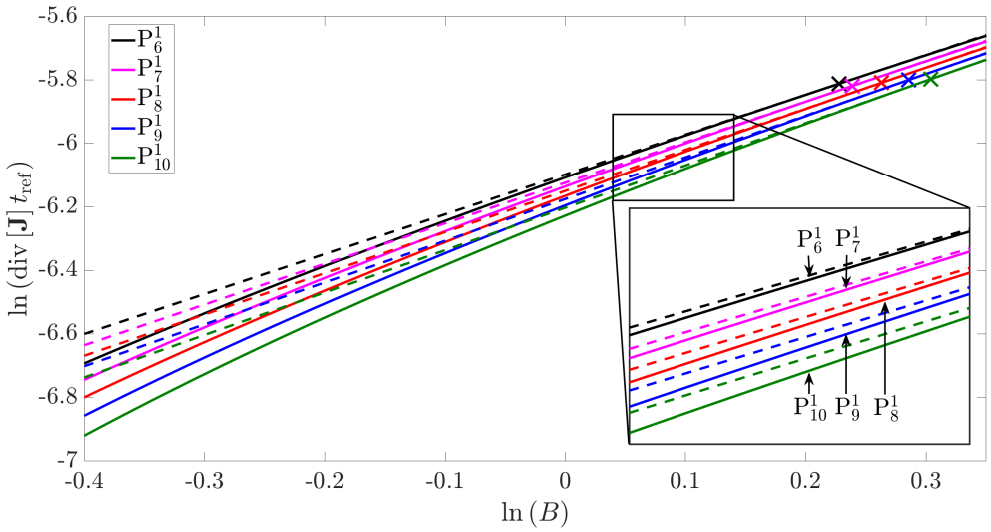

Fig. 4.2 Variation of the natural logarithm of the divergence with respect to $\ln(B)$ for processes $\mathrm{P}_6^1 - \mathrm{P}_{10}^1$. The crosses indicate the points at the boundary of instability, and the dashed lines indicate the gradient at these points.

From Figure 4.2 it can be seen that the gradients at the boundary of instability are approximately parallel for processes $\mathrm{P}_6^1 - \mathrm{P}_{10}^1$. A similar result is obtained for processes $\mathrm{P}_1^1 - \mathrm{P}_5^1$ and $\mathrm{P}_{11}^1 - \mathrm{P}_{15}^1$ for the variation of $\ln(\mathrm{div}\,[\mathbf{J}]\,t_{\mathrm{ref}})$ with $\ln(B)$.

The second coefficient $m_{\mathrm{Da_{res}}}$ is evaluated at the boundary of stability while keeping the values of B, γ and St constant, as shown in Equation (4.19b). The gradients of $\ln(\mathrm{div}\,[\mathbf{J}]\,t_{\mathrm{ref}})$ with respect to $\ln(\mathrm{Da_{res}})$ for processes $\mathrm{P}_6^1 - \mathrm{P}_{10}^1$ are shown in Figure 4.3.

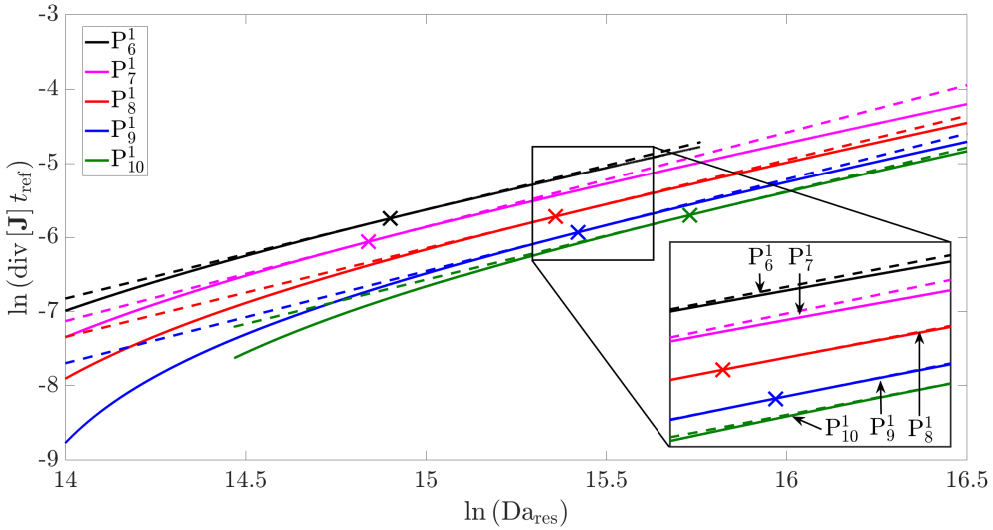

Fig. 4.3 Variation of the natural logarithm of the divergence with respect to $\ln(\mathrm{Da}_{\mathrm{res}})$ for processes $P_6^1 - P_{10}^1$. The crosses indicate the points at the boundary of instability, and the dashed lines indicate the gradient at these points.

In Figure 4.3 it can be seen that the values of $\mathrm{Da}_{\mathrm{res}}$, at which the system becomes unstable, are different for each process. The gradients obtained at these points are still approximately parallel for processes $P_6^1 - P_{10}^1$. Similar results are obtained for processes $P_1^1 - P_5^1$ and $P_{11}^1 - P_{15}^1$.

The third coefficient m_γ is evaluated at the boundary of stability while keeping the values of B, $\mathrm{Da}_{\mathrm{res}}$ and St constant, as shown in Equation (4.19c). The gradients of $\ln(\mathrm{div}[\mathbf{J}]\, t_{\mathrm{ref}})$ with respect to $\ln(\gamma)$ for processes $P_6^1 - P_{10}^1$ are shown in Figure 4.4.

The values of γ at which processes $P_6^1 - P_{10}^1$ becomes unstable are different for each process. Still, the gradients of $\ln(\mathrm{div}[\mathbf{J}]\, t_{\mathrm{ref}})$ at these points are parallel as can be seen in Figure 4.4. The same conclusions can be made about the results obtained for processes $P_1^1 - P_5^1$ and $P_{11}^1 - P_{15}^1$.

The fourth coefficient m_{St} is evaluated at the boundary of stability while keeping the values of B, γ and $\mathrm{Da}_{\mathrm{res}}$ constant, as shown in Equation (4.19d). The gradients of $\ln(\mathrm{div}[\mathbf{J}]\, t_{\mathrm{ref}})$ with respect to $\ln(\mathrm{St})$ for processes $P_6^1 - P_{10}^1$ are shown in Figure 4.5.

The gradients obtained at the point of instability for the variable St are again approximately parallel for processes $P_6^1 - P_{10}^1$. As was the case for the calculations of the previous three coefficients there is a good match for m_{St} obtained for processes $P_1^1 - P_5^1$ and $P_{11}^1 - P_{15}^1$.

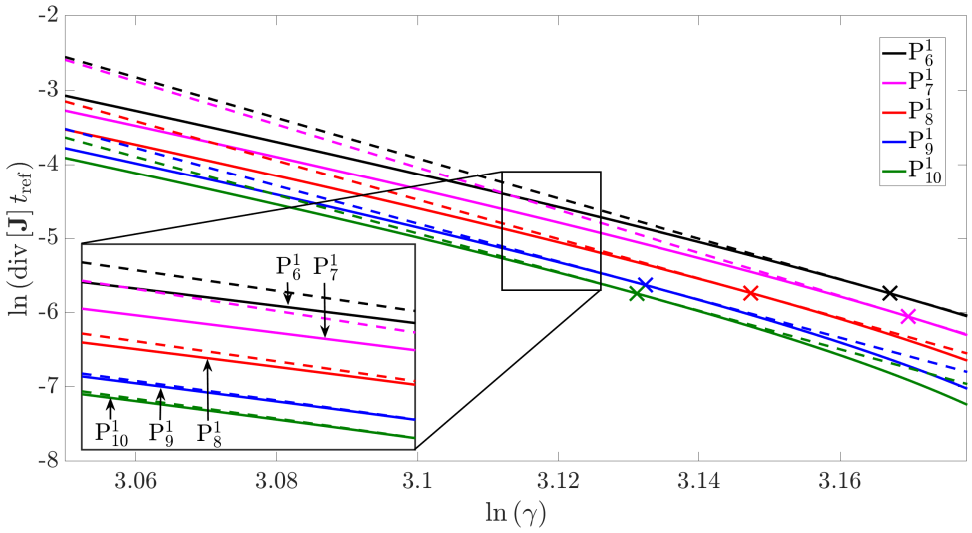

Fig. 4.4 Variation of the natural logarithm of the divergence with respect to $\ln(\gamma)$ for processes $P_6^1 - P_{10}^1$. The crosses indicate the points at the boundary of instability, and the dashed lines indicate the gradient at these points.

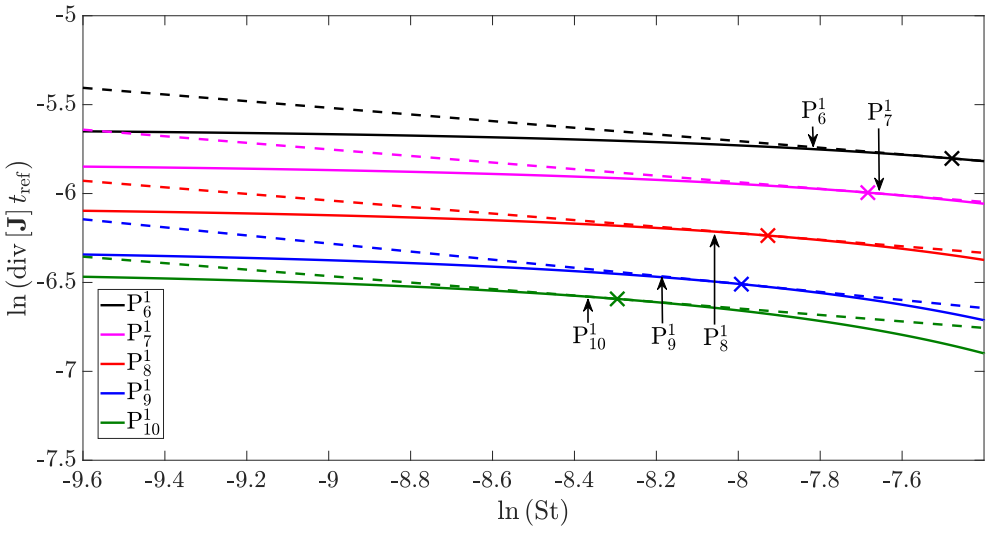

Fig. 4.5 Variation of the natural logarithm of the divergence with respect to $\ln(\mathrm{St})$ for processes $P_6^1 - P_{10}^1$. The crosses indicate the points at the boundary of instability, and the dashed lines indicate the gradient at these points.

If the gradients are parallel, the gradient coefficients obtained are very close to each other, hence making the assumption of using a single value of m reasonable in order to characterise the behaviour of the batch reactor system at the boundary of stability. The fact that the lines obtained for each variable give a very similar gradient value is promising and gives a good foundation for the use of the stability criterion $\mathscr{K}$. The coefficient values with their averages and deviations are summarised in Table 4.1.

Table 4.1 Values of coefficients for processes $P_1^1 - P_{15}^1$, including averages (Avg) and deviations (Dev).

Process	m_B	m_γ	$m_{\mathrm{Da_{res}}}$	m_{St}	Process	m_B	m_γ	$m_{\mathrm{Da_{res}}}$	m_{St}
P_1^1	1.24	−27.0	1.19	−0.187	P_{10}^1	1.33	−26.0	1.19	−0.180
P_2^1	1.27	−26.9	1.19	−0.186	P_{11}^1	1.26	−27.3	1.20	−0.189
P_3^1	1.29	−26.9	1.19	−0.186	P_{12}^1	1.26	−27.2	1.20	−0.191
P_4^1	1.24	−26.8	1.19	−0.187	P_{13}^1	1.26	−27.2	1.20	−0.187
P_5^1	1.33	−27.0	1.19	−0.184	P_{14}^1	1.26	−27.2	1.20	−0.188
P_6^1	1.25	−27.2	1.21	−0.191	P_{15}^1	1.26	−27.2	1.20	−0.188
P_7^1	1.38	−27.0	1.27	−0.185					
P_8^1	1.30	−26.6	1.20	−0.184	Avg	1.28	−26.9	1.21	−0.187
P_9^1	1.32	−26.0	1.19	−0.182	Dev	±0.07	±0.67	±0.04	±0.01

Although each of processes $P_1^1 - P_{15}^1$ has very different kinetic parameters and reaction orders, the gradient coefficients are almost equal for each process. Differences in the gradient coefficient values are obtained for two reasons: firstly differences in each process will lead to slight differences in coefficient values. Secondly, and more importantly, detecting the exact point at which thermal instability occurs cannot be found with 100% accuracy, but it is found by trial and error. This is assumed to be the major source of the deviations for coefficients m_B, $m_{\mathrm{Da_{res}}}$, m_γ and m_{St}.

Due to the variation of variables B, Da, γ and St in a broad spectrum the coefficients m_B, $m_{\mathrm{Da_{res}}}$, m_γ and m_{St} are suggested to be used for the stability function of exothermic batch processes with reaction kinetics mainly dependent on a single component.

4.3.3 Verification of criterion $\mathscr{K}$ for reaction scheme 1

In this section the function of thermal stability criterion $\mathscr{K}$, given in Equation (4.22), and the coefficients found in Table 4.1 are verified using the thermal runaway reactions for reaction scheme 1 shown in Section 2.4.

Important to note for this analysis is at which time criterion $\mathscr{K}$ identifies thermal runaway behaviour, and when the real system becomes thermally unstable. The profiles for criterion $\mathscr{K}$ for processes $P_1^1 - P_5^1$, relating to temperature profiles in Figure 2.2, are shown in Figure 4.6.

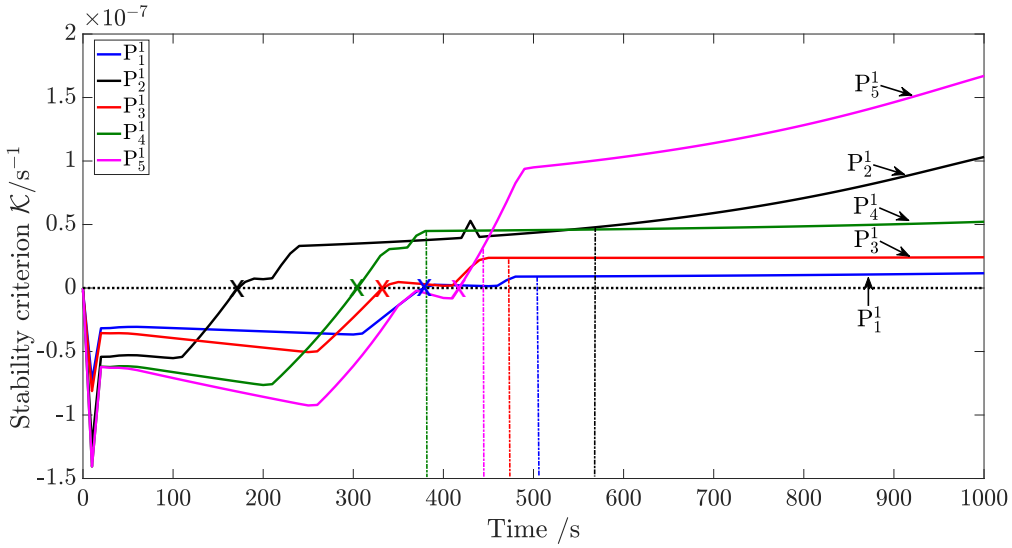

Fig. 4.6 Profiles of stability criterion $\mathscr{K}$ for processes $P_1^1 - P_5^1$. The vertical lines indicate where each process becomes unstable, according to temperature profiles in Figure 2.2. The crosses indicate where criterion $\mathscr{K}$ identifies the beginning of thermal runaway behaviour.

In Figure 4.6 it is seen that the crosses, indicating when criterion $\mathscr{K}$ identifies thermal instability, occur before the vertical dash-dotted lines, representing when the system actually becomes unstable. There is a gap of approximately 100 s, apart from process P_2^1 where the gap is 350 s. This would give enough time for an advanced control system to react to potential thermal runaway behaviour. Therefore, the coefficients found in Table 4.1 result in a conservative measure of stability. How conservative this measure is will be evident when process intensification is considered. The profiles for criterion $\mathscr{K}$ for processes $P_6^1 - P_{10}^1$, relating to temperature profiles in Figure 2.3, are shown in Figure 4.7.

In Figure 4.7 it is seen again that thermal instability is predicted before it occurs. Interesting to note is the profile of $\mathscr{K}$ for processes P_9^1 and P_{10}^1: as the thermal runaway occurs, the value of criterion $\mathscr{K}$ decreases. This is the case because the reaction occurring is so fast that the reagents are consumed at an increased rate. Therefore the potential to cause thermal runaways decreases, reducing the value of criterion $\mathscr{K}$.

Hence, for reaction scheme 1 the form of thermal stability criterion $\mathscr{K}$ is shown to work for batch processes.

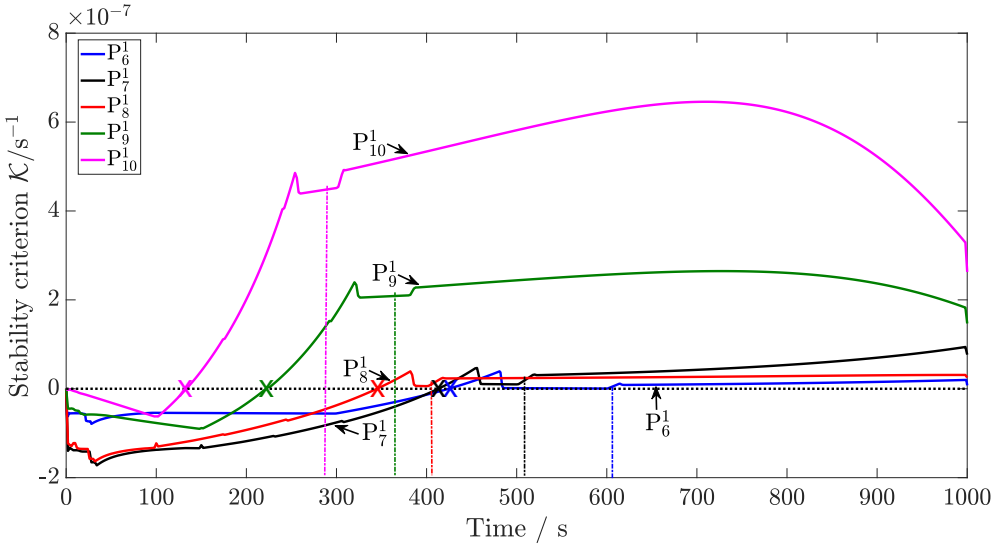

Fig. 4.7 Profiles of stability criterion $\mathscr{K}$ for processes $P_6^1 - P_{10}^1$. The vertical lines indicate where each process becomes unstable, according to temperature profiles in Figure 2.3. The crosses indicate where criterion $\mathscr{K}$ identifies the beginning of thermal runaway behaviour.

4.4 Thermal stability criterion $\mathscr{K}$ for reaction scheme 2

Reaction scheme 2, with respect to reaction scheme 1, introduces one more reagent B into the single reaction occurring. To account for this increase in complexity, the only difference in the derivation of criterion $\mathscr{K}$ is the expression for the resultant Damköhler number. For reaction scheme 2 the resultant Damköhler number is given by:

$$\mathrm{Da}_{\mathrm{res}} = \nu_{\mathrm{A}} n_{\mathrm{A}} \mathrm{Da}_{\mathrm{A}} + \nu_{\mathrm{B}} n_{\mathrm{B}} \mathrm{Da}_{\mathrm{B}} \tag{4.23}$$

Apart from this difference, the derivation outlined in Equations (4.18)−(4.22) is identical for reaction scheme 2.

The issue now becomes if the gradient coefficients found for this reaction scheme are similar to those found for reaction scheme 1. This is examined in detail in the following section.

4.4.1 Evaluation of gradient coefficients m_B, m_γ, $m_{\mathrm{Da}_{\mathrm{res}}}$, and m_{St}

The gradient at the boundary of stability with respect to the Damköhler number, $\mathrm{Da}_{\mathrm{res}}$, is analysed first. To combine the influence of both reactants A and B, $\mathrm{Da}_{\mathrm{res}}$ is given by

Equation (4.10). In contrast to the base processes $P_1^2 - P_{20}^2$, first the pre-exponential Arrhenius coefficient k_0 is increased until loss of stability. A thermal runaway is caused by increasing the rate of reaction until the heat generated by the reaction exceeds the cooling capacity. All remaining parameters of each process are kept constant. The variations in $\ln(\mathrm{div}[\mathbf{J}]t_{\mathrm{ref}})$ with respect to $\ln(\mathrm{Da}_{\mathrm{res}})$ for processes $P_1^2 - P_5^2$ are given in Figure 4.8.

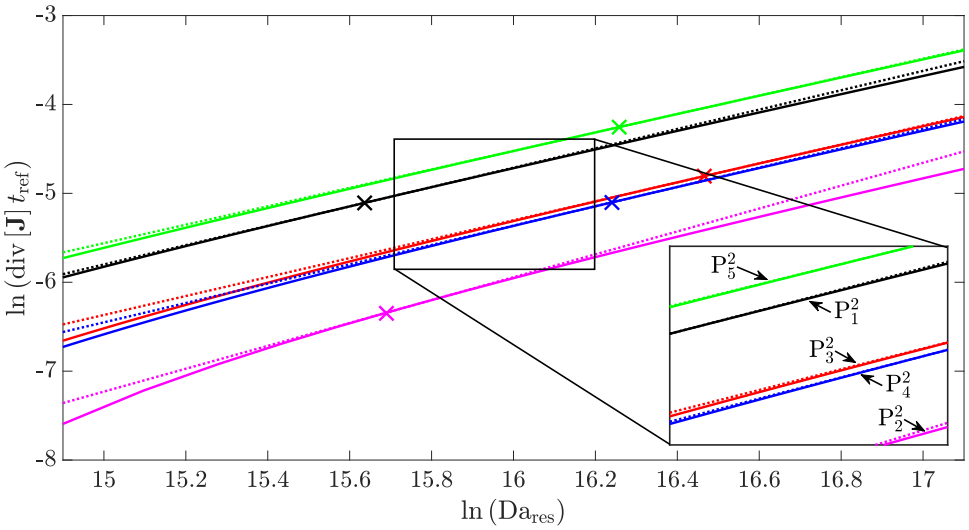

Fig. 4.8 Variation of $\ln(\mathrm{div}[\mathbf{J}]t_{\mathrm{ref}})$ with respect to $\ln(\mathrm{Da}_{\mathrm{res}})$ for processes $P_1^2 - P_5^2$. The crosses indicate the points at the boundary of instability, and the dashed lines indicate the gradient at these points.

At the point where systems $P_1^2 - P_{20}^2$ become unstable the value of $\mathrm{Da}_{\mathrm{res}}$ is recorded and the gradient of $\ln(\mathrm{div}[\mathbf{J}]t_{\mathrm{ref}})$ at that point is found. This is indicated in Figure 4.8 as dashed lines. As can be seen, the lines are close to parallel. Therefore, the most conservative gradient obtained will give a good description of the divergence at the boundary of stability. Similar profiles and gradients are obtained for processes $P_6^2 - P_{20}^2$, as will be shown below. The evaluated gradient coefficients $m_{\mathrm{Da}_{\mathrm{res}}}$ for $\ln(\mathrm{div}[\mathbf{J}]t_{\mathrm{ref}})$ with respect to $\ln(\mathrm{Da}_{\mathrm{res}})$ at the boundary of stability for processes $P_1^2 - P_{20}^2$ are shown in Table 4.2.

Table 4.2 Gradient coefficient $m_{\mathrm{Da}_{\mathrm{res}}}$ values for processes $P_1^2 - P_{20}^2$.

Process	P_1^2	P_2^2	P_3^2	P_4^2	P_5^2	P_6^2	P_7^2	P_8^2	P_9^2	P_{10}^2
$m_{\mathrm{Da}_{\mathrm{res}}}$	1.09	1.13	1.05	1.04	1.04	1.11	1.11	1.08	1.13	1.13
Process	P_{11}^2	P_{12}^2	P_{13}^2	P_{14}^2	P_{15}^2	P_{16}^2	P_{17}^2	P_{18}^2	P_{19}^2	P_{20}^2
$m_{\mathrm{Da}_{\mathrm{res}}}$	1.13	1.16	1.08	1.03	1.04	1.15	1.09	1.16	1.11	1.09

The most conservative gradient coefficients are guaranteed to ensure stability for the processes examined. Hence the smallest values in magnitude for $m_{\mathrm{Da_{res}}}$ and all remaining gradient coefficients are chosen to evaluate $\mathscr{E}$. Therefore a value of $m_{\mathrm{Da_{res}}} = 1.03$ is used for thermal stability detection of processes in reaction scheme 2.

For the dependence on the divergence of the Jacobian matrix with respect to the Barkelew number B the same logic is applied as for the Damköhler number. In processes $\mathrm{P}_1^2 - \mathrm{P}_{20}^2$ the enthalpy of reaction ΔH_r is varied until a thermal runaway occurs. All remaining parameters are kept constant during this analysis. The profiles of $\ln(\mathrm{div}\,[\mathbf{J}]\,t_{\mathrm{ref}})$ with respect to $\ln(B)$ for processes $\mathrm{P}_1^2 - \mathrm{P}_5^2$ are given in Figure 4.9.

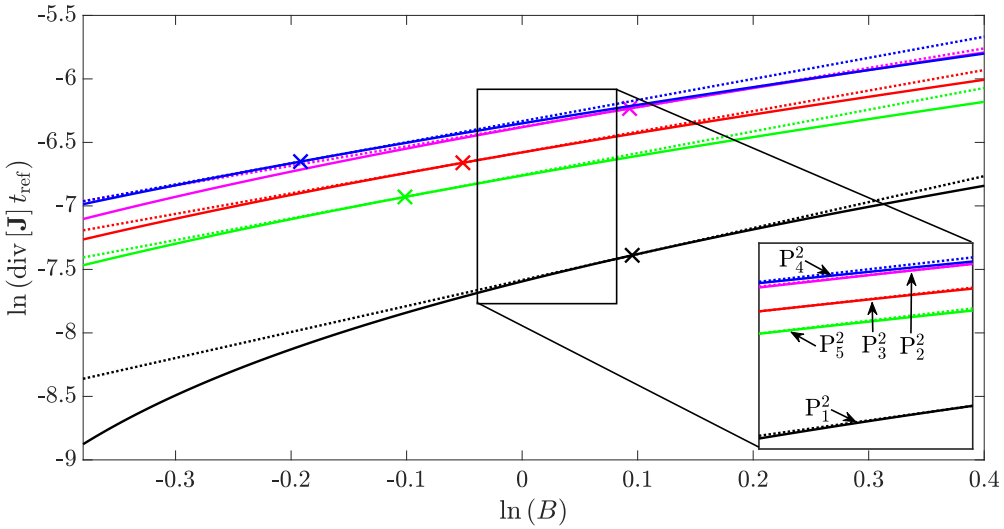

Fig. 4.9 Variation of $\ln(\mathrm{div}\,[\mathbf{J}]\,t_{\mathrm{ref}})$ with respect to $\ln(B)$ for processes $\mathrm{P}_1^2 - \mathrm{P}_5^2$. The crosses indicate the points at the boundary of instability, and the dashed lines indicate the gradient at these points.

As for the Damköhler number, the lines obtained for processes $\mathrm{P}_1^2 - \mathrm{P}_5^2$ at the boundary of stability are nearly parallel. The same behaviour is observed for processes $\mathrm{P}_6^2 - \mathrm{P}_{20}^2$. The values of m_B for this reaction scheme are given in Table 4.3.

Table 4.3 Gradient coefficient m_B values for processes $\mathrm{P}_1^2 - \mathrm{P}_{20}^2$.

Process	P_1^2	P_2^2	P_3^2	P_4^2	P_5^2	P_6^2	P_7^2	P_8^2	P_9^2	P_{10}^2
m_B	2.05	1.54	1.62	1.66	1.71	1.55	1.55	1.67	1.60	1.72
Process	P_{11}^2	P_{12}^2	P_{13}^2	P_{14}^2	P_{15}^2	P_{16}^2	P_{17}^2	P_{18}^2	P_{19}^2	P_{20}^2
m_B	1.57	1.47	1.53	1.58	1.80	1.34	1.30	1.35	1.28	1.34

In order to get a conservative estimate of the divergence value at the boundary of stability, the most conservative gradient value from the ones found in Table 4.3 is used, *i.e.* specifically $m_B = 1.28$.

The reduction in activation energy E_a increases the reaction rate, hence resulting in more heat generation. Once the heat generated exceeds the cooling capacity of the system and a thermal runaway occurs, the respective value of E_a is recorded. All remaining parameters are kept constant during this analysis. The profiles of $\ln(\mathrm{div}[\mathbf{J}]t_{\mathrm{ref}})$ with respect to the Arrhenius number $\ln(\gamma)$ for processes $\mathrm{P}_1^2 - \mathrm{P}_5^2$ are given in Figure 4.10.

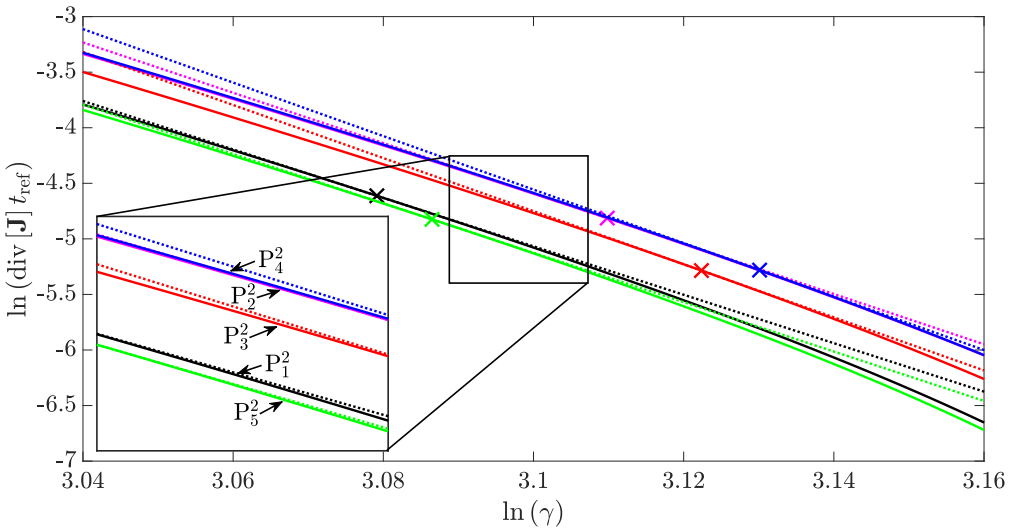

Fig. 4.10 Variation of $\ln(\mathrm{div}[\mathbf{J}]t_{\mathrm{ref}})$ with respect to $\ln(\gamma)$ for processes $\mathrm{P}_1^2 - \mathrm{P}_5^2$. The crosses indicate the points at the boundary of instability, and the dashed lines indicate the gradient at these points.

As was observed above, the gradients obtained at the boundary of stability are very similar for all processes $\mathrm{P}_1^2 - \mathrm{P}_{20}^2$. The values of m_γ for this reaction scheme are given in Table 4.4.

Table 4.4 Gradient coefficient m_γ values for processes $\mathrm{P}_1^2 - \mathrm{P}_{20}^2$.

Process	P_1^2	P_2^2	P_3^2	P_4^2	P_5^2	P_6^2	P_7^2	P_8^2	P_9^2	P_{10}^2
m_γ	-21.8	-22.6	-23.9	-24.1	-22.2	-23.7	-23.8	-24.7	-24.7	-23.1
Process	P_{11}^2	P_{12}^2	P_{13}^2	P_{14}^2	P_{15}^2	P_{16}^2	P_{17}^2	P_{18}^2	P_{19}^2	P_{20}^2
m_γ	-22.4	-23.3	-22.5	-23.8	-22.2	-22.3	-23.05	-24.5	-24.3	-23.3

The most conservative value obtained from these processes is used in order to predict the value of the divergence close to the boundary of instability, *i.e.* specifically $m_\gamma = -21.8$.

The variation of $\mathrm{div}\,[\mathbf{J}]$ with respect to the Stanton number St for processes $\mathrm{P}_1^2 - \mathrm{P}_{20}^2$ is analysed by varying the heat transfer coefficient U with respect to the parameters of processes $\mathrm{P}_1^2 - \mathrm{P}_{20}^2$. The profiles obtained for $\ln(\mathrm{div}\,[\mathbf{J}]\,t_{\mathrm{ref}})$ with respect to $\ln(\mathrm{St})$ for processes $\mathrm{P}_1^2 - \mathrm{P}_5^2$ are given in Figure 4.11.

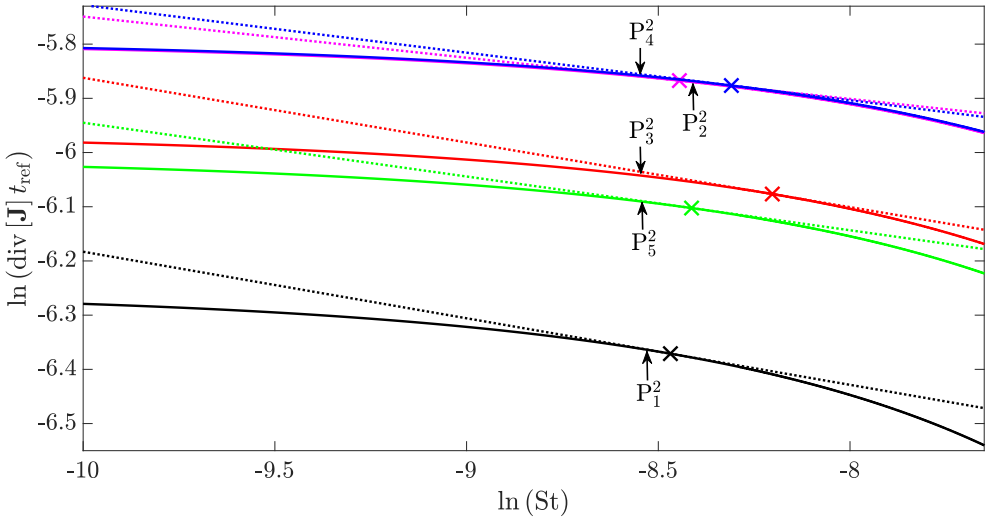

Fig. 4.11 Variation of $\ln(\mathrm{div}\,[\mathbf{J}]\,t_{\mathrm{ref}})$ with respect to $\ln(\mathrm{St})$ for processes $\mathrm{P}_1^2 - \mathrm{P}_5^2$. The crosses indicate the points at the boundary of instability, and the dashed lines indicate the gradient at these points.

The gradients obtained for $\ln(\mathrm{div}\,[\mathbf{J}]\,t_{\mathrm{ref}})$ at the boundary of stability were very close to each other. This is also the case for processes $\mathrm{P}_1^2 - \mathrm{P}_{20}^2$. The values obtained for the gradient coefficient m_{St} are shown in Table 4.5.

Table 4.5 Gradient coefficient m_{St} values for processes $\mathrm{P}_1^2 - \mathrm{P}_{20}^2$.

Process	P_1^2	P_2^2	P_3^2	P_4^2	P_5^2	P_6^2	P_7^2	P_8^2	P_9^2	P_{10}^2
$m_{\mathrm{St}}/0.1$	-1.83	-1.76	-1.90	-1.99	-1.99	-1.82	-1.86	-1.85	-1.89	-1.74
Process	P_{11}^2	P_{12}^2	P_{13}^2	P_{14}^2	P_{15}^2	P_{16}^2	P_{17}^2	P_{18}^2	P_{19}^2	P_{20}^2
$m_{\mathrm{St}}/0.1$	-1.89	-1.83	-1.86	-1.94	-1.89	-1.81	-1.75	-1.97	-1.91	-1.74

From Table 4.5 the most conservative gradient obtained can therefore be used to predict the value of the divergence as the system comes closer to the boundary of stability, *i.e.* specifically $m_{\mathrm{St}} = -0.174$.

The most conservative gradient coefficients are guaranteed to ensure stability for the processes examined. Hence the smallest values in magnitude from Tables 4.2−4.5 are chosen to be used for function $\mathscr{K}$. The gradient coefficients used for all following simulations throughout this thesis are given in Table 4.6.

Table 4.6 Most conservative gradient coefficients used for simulations.

Gradient coefficient	m_B	$m_{\mathrm{Da_{res}}}$	m_γ	m_{St}
Value	1.28	1.03	-21.8	-0.174

The results obtained for all gradient coefficients are in accord with the results obtained for reaction scheme 1. Small deviations in the values for $m_{\mathrm{Da_{res}}}$ and m_{St} are present. Both deviations result in a more conservative prediction of instability by criterion $\mathscr{K}$. A significant deviation of the value for m_γ is observed, which also results in a more conservative stability detection. The same value for m_B is obtained in this work as was done for reaction scheme 1. The differences in analysis with respect to reaction scheme 1 are obtained because the most conservative gradient coefficients are used, and not the average values. Furthermore, slight differences arise due to the complication that it is very difficult to find the exact point where stability is lost.

The reliability of predicting thermal runaway behaviour with stability criterion $\mathscr{K}$ for batch processes with reaction scheme 2 is analysed in detail in the following section.

4.4.2 Verification of criterion $\mathscr{K}$ for reaction scheme 2

Reaction scheme 2 consists of a single reaction, the rate of which depends on reagents A and B. Temperature profiles where examples of thermal runaways are shown are given in Figures 2.4 and 2.5. The respective profiles for thermal stability criterion $\mathscr{K}$ for processes $\mathrm{P}_1^2 - \mathrm{P}_5^2$ are shown in Figure 4.12.

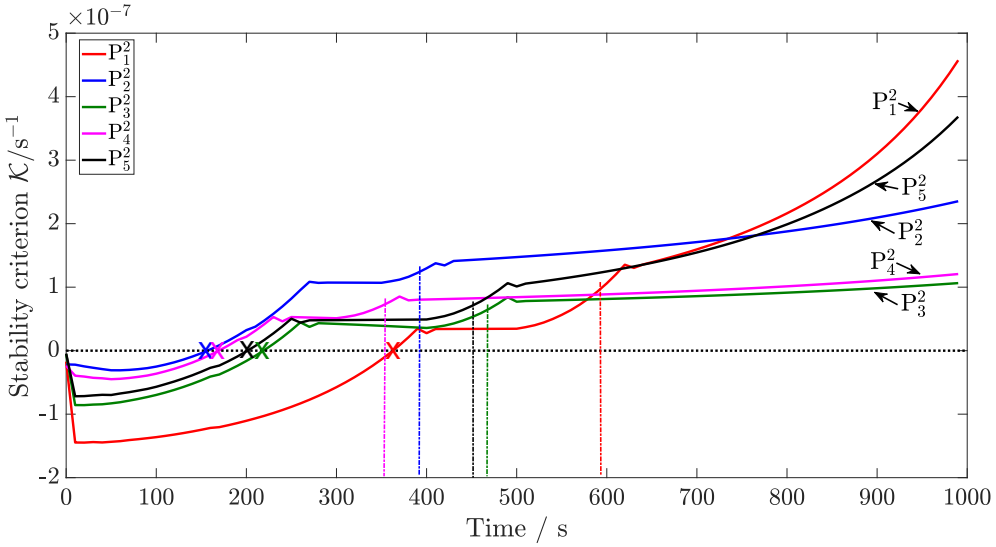

Fig. 4.12 Profiles of stability criterion $\mathscr{K}$ for processes $P_1^2 - P_5^2$. The vertical lines indicate where each process becomes unstable, according to Figure 2.3. The crosses indicate where criterion $\mathscr{K}$ identifies the beginning of thermal runaway behaviour.

In Figure 4.12 it is seen that the crosses, indicating when criterion $\mathscr{K}$ predicts process instability, occur before each process becomes thermally unstable, represented by the vertical dash-dotted lines. The time between the predicted instability and the actual loss of stability is approximately 250 s. This is equivalent to approximately 4 minutes, which is enough time for a control system to react to keep each batch process under control. After each batch process exerts thermal runaway behaviour, the value of $\mathscr{K}$ keeps increasing with time, showing an increased rate of heat generation during the process The same analysis as for processes $P_1^2 - P_5^2$ is now carried out for processes $P_6^2 - P_{10}^2$. The profiles for thermal stability criterion $\mathscr{K}$ for processes $P_6^2 - P_{10}^2$ are shown in Figure 4.13.

Similar results are obtained for processes $P_6^2 - P_{10}^2$ in Figure 4.13 as for processes $P_1^2 - P_5^2$: thermal stability criterion $\mathscr{K}$ predicts unstable process behaviour before it occurs. Approximately 4 minutes are between the prediction and occurrence of thermal runaway behaviour. Therefore a degree of conservativeness is present when using thermal stability criterion $\mathscr{K}$. Whether or not the conservative nature of criterion $\mathscr{K}$ allows for process intensification when embedded within an MPC scheme will be examined in Chapter 5.

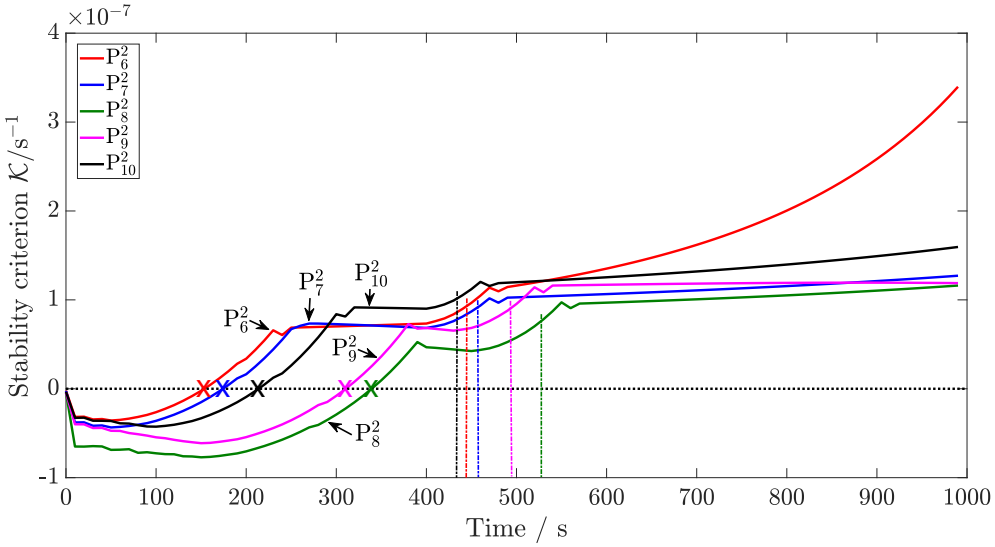

Fig. 4.13 Profiles of stability criterion $\mathscr{K}$ for processes $P_6^2 - P_{10}^2$. The vertical lines indicate where each process becomes unstable, according to Figure 2.3. The crosses indicate where criterion $\mathscr{K}$ identifies the beginning of thermal runaway behaviour.

4.5 Generalisation of thermal stability criterion $\mathscr{K}$

Stability criterion $\mathscr{K}$ has so far been derived for single reaction processes, *i.e.* reaction schemes 1 and 2. In this section the generalisation to multiple reaction systems is carried out and its validity is examined. The thermal stability criterion for a multi-reaction system is given by the same expression as for a single reaction system:

$$\mathscr{K}^{(s)} = \text{div}\left[\mathbf{J}^{(s)}\right] - \left|\mathscr{E}^{(s)}\right| \tag{4.24}$$

where it is now necessary to find an expression for $\mathscr{E}$ for multiple reaction systems.

The generalised expression for $\mathscr{E}^{(s)}$ is given by Equation (4.20b):

$$\mathscr{E}^{(s)} = \text{div}\left[\mathbf{J}^{(s-1)}\right] + \text{div}\left[\mathbf{J}^{(s-1)}\right] \cdot \text{d}\ln\left(\text{div}\left[\mathbf{J}^{(s)}\right] t_{\text{ref}}\right) \tag{4.20b}$$

The generalised form of the divergence was derived in Equation (4.13). Hence it is now necessary to find an expression for $\text{d}\ln\left(\text{div}\left[\mathbf{J}^{(s)}\right] t_{\text{ref}}\right)$ within Equation (4.20b) given above. From Equation (4.13) it is true in general that $\text{div}\,[\mathbf{J}]$ is a function of $\mathscr{D}_i$ and St for a total of M reactions. Therefore Equation (4.13) is given by the following:

$$\text{div}\,[\mathbf{J}]\, t_{\text{ref}} = f\left(\mathscr{D}_i, \text{St}\right), \qquad i = 1, 2, \ldots, M \tag{4.25}$$

where $\mathscr{D}_i$ is the part of the divergence which is only influenced by each individual reaction.

The form of the total divergence of the Jacobian, $\operatorname{div}[\mathbf{J}]\, t_{\mathrm{ref}}$, now allows a total derivative to be carried out:

$$\mathrm{d}\left(\operatorname{div}[\mathbf{J}]\cdot t_{\mathrm{ref}}\right)=\sum_{i=1}^{M}\frac{\partial\left(\operatorname{div}[\mathbf{J}]\, t_{\mathrm{ref}}\right)}{\partial\left(\mathscr{D}_i\right)}\mathrm{d}\left(\mathscr{D}_i\right)+\frac{\partial\left(\operatorname{div}[\mathbf{J}]\, t_{\mathrm{ref}}\right)}{\partial\left(\mathrm{St}\right)}\mathrm{d}\left(\mathrm{St}\right) \tag{4.26}$$

Using the expression for the differential of a logarithm in Equation (4.17), Equation (4.26) can be reformulated to give the following expression including logarithmic terms:

$$\begin{aligned}\mathrm{d}\left(\operatorname{div}[\mathbf{J}]\, t_{\mathrm{ref}}\right)=&\sum_{i=1}^{M}\mathscr{D}_i\frac{\partial\left(\operatorname{div}[\mathbf{J}]\, t_{\mathrm{ref}}\right)}{\partial\left(\mathscr{D}_i\right)}\mathrm{d}\left[\ln\left(\mathscr{D}_i t_{\mathrm{ref}}\right)\right]\\&+\left(\operatorname{div}[\mathbf{J}]\, t_{\mathrm{ref}}\right)\frac{\partial\left[\ln\left(\operatorname{div}[\mathbf{J}]\, t_{\mathrm{ref}}\right)\right]}{\partial\ln\left(\mathrm{St}\right)}\mathrm{d}\left[\ln\left(\mathrm{St}\right)\right]\end{aligned} \tag{4.27}$$

In Section 4.3.1 it is shown how the divergence of the Jacobian for a single reaction can be used to find an expression for $\mathscr{E}$. Similarly, the summation of the individual contribution for each reaction will lead to the generalised expression of $\mathscr{E}$ for a multiple reaction system. To find such an expression, it is required to find an equation for $\mathrm{d}\left[\ln\left(\mathscr{D}_i t_{\mathrm{ref}}\right)\right]$ within Equation (4.27). From Equation (4.12) the function for $\mathscr{D}_i$ is given by:

$$\mathscr{D}_i=f\left(B_i,\gamma_i,\mathrm{Da}_{\mathrm{res},i}\right) \tag{4.28}$$

Equation (4.28) is used to derive the total derivative of $\mathrm{d}\left[\ln\left(\mathscr{D}_i t_{\mathrm{ref}}\right)\right]$ given in Equation (4.27):

$$\begin{aligned}\mathrm{d}\left[\ln\left(\mathscr{D}_i t_{\mathrm{ref}}\right)\right]=&\frac{\partial\ln\left(\mathscr{D}_i t_{\mathrm{ref}}\right)}{\partial\ln\left(B_i\right)}\mathrm{d}\ln\left(B_i\right)+\frac{\partial\ln\left(\mathscr{D}_i t_{\mathrm{ref}}\right)}{\partial\ln\left(\gamma_i\right)}\mathrm{d}\ln\left(\gamma_i\right)\\&+\frac{\partial\ln\left(\mathscr{D}_i t_{\mathrm{ref}}\right)}{\partial\ln\left(\mathrm{Da}_{\mathrm{res},i}\right)}\mathrm{d}\ln\left(\mathrm{Da}_{\mathrm{res},i}\right)\end{aligned} \tag{4.29a}$$

$$\mathrm{d}\left[\ln\left(\mathscr{D}_i t_{\mathrm{ref}}\right)\right]=m_B\mathrm{d}\ln\left(B_i\right)+m_\gamma\mathrm{d}\ln\left(\gamma_i\right)+m_{\mathrm{Da}_{\mathrm{res}}}\mathrm{d}\ln\left(\mathrm{Da}_{\mathrm{res},i}\right) \tag{4.29b}$$

The Stanton number coefficient m_{St} does not appear in Equation (4.29b), as each individual reaction does not have an effect on this dimensionless variable. Therefore this is taken into account separately. As was the case for a single reaction in Section 4.3.1, the gradient

coefficient for the Stanton number is given by:

$$\frac{\partial \ln\left(\operatorname{div}\left[\mathbf{J}\right] t_{\mathrm{ref}}\right)}{\partial \ln\left(\mathrm{St}\right)} = m_{\mathrm{St}} \tag{4.30}$$

The values of coefficients m_B, m_γ, $m_{\mathrm{Da_{res}}}$, and m_{St} were derived in the previous sections for a wide variety of possible reaction kinetics for a single reaction. Hence it is tested if the values found can be applied for a general reaction i within a reaction network. The trajectory of each individual dimensionless variable B_i, γ_i and $\mathrm{Da}_{\mathrm{res},i}$ will be different for each reaction and needs to be evaluated separately. It is further noted from Equation (4.13) that:

$$\frac{\partial\left(\operatorname{div}\left[\mathbf{J}\right] t_{\mathrm{ref}}\right)}{\partial\left(\mathscr{D}_i\right)} = 1 \qquad i = 1, 2, ..., M \tag{4.31}$$

This result, together with Equations (4.29b) and (4.30), allows the simplification of the derivative of the divergence of a general reaction system, given in Equation (4.27):

$$\begin{aligned}\operatorname{div}\left[\mathbf{J}\right] \mathrm{d}\ln\left(\operatorname{div}\left[\mathbf{J}\right]\right) = \sum_{i=1}^{M} \mathscr{D}_i \left[m_B \mathrm{d}\ln\left(B_i\right) + m_\gamma \mathrm{d}\ln\left(\gamma_i\right) + m_{\mathrm{Da_{res}}} \mathrm{d}\ln\left(\mathrm{Da}_{\mathrm{res},i}\right)\right] \\ + \left(\operatorname{div}\left[\mathbf{J}\right] t_{\mathrm{ref}}\right) m_{\mathrm{St}} \,\mathrm{d}\left[\ln\left(\mathrm{St}\right)\right]\end{aligned} \tag{4.32}$$

In Equation (4.32) several interesting features can be observed: each reaction contributes towards the total divergence weighted by its individual divergence $\mathscr{D}_i$, therefore giving a weighting for the thermal runaway behaviour. This means that if a reaction is very slow or produces very little heat, its value for $\mathscr{D}_i$ is small and hence its contribution to the thermal runaway is small, too. The Stanton number appears separately, as discussed above. The contribution of the Stanton number is the same, no matter how many reactions take place. This is intuitive, as the Stanton number only depends on the cooling jacket properties, and not the reaction kinetics within the reactor.

The final step of the derivation requires to find an expression for $\mathscr{E}$. As was the case in Section 4.3.1, it is necessary to find an expression for $\mathscr{E}^{(s)}$ at time step (s) as a function of each individual contribution towards the total divergence in time step $(s-1)$, $\mathscr{D}_i^{(s-1)}$, and the dimensionless variables at time steps $(s-1)$ and (s). For multiple reactions the function

for $\mathscr{E}^{(s)}$ is given by:

$$\mathscr{E}^{(s)} = f\left(\mathscr{D}_i^{(s-1)}, B_i^{(s)}, B_i^{(s-1)}, \gamma_i^{(s)}, \gamma_i^{(s-1)}, \mathrm{Da}_{\mathrm{res},i}^{(s)}, \mathrm{Da}_{\mathrm{res},i}^{(s-1)}, \mathrm{St}^{(s)}, \mathrm{St}^{(s-1)}\right) \qquad (4.33)$$
$$i = 1,2,...,M$$

where $\mathscr{D}_i^{(s-1)}$ is a function of all dimensionless groups mentioned in time step $(s-1)$.

From Equations (4.20b) and (4.32) the correction function $\mathscr{E}^{(s)}$ at time step (s) can be found:

$$\begin{aligned}\mathscr{E}^{(s)} = &\mathrm{div}\left[\mathbf{J}^{(s-1)}\right] + \sum_{i=1}^{M} \mathscr{D}_i^{(s-1)} \left[m_B \frac{B_i^{(s)} - B_i^{(s-1)}}{B_i^{(s-1)}} + m_\gamma \frac{\gamma_i^{(s)} - \gamma_i^{(s-1)}}{\gamma_i^{(s-1)}} \right. \\ &\left. + m_{\mathrm{Da_{res}}} \frac{\mathrm{Da}_{\mathrm{res},i}^{(s)} - \mathrm{Da}_{\mathrm{res},i}^{(s-1)}}{\mathrm{Da}_{\mathrm{res},i}^{(s-1)}} \right] + \mathrm{div}\left[\mathbf{J}^{(s-1)}\right] m_{\mathrm{St}} \frac{\mathrm{St}^{(s)} - \mathrm{St}^{(s-1)}}{\mathrm{St}^{(s-1)}}\end{aligned} \qquad (4.34)$$

which includes all the variables as required in Equation (4.33).

Now that the necessary form of $\mathscr{E}^{(s)}$ is derived, thermal stability criterion $\mathscr{K}$ can be evaluated according to the definition given in Equation (4.24):

$$\begin{aligned}\mathscr{K}^{(s)} = &\mathrm{div}\left[\mathbf{J}^{(s)}\right] - \left| \mathrm{div}\left[\mathbf{J}^{(s-1)}\right] + \sum_{i=1}^{M} \mathscr{D}_i^{(s-1)} \left[m_B \frac{B_i^{(s)} - B_i^{(s-1)}}{B_i^{(s-1)}} + m_\gamma \frac{\gamma_i^{(s)} - \gamma_i^{(s-1)}}{\gamma_i^{(s-1)}} \right. \right. \\ &\left. \left. + m_{\mathrm{Da_{res}}} \frac{\mathrm{Da}_{\mathrm{res},i}^{(s)} - \mathrm{Da}_{\mathrm{res},i}^{(s-1)}}{\mathrm{Da}_{\mathrm{res},i}^{(s-1)}} \right] + \mathrm{div}\left[\mathbf{J}^{(s-1)}\right] m_{\mathrm{St}} \frac{\mathrm{St}^{(s)} - \mathrm{St}^{(s-1)}}{\mathrm{St}^{(s-1)}} \right|\end{aligned} \qquad (4.35)$$

This concludes the generalisation of thermal stability criterion $\mathscr{K}$ for multiple reaction systems. It can be seen clearly that the stability criterion $\mathscr{K}$ for multiple reaction systems, given in Equation (4.35), is of similar form as for a single chemical reaction. The derived equation for multiple reaction systems adds the contribution of each individual reaction to the total divergence of the Jacobian.

The validity of the derived general form of criterion $\mathscr{K}$ is examined for reaction schemes 3 and 4, each containing 4 and 6 simultaneous reactions, respectively.

4.5.1 Verification for reaction scheme 3

Reaction scheme 3 consists of 4 reactions occurring simultaneously. For this reaction scheme the specific expression for criterion $\mathscr{K}$, using the generalised expression in Equation (4.35),

is given by:

$$\begin{aligned}\mathscr{K}^{(s)} =& \operatorname{div}\left[\mathbf{J}^{(s)}\right] - \Bigg| \operatorname{div}\left[\mathbf{J}^{(s-1)}\right] \cdot \\ &+ \sum_{i=1}^{4} \mathscr{D}_i^{(s-1)} \left(m_B \frac{B_i^{(s)} - B_i^{(s-1)}}{B_i^{(s-1)}} + m_\gamma \frac{\gamma_i^{(s)} - \gamma_i^{(s-1)}}{\gamma_i^{(s-1)}} + m_{\mathrm{Da_{res}}} \frac{\mathrm{Da}_{\mathrm{res},i}^{(s)} - \mathrm{Da}_{\mathrm{res},i}^{(s-1)}}{\mathrm{Da}_{\mathrm{res},i}^{(s-1)}} \right) \\ &+ \operatorname{div}\left[\mathbf{J}^{(s-1)}\right] m_{\mathrm{St}} \frac{\mathrm{St}^{(s)} - \mathrm{St}^{(s-1)}}{\mathrm{St}^{(s-1)}} \Bigg| \end{aligned} \tag{4.36}$$

As an example, the form of $\mathscr{D}_1^{(s-1)}$ in Equation (4.36) is given by the following expression:

$$\begin{aligned}\mathscr{D}_1^{(s-1)} = \Bigg[& - \nu_{\mathrm{A},1}\, n_{\mathrm{A},1}\, \mathrm{Da}_{\mathrm{A},1}^{(s-1)} - \nu_{\mathrm{B},1}\, n_{\mathrm{B},1}\, \mathrm{Da}_{\mathrm{B},1}^{(s-1)} \\ & + \gamma_1^{(s-1)}\, B_1^{(s-1)}\, \mathrm{Da}_{\mathrm{B},1}^{(s-1)} \Bigg] \exp\left(-\gamma_1^{(s-1)}\right) \end{aligned} \tag{4.37}$$

Keeping in mind the temperature profiles of the thermal runaway reactions shown in Section 2.4.3, it is required to compare when the system actually becomes unstable, when criterion $\mathscr{K}$ identifies the system to become unstable, and what the value of $\mathscr{K}$ is at the point in time when stability is lost. As was indicated in Figures 2.6 and 2.7, the time at which stability is lost is indicated by dash-dotted lines parallel to the y-axis. The stability criterion profiles for processes $\mathrm{P}_1^3 - \mathrm{P}_3^3$ are shown in Figure 4.14.

In Figure 4.14 it is seen that for each process the criterion gives a positive number at the point in time where stability is lost, indicated by the dash-dotted lines. This is in agreement with the results for reaction schemes 1 and 2, where similar results were obtained for single reaction systems. Hence criterion $\mathscr{K}$ correctly indicates that an unstable process is present when the thermal stability of the system is lost.

Now the points at which stability criterion $\mathscr{K}$ predicts the stability are analysed: the crosses in Figure 4.14 indicate where each profile for $\mathscr{K}$ has a value of zero. This is the switch-over point which indicates a thermally unstable process is present. The first positive feature is that instability is predicted before it actually occurs. This can be observed in Figure 4.14 as the crosses occur before the dash-dotted lines indicating the loss of stability in the system. Furthermore, the difference in time between the real loss of stability and the prediction of the

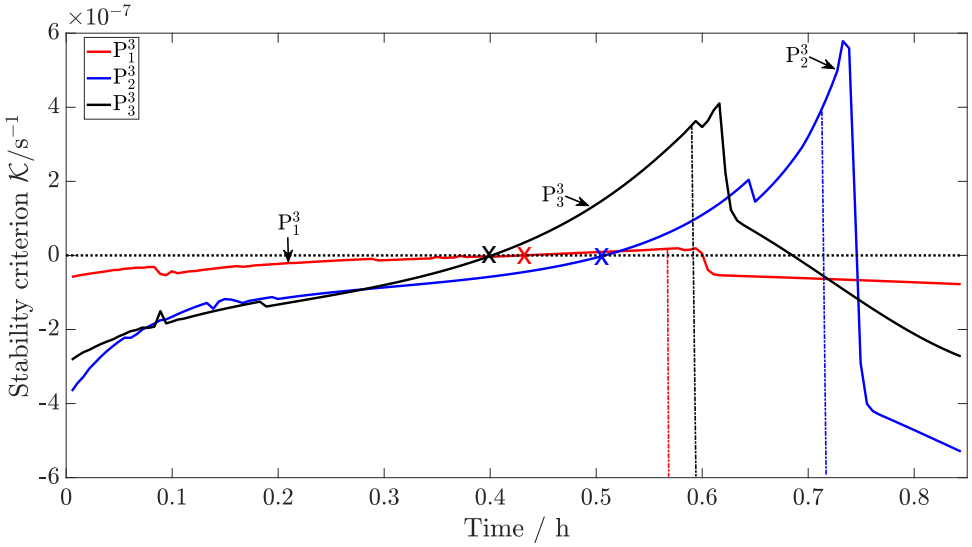

Fig. 4.14 Profiles of stability criterion $\mathscr{K}$ for processes $P_1^3 - P_3^3$. The vertical lines indicate where each process becomes unstable, according to Figure 2.6. The crosses indicate where criterion $\mathscr{K}$ identifies the beginning of thermal runaway behaviour.

loss of stability are separated by approximately 0.2 h, which is equivalent to 12 minutes. This should give enough time for an advanced control scheme to be able to modify the control actions to keep the system in a stable regime.

For each process given in Figure 4.14 the value of $\mathscr{K}$ reduces sharply after approximately 0.3 h, after the actual loss of stability has occurred. This is the case as the sharp increase in reaction temperature leads to a sharp increase in the rate of consumption of reagents. Criterion $\mathscr{K}$ incorporates the trajectories of both, temperatures and concentrations, which is why a sudden drop in concentrations will lead to a sudden change in the value of $\mathscr{K}$. The fact that the value becomes negative after the loss of stability has occurred is not in contradiction to the definition of $\mathscr{K}$. The purpose of thermal stability criterion $\mathscr{K}$ is to identify the point at which stability is lost, and not to predict how unstable a process is once stability is lost.

The analysis of processes $P_1^3 - P_3^3$ is now carried out for processes $P_4^3 - P_6^3$. The thermal stability criterion profiles for processes $P_4^3 - P_6^3$ are shown in Figure 4.15.

For processes $P_4^3 - P_6^3$ in Figure 4.15 the times when stability is lost are indicated by the vertical dash-dotted lines, as was shown in Figure 2.7. Similar to processes $P_1^3 - P_3^3$, the values of $\mathscr{K}$ at the actual loss of stability is positive. Hence criterion $\mathscr{K}$ correctly classifies the point at which the loss of stability occurs. Furthermore, the crosses within Figure 4.15 show that criterion $\mathscr{K}$ predicts the stability to be lost at times occurring before the actual stability is lost. This is logical since the values of $\mathscr{K}$ are initially negative, becoming positive

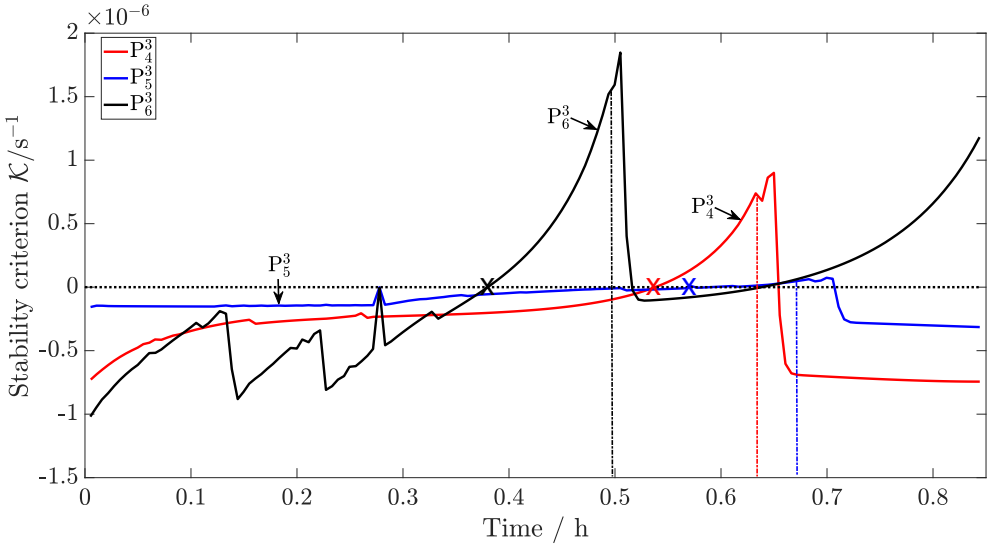

Fig. 4.15 $\mathscr{K}$ criterion profiles for processes $P_4^3 - P_6^3$. The dotted line within the figure indicates where $\mathscr{K} = 0$. The crosses indicate where thermal stability criterion $\mathscr{K}$ detects an unstable process. The dash-dotted lines parallel to the y-axis indicate when stability is lost in the system.

when the stability is actually lost. The difference in time between the predicted loss of stability, and the actual loss of stability, as indicated on the temperature profiles on Figure 2.7, is approximately 0.1 h for each process, hence giving 6 minutes for an advanced control scheme to react.

For process P_6^3 it is further noted that the profile of $\mathscr{K}$ at times before 0.4 h, the time when instability is predicted, follows an oscillatory profile. As can be observed in Figure 2.7, the temperature profile at times before 0.4 h follows an oscillatory profile as well. This is the case because the PI controller acts very fast to cool the system once the initial set-point temperature of 389 K is reached. Since the PI controller was not tuned in order to give the best performance, this oscillatory effect is present for the temperature profile. The value of $\mathscr{K}$ is evaluated using information from the temperature and concentration trajectories of the system. Hence, sharp changes in the temperature will result in sharp changes in the value of $\mathscr{K}$. Therefore the initial profile of $\mathscr{K}$ is given by the profile shown in Figure 4.15. The other significant feature of the profile of $\mathscr{K}$ for process P_6^3 is that the value of $\mathscr{K}$ increases after the loss of stability has occurred. This is different to processes $P_1^3 - P_5^3$, where the value of $\mathscr{K}$ entered the negative region and decreased afterwards. In this case the reaction still has enough reagents to cause an accelerated rate of increase in temperature, which can be observed in Figure 2.7. As $\mathscr{K}$ follows the temperature and concentration profiles, in this

process the effect of the temperature increasing at an accelerated rate outweighs the decrease in concentration, therefore increasing the value of $\mathscr{K}$.

4.5.2 Verification for reaction scheme 4

The most complex reaction network in this work is considered next, given by reaction scheme 4. The reactions occurring in this reaction scheme are given in Section 2.2.4. The equation of thermal stability criterion $\mathscr{K}$ used for this reaction scheme is similar to the expression in Equation (4.36) for reaction scheme 3. For reaction scheme 2 the effect of the additional two reactions and the respective expression for the divergence of the Jacobian have to be added. The two components added to Equation (4.36) are given by:

$$\begin{aligned}
&+\mathscr{D}_5^{(s-1)}\left[m_B\frac{B_5^{(s)}-B_5^{(s-1)}}{B_5^{(s-1)}}+m_\gamma\frac{\gamma_5^{(s)}-\gamma_5^{(s-1)}}{\gamma_5^{(s-1)}}+m_{\mathrm{Da_{res}}}\frac{\mathrm{Da}_{\mathrm{res},5}^{(s)}-\mathrm{Da}_{\mathrm{res},5}^{(s-1)}}{\mathrm{Da}_{\mathrm{res},5}^{(s-1)}}\right]\\
&+\mathscr{D}_6^{(s-1)}\left[m_B\frac{B_6^{(s)}-B_6^{(s-1)}}{B_6^{(s-1)}}+m_\gamma\frac{\gamma_6^{(s)}-\gamma_6^{(s-1)}}{\gamma_6^{(s-1)}}+m_{\mathrm{Da_{res}}}\frac{\mathrm{Da}_{\mathrm{res},6}^{(s)}-\mathrm{Da}_{\mathrm{res},6}^{(s-1)}}{\mathrm{Da}_{\mathrm{res},6}^{(s-1)}}\right]
\end{aligned} \tag{4.38}$$

The expressions for $\mathscr{D}_1^{(s-1)}$ to $\mathscr{D}_4^{(s-1)}$ for reaction scheme 4 are the same as for reaction scheme 3. The expressions for $\mathscr{D}_5^{(s-1)}$ and $\mathscr{D}_6^{(s-1)}$ are calculated in the same manner as $\mathscr{D}_1^{(s-1)}$ in Equation (4.37).

The verification of $\mathscr{K}$ requires to check where the systems shown in Figure 2.8 and 2.9 becomes unstable, and where $\mathscr{K}$ predicts them to be unstable. Furthermore it is important to see what the value of $\mathscr{K}$ is at the point where stability is actually lost, indicated by dash-dotted lines. A plot of $\mathscr{K}$ for processes $\mathrm{P}_1^4-\mathrm{P}_3^4$ is shown in Figure 4.16.

Firstly it is noted from Figure 4.16 that, as for reaction scheme 3, the prediction of stability indicated by the crosses occurs before the systems lose stability, as indicated by the vertical dash-dotted lines. Secondly, at times where stability is lost, given by 0.61 h, 0.73 h and 0.48 h for processes P_1^4, P_2^4 and P_3^4, respectively, the values of $\mathscr{K}$ are all positive, hence classifying this as an unstable point. The difference in times between the prediction of instability (crosses) and the times of actual loss of stability (dash-dotted lines) is approximately 0.1 h for each process, hence giving a time of approximately 6 minutes to react. This is more than enough for advanced control schemes, and not too large to make the stability prediction too conservative. In case of plant-model mismatch this property is very useful, as predicting instability before it occurs is essential.

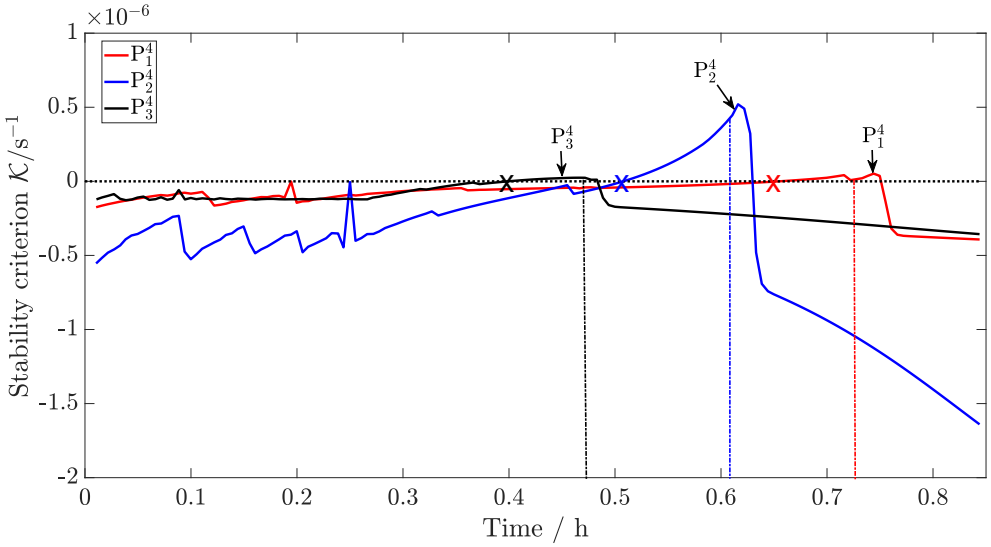

Fig. 4.16 $\mathscr{K}$ criterion profiles for processes $P_1^4 - P_3^4$. The dotted line indicates where $\mathscr{K} = 0$. The crosses indicate where thermal stability criterion $\mathscr{K}$ detects an unstable process. The dash-dotted lines parallel to the y-axis indicate when stability is lost in the system.

For process P_1^4 the same oscillatory behaviour as for process P_6^3 can be observed. This is again due to the PI controller at the initial stable operating temperature: since the PI controller is not perfectly tuned, the cooling action cools down the system very quickly, causing oscillatory behaviour in the temperature as can be seen in Figure 2.8. Since criterion $\mathscr{K}$ takes into account information from the temperature and concentration trajectories, the sudden changes in temperature in Figure 2.8 will cause similar effects on the trajectory of $\mathscr{K}$. This is exactly what is observed for process P_1^4 in Figure 4.16. The stability criterion profiles for processes $P_4^4 - P_6^4$ are shown in Figure 4.17.

In Figure 4.17 the dash dotted lines indicate where the stability is lost for processes $P_4^4 - P_6^4$, as shown for the temperature profiles in Figure 2.9. All values of $\mathscr{K}$ at the indicated times are positive, hence being in accord with the previous results. Furthermore, the crosses indicate that before the system loses stability, criterion $\mathscr{K}$ detects instability at times of 0.44 h, 0.61 h and 0.49 h for processes P_4^4, P_5^4, and P_6^4, respectively. After instability occurs for processes P_4^4 and P_5^4 the profiles of $\mathscr{K}$ decrease, showing that the reduction in concentration of reagents stabilises the system. This stabilising effect comes too late, as the system has already entered the unstable regime. For process P_6^4 the profile for $\mathscr{K}$ increases after instability occurs. This, as was the case for process P_6^3, is due to the rapidly increasing system temperature. This causes an accelerated rate at which the temperature increases. Therefore the value of $\mathscr{K}$ increases in this manner also.

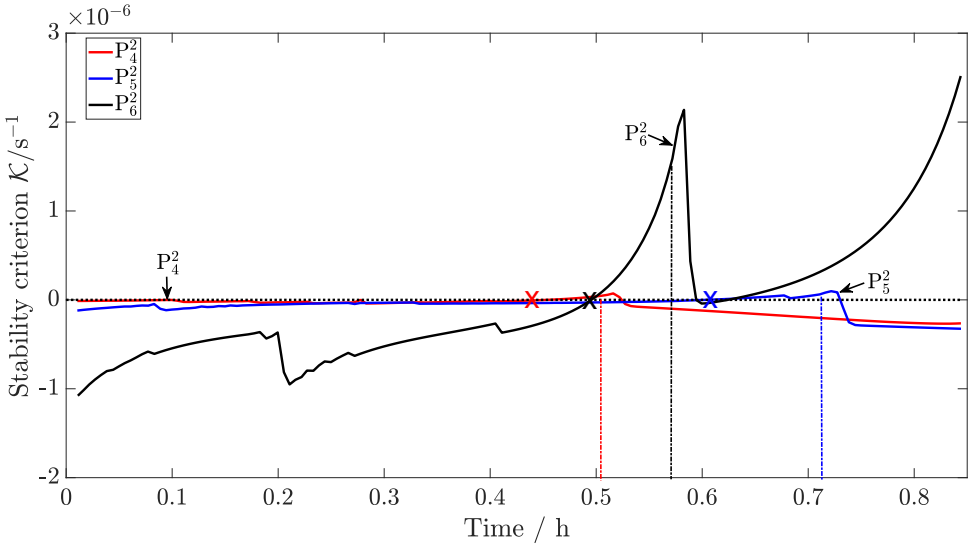

Fig. 4.17 $\mathscr{K}$ criterion profiles for processes $P_4^4 - P_6^4$. The dotted line indicates where $\mathscr{K} = 0$. The crosses indicate where thermal stability criterion $\mathscr{K}$ detects an unstable process. The dash-dotted lines parallel to the y-axis indicate when stability is lost in the system.

4.6 Chapter summary

In this chapter the generalisation of the divergence criterion for any reaction network was derived. Based on this the general form of thermal stability criterion $\mathscr{K}$ was derived.

The derivation of criterion $\mathscr{K}$ resulted in gradient coefficients with respect to four major dimensionless numbers defining the divergence criterion: the Barkelew number B, the resultant Damköhler number Da_{res}, the Arrhenius number γ, and the Stanton number St. For reaction schemes 1 and 2 it is found that the values found for these gradient coefficients m at the boundary of stability can be quantified by a single number for each dimensionless variable. Therefore, the divergence criterion at the boundary of instability can be estimated with the function $\mathscr{E}$ for a large variety of reaction parameters.

The evaluation of $\mathscr{E}$ for reaction schemes 1 and 2 considers a single exothermic reaction. When extended to a reaction network, it is found that the same values for the gradient coefficients m can be applied to predict thermal runaway behaviour. This is shown by considering the example thermal runaway reactions for reaction schemes 3 and 4.

The prediction of thermal runaway behaviour with criterion $\mathscr{K}$ is shown to be reliable for all complex reaction schemes considered, hence suggesting applicability to any exothermic reaction occurring in batch reactors. Criterion $\mathscr{K}$ has not been applied to fed-batch systems for which the dynamic behaviour, *i.e.* mass and energy balances, differs.

The instability is predicted approximately 4 minutes before thermal runaway behaviour occurs, hence giving enough time for a control system to react. After showing that criterion $\mathscr{K}$ can be used for the reliable detection of instability in batch processes, the next chapter uses this measure of stability with MPC framework 1 for process intensification.

Chapter 5

Embedding stability criterion $\mathscr{K}$ within MPC for batch process intensification

In this chapter the main focus is process intensification using thermal stability criterion $\mathscr{K}$, as it was derived in Chapter 4. As was done for Lyapunov exponents and the divergence criterion, MPC framework 1 from Section 2.5.1 is used for this purpose. MPC framework 1 incorporates a thermal stability constraint, which in this chapter is criterion $\mathscr{K}$. This MPC framework, embedded with Lyapunov exponents in Section 3.2, was shown to result in process intensification which reduces the batch duration, whilst ensuring stable operation.

To examine how well batch processes can be intensified, reaction schemes 1 to 4, and the nitration of toluene introduced in Section 2.2 are considered. Important to note is the following feature when using thermal stability criterion $\mathscr{K}$ to predict instability in the batch processes: for all reaction schemes considered, instability is predicted approximately 4 minutes before the actual process becomes unstable. How much this degree of conservativeness influences process intensification is therefore one of the major motivations for this chapter.

Furthermore, it is essential that the computational time does not exceed the time available for each MPC step, in this case 10 s per step. When using Lyapunov exponents within MPC frameworks it is found in Section 3.2.4 that the computational time required per MPC step increases exponentially with the number of exponents required. Thermal stability criterion $\mathscr{K}$ requires one number to be evaluated in order to quantify stability. Therefore it is expected to achieve greater computational efficiency when using criterion $\mathscr{K}$, making it more applicable for potential industrial applications.

5.1 Reaction scheme 1

In Section 4.3.3 it is shown that criterion $\mathscr{K}$ results in reliable predictions of thermal stability. How well MPC framework 1 embedded with criterion $\mathscr{K}$ works for process intensification is considered next. The temperature profiles for processes $P_6^1 - P_{10}^1$ are shown in Figure 5.1.

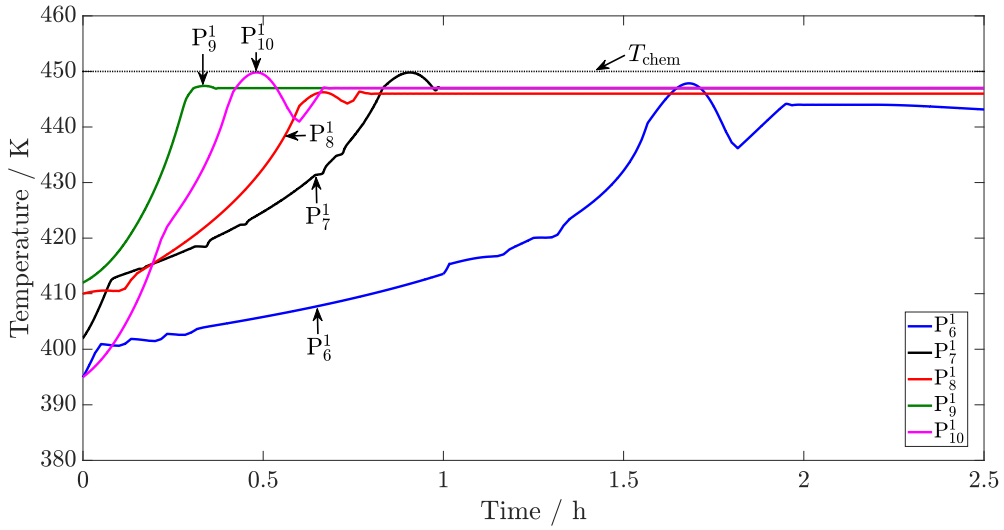

Fig. 5.1 Temperature profiles for processes $P_6^1 - P_{10}^1$ with MPC framework 1 embedded with stability criterion $\mathscr{K}$. The horizontal dotted line indicates the maximum allowable temperature of T_{chem}.

In Figure 5.1 it is seen that MPC framework 1 embedded with criterion $\mathscr{K}$ results in stable process control, not exceeding the maximum allowable temperature of 450 K at any point. For each process sudden drops in temperature can be observed along the temperature profiles. This is due to the process running close to what criterion $\mathscr{K}$ predicts as being thermally unstable. The temperature profiles obtained with criterion $\mathscr{K}$ show better intensification than MPC framework 1 with the divergence criterion, the criterion that $\mathscr{K}$ is based on.

If better intensification is achieved is seen when considering the conversion profiles. The conversion of reagent A for processes $P_6^1 - P_{10}^1$ controlled by MPC framework 1 is shown in Figure 5.2.

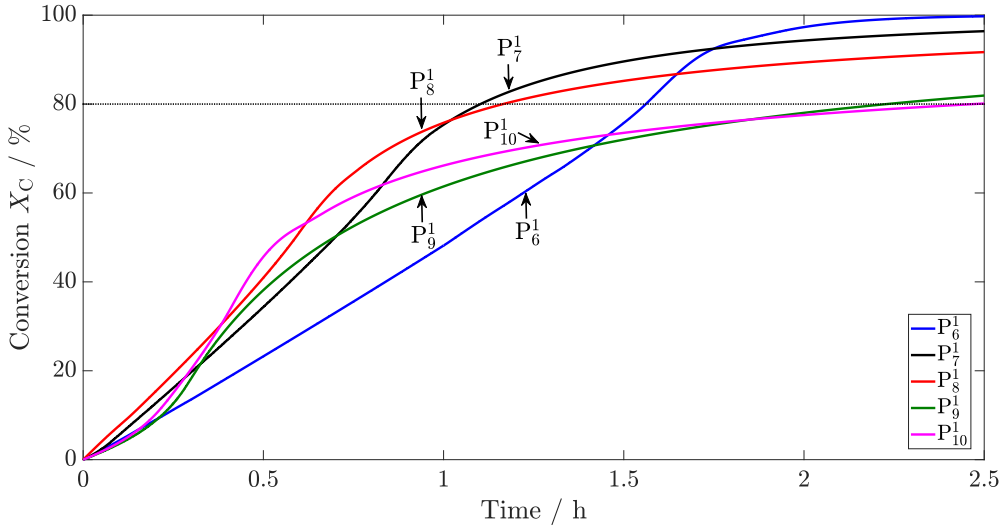

Fig. 5.2 Conversion profiles for processes $P_6^1 - P_{10}^1$ with MPC framework 1 embedded with stability criterion $\mathscr{K}$. The horizontal dotted line indicates the target conversion of $X_C = 80\%$.

In Figure 5.2 it is seen that the target conversion of $X_C = 80\%$ is achieved with MPC framework 1 within 3 h. Similar results are obtained for all remaining processes. The results for all simulations controlled with MPC framework 1 with criterion $\mathscr{K}$ embedded, as well as the processing times when MPC framework 2 with a constant set-point temperature, are shown in Table 5.1.

When comparing the processing times in Table 5.1 when using MPC frameworks 1 and 2 it is clear that process intensification using standard MPC with criterion $\mathscr{K}$ embedded leads to a significant improvement in efficiency. The processing times are reduced by at least 2-fold. This is achieved safely by continuously increasing the reactor temperature as shown in Figure 5.1. The maximum temperature T_{chem} is never exceeded but reached safely for every process for reaction scheme 1.

Comparing the results in Table 5.1 with the results obtained for MPC framework 1 with Lyapunov exponents in Table 3.1, it is seen that the average computational times required per MPC step, $\bar{t}_{comp}$, are shorter by approximately 1 s when embedding criterion $\mathscr{K}$. MPC framework 2 results in shorter computational times than MPC framework 1 with criterion $\mathscr{K}$ embedded, never exceeding 0.60 s per MPC step. Whether or not embedding criterion $\mathscr{K}$ results in a computationally more efficient control scheme than the use of Lyapunov exponents for more complex reaction networks will be examined in the following sections.

Table 5.1 Simulation results for process intensification with MPC frameworks 1 and 2 for reaction scheme 1.

	MPC framework 1 with criterion $\mathscr{K}$			MPC framework 2
	t_{reac}/h	T_{peak}/K	$\bar{t}_{\text{comp}}$/CPUs	t_{reac}/h
P_1^1	1.5	447	1.15	6.5
P_2^1	1.5	446	1.81	7.4
P_3^1	1.5	449	1.56	15.7
P_4^1	1.9	448	1.21	20.3
P_5^1	2.7	448	1.16	47.3
P_6^1	1.6	448	1.34	6.6
P_7^1	1.1	450	0.79	6.1
P_8^1	1.2	446	1.26	4.9
P_9^1	2.2	447	1.26	12.5
P_{10}^1	2.5	450	1.43	35.9
P_{11}^1	0.8	449	0.97	2.0
P_{12}^1	0.9	449	1.13	2.0
P_{13}^1	1.2	450	1.84	2.6
P_{14}^1	1.5	449	1.24	3.1
P_{15}^1	1.8	448	1.05	3.8

5.2 Reaction scheme 2

The same analysis as for reaction scheme 1 is carried out for reaction scheme 2 in this section. In Section 4.4 stability criterion $\mathscr{K}$ was shown to give reliable predictions of thermal runaway behaviour for reaction scheme 2. As for reaction scheme 1, it is now of interest to see how the conservative nature of criterion $\mathscr{K}$ effects process intensification. The temperature profiles for processes $P_6^2 - P_{10}^2$ are shown in Figure 5.3.

In Figure 5.3 it is seen that stable control is achieved for processes $P_6^2 - P_{10}^2$ when using MPC framework 1 with embedded stability criterion $\mathscr{K}$. The maximum allowable temperature of $T_{\text{chem}} = 470\,\text{K}$ is not exceeded. Therefore feasible processes are obtained. The conservative nature of criterion $\mathscr{K}$ does not lead to excessive cooling of the batch reactor. To examine the

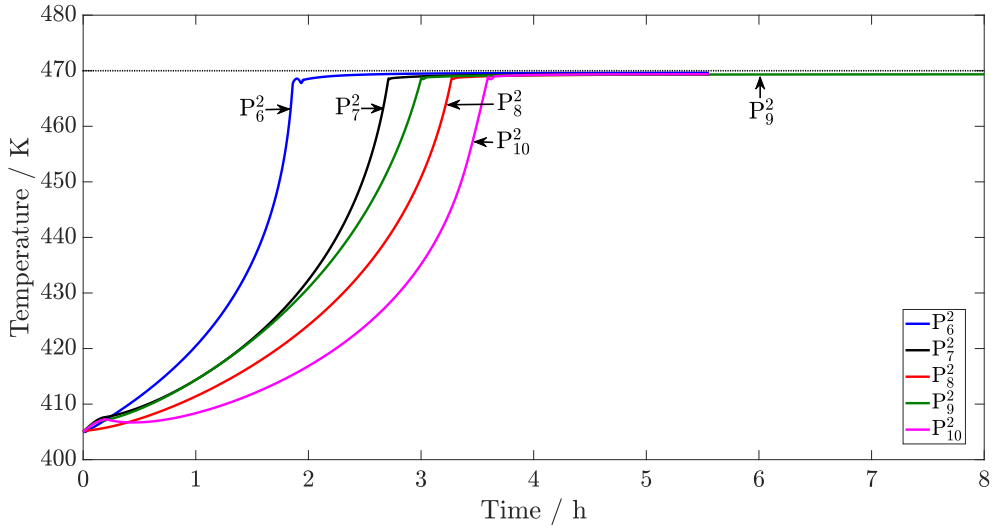

Fig. 5.3 Temperature profiles for processes $P_6^2 - P_{10}^2$ with MPC framework 1. The horizontal dotted line indicates the maximum allowable temperature of T_{chem}.

intensification achieved with this control framework the conversion profiles X_C for processes $P_6^2 - P_{10}^2$ are shown in Figure 5.4.

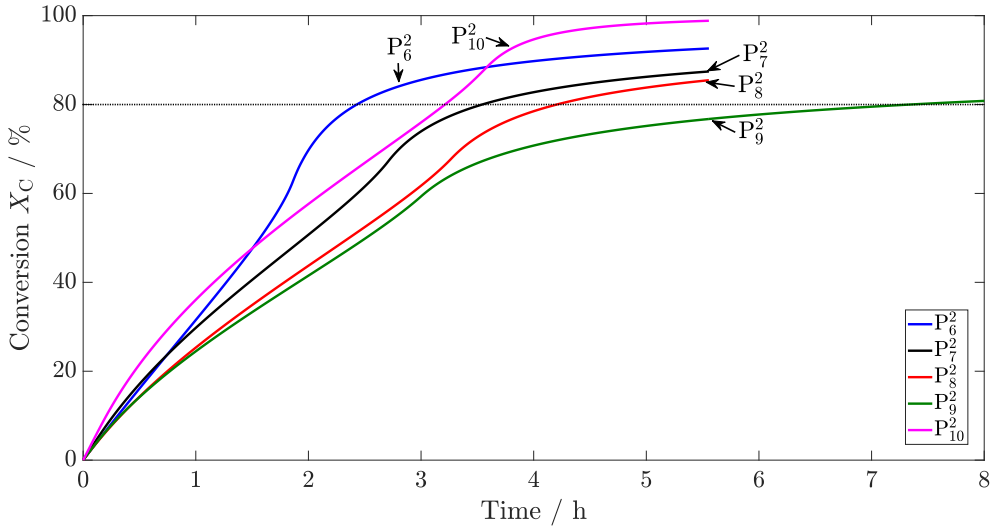

Fig. 5.4 Conversion profiles for processes $P_6^2 - P_{10}^2$ with MPC framework 1. The horizontal dotted line indicates the target conversion of $X_C = 80\%$.

In Figure 5.4 it is seen that within 7.5 h the target conversion is reached for each of processes $P_6^2 - P_{10}^2$. Similar results are obtained for all remaining processes of reaction scheme 2.

The results for all simulations with reaction scheme 2 controlled with MPC framework 1 with criterion $\mathscr{K}$ embedded, as well as the process times obtained for MPC framework 2 with a constant set-point temperature, are shown in Table 5.2.

Table 5.2 Simulation results for process intensification of batch processes $P_1^2 - P_{20}^2$ with MPC frameworks 1 and 2.

	MPC framework 1 with criterion $\mathscr{K}$			MPC framework 2
	t_{reac}/h	T_{peak}/K	$\bar{t}_{comp}$/CPUs	t_{reac}/h
P_1^2	4.5	469	1.17	13.4
P_2^2	3.1	469	1.04	40.3
P_3^2	2.4	469	1.15	9.9
P_4^2	1.9	469	1.07	10.6
P_5^2	4.5	469	1.20	13.9
P_6^2	2.4	470	1.30	20.2
P_7^2	3.5	469	1.35	31.0
P_8^2	4.2	469	1.35	35.5
P_9^2	7.2	469	1.25	>100
P_{10}^2	3.2	469	1.07	7.2
P_{11}^2	2.0	469	1.06	6.9
P_{12}^2	2.2	469	1.10	7.1
P_{13}^2	1.1	470	1.07	7.9
P_{14}^2	7.3	469	1.12	>100
P_{15}^2	7.2	469	1.09	>100
P_{16}^2	2.1	469	1.08	6.0
P_{17}^2	2.7	469	1.11	5.4
P_{18}^2	2.5	470	1.17	5.6
P_{19}^2	2.5	469	1.05	5.6
P_{20}^2	2.3	469	1.05	5.4

As was the case for reaction scheme 1 in Table 5.1, MPC framework 1 with criterion $\mathscr{K}$ embedded results in stable process control reducing the process time t_{reac} by at least 2-fold when compared to constant temperature processes. The peak temperature of processes

controlled by MPC framework 1 in Table 5.2 does not exceed the maximum allowable temperature of $T_{\text{chem}} = 470\,\text{K}$, therefore resulting in feasible processes. The computational time per MPC step, when compared to the results obtained with Lyapunov exponents in Table 3.2, are consistently shorter. Therefore, a computationally more efficient MPC framework is obtained by embedding criterion $\mathscr{K}$ than for standard MPC with an extended control and prediction horizon and MPC embedded with Lyapunov exponents.

5.3 Reaction scheme 3

In this section the process intensification of reaction scheme 3 is considered. In this reaction scheme 4 simultaneous reactions occur according to Section 2.2.3. Given each MPC framework, the resulting temperature and conversion profiles are examined. Important for the application to industrial processes is the time to reach the target conversion, which for this reaction scheme is set to $X_{\text{A,target}} = 70\%$. Furthermore it is essential that each process is kept under control, never exceeding the maximum allowable temperature of $T_{\text{chem}} = 470\,\text{K}$. Finally, the computational time required for every MPC iteration for each MPC framework is compared. The smaller the computational time, the more feasible its application to industry. Furthermore, it is important that the computational time is below the time available given by the control horizon, *i.e.* below 10 s.

For clarity only figures for processes P_5^3 and P_6^3 are shown below for reaction scheme 3. Similar solutions to those obtained for processes P_5^3 and P_6^3 are obtained for all remaining processes of reaction scheme 3. The temperature profiles when each MPC framework is applied to these processes are shown in Figure 5.5.

MPC framework 3 results in thermal runaway behaviour even with an extended control and prediction horizon. The temperature increases in an uncontrolled manner, exceeding the maximum allowable temperature. The maximum temperatures of 910 K and 1200 K are reached at times of 0.9 h and 1.5 h for processes P_5^3 and P_6^3, respectively. At these temperatures an explosion would occur in reality if no preventative actions were to be taken. The cooling capacity is not able to keep the process under control with this MPC framework, because the unstable behaviour is detected too late.

MPC framework 2 results in constant temperature throughout each process. No thermal runaway occurs for processes P_5^3 and P_6^3, as the temperature is kept constant during the process. The trade-off of having an overly conservative process run at a constant temperature is evident when considering the conversion profiles for each process.

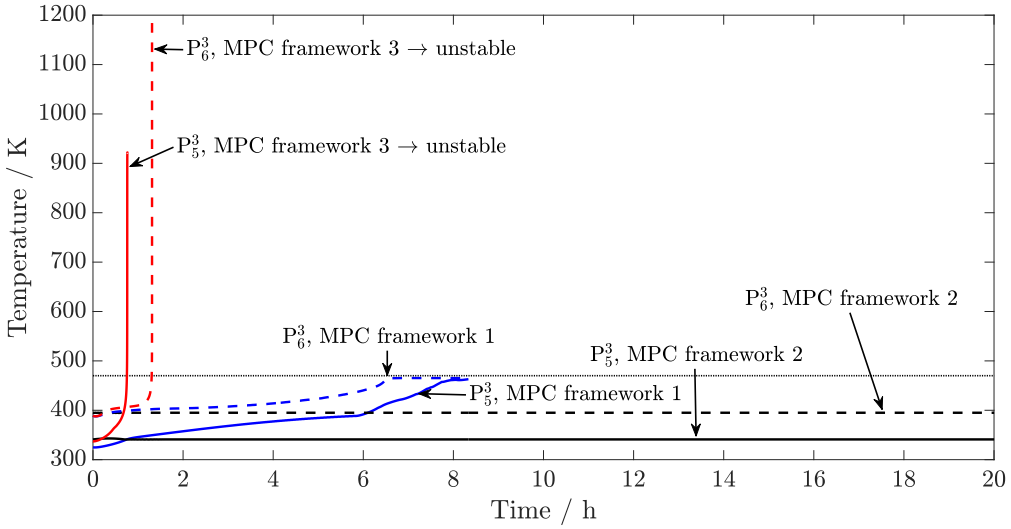

Fig. 5.5 Temperature profiles for processes P_5^3 and P_6^3 with all three MPC frameworks. The blue, black and red lines show the temperature profiles for MPC frameworks 1, 2 and 3, respectively. The dotted line indicates the maximum allowable temperature of $T_{\text{chem}} = 470$ K.

MPC framework 1, embedding criterion $\mathscr{K}$, shows a continuous increase in system temperature, without exceeding the maximum allowable temperature T_{chem}. For processes P_5^3 and P_6^3 stable reactions are obtained. The initial temperatures for these processes are equal to the ones given for MPC framework 3. This continuous increase in temperature will result in a more efficient process when compared to MPC framework 2. This will be shown in the conversion profiles below. Furthermore, the upper limit of the temperature, T_{chem}, is not exceeded.

To examine further how well each process is intensified, the conversion profiles for each MPC framework are considered next. The time required to reach the target conversion of 70% is found and compared. The smaller the time required, the more the process is intensified. As was shown for the temperature profiles, it is expected that the processes controlled by MPC framework 3 are intensified most whilst keeping the process under control.

For clarity again only processes P_5^3 and P_6^3 are considered, as these can be compared to the temperature profiles given in Figure 5.5. The profiles for the conversion of reagent A for processes P_5^3 and P_6^3 are shown in Figure 5.6.

Stable control is achieved with MPC framework 2, at the expense of long reaction times: the target conversion is reached after 78 h and 61 h for processes P_5^3 and P_6^3, respectively.

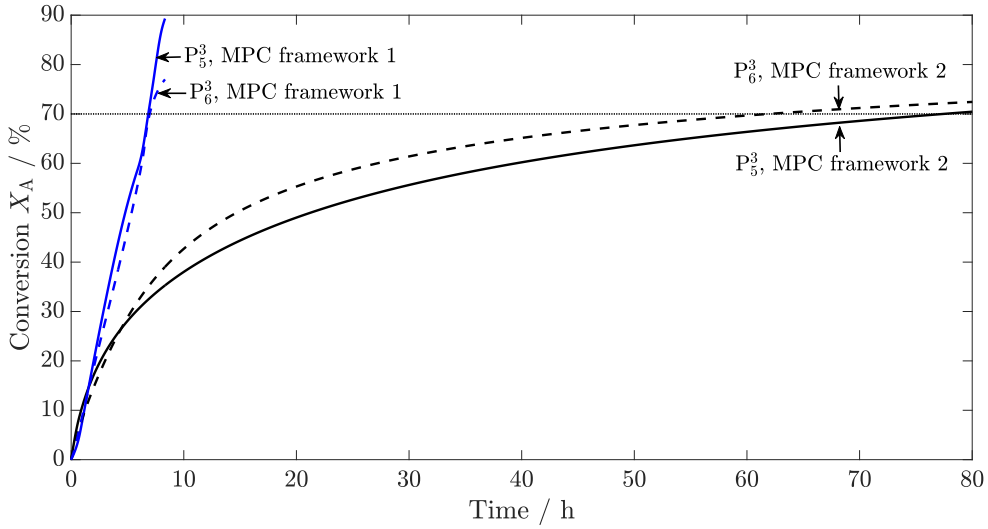

Fig. 5.6 Conversion profiles of reagent A for processes P_5^3 and P_6^3 controlled by MPC frameworks 1 and 2, given by the blue and black lines, respectively. The dotted line indicates the target conversion of $X_{A,target} = 70\%$.

Having a constant reaction temperature hence has advantages in terms of reactor stability, and disadvantages in terms of efficiency.

MPC framework 1 results in stable control, as was shown in Figure 5.5, whilst increasing the reaction temperature continuously. The target conversion of 70% is reached after 7.0 h and 7.1 h for processes P_5^3 and P_6^3, respectively. This is a significant decrease in reaction time with respect to MPC framework 2, while also keeping the process under control at every point in time.

With processes $P_1^3 - P_6^3$ controlled by MPC frameworks 1, 2 and 3 it is shown that MPC framework 1 results in stable control, while intensifying each process. The decrease in reaction time when compared to MPC framework 2 is at least 3-fold. MPC framework 3 shows unstable behaviour, causing thermal runaways. This is the case although a larger control and prediction horizon than for the other MPC frameworks is used.

The last important feature of all these MPC frameworks to note is the computational time required to use each of these MPC frameworks. The smaller the computational time, the more feasible the application to industrial processes. The average computational times per MPC step, $\bar{t}_{comp}$, together with the time to reach the target conversion, t_{reac}, and the peak temperature throughout each process, T_{peak}, are summarised in Table 5.3.

Table 5.3 Summary of results obtained for reaction scheme 3 controlled by each of the three MPC frameworks presented, including t_{reac}, T_{peak}, and $\bar{t}_{comp}$.

	MPC framework 1			MPC framework 2			MPC framework 3	
	t_{reac}/h	T_{peak}/K	$\bar{t}_{comp}$/CPUs	t_{reac}/h	T_{peak}/K	$\bar{t}_{comp}$/CPUs	T_{peak}/K	$\bar{t}_{comp}$/CPUs
P_1^3	5.2	467	0.51	>150	355	0.11	705	2.2
P_2^3	2.7	469	0.82	6.1	368	0.50	510	2.5
P_3^3	2.7	469	0.94	16.7	383	0.97	485	3.3
P_4^3	5.1	468	0.58	147	399	0.62	921	3.5
P_5^3	7.0	467	0.67	78	344	0.57	923	3.1
P_6^3	7.0	469	0.59	61	401	0.41	1204	3.8

From Table 5.3 it is seen that MPC framework 3 results in peak temperatures $T_{peak} > T_{chem}$, hence resulting in infeasible processes. As shown in Figure 5.5, the temperature profiles rise sharply due to thermal runaway behaviour. Furthermore, MPC framework 3 requires the largest computational time per MPC step. This is the case because this MPC framework has the longest control and prediction horizon. Important to note is that this MPC framework is not able to keep the processes under control. A longer prediction horizon would be required to achieve stable control, leading to even larger computational times. Since the computational time is already close to or larger than 10 s, this poses a problem for potential industrial applications.

MPC framework 2 gives close to constant temperature profiles as shown in Figure 5.5. The initial temperatures are very close to the maximum temperatures T_{peak}. The time to reach the final conversion of 70% varies strongly from 6.1 h for process P_2^3 to more than 150 h for process P_1^3. This sets the baseline relative to which the intensification of MPC framework 1 is compared to. The initial temperatures for each process controlled with MPC framework 2 is close to the boundary of stability initially: a further increase in the initial temperature of 1 K would results in an unstable process. The computational time given in Table 5.3 for MPC framework 2 is the smallest amongst all MPC frameworks which is expected: a smaller control horizon with the objective of just keeping a constant temperature is much simpler than for the other MPC frameworks.

MPC framework 1, embedding criterion $\mathscr{K}$, results in peak temperatures below the maximum allowable temperature T_{chem}. As is seen in Figure 5.5 the temperature is increased in a controlled manner throughout the process, hence resulting in an intensified reaction. From the times required to reach the target conversion, t_{reac}, given in Table 5.3 it is seen that a speed-up of at least 3-fold is achieved when implementing MPC framework 1, compared

to MPC framework 2. A controlled intensification results in much shorter reaction times, increasing the efficiency of the respective batch reactors. The computational times $\bar{t}_{\text{comp}}$ shown are larger than those for MPC framework 2, but less than half of those for MPC framework 3. To achieve stable control with MPC framework 3 even larger control and prediction horizons are necessary which increase the computational time even further. Hence, MPC framework 1 with embedded criterion $\mathscr{K}$ results in an efficient control system in terms of computational and economical cost.

5.4 Reaction scheme 4

As for reaction scheme 3, each MPC framework is applied to every process given in reaction scheme 4. The efficiency of each control scheme, as well as the ability to keep each process under control, is examined. Together with the computational time required to evaluate each MPC step the feasibility of each MPC framework for potential industrial application is analysed. For clarity, only the temperature and conversion profiles of processes P_1^4 and P_2^4 are shown in this section. Results with the same key features are obtained for all remaining processes of reaction scheme 4. The temperature profiles of processes P_1^4 and P_2^4 are given in Figure 5.7.

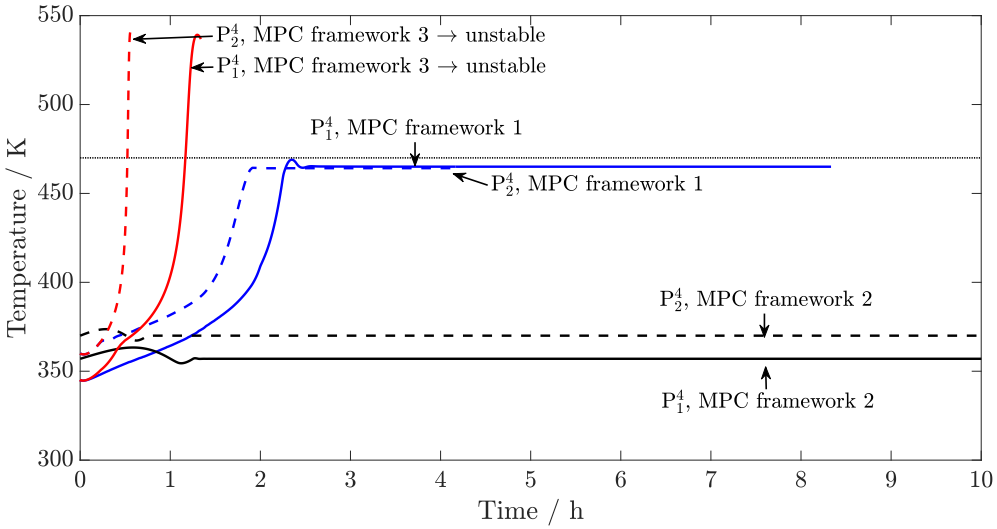

Fig. 5.7 Temperature profiles for processes P_1^4 and P_2^4 with all three MPC frameworks. The blue, black and red lines show the temperature profiles for MPC frameworks 1, 2 and 3, respectively. The dotted line indicates the maximum allowable temperature of $T_{\text{chem}} = 470$ K.

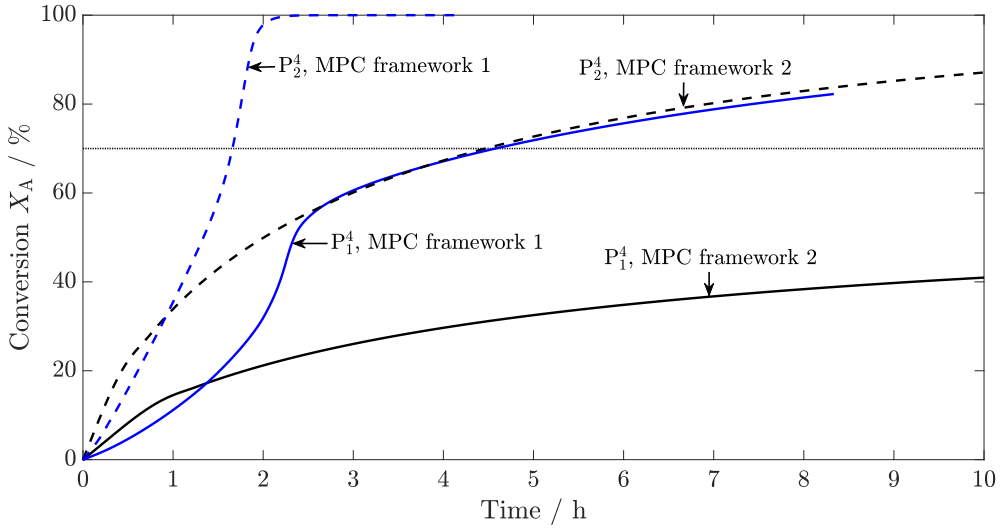

Fig. 5.8 Conversion profiles of reagent A for processes P_1^4 and P_2^4 controlled by MPC frameworks 1 and 2, given by the blue and black lines, respectively. The dotted line indicates the target conversion of $X_{A,target} = 70\%$.

MPC framework 3 results in unstable process behaviour, as the temperature profiles in Figure 5.7 exceed the maximum allowable temperature of $T_{chem} = 470$ K. The maximum temperature peaks for processes P_1^4 and P_2^4 occur at 540 K for both processes. It is clear that these processes exhibit thermal runaway behaviour and hence are not acceptable for real applications.

A constant set-point temperature results in stable control for processes P_1^4 and P_2^4. During the first approximately 1.2 h fluctuations in temperature occur, which then get controlled well throughout the remainder of the simulation.

MPC framework 1 leads to a continuous increase in the reaction temperature for processes P_1^4 and P_2^4. The temperature profiles never exceed the maximum allowable temperature T_{chem} and hence give thermally stable processes, as opposed to MPC framework 3. Furthermore, changes in the temperature profiles can be observed: when criterion $\mathscr{K}$ classifies the system to become unstable, the cooling flow rate is suddenly increased. This causes the temperature profiles to flatten, after which the system is again controlled along the boundary of stability until the maximum allowable temperature is reached. The extent to which these processes are more efficient than those controlled by MPC framework 2 is discussed in detail below with the help of conversion profiles. The conversion profiles of reagent A for processes P_1^4 and P_2^4 are shown in Figure 5.8.

Table 5.4 Summary of results obtained fro reaction scheme 4 controlled by each of the three MPC frameworks presented, including t_{reac}, T_{peak}, and $\bar{t}_{comp}$.

	MPC framework 1			MPC framework 2			MPC framework 3	
	t_{reac}/h	T_{peak}/K	$\bar{t}_{comp}$/CPUs	t_{reac}/h	T_{peak}/K	$\bar{t}_{comp}$/CPUs	T_{peak}/K	$\bar{t}_{comp}$/CPUs
P_1^4	4.6	469	0.86	>200	363	0.54	540	2.63
P_2^4	1.7	465	1.41	4.5	373	0.92	541	2.29
P_3^4	2.1	468	1.65	>200	386	1.28	542	11.2
P_4^4	35	468	1.21	124	380	1.05	539	10.4
P_5^4	4.2	467	1.16	60	346	0.93	918	2.89
P_6^4	15	465	1.12	55	385	0.94	589	13.0

Long times to reach the target conversion of 70%, given by the dotted line in Figure 5.8, are necessary when keeping a constant reaction temperature as is done for MPC framework 2. The target conversion is reached after more than 200 h and after 4.5 h for processes P_1^4 and P_2^4, respectively.

To see how well these processes can be intensified, MPC framework 1 has to be considered. The intensification of MPC framework 1 results in conversion times of 4.6 h and 1.7 h for processes P_1^4 and P_2^4, respectively. This is much shorter than the times obtained for MPC framework 2, whilst resulting in stable control as opposed to MPC framework 3. Hence a 3-fold decrease in reaction time is achieved by continuously increasing the reaction temperature along the boundary of stability.

As was observed for reaction schemes 1 to 3, MPC framework 1 results in intensified batch processes outperforming MPC framework 2 with a constant set-point temperature. Stable processes were obtained for MPC framework 1 unlike MPC framework 3, which employs a standard MPC framework with an extended control and prediction horizon.

In industry it is not only necessary to obtain stable processes, but the computational time required to evaluate the MPC steps is essential as well. If the computational time exceeds 10 s, which represents the time to implement the first control step by the MPC algorithm, this control scheme cannot be implemented. The average computational times per MPC step, $\bar{t}_{comp}$, the time to reach the target conversion, t_{reac}, and the peak temperature throughout each process, T_{peak}, for reaction scheme 4 are summarised in Table 5.4.

MPC framework 3 requires the longest times to evaluate the control values due to the larger control and prediction horizon. The computational times are not within the limit of 10 s set by the length of the control steps implemented in the MPC algorithm for processes P_3^4, P_4^4 and

P_6^4. The controls obtained result in unstable control which is unacceptable for implementation in industry. This can be further seen from the temperature peaks obtained for each process when controlled with MPC framework 1 within Table 5.4. The temperature peak exceeds $T_{\text{chem}} = 470$ K for every process, showing that thermal runaway behaviour is obtained. If this scheme were to be used, an even longer control and prediction horizon would be required. This further increases the computational time required, making it potentially infeasible for implementation in industry.

MPC framework 2 gives the shortest computational times $\bar{t}_{\text{comp}}$, since this control scheme does not require the evaluation of a large control and prediction horizon. Keeping a constant set-point temperature results in a simple and computationally efficient control scheme. The drawbacks of this control scheme are the lack of intensification, resulting in long processing times as can be seen from the values of t_{reac} in Table 5.4. The temperature peak for each process is close to the initial temperature, which is equal to the set-point temperature throughout each process.

MPC framework 1 gives the best compromise between computational time required, stability obtained, and intensification achieved. The computational times $\bar{t}_{\text{comp}}$ for MPC framework 1 obtained in Table 5.4 are shorter than for MPC framework 3, as a shorter horizon is used for each MPC step. The temperature peak is below the maximum allowable temperature of 470 K for each process, hence showing a stable process is present. The time required to reach the target conversion of 70% is much shorter for MPC framework 1 than it is for MPC framework 2: an at least 3-fold decrease in reaction time is achieved with the intensification. Hence this MPC framework leads to the stable intensification of batch processes with multiple reactions, as was also shown for reaction scheme 3.

5.5 Nitration of toluene

The nitration of toluene presents a challenging case study of an exothermic reaction network of industrial interest. The parameters defining this reaction network are given in Sections 2.2.5. The goal of this case study is to show that criterion $\mathscr{K}$ can be applied successfully to an industrially relevant reaction and give similar results in terms of intensification, as for reaction schemes 1 to 4. This case study was considered in Section 3.2.4 with the use of Lyapunov exponents. Similar simulations are carried here with criterion $\mathscr{K}$ to compare the extent of intensification and computational time required for each step in the MPC algorithm.

The intensification of the nitration of toluene is carried out with MPC framework 1 by starting the same reaction at three different initial temperatures. The temperature and conversion profiles for these processes will be presented to show that stable profiles are obtained.

For this case study the maximum allowable temperature is set to $T_{\text{chem}} = 510$ K. The objective function is formulated such that the most efficient process is found:

$$\min_{u(t)} \Phi\left(x(t), y(t), u(t)\right) = -\left[\text{o-}C_7H_7NO_2\right]\left(t_f\right) \tag{5.1}$$

The target concentration of o-nitrotoluene is set to $\left[\text{o-}C_7H_7NO_2\right]\left(t_f\right) = 2.5\,\text{kmol}\,\text{m}^{-3}$. The application of MPC framework 1 uses a control horizon of $t_c = 60$ s, with steps of length 10 s, and a prediction horizon of $t_p = 100$ s. The time required to find the control values set has to be shorter than the length of the first control value implemented. Three different starting temperatures of 430 K, 440 K, and 450 K are used to show that MPC framework 1 with criterion $\mathscr{K}$ results in stable control for each of these cases. The temperature profiles for each process are shown in Figure 5.9.

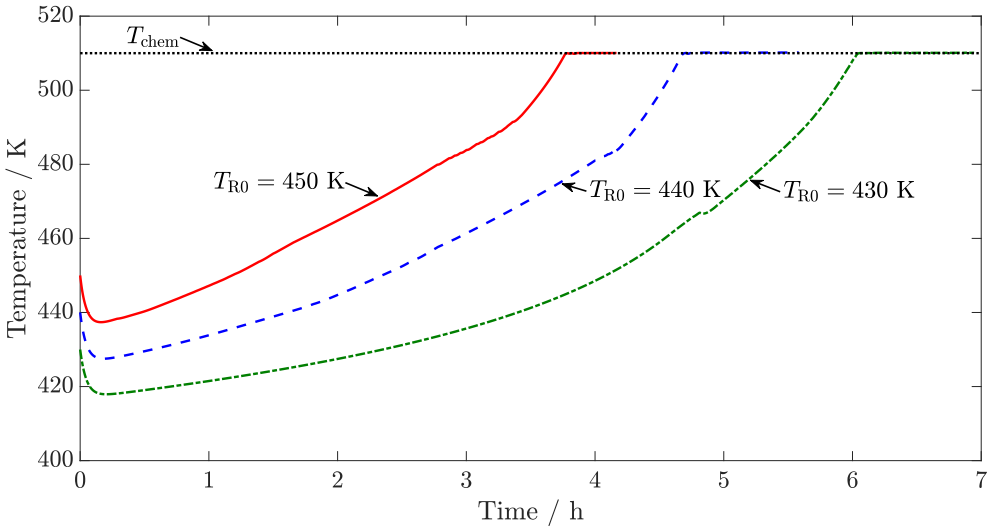

Fig. 5.9 Temperature profiles for intensified processes of the nitration of toluene. The solid line relates to $T_{\text{R0}} = 450$ K, the dashed line relates to $T_{\text{R0}} = 440$ K and the dash-dotted line relates to $T_{\text{R0}} = 430$ K. The dotted line indicates the maximum allowable temperature of $T_{\text{chem}} = 510$ K.

In Figure 5.9 no unstable process is obtained for any of the three processes. The maximum allowable temperature $T_{\text{chem}} = 510$ K is not exceeded for each process, hence each process is successfully intensified while satisfying the stability constraint given by thermal stability

criterion $\mathscr{K}$. It is therefore concluded that MPC framework 1 works successfully for this industrially relevant reaction system.

Interesting to note is the initial decrease in the reactor temperature observed in Figure 5.9. This initial temperature drop occurs due to the first reaction being endothermic, as well as the water within the cooling jacket removing heat even without coolant flow. Once enough heat is released by the nitration reactions, as shown in Table 2.2, the reactor temperature starts to increase. The same behaviour is observed when using Lyapunov exponents as the measure of stability, as is seen in Figure 3.16. Therefore the initial decrease in temperature does not occur due to criterion $\mathscr{K}$ incorrectly identifying unstable processes.

The time required until the target concentration of o-nitrotoluene shows how well the intensification with MPC framework 1 performs for batch processes. The concentration profiles for each product obtained during the process are shown for each starting temperature in Figure 5.10.

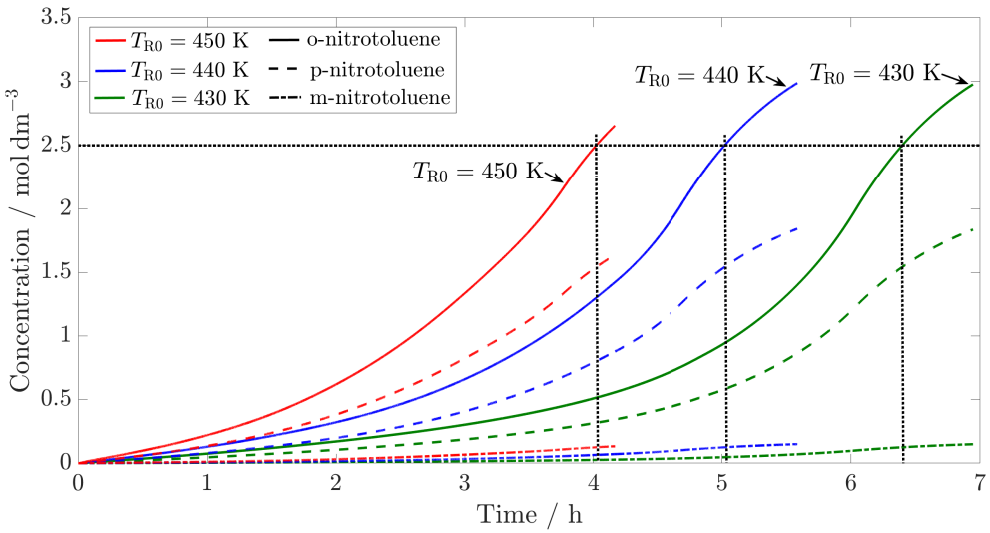

Fig. 5.10 Concentration profiles for the nitration of toluene reaction system. The profiles are obtained by control with MPC framework 1. The dotted line indicates the target concentration for o-nitrotoluene.

The concentration for o-nitrotoluene, given by the solid lines in Figure 5.10, reaches the target concentration of 2.5 kmol m^{-3} within 7 hours, which is similar to the results obtained when using Lyapunov exponents instead of criterion $\mathscr{K}$. Furthermore, the ratio of each nitrotoluene product obtained from the three different initial temperatures is equal in each case, as shown by the vertical dotted lines in Figure 5.10. In Section 2.2.5, where MPC

framework 1 with Lyapunov exponents was employed, the computational time required for each starting temperature was approximately 9 s which is very close to the upper limit of the permissible computational time. The computational times required per MPC step when using criterion $\mathscr{K}$ are given in Table 5.5.

Table 5.5 Computational time required by MPC framework 1 with criterion $\mathscr{K}$ for the intensification of the nitration of toluene with different starting temperatures T_{R0}.

	$T_{R0} = 430$ K	$T_{R0} = 440$ K	$T_{R0} = 450$ K
$\bar{t}_{comp}$ / CPUs	1.21	1.75	1.43

From Table 5.5 it is seen that the computational time required with MPC framework 1 is reduced by at least 4-fold compared to the framework using Lyapunov exponents as the measure of thermal stability. This shows that the same extent of intensification can be achieved with a more efficient MPC framework, whilst keeping the system under control at all times.

This last case study shows how the generalised expression for thermal stability criterion $\mathscr{K}$ can be implemented within a standard MPC framework, allowing a continuous increase in reactor temperature whilst keeping the respective batch process under control. This framework is valid for industrially relevant reactions, as is shown above. The computational time required is significantly shorter than for the framework with Lyapunov exponents, hence resulting in an efficient and safe control scheme for highly exothermic batch processes.

5.6 Chapter summary

In this chapter the generalised expression for stability criterion $\mathscr{K}$ derived in Chapter 4 was applied to MPC framework 1. The resulting processes are found to be stable for all reaction schemes introduced in Section 2.2. Furthermore, it is found that intensification of all batch processes is achieved, reducing the processing time significantly compared to constant temperature processes obtained with MPC framework 2.

As was the case for reaction schemes 1 and 2, a standard MPC algorithm with extended control and prediction horizons, given by MPC framework 3, results in unstable control if process intensification is attempted for reaction schemes 3 and 4. It is found that the computational time required for the extended control and prediction horizons exceeds the time available in several occasions. To achieve stable control with standard MPC frameworks a further increase in control and prediction horizon is required which results in even larger computational times. This makes the use of standard MPC frameworks for the intensification of batch processes infeasible.

In reaction schemes 3 and 4 multiple reactions occur simultaneously. The generalised expression of criterion $\mathscr{K}$ embedded in MPC framework is found to give stable process control for these reaction schemes, too. The computational time required per MPC step is found not to increase significantly with the number of reagents and reactions, which is the case for the implementation using Lyapunov exponents (see Section 3.2.4). This is the case, because the evaluation of criterion $\mathscr{K}$ requires one single function evaluation independent of the number of reagents and reactions, whilst the evaluation of Lyapunov exponents increases with number of components.

The industrial case study of the nitration of toluene is controlled using MPC framework 1 with criterion $\mathscr{K}$ embedded. It is found that, as for reaction schemes 3 and 4, the computational time required per MPC step does not increase significantly. This is a major improvement over MPC framework 1 with Lyapunov exponents, because the upper limit of 10 s per MPC step is reached for the control scheme using Lyapunov exponents. Similar process intensification is achieved for MPC framework 1 with criterion $\mathscr{K}$ as for the implementation using Lyapunov exponents embedded.

Chapter 6

Robust MPC under process uncertainty with stability criteria

As introduced in Section 1.3.4, process uncertainty has significant effects on process control. First principles models of batch reactors have found wide applications in the literature (Maxeiner and Engell, 2017). Therefore, uncertainty in the model structure is not considered in this work. The parameters of the model on the other hand are still uncertain and subject to potential change during the process (Wang *et al.*, 2018). Hence, parametric uncertainty is considered for the safe intensification of batch processes. The model structure, on the other hand, is assumed to be perfectly known.

6.1 Analysis of parametric uncertainty

Before parametric uncertainty can be included, the parameters of interest have to be found. As is the case for criterion $\mathscr{K}$ and Lyapunov exponents, the variables affecting the energy balance of the reactor contents are of major interest. The energy balance of the reactor mixture is given in Section 2.3 as:

$$\frac{\mathrm{d}}{\mathrm{d}t}\left(\rho_{\mathrm{R}} C_{p,\mathrm{R}} T_{\mathrm{R}} V_{\mathrm{R}}\right) = \sum_{i=1}^{M}\left[r_i\left(\Delta H_{r,i}\right) V_{\mathrm{R}}\right] - UA\left(T_{\mathrm{R}} - T_{\mathrm{C}}\right) \tag{2.22}$$

From Equation (2.22) it is seen, that the following parameters of reaction i influence the heat generation within the reactor:

- $\Delta H_{r,i}$

- $k_{0,i}$
- $E_{a,i}$

Furthermore, a lack of cooling may lead to thermal runaway behaviour. Hence, for considerations of robustness, the heat transfer coefficient U is considered also. It is further assumed that parameters with respect to the reaction mechanism, such as stoichiometric coefficients and reaction orders, are known for certain. The values of density and heat capacity can be measured to relatively high accuracy in industry, and are therefore not expected to have large effects control performance due to uncertainty.

In the previous sections it was shown that batch process intensification can be achieved when embedding thermal stability criterion $\mathscr{K}$ and Lyapunov exponents within a suitable MPC framework, if the process models are known exactly. Hence, it is required to examine how parametric uncertainty affects the prediction of thermal runaway behaviour when using Lyapunov exponents and criterion $\mathscr{K}$.

Considering process P_1^1 as an example, the following analysis is carried out for one of the parameters identified, *e.g.* the enthalpy of reaction ΔH_r:

1. define a normal distribution for ΔH_r, using the value given by process P_1^1 in Table A.1 as the arithmetic mean
2. for a given relative standard deviation, sample 100 values for ΔH_r
3. for the sampled values of ΔH_r use criterion $\mathscr{K}$ and Lyapunov exponents to predict the stability of process P_1^1 with PI control, as was done in Section 2.4.1
4. examine how wide the confidence interval of criterion $\mathscr{K}$ and Lyapunov exponents is in terms of predicting thermal runaway behaviour
5. repeat for remaining parameters k_0, E_a, and U

Once the effect of parametric uncertainty on the quality of predicting thermal runaway behaviour with criterion $\mathscr{K}$ and Lyapunov exponents is understood, MPC frameworks including uncertainty are considered.

6.1.1 Uncertainty of enthalpy of reaction

The probability distribution used for the analysis of robustness with respect to the enthalpy of reaction ΔH_r for process P_1^1 is given by:

$$\Delta H_r \sim \mathscr{N}\left(\mathrm{E}\left[\Delta H_r\right], \sigma^2_{\Delta H_r}\right) \tag{6.1a}$$

where $\mathrm{E}[\Delta H_r]$ is the mean and $\sigma_{\Delta H_r}$ is the standard deviation of ΔH_r. The numerical values are given by:

$$\mathrm{E}[\Delta H_r] = -75\,\mathrm{kJ\,mol^{-1}} \tag{6.1b}$$

$$\sigma_{\Delta H_r} = 1.91\,\mathrm{kJ\,mol^{-1}} \tag{6.1c}$$

The standard deviation is obtained in the following manner: for a 95% confidence interval in the mean value of the enthalpy of reaction given a 10% range, the z-value of a normal distribution is given by (Rasmussen and Williams, 2006):

$$1.96 = \frac{0.95\mathrm{E}[\Delta H_r] - \mathrm{E}[\Delta H_r]}{\sigma_{\Delta H_r}} \tag{6.2a}$$

$$\sigma_{\Delta H_r} = \frac{-0.05\mathrm{E}[\Delta H_r]}{1.96} \tag{6.2b}$$

$$\sigma_{\Delta H_r} = 1.91\,\mathrm{kJ\,mol^{-1}} \tag{6.2c}$$

The normal distribution given in Equation (6.1) is used to examine the effect of perturbing the value of ΔH_r by 10%. The temperature profile of the unperturbed process P_1^1 is given in Figure 2.2.

The profiles for criterion $\mathscr{K}$ and the local Lyapunov exponent with respect to reactor temperature, $\Lambda_{1,3}$, when using a perturbation of 10% in the value of ΔH_r are shown in Figure 6.1 and Figure 6.2, respectively.

Figure 6.1 shows that, if there is 95% certainty that the value of ΔH_r is within 10% of the mean value shown in Equation (6.1), criterion $\mathscr{K}$ results in different prediction of thermal stability: if the magnitude of ΔH_r is reduced the reaction becomes less exothermic, hence resulting in a thermal runaway reaction later. This is shown by the red line in Figure 6.1. If the magnitude of ΔH_r is increased on the other hand, unstable operation is predicted from the beginning of the process. This is the case because a 5% increase in enthalpy of reaction would result in thermal runaway behaviour for process P_1^1. Therefore, using this increased value of ΔH_r with criterion $\mathscr{K}$ for process intensification should result in more conservative control than that obtained in Section 5.1.

The local Lyapunov exponents $\Lambda_{1,3}$ in Figure 6.2 shows similar results to those for criterion $\mathscr{K}$ in Figure 6.1: an increase in the magnitude of ΔH_r leads to the prediction of thermal

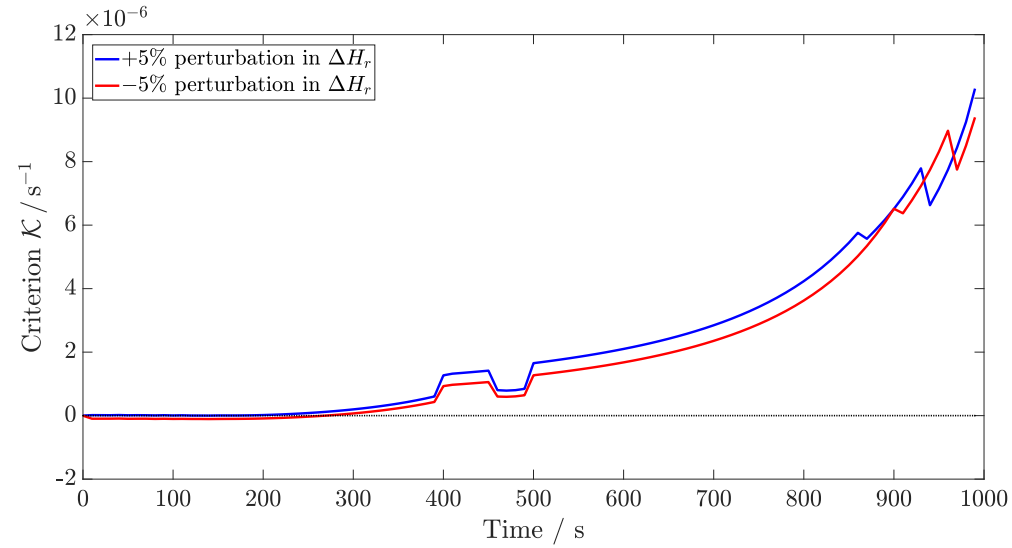

Fig. 6.1 Profile of criterion $\mathscr{K}$ for process P_1^1 with uncertainty in the value of ΔH_r according to Equation (6.1). The predictions using a positive 5% perturbation in the magnitude of ΔH_r and a negative perturbation of 5% in the magnitude of ΔH_r are shown by the blue and red lines, respectively.

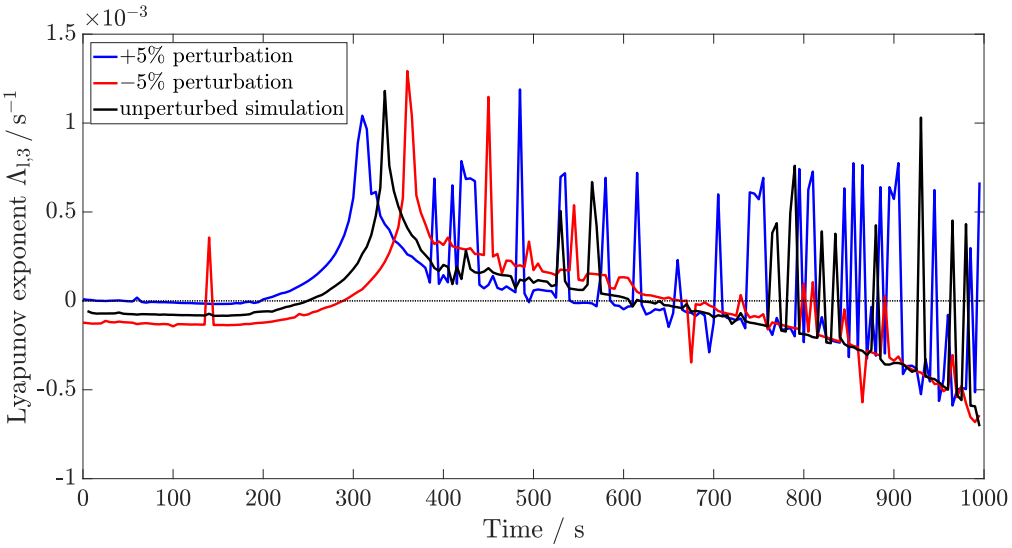

Fig. 6.2 Profile of Lyapunov exponent $\Lambda_{l,3}$ for process P_1^1 with uncertainty in the value of ΔH_r according to Equation (6.1). The predictions using a positive 5% perturbation in the magnitude of ΔH_r, a negative perturbation of 5% in the magnitude of ΔH_r, and the actual value of ΔH_r are shown by the blue, red and black line, respectively.

instability from the beginning of the process. If a smaller value of ΔH_r is used for the Lyapunov exponents than is present in the real process, instability will be predicted later at approximately 300 s in Figure 6.2. Once thermal runaway behaviour occurs significant oscillations in the value of $\Lambda_{1,3}$ are observed, as was the case for the unperturbed example processes shown in Section 3.2.3.

6.1.2 Uncertainty of Arrhenius pre-exponential factor

The probability distribution of the Arrhenius pre-exponential factor k_0 used to examine the robustness of criterion $\mathscr{K}$ and Lyapunov exponents is as follows:

$$k_0 \sim \mathscr{N}\left(\mathrm{E}\left[k_0\right], \sigma_{k_0}^2\right) \tag{6.3a}$$

where

$$\mathrm{E}\left[k_0\right] = 2.76 \times 10^6\,\mathrm{m^3\,kmol^{-1}\,s^{-1}} \tag{6.3b}$$

$$\sigma_{k_0} = 7.04 \times 10^4\,\mathrm{m^3\,kmol^{-1}\,s^{-1}} \tag{6.3c}$$

The value for the standard deviation σ_{k_0} is obtained in a similar fashion to that shown in Equation (6.2) for the enthalpy of reaction ΔH_r.

The normal distribution shown in Equation (6.3) is used to obtain a 95% confidence interval when perturbing the value of k_0 by $\pm 5\%$. For each perturbed value of k_0 criterion $\mathscr{K}$ and the Lyapunov exponent for the reactor temperature $\Lambda_{1,3}$ are evaluated. The profiles of criterion $\mathscr{K}$ and the local Lyapunov exponent $\Lambda_{1,3}$ for process P_1^1 are shown in Figure 6.3 and Figure 6.4, respectively.

Figure 6.3 shows similar results as for the enthalpy of reaction: according to the heat generation within the reactor, a 5% change in the enthalpy of reaction is equivalent to a 5% increase in reaction rate, which is given by a 5% increase in k_0. Hence, an increase of 5% in the value of k_0 will make criterion $\mathscr{K}$ predict thermal runaway behaviour from the beginning, whereas a decrease of 5% in the value of k_0 results in delayed thermal runaway prediction. Therefore, as the estimated value of k_0 increases, the model predicts a system with higher potential of thermal runaway behaviour. If MPC is used to intensify this process, a more conservative increase in reactor temperature will therefore be necessary.

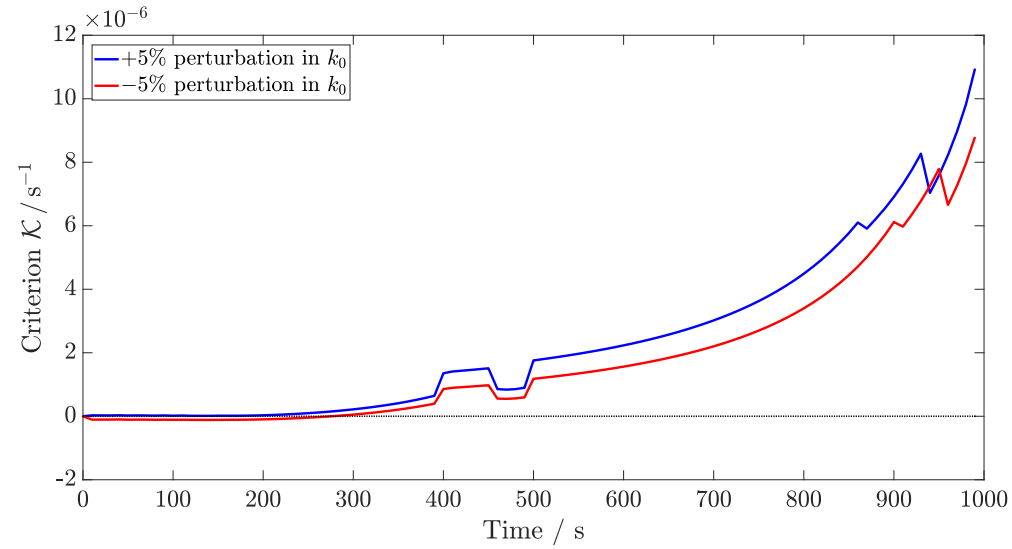

Fig. 6.3 Profile of criterion $\mathscr{K}$ for process P_1^1 with uncertainty in the value of k_0 according to Equation (6.3). The predictions using a positive 5% perturbation in k_0 and a negative perturbation of 5% in k_0 are shown by the blue and red lines, respectively.

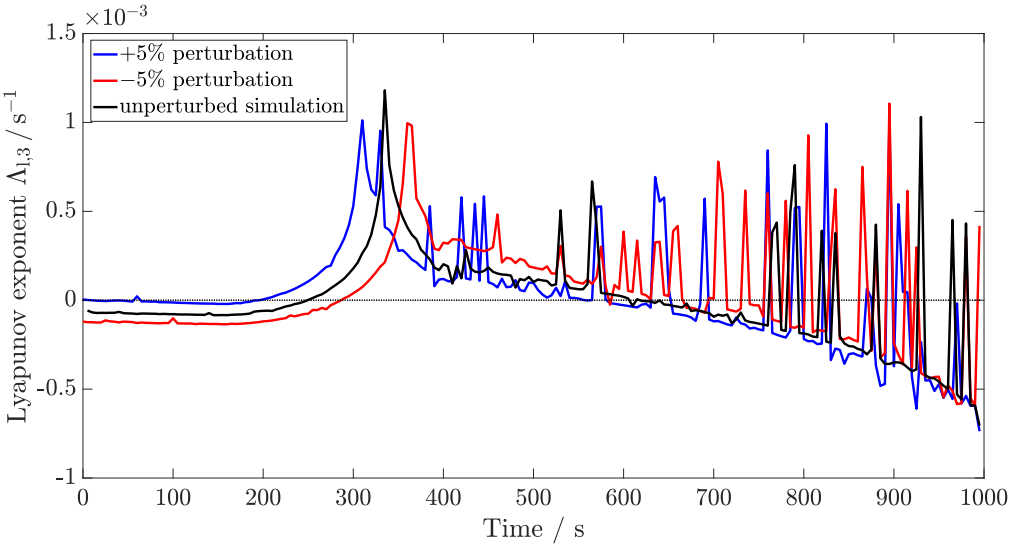

Fig. 6.4 Profile of Lyapunov exponent $\Lambda_{1,3}$ for process P_1^1 with uncertainty in the value of k_0 according to Equation (6.3). The predictions using a positive 5% perturbation in k_0, a negative perurbation of 5% in k_0, and the actual value of k_0 are shown by the blue, red and black line, respectively.

Figure 6.4 shows similar results to those shown for ΔH_r in Figure 6.2: a positive perturbation of 5% in the value of k_0 increases the rate of reaction and therefore the heat generation. Instability is hence predicted before the nominal prediction using the correct value of k_0, shown by the black line. This means that if too large a value of k_0 is used for Lyapunov exponents, a more conservative prediction of thermal runaway behaviour is present. A reduction in the value of k_0 results in later prediction of thermal runaway behaviour, since the process is assumed to be reacting more slowly. This delayed instability prediction can be seen by the red line in Figure 6.6.

6.1.3 Uncertainty of activation energy

The last reaction parameter to be considered for the robustness analysis is the activation energy E_a. As was carried out for the enthalpy of reaction and the Arrhenius pre-exponential factor, 100 values of E_a are sampled from a normal distribution. As is shown in Table A.2, the values of activation energy are given as E_a/R which results in units of Kelvin. The normal distribution is hence is given by:

$$E_a/R \sim \mathcal{N}\left(\mathrm{E}\left[E_a/R\right], \sigma^2_{E_a/R}\right) \tag{6.4a}$$

where

$$\mathrm{E}\left[E_a/R\right] = 9525\,\mathrm{K} \tag{6.4b}$$

$$\sigma_{E_a/R} = 243\,\mathrm{K} \tag{6.4c}$$

The value for the standard deviation $\sigma_{E_a/R}$ is obtained in a similar fashion to that shown in Equation (6.2) for the enthalpy of reaction ΔH_r.

The value of E_a/R is perturbed by 5% to examine the 95% confidence interval of the predictions with criterion $\mathscr{K}$ and Lyapunov exponents. For each perturbed value of E_a/R the profiles of criterion $\mathscr{K}$ and the local Lyapunov exponent $\Lambda_{1,3}$ for process P_1^1 are shown in Figure 6.5 and Figure 6.6, respectively.

Figure 6.5 shows a different result to that observed for uncertainty in ΔH_r and k_0: a 5% perturbation in the value of E_a/R results in a much larger range of values for criterion $\mathscr{K}$. This is the case, because the effect of the uncertainty in the activation energy is amplified by the exponential within the Arrhenius expression $(\exp(-E_a/(RT_\mathrm{R}))$. A smaller value in the activation energy results in a faster reaction rate. This effect is amplified by the exponential

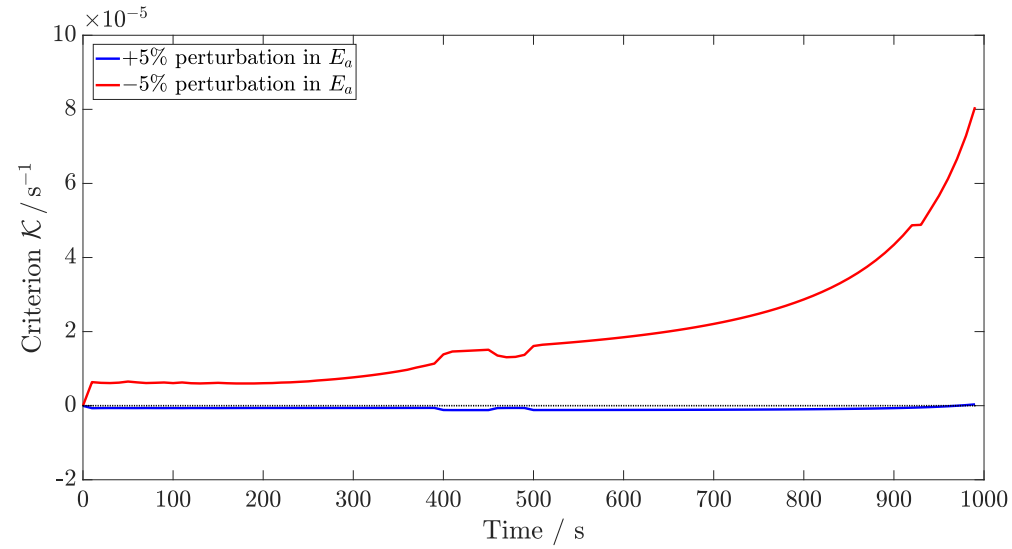

Fig. 6.5 Profile of criterion $\mathscr{K}$ for process P_1^1 with uncertainty in the value of E_a/R according to Equation (6.4). The predictions using a positive 5% perturbation in E_a/R and a negative perturbation of 5% in E_a/R are shown by the blue and red lines, respectively.

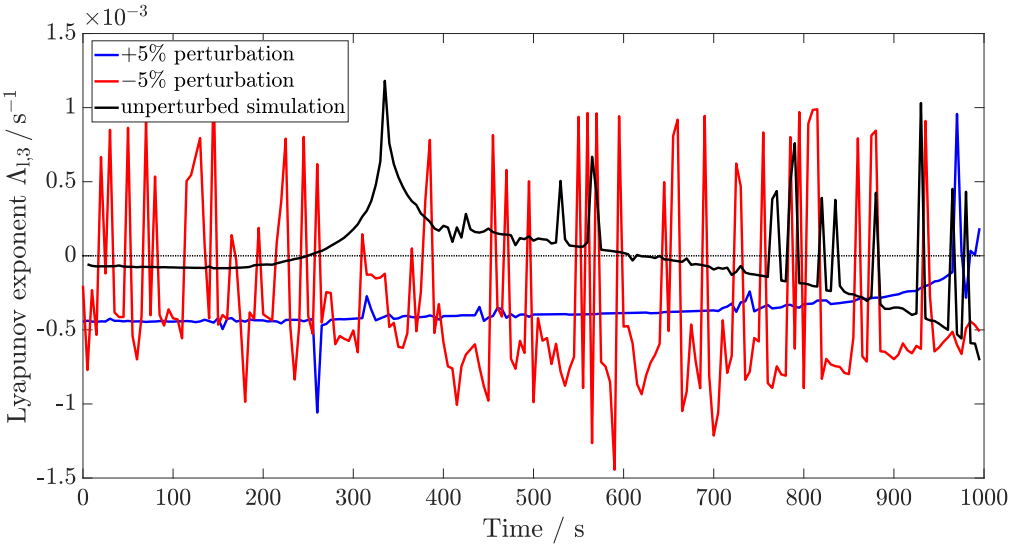

Fig. 6.6 Profile of Lyapunov exponent $\Lambda_{1,3}$ for process P_1^1 with uncertainty in the value of E_a/R according to Equation (6.4). The predictions using a positive 5% perturbation in E_a/R, a negative perurbation of 5% in E_a/R, and the actual value of E_a/R are shown by the blue, red and black line, respectively.

term. Therefore, the effect of decreasing the activation energy results in stronger deviations in the thermal runaway prediction with criterion $\mathscr{K}$. An increase of 5% in the value of E_a/R reduces the rate of reaction to such an extent, that thermal runaway behaviour only occurs towards the end of the time frame as shown in Figure 6.5.

When incorporated within an MPC framework, the prediction of thermal stability with criterion $\mathscr{K}$ and Lyapunov exponents will be more sensitive to deviations in the activation energy.

For Lyapunov exponents large oscillations for the negatively perturbed value of activation energy, given by the red lines, are observed in Figure 6.6. A reduction of 5% in the value of E_a increases the rate of reaction significantly, including the temperature effect explained above. Hence, unstable behaviour is predicted from the beginning which results, as discussed before, results in large oscillations for the value of $\Lambda_{l,3}$. In Figure 6.6 this is shown by the red line. An increase of 5% in the value of E_a reduces the reaction rate due to the Arrhenius expression used. Therefore, the local Lyapunov exponent for reactor temperature only predicts unstable behaviour towards the end of the process at approximately 960 s, given by the blue line. From the Lyapunov exponent using the exact parameter value, given by the black line, it is seen that unstable behaviour occurs much earlier during the process at approximately 280 s. Therefore, variations in the activation energy of $\pm 5\%$ results in a large spread of thermal stability predictions.

6.1.4 Uncertainty of heat transfer coefficient

The cooling of the reactor strongly affects the thermal runaway behaviour of batch reactors. Therefore, uncertainty in the heat transfer coefficient can have drastic effects on the prediction of thermal instability. As was carried out for the reaction parameters, a normal distribution for the value of U is used to obtain 100 samples for which thermal stability is predicted using criterion $\mathscr{K}$ and Lyapunov exponent $\Lambda_{l,3}$. In this analysis it is assumed that the value of U does not change throughout the process but stays constant at the sampled value. Otherwise the influence of uncertainty in the value of U could not be observed easily. The normal distribution for the heat transfer coefficient U is given by:

$$U \sim \mathscr{N}\left(\mathrm{E}\left[U\right], \sigma_U^2\right) \tag{6.5a}$$

where

$$\mathrm{E}[U] = 720\,\mathrm{W\,m^{-2}\,K^{-1}} \tag{6.5b}$$

$$\sigma_U = 18.4\,\mathrm{W\,m^{-2}\,K^{-1}} \tag{6.5c}$$

The value for the standard deviation σ_U is obtained in a similar fashion to that shown in Equation (6.2) for the enthalpy of reaction ΔH_r.

A 95% confidence interval for the thermal runaway prediction using Lyapunov exponents and criterion $\mathscr{K}$ is obtained by perturbing the value of U by $\pm 5\%$ and with Equation (6.5). The profiles of criterion $\mathscr{K}$ and the local Lyapunov exponent $\Lambda_{l,3}$ for process P_1^1 are shown in Figure 6.7 and Figure 6.8, respectively.

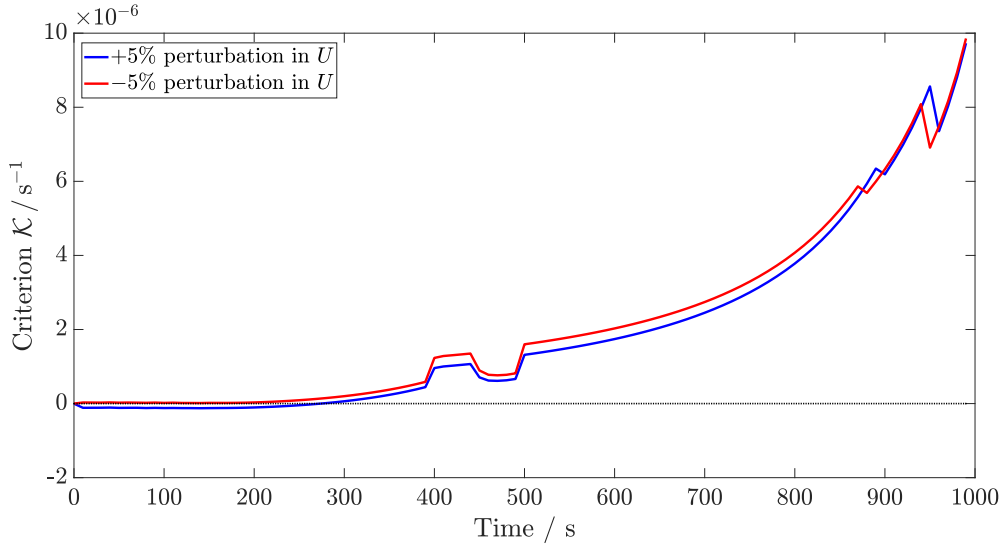

Fig. 6.7 Profile of criterion $\mathscr{K}$ for process P_1^1 with uncertainty in the value of U according to Equation (6.5). The predictions using a positive 5% perturbation in U and a negative perturbation of 5% in U are shown by the blue and red lines, respectively.

Figure 6.7 for criterion $\mathscr{K}$ shows similar results to those for k_0 and ΔH_r with one significant difference: an increase in the value of U will decrease the thermal runaway potential, since an increase in heat transfer coefficient leads to better cooling of the system. Similarly, decreasing the value of U will result in a more unstable process. The resulting profiles of criterion $\mathscr{K}$ are not affected as strongly by the perturbation in U as for the activation energy, because no exponential term is involved in the cooling of the reactor.

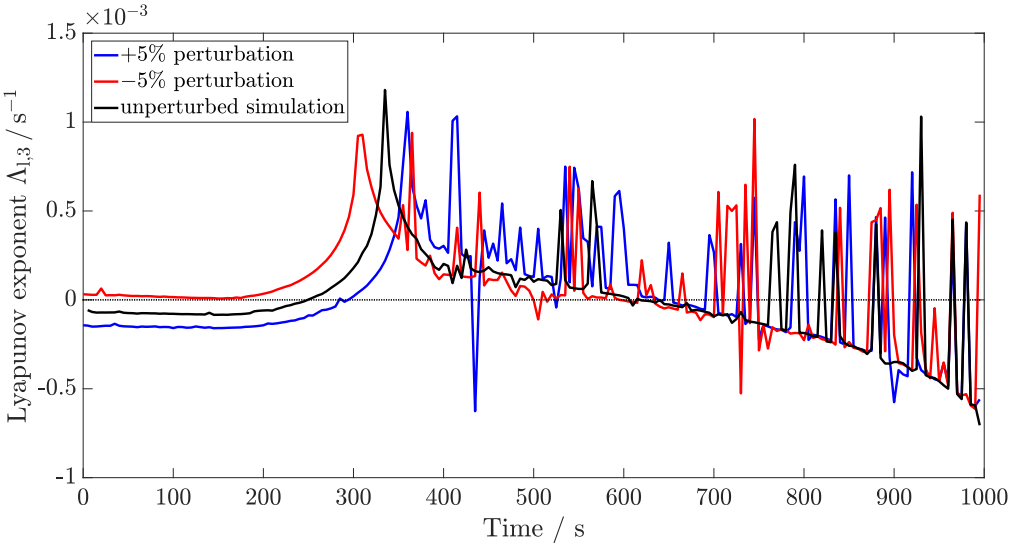

Fig. 6.8 Profile of Lyapunov exponent $\Lambda_{1,3}$ for process P_1^1 with uncertainty in the value of U according to Equation (6.5). The predictions using a positive 5% perturbation in U, a negative perurbation of 5% in U, and the actual value of U are shown by the blue, red and black line, respectively.

Figure 6.8 for Lyapunov exponents shows similar results for perturbations in the value of U as for ΔH_r and k_0, but in the reverse direction. An increase in the value of U leads to better cooling, hence resulting in a delayed stability prediction. A decrease in the value of U by 5% leads to worse cooling performance, and hence Lyapunov exponents predict thermal runaway behaviour to occur earlier than it actually does. The most significant effect of uncertainty when using Lyapunov exponents for stability detection is still the activation energy E_a, as can be seen in Figure 6.6.

6.2 Scenario-based MPC framework

In the previous section it was shown that uncertainty in the enthalpy of reaction, Arrhenius pre-exponential factor, activation energy and heat transfer coefficient indeed affect the prediction of thermal stability using criterion $\mathscr{K}$ and Lyapunov exponents. To ensure safe operation of industrial processes, it is therefore of utmost importance that the MPC framework employed takes this uncertainty into consideration.

As was discussed in Section 1.3.4, several methods of dealing with parametric uncertainty exist in literature. In a similar manner to the analysis in Section 6.1, several sets of parameters can be sampled from normal distributions of each individual parameter. For each set of

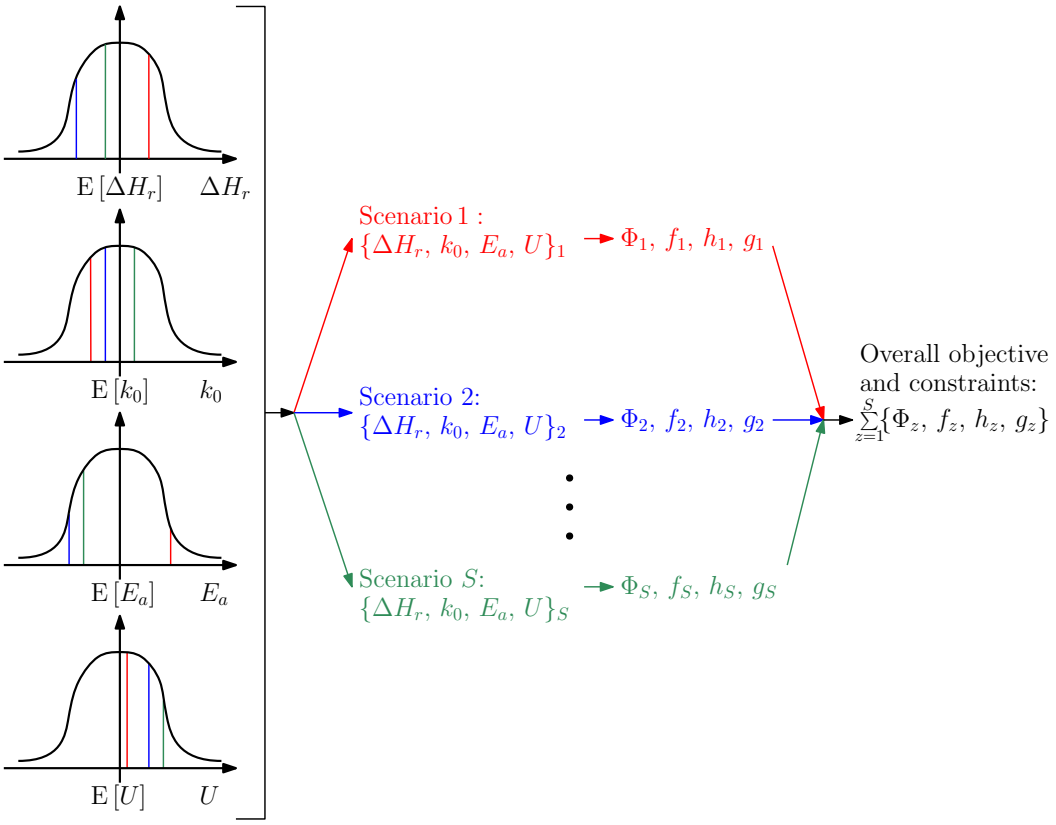

Fig. 6.9 Schematic showing scenario-based MPC with sampling of parameter values to obtain the overall problem solved by the MPC algorithm.

parameters a scenario is created, which is included within the MPC framework. This method is called *scenario-based* MPC.

Unlike the formulation shown in Equation (2.23) the optimisation and constraints of the MPC algorithm are not considered for the nominal model, but for several scenarios with sampled parameter values. Hence, the modified formulation is as follows:

$$\min_{u} \sum_{z=1}^{S} \int_{t_0^{(s)}}^{t_0^{(s)}+t_p} \Phi_z \, \mathrm{d}t \tag{6.6a}$$

subject to:

$$f_z\left(x, y_z, u, t\right) = \dot{x} \qquad z = 1, 2, \ldots, S \tag{6.6b}$$

$$h_z\left(x, y_z, u, t\right) = 0 \qquad z = 1, 2, \ldots, S \tag{6.6c}$$

$$g_z\left(x, y_z, u, t\right) \leq 0 \qquad z = 1, 2, \ldots, S \tag{6.6d}$$

$$t_0^{(s)} \leq t^{(s)} \leq t_0^{(s)} + t_p \tag{6.6e}$$

where the subscript z indicates each individual scenario, Φ_z is the objective function for each scenario, and it is assumed that S scenarios are simulated for each MPC step.

Thermal stability criterion $\mathscr{K}$ and Lyapunov exponents are used as stability criteria for the MPC formulation in Equation (6.6). The implementation of scenario-based MPC is schematically shown in Figure 6.9.

The performance of scenario-based MPC is investigated using reaction schemes 1 and 2, as well as the nitration of toluene. As was the case for nominal MPC cases, *i.e.* the simulations with certain system parameters, the processing time, computational time and the stability are the main points of comparison.

6.2.1 Reaction scheme 1

The performance of scenario-based MPC embedded with criterion $\mathscr{K}$ and Lyapunov exponents is assessed by simulating process P_1^1 for different numbers of scenarios, each using a sample of parameters ΔH_r, k_0, E_a and U according to Figure 6.9. As the number of scenarios increases, the number of parameter sets sampled increases. Therefore, with an increasing number of scenarios it is more likely to obtain a set of parameters which would result in a more unstable system than the real system being controlled. The MPC framework is required to ensure that each scenario with its set of sampled parameters is stable. Therefore, as the number of scenarios increases, the probability of the MPC framework having to control more unstable processes than the nominal system increases. Hence, it is expected that the number of simulations of the real process resulting in thermal runaway behaviour decreases as the number of scenarios increases.

100 simulations are carried out with 1, 2, 3, 5, 8 and 10 scenarios for process P_1^1 with MPC framework 1 embedded with criterion $\mathscr{K}$ and with Lyapunov exponents. The fraction of processes that are unstable with this control scheme for each number of scenarios S is shown in Figure 6.10.

In Figure 6.10 it is seen that once 5 scenarios are used with criterion $\mathscr{K}$, no thermal runaway behaviour is observed. If Lyapunov exponents are used, 3 or more scenarios result in mostly stable processes without thermal runaways. Important to note is that only 100 simulations have been carried out. Therefore, this is not a guarantee that safe operation is obtained under all conditions. Nevertheless, a clear improvement is achieved in terms of stability as the number of scenarios is increased within the MPC framework.

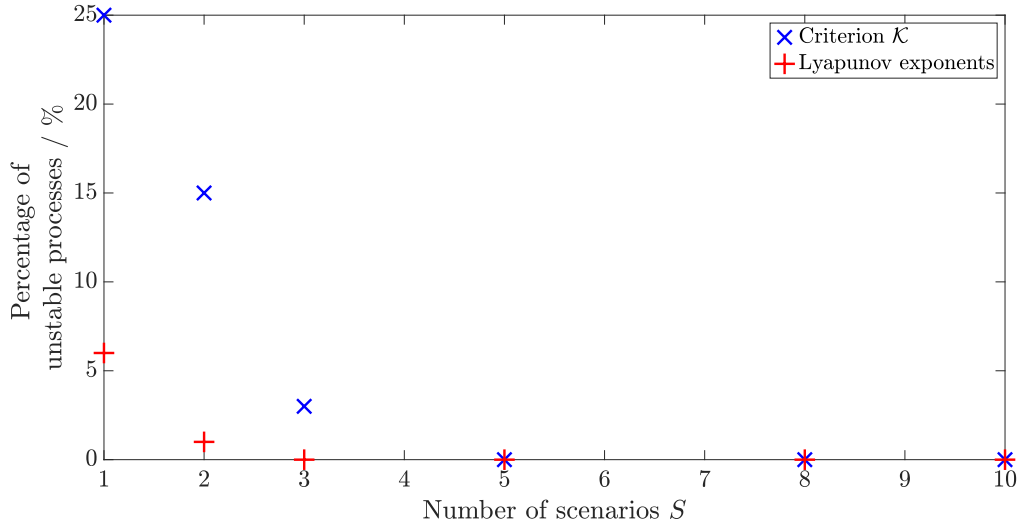

Fig. 6.10 Fraction of simulations of process P_1^1 resulting in thermal runaway behaviour for each number of scenarios. The percentages are evaluated based on 100 simulations carried out for each control scheme.

A reduction in the number of unstable processes means that more conservative control is obtained. This, on the other hand, could mean that no reduction in processing time t_{reac} is obtained when compared to processes controlled by MPC framework 2. The target conversion for process P_1^1 is $X_{\text{C,target}} = 80\%$. The average times required to reach this target conversion for each number of scenarios is shown in Figure 6.11.

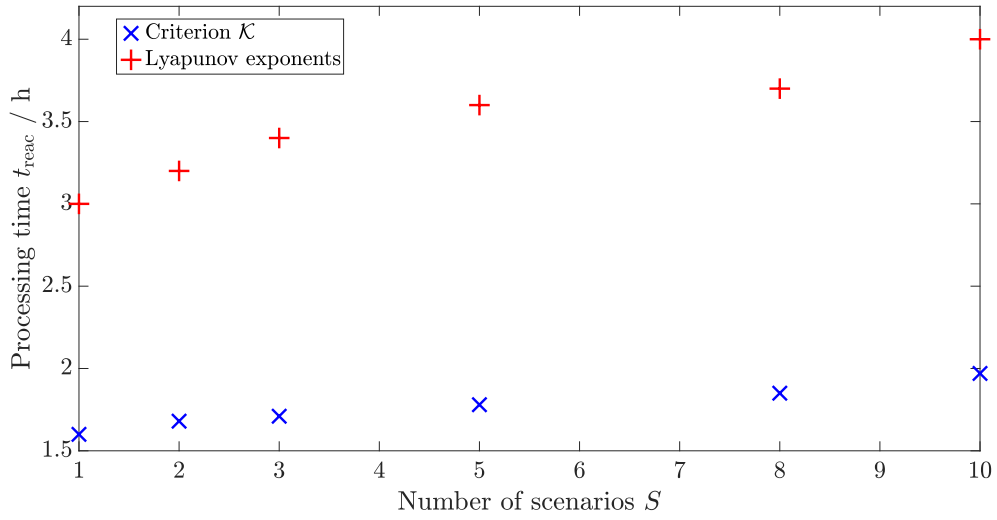

Fig. 6.11 Processing times t_{reac} to reach the target conversion of $X_{\text{C,target}} = 80\%$ for process P_1^1 with each number of scenarios.

As expected, t_{reac} increases with the number of scenarios used. Nevertheless, if criterion $\mathscr{K}$ is used the value of t_{reac} does not exceed 2 h. The time required to reach the target conversion with MPC framework 2 is 6.5 h, as shown in Table 3.1. Therefore the increase in conservativeness by using several scenarios within an MPC framework with criterion $\mathscr{K}$ still results in significant process intensification. If Lyapunov exponents are used process intensification is also achieved, but the processing times are considerably higher than with criterion $\mathscr{K}$.

On average, the time to reach the target conversion with Lyapunov exponents is double that of using criterion $\mathscr{K}$ for process P_1^1. Due to the horizon of $t_{\text{Lyap}} = 5000$ s over which Lyapunov exponents are evaluated a small uncertainty in a parameter will have a larger effect on the Lyapunov exponent value than on criterion $\mathscr{K}$, which is evaluated at the current point in time only. Therefore, using scenarios with uncertain parameters will result in more conservative predictions of thermal stability if Lyapunov exponents are used. Hence, larger processing times and fewer unstable processes are observed if Lyapunov exponents, as opposed to criterion $\mathscr{K}$, is used.

The last important feature of this control scheme is the computational time required for each MPC step, $\bar{t}_{\text{comp}}$. If $\bar{t}_{\text{comp}}$ exceeds 10 s, then the time required to evaluate the optimal control value is larger than the time available. This is not acceptable when using such control schemes in industry. The computational times $\bar{t}_{\text{comp}}$ for multiple scenario-based MPC for process P_1^1 is shown in Figure 6.12.

In Figure 6.12 it is observed that as the number of scenarios increases, larger computational times are required per MPC step. If 8 scenarios or more are used with criterion $\mathscr{K}$, the upper limit of computational time of 10 s is reached. Similar results are obtained for the implementation with Lyapunov exponents. Therefore the number of scenarios has to be chosen carefully such that feasible control with respect to time available is obtained.

From the results shown in Figures 6.10−6.12 it is seen that when embedding criterion $\mathscr{K}$ within MPC framework 1, using 5 scenarios results in most processes being stable, as well as the computational time not exceeding the 10 s limit. Process intensification is still achieved, with t_{reac} only 10% larger than for the single scenario case. When using Lyapunov exponents 3 or more scenarios can be used to make sure stable processes are present. A reduced number in scenarios reduces the computational time per MPC step required. Processing times when using Lyapunov exponents with scenario-based MPC are longer than using criterion $\mathscr{K}$, but still significantly shorter than constant temperature processes. Therefore a robust MPC framework with embedded criterion $\mathscr{K}$ and embedded Lyapunov exponents is obtained.

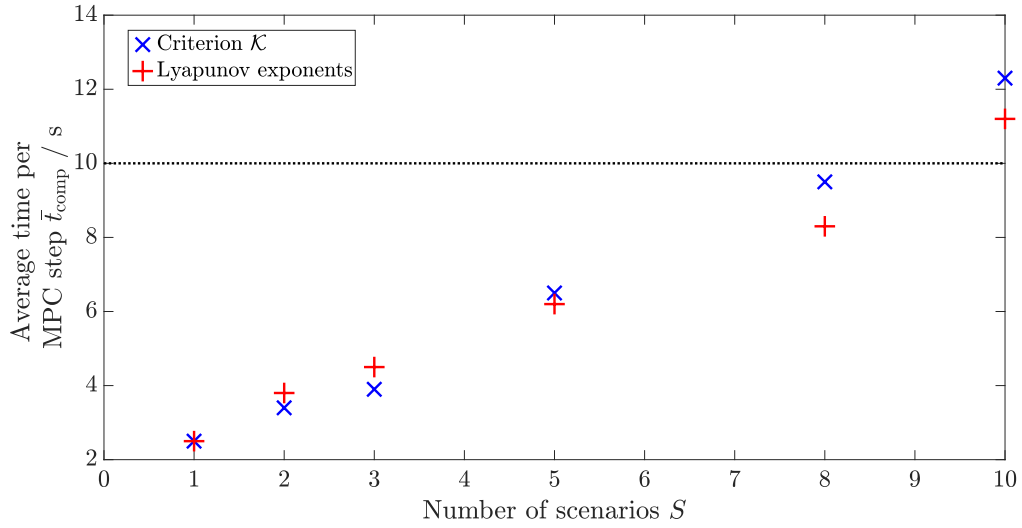

Fig. 6.12 Computational times $\bar{t}_{\text{comp}}$ per MPC step for process P_1^1 with each number of scenarios. The horizontal dashed line indicates the upper limit of the computational time available for the MPC framework used.

6.2.2 Reaction scheme 2

The same analysis as for process P_1^1 above is now carried out for process P_4^2 which represents a more complicated reaction system, as described in Section 2.2.2. The uncertain parameters are the same as for process P_1^1, with the mean values given in Table A.2.

100 simulations are carried out for 1, 2, 3, 5, 8, and 10 scenarios for MPC framework 1 with both, embedded criterion $\mathscr{K}$ and embedded Lyapunov exponents. How many of the resulting processes exhibit thermal runaway behaviour is shown in Figure 6.13.

In Figure 6.13 it is seen that as the number of scenarios increases, the percentage of thermal runaway processes decreases. This is the case, because a larger number of scenarios increases the chance of predicting more unstable process behaviour, hence resulting in more conservative control. The percentage of thermal runaway processes initially is higher for process P_4^2 than it is for process P_1^1. Furthermore, the number of unstable processes when using Lyapunov exponents is much lower if using less than 5 scenarios, which is also observed for process P_1^1. Therefore, using Lyapunov exponents embedded within scenario-based MPC results in a more conservative control scheme with fewer thermal runways for a small number of scenarios.

As for process P_1^1, once 5 scenarios are used within the MPC framework, no thermal runaway behaviour is observed with criterion $\mathscr{K}$. As for process P_1^1, if using Lyapunov exponents

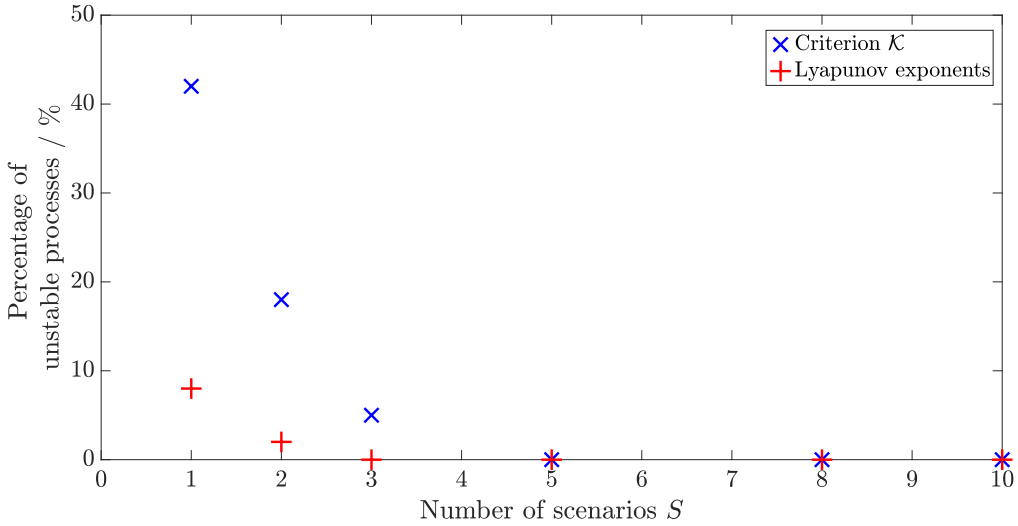

Fig. 6.13 Fraction of simulations of process P_4^2 resulting in thermal runaway behaviour for each number of scenarios. The percentages are evaluated based on 100 simulations carried out for each control scheme.

no thermal runaways are observed if more than 3 scenarios are used. These observations are made from 100 simulations and hence do not guarantee that stable operation is always obtained if 5 scenarios for criterion $\mathcal{K}$ and 3 scenarios for Lyapunov exponents are used. Since the conservativeness of the robust control system increases with the number of scenarios used, it is interesting to see how this affects the processing time t_{reac}. The results are shown in Figure 6.14.

Similar to process P_1^1, in Figure 6.14 it is seen that t_{reac} increases with the number of scenarios used. The processing time when using standard MPC with a constant set-point temperature, as is shown for MPC framework 2 in Table 3.2, is given by $t_{\text{reac}} = 10.6$ h. Comparing the results for t_{reac} and the processing times using MPC framework 2 with the results shown in Figure 6.14 it is observed that significant process intensification is achieved with the scenario-based MPC framework. If 5 scenarios are used with criterion $\mathcal{K}$, the reaction time is still reduced by a factor of 5.

The use of Lyapunov exponents with 3 scenarios results in a processing time of approximately 3 h, which is a 3-fold reduction in processing time when compared to the constant temperature process as shown in Table 3.2. As is observed for process P_1^1 above, using Lyapunov exponents results in less thermal runaway processes and longer processing times. This is in line with the results for process P_1^1.

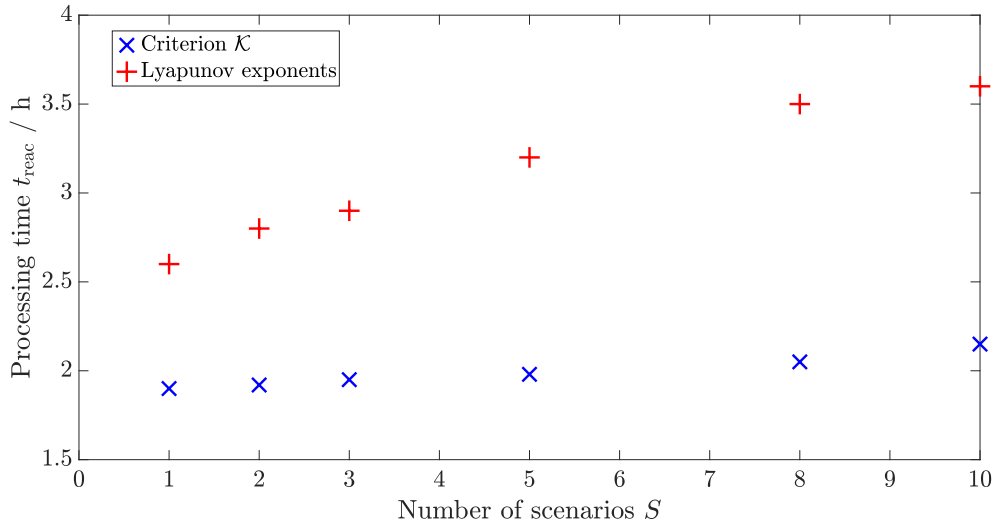

Fig. 6.14 Processing times t_{reac} to reach the target conversion of $X_{\text{C,target}} = 80\%$ for process P_4^2 with each number of scenarios.

Lastly, for potential use in industry, the computational times required per MPC step have to be considered. The computational cost of using the scenario-based MPC approach are shown in Figure 6.15.

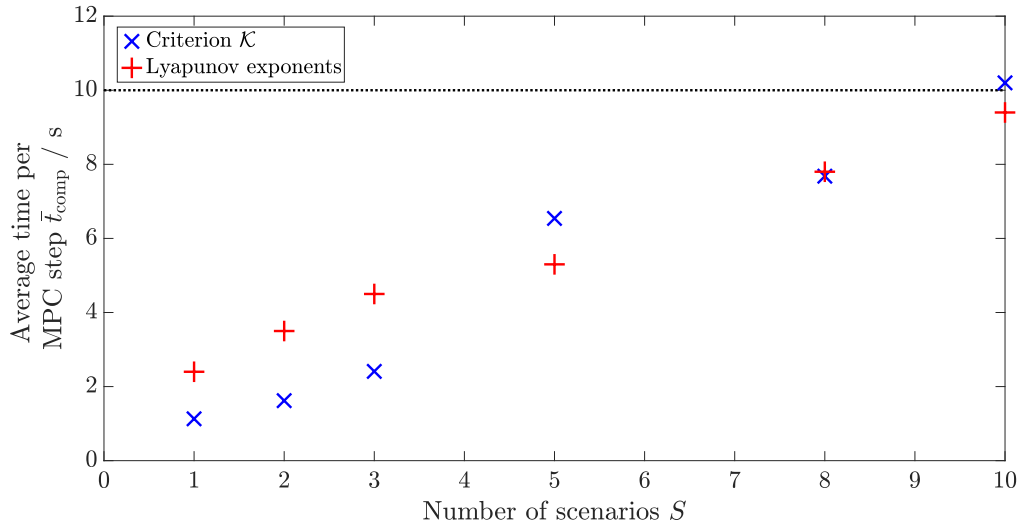

Fig. 6.15 Computational times $\bar{t}_{\text{comp}}$ per MPC step for process P_4^2 with each number of scenarios. The horizontal dashed line indicates the upper limit of the computational time available for the MPC framework used.

Similarly to Figure 6.15, as the number of scenarios increases the computational time per MPC step increases. Once 10 scenarios are used with criterion $\mathscr{K}$, the limit of 10 s available for the MPC algorithm is exceeded. 8 scenarios could still be used for process P_4^2, but the computational time of 7.7 s is close to the 10 s limit.

If Lyapunov exponents are used, similar computational times per MPC step are observed as with criterion $\mathscr{K}$. This is interesting, since the computational cost of evaluating Lyapunov exponents is much larger than that of criterion $\mathscr{K}$. Similar results were obtained for the nominal MPC framework results in Tables 3.2 and 5.2.

In industrial applications data acquisition during the process and potential model re-fitting would require time also. Hence, scenario-based MPC with 5 scenarios for criterion $\mathscr{K}$ and 3 scenarios for Lyapunov exponents give the best compromise between stable operation, process intensification and computational time for process P_4^2.

6.2.3 Nitration of toluene

The industrial case study of the nitration of toluene is the last case study for scenario-based MPC. As for reaction schemes 1 and 2 in the sections above, different numbers of scenarios are used and the performance of the MPC controlled systems embedded with criterion $\mathscr{K}$ and Lyapunov exponents are compared by considering the effect on stability, intensification and computational time. The initial temperature of the process is set to 450 K.

The percentage of processes exhibiting thermal runaway behaviour when using different numbers of scenarios with criterion $\mathscr{K}$ and with Lyapunov exponents is shown in Figure 6.16.

The nitration of toluene, as shown in Section 2.2.5, includes one endothermic reaction in the reaction network. A much smaller percentage of thermal runaway behaviour is observed for the nitration of toluene even with one scenario when compared to scenario-based MPC for processes P_1^1 and P_4^2. When using 3 or more scenarios a reduction of thermal runaway behaviour to 0% is achieved with criterion $\mathscr{K}$. Lyapunov exponents embedded within the scenario-based MPC framework results in no thermal runaways if 2 or more scenarios are included. As previously mentioned, these percentages are taken from 100 simulations carried out for each stability criterion embedded within MPC.

The processing times to reach the target concentration of o-nitrotoluene of $2.5\,\mathrm{kmol\,m^{-3}}$ are shown in Figure 6.17.

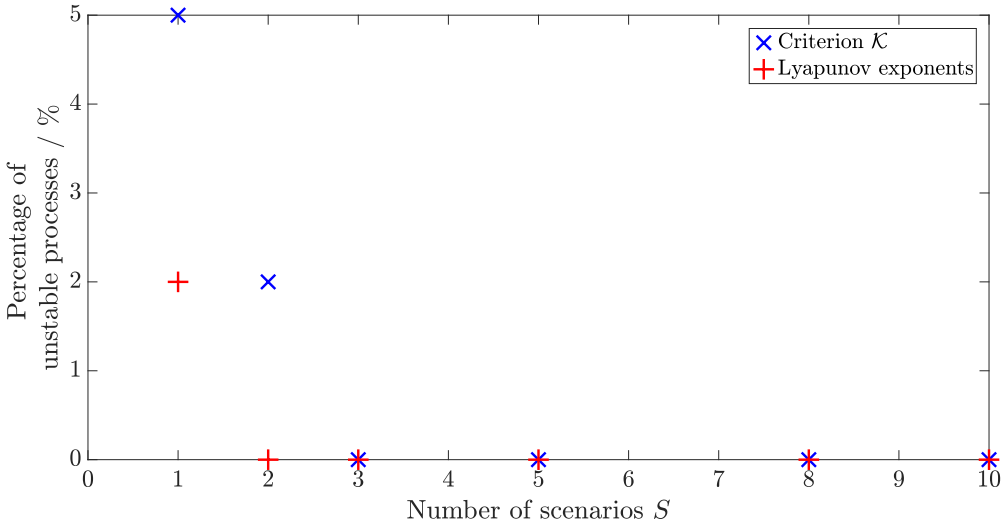

Fig. 6.16 Fraction of simulations for the nitration of toluene resulting in thermal runaway behaviour for each number of scenarios. The percentages are evaluated based on 100 simulations carried out for each control scheme.

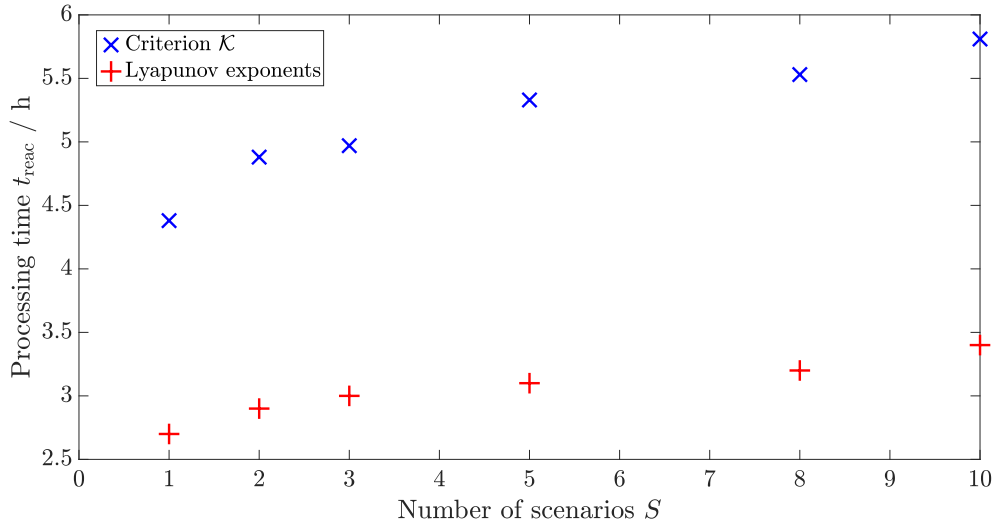

Fig. 6.17 Processing times t_{reac} to reach the target concentration of o-nitrotoluene for the nitration of toluene with each number of scenarios.

As the number of scenarios increases, the time required to reach the final concentration increases. Compared to the results shown in Section 5.5, the average processing time to reach the target concentration is 0.4 h larger if using a single scenario with thermal stability criterion $\mathcal{K}$. In Section 3.2.6 it is shown that constant temperature MPC results in processing times of

approximately 13 h. Hence, even with 10 scenarios and criterion $\mathscr{K}$, a 2-fold reduction in processing time can be achieved. Therefore, the conservative nature of scenario-based MPC does not hinder the ability to intensify processes with MPC framework 1.

Similar results are observed when embedding Lyapunov exponents within the scenario-based MPC framework. The processing times using Lyapunov exponents are shorter than those with criterion $\mathscr{K}$. This is the same behaviour as observed in the nominal MPC case studies. Furthermore, as the number of scenarios employed increases, the control scheme becomes more conservative hence resulting in longer processing times.

The increase in computational time due to the increased number of scenarios used for MPC is extremely important for this case study, as an industrial process is considered. The average computational times per MPC step obtained using scenario-based MPC are shown in Figure 6.18.

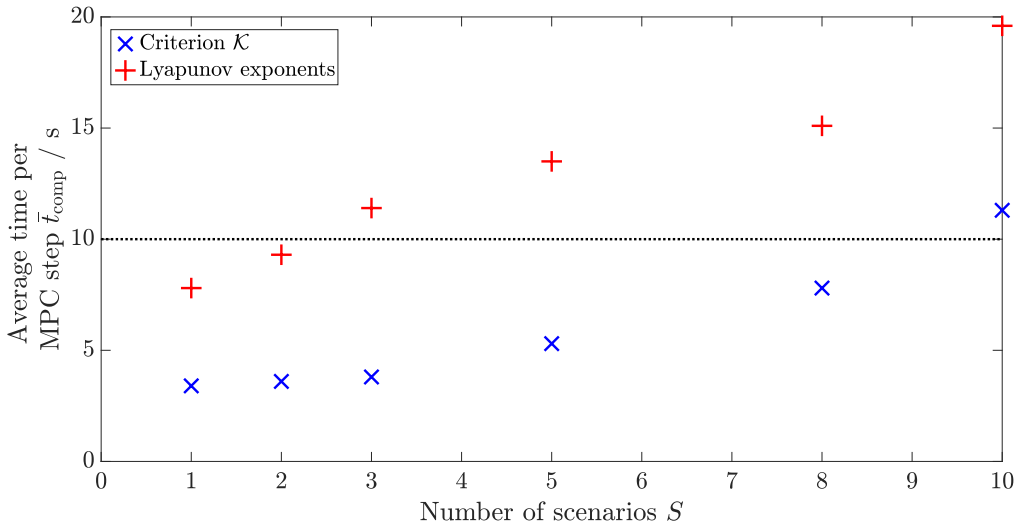

Fig. 6.18 Computational times $\bar{t}_{\mathrm{comp}}$ per MPC step for the nitration of toluene with each number of scenarios. The horizontal dashed line indicates the upper limit of the computational time available for the MPC framework used.

With criterion $\mathscr{K}$, for 1 to 3 scenarios used the computational time is approximately 4 s. If more than 5 scenarios are used the computational time increases significantly. This feature is most likely observed due to 4 cores being available in the computer for each simulation. As the number of scenarios used exceeds 4, significant lag times are present for the evaluation of the additional scenarios. If up to 4 scenarios are present, the increase in computational time is most likely caused by an increase in communication time between the cores for the

overall MPC algorithm. Using up to 5 scenarios again results in an MPC framework which leaves enough time for data processing.

When using Lyapunov exponents a more significant increase in computational time per MPC step is observed. Compared to processes P_1^1 and P_4^2 the number of Lyapunov exponents increases, hence resulting in larger computational overhead per MPC step. Therefore, if using more than 2 scenarios, the 10 s limit given by the MPC algorithm is exceeded. If larger systems were to be controlled with scenario-based MPC embedded with Lyapunov exponents, an even larger number of exponents would be required, further increasing the computational time. Hence, significant speed-up of the MPC framework with Lyapunov exponents is required for potential application in industry with the scenario-based approach.

6.2.4 Effect of exothermicity on robustness

In the previous sections it is observed that with 1 scenario the highest percentage of thermal runaway processes is observed for process P_4^2, followed by process P_1^1 and the nitration of toluene. This feature is observed when comparing Figures 6.10, 6.13 and 6.16 for up to two scenarios for the implementation with both, criterion $\mathscr{K}$ and Lyapunov exponents. To understand the difference in the percentage of thermal runaway simulations observed for each process, the initial values of criterion $\mathscr{K}$ are compared, given in Table 6.1.

Table 6.1 Initial values of criterion $\mathscr{K}$ for processes P_1^1 and P_4^2, and the nitration of toluene.

	Process P_1^1	Process P_4^2	Nitration of toluene
Initial value of criterion $\mathscr{K}$	-1.56×10^{-6}	8.74×10^{-9}	-0.0123

In Table 6.1 it is seen that the initial value of criterion $\mathscr{K}$ for process P_4^2 is the largest, and hence representing the most thermally unstable process amongst the ones considered. The thermally most stable process on the other hand is given by the nitration of toluene, since criterion $\mathscr{K}$ for this process has the most negative value.

Therefore it is apparent that uncertainty in simulations for process P_4^2 will have the most significant effect on thermal runaway behaviour, because this process is most thermally unstable initially. The nitration of toluene results in the fewest thermal runaway simulations because, as given by the value for criterion $\mathscr{K}$, this process initially is the thermally most stable process amongst the three processes considered for the robustness analysis.

6.3 Worst case MPC

In Section 1.3.4 the *worst case* approach was briefly introduced. For the processes considered in this work it can easily be observed how a change in the identified parameters leads to higher potential of thermal runaway behaviour:

- increase in $\Delta H_r \rightarrow$ increased heat generation
- increase in $k_0 \rightarrow$ faster reaction rate $\rightarrow$ increased heat generation
- decrease in $E_a \rightarrow$ faster reaction rate $\rightarrow$ increased heat generation
- decrease in $U \rightarrow$ decreased rate of heat removal

Therefore, given a range of values each parameter is allowed to take, the worst set of parameters, *i.e.* the set of parameters resulting in most heat generation, can be found easily. Since process stability is of utmost importance the worst case MPC method will be used also. To consider the overall most exothermic scenario, the worst parameter values in every dimension are chosen. The dimensions in this thesis are given by the different parameters mentioned above.

Similarly to the scenario-based MPC analysis, reaction schemes 1 and 2, as well as the nitration of toluene are considered below. MPC framework 1 embedded with criterion $\mathscr{K}$ and with Lyapunov exponents are both used. The performance of each control scheme is compared in terms of number of processes causing thermal runaways, processing time and computational time per MPC step.

In industry the following situation is commonly present: a set of parameter values is obtained from experiments and analysis of process data. The values obtained have some uncertainty associated with them, such that normal distributions can be constructed to describe possible values for each individual parameter. Depending on the range of values within the 95% confidence interval, the normal distribution can be wider or narrower. In this thesis the range of possible values is set to 1%, 3%, 5%, 8% and 10% of the parameter value. From the distributions with varying ranges in values within the 95% confidence interval the worst case set of parameters is then chosen to simulate the process model. This represents the worst case model used within the control scheme.

Since this work is of theoretical nature, the sets of parameter values initially assumed for the above analysis have to be generated themselves. To carry out the above analysis the initial value of each parameter is sampled from the normal distributions in Equations (6.1)−(6.5). This sampling is carried out 100 times, resulting in 100 different initial estimates of the system parameters. In this way comparable results to those for the scenario-based MPC

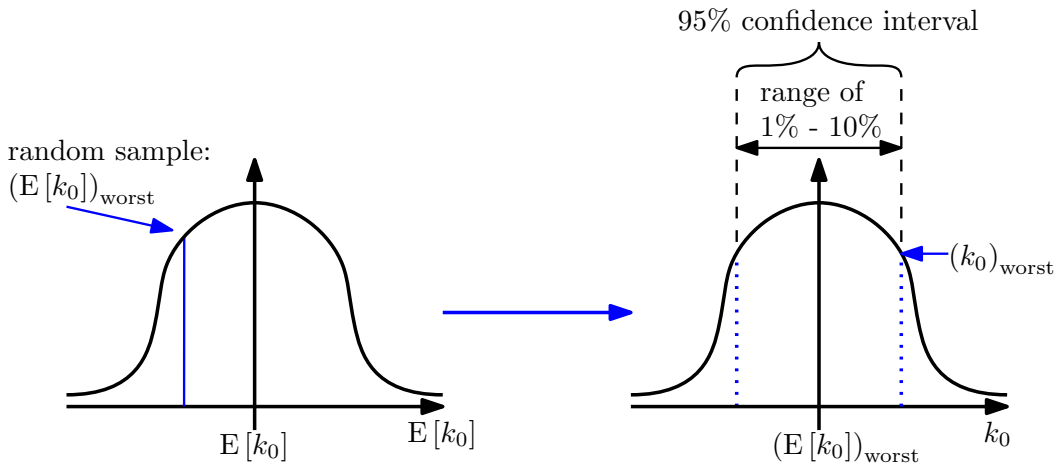

Fig. 6.19 Schematic showing the sampling procedure to obtain the worst value of k_0 for the worst case MPC algorithm.

approach are obtained. The above procedure is schematically shown for the Arrhenius pre-exponential factor k_0 in Figure 6.19.

Consider process P_1^1, for which the mean and standard deviation of k_0 are shown in Equation (6.3). For a deviation of 8% from the mean the following worst case value would be used:

$$k_0 \sim \mathcal{N}\left(\mathrm{E}[k_0], \sigma_{k_0}^2\right) \tag{6.7a}$$

$$k_0 \sim \mathcal{N}\left(2.76 \times 10^6, 4.96 \times 10^9\right) \tag{6.7b}$$

A random sample from the above distribution yields:

$$(\mathrm{E}[k_0])_{\mathrm{worst}} = 2.60 \times 10^6 \tag{6.8}$$

The worst case scenario mean, $(\mathrm{E}[k_0])_{\mathrm{worst}}$, is used to find the standard deviation of the new distribution, including the required 8% deviation from the mean which sets the 95% confidence interval:

$$\sigma_{\mathrm{worst}} = \frac{(\mathrm{E}[k_0])_{\mathrm{worst}}}{1.96} \times 0.08 \tag{6.9a}$$

$$\sigma_{\mathrm{worst}} = 1.06 \times 10^5 \tag{6.9b}$$

An increase in the Arrhenius pre-exponential factor will result in a faster reaction. Hence, the worst case value for k_0 from the new distribution, whilst staying within the 95% confidence

interval, is given by:

$$(k_0)_{\text{worst}} = (\mathrm{E}[k_0])_{\text{worst}} + \sigma_{\text{worst}} \tag{6.10a}$$

$$(k_0)_{\text{worst}} = 2.60 \times 10^6 + 1.06 \times 10^5 \tag{6.10b}$$

$$(k_0)_{\text{worst}} = 2.71 \times 10^6 \tag{6.10c}$$

The same procedure is carried out for all remaining parameters. It is expected that as the deviation from the mean values increases, the resulting control system becomes more conservative. As the processes become more conservative the number of thermal runaway reactions decreases, and processing times increase. These properties are examined below for processes P_1^1, P_4^2 and the nitration of toluene.

6.3.1 Reaction scheme 1

The worst case MPC approach is first tested with the simplest reaction given by process P_1^1. In this case 100 simulations are carried out, each with a mean value of the uncertain parameters sampled from the respective distributions. The target conversion of each process is set to $X_{\mathrm{C,target}} = 80\%$. If the temperature of a simulation exceeds the upper limit of $T_{\mathrm{chem}} = 450\,\mathrm{K}$ it is considered to be unstable. The percentage of reactions exceeding the maximum temperature limit and resulting in thermal runaway behaviour is shown in Figure 6.20.

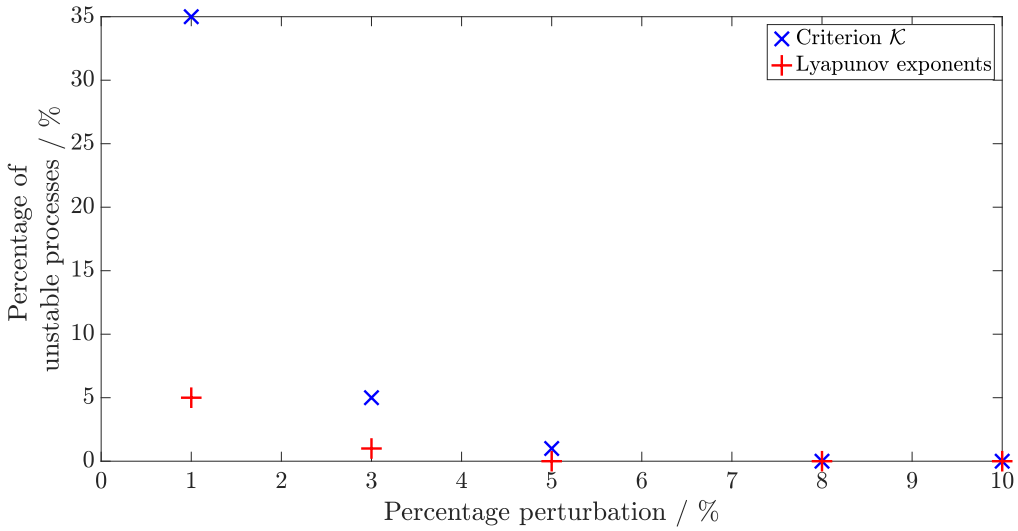

Fig. 6.20 Fraction of simulations for process P_1^1 resulting in thermal runaway behaviour for each percentage perturbation resulting in the worst case model.

In Figure 6.20 similar profiles as for scenario-based MPC are observed: as the percentage change in parameter values towards the most exothermic and hence worst case increases, more robust control is achieved. As outlined above, this is the case due to the stability criteria assuming worse systems than actually present, hence applying more cooling and keeping the processes under control. Embedding Lyapunov exponents within a worst case MPC approach results in a larger fraction of processes begin stable initially when compared to using criterion $\mathscr{K}$. This is in line with the results obtained for scenario-based MPC. Once a percentage change of 8% or more is applied, all simulated processes turn out to be stable. 100 simulations are used to generate these results, therefore it is not guaranteed that all reactions will be stable if an 8% change within a 95% confidence interval is used.

How the increase in robustness affects the process intensification is considered next. The effect of the percentage change in parameters on the processing time is shown Figure 6.21.

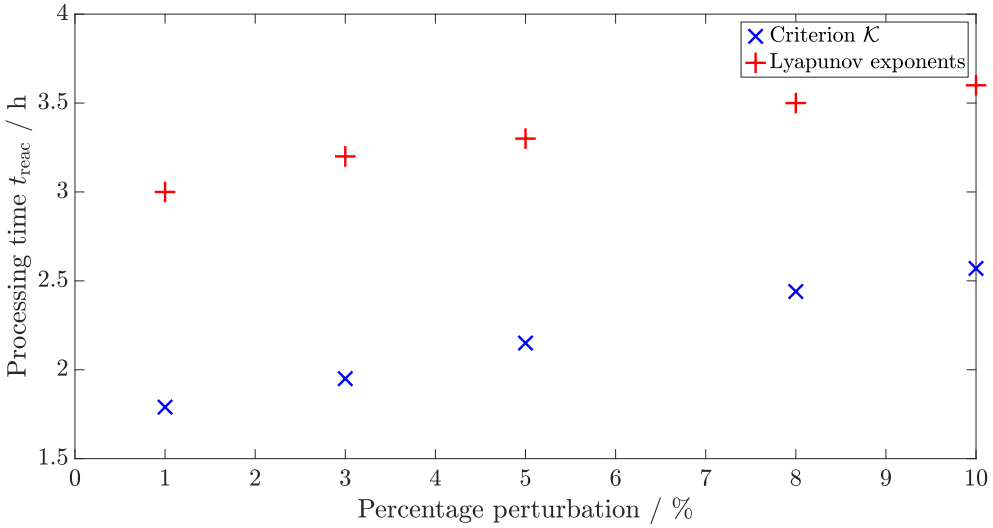

Fig. 6.21 Processing times t_{reac} to reach the target conversion for process P_1^1 for each percentage perturbation resulting in the worst case model.

As observed for scenario-based MPC, embedding criterion $\mathscr{K}$ within worst case MPC results in shorter processing times than the use of Lyapunov exponents. As the conservativeness of the model increases, the processing time increases, which is expected. For a percentage change in parameter values that shows no thermal runaway behaviour, *i.e.* 5% for Lyapunov exponents and 8% for criterion $\mathscr{K}$, comparable processing times to those for scenario-based MPC are obtained. Since only one scenario is used for the worst case MPC formulation, it is expected that the computational time does not increase with an increase in conservativeness

of the model. The computational times per MPC step obtained for each set of simulations are shown in Figure 6.22.

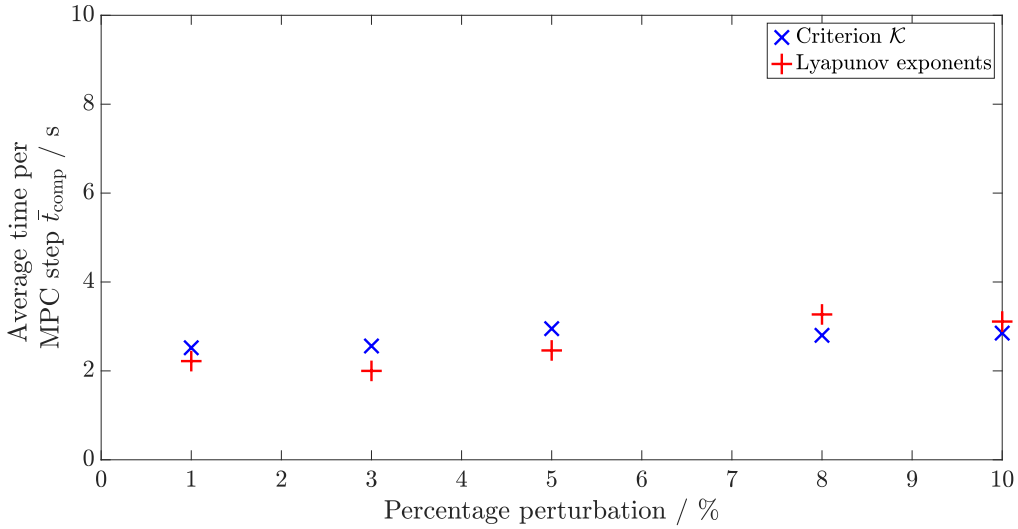

Fig. 6.22 Computational times $\bar{t}_{\text{comp}}$ per MPC step for process P_1^1 for each percentage perturbation resulting in the worst case model.

Each control step within the MPC framework accounts for 10 s in the reaction. Therefore the upper limit of computational time per MPC step available is 10 s. In Figure 6.22 it is seen that this upper limit is not reached for the implementation with both criterion $\mathcal{K}$ and Lyapunov exponents. An average time per MPC step of approximately 3 s is required for worst case MPC with either stability criterion. This is computationally more efficient than the scenario-based approach, which as the number of scenarios used increases, results in significantly larger computational times.

Considering the similarity in processing times for the same extent of preventing thermal runaway reactions, worst case MPC with Lyapunov exponents and criterion $\mathcal{K}$ results in a more efficient control framework than scenario-based MPC with the same stability criteria. Whether or not this advantage persists for more complex reactions is examined below.

6.3.2 Reaction scheme 2

The same analysis as for process P_1^1 is now carried out for process P_4^2. Worst case MPC is used with Lyapunov exponents and criterion $\mathcal{K}$. 100 simulations are carried out and the fraction of processes exceeding the maximum temperature limit of 470 K is shown in Figure 6.23.

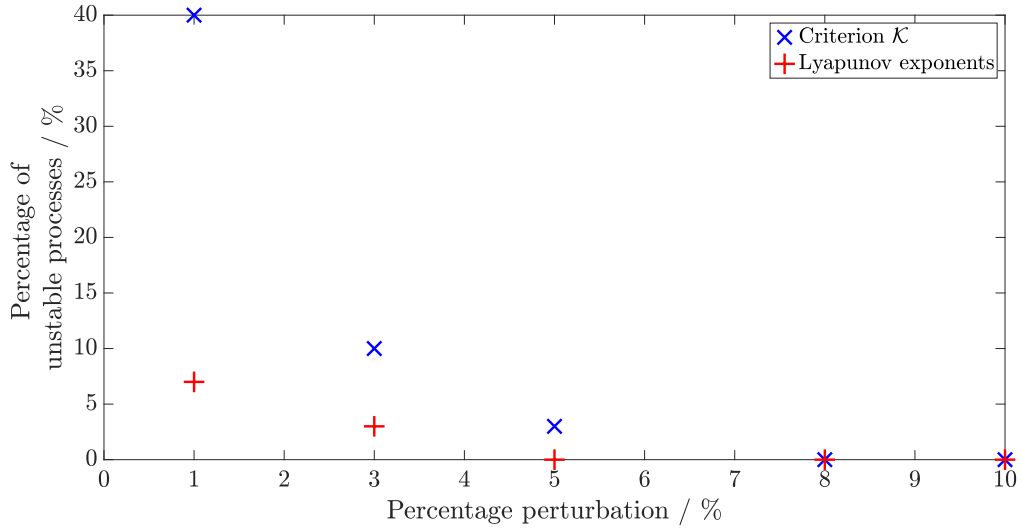

Fig. 6.23 Fraction of simulations for process P_4^2 resulting in thermal runaway behaviour for each percentage perturbation resulting in the worst case model.

The fraction of processes resulting in thermal runaway behaviour is larger for process P_4^2 than for process P_1^1, due to the thermal runaway potential discussed in Section 6.2.4. Therefore, uncertainty in the process parameters will have a larger effect on thermal stability.

For a percentage change in parameter values of at least 8%, embedded criterion $\mathscr{K}$ within a worst case MPC formulation results in no thermal runaways for the 100 simulations carried out in this work. As was the case for process P_1^1, a change in parameter values of at least 5% for the implementation with Lyapunov exponents results in no thermal runaway reactions. These percentage changes in parameter values are again within the 95% confidence interval of the respective parameters.

The effect on processing times due to increasing the conservativeness of the model used for criterion $\mathscr{K}$ and Lyapunov exponents with the worst case MPC approach is summarised in Figure 6.24.

In Figure 6.24 it is seen that when using percentage changes in parameter values that result in no thermal runaways, the processing times obtained are comparable to those obtained with scenario-based MPC in Figure 6.14. The processing times using Lyapunov exponents are larger than those for criterion $\mathscr{K}$. This is obtained since the horizon over which Lyapunov exponents are evaluated increase the effect of uncertainty within the model.

The computational times per MPC step are expected to be approximately the same for each different percentage change in parameter value, as was the case for process P_1^1. The

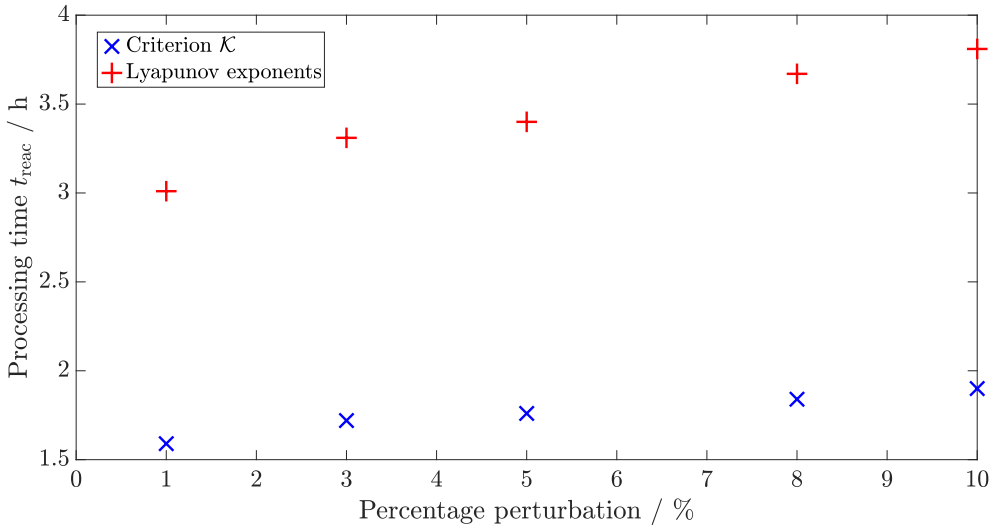

Fig. 6.24 Processing times t_{reac} to reach the target conversion of 80% for process P_4^2 for each percentage perturbation resulting in the worst case model.

computational times per MPC step observed for process P_4^2 with worst case MPC are shown in Figure 6.25.

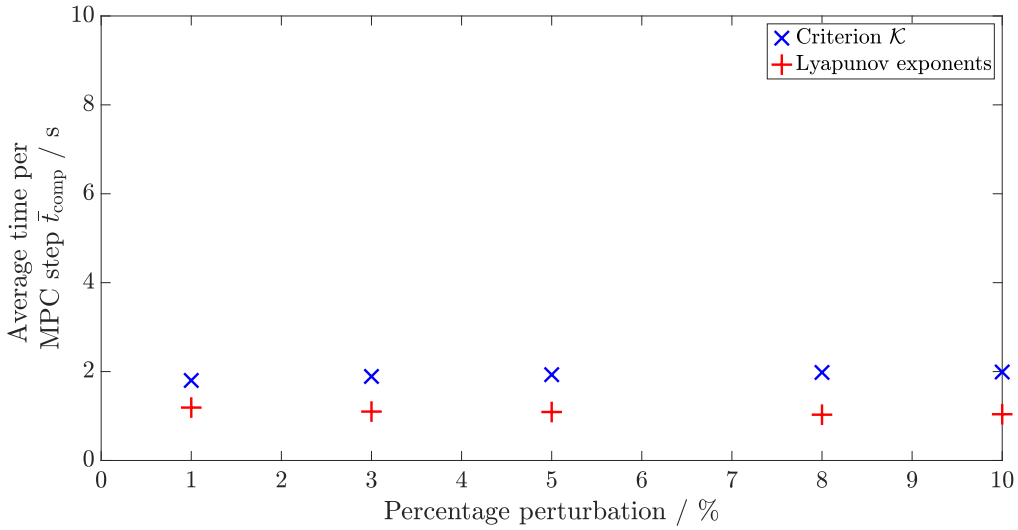

Fig. 6.25 Computational times $\bar{t}_{\text{comp}}$ per MPC step for process P_4^2 for each percentage perturbation resulting in the worst case model.

Similarly to process P_1^1 the computational times are approximately constant, because a single scenario is used for each set of simulations. The computational times per MPC step are

smaller than 2 s, which gives enough time to carry out other evaluations and estimations within the 10 s horizon available due to the MPC framework used.

Interesting to note is that for single reaction process P_4^2 the value of $\bar{t}_{comp}$ is smaller when using Lyapunov exponents as opposed to criterion $\mathscr{K}$. This is the case even though the evaluation of Lyapunov exponents is more computationally expensive than criterion $\mathscr{K}$. Nevertheless, as the number of reactions and reagents within the system increases, the computational time to evaluate criterion $\mathscr{K}$ is not expected to increase significantly, whereas the computational time when embedding Lyapunov exponents will increase significantly. This effect is investigated further for the industrially relevant nitration of toluene, which consists of 4 reactions occurring simultaneously.

6.3.3 Nitration of toluene

The last reaction considered in the analysis of MPC with the worst case scenario is the nitration of toluene. As was done for reaction schemes 1 and 2, the worst case given a maximum percentage change in the relevant parameters is chosen for the stability criterion evaluations. It is again assumed that a 95% confidence interval is present in the mean value of each parameter. The percentage deviation is then applied with respect to the sampled mean and the calculated standard deviation of each respective parameter.

When increasing the percentage change in each parameter towards its worst case, a model with higher potential of thermal runaway behaviour is obtained. Hence, it is expected that as the percentage change increases, processing times decrease and the number unstable processes decreases. This was observed for reaction schemes 1 and 2 above for criterion $\mathscr{K}$ and Lyapunov exponents. 100 simulations are carried out and based on these results the fraction of processes resulting in thermal runaway behaviour is shown in Figure 6.26.

In Figure 6.26 it is seen that an increase in the change of parameter values results in fewer thermal runaway processes. This is the case because the parameters obtained with a larger perturbation result in a model that samples a larger range of parameters which would cause thermal runaways. As the potential of thermal runaway of the model used increases, the likelihood of keeping the nominal process under control increases. This is in line with the results obtained for worst case MPC for reaction schemes 1 and 2. For a 3% change in the parameter values no thermal runaway behaviour is observed for the simulations carried out with both criterion $\mathscr{K}$ and Lyapunov exponents. According to the discussion in Section 6.2.4, many less thermal runaway processes are observed compared to reaction schemes 1 and 2.

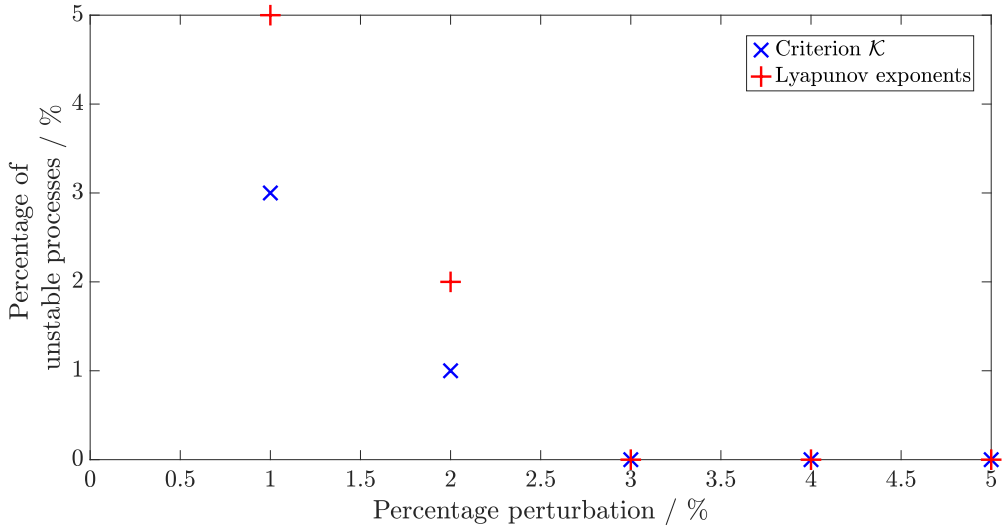

Fig. 6.26 Fraction of simulations for the nitration of toluene resulting in thermal runaway behaviour for each percentage perturbation resulting in the worst case model.

The effect of increasing the thermal runaway potential of the model used on the processing time is shown in Figure 6.27.

Similar to the results shown for reaction schemes 1 and 2, as the percentage change in parameter values increases, a higher processing time t_{reac} is required to reach the target concentration. This is as expected, because an overall more conservative control scheme is obtained as the percentage change in parameter values increases. Important to note is the longer processing time when using criterion $\mathscr{K}$ with worst case MPC. For each set of simulations it is found that approximately 1 h more is required when stability criterion $\mathscr{K}$ is used instead of Lyapunov exponents. How the two different MPC schemes compare in terms of computational time required per MPC step, $\bar{t}_{\text{comp}}$, is shown in Figure 6.28.

As the percentage change in parameter values increases, still a single scenario is simulated to evaluate each stability criterion. Hence no increase in computational time is observed. Due to the computational cost of evaluating Lyapunov exponents for each reagent and the reactor temperature, the computational cost per MPC step when using Lyapunov exponents is approximately double that of using criterion $\mathscr{K}$ with MPC. Using worst case MPC with Lyapunov exponents is close to the upper limit of 10 s available for each MPC iteration. Therefore significant speed-up of this control scheme would be required for industrial implementation. The MPC framework using worst case scenarios and criterion $\mathscr{K}$ on the other hand takes approximately 4 s per MPC step and therefore enough time for data

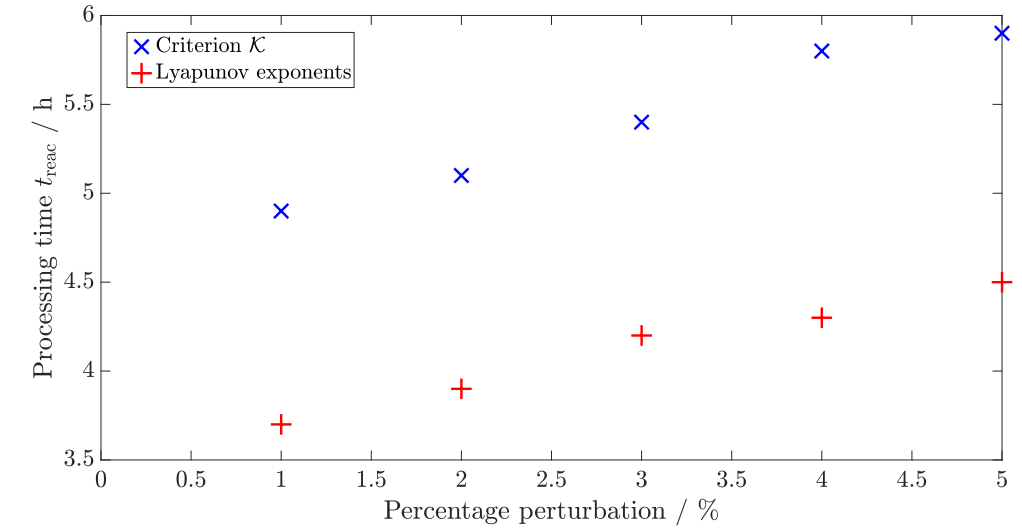

Fig. 6.27 Processing times t_{reac} to reach the target concentration of o-nitrotoluene for the nitration of toluene for each percentage perturbation resulting in the worst case model.

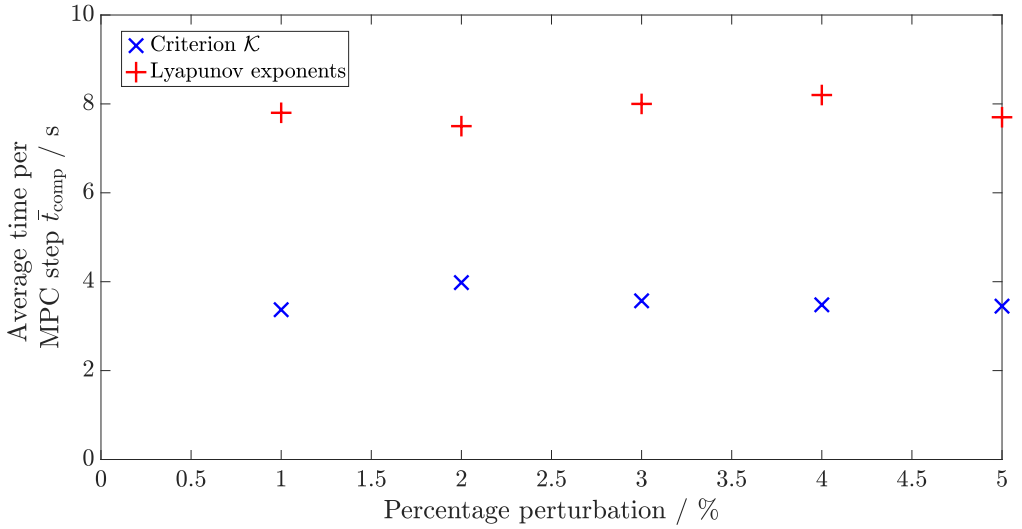

Fig. 6.28 Computational times $\bar{t}_{\text{comp}}$ per MPC step for the nitration of toluene for each percentage perturbation resulting in the worst case model.

processing at each MPC iteration is available. This is in line with the results obtained for worst case MPC with reaction schemes 1 and 2 above.

6.4 Chapter summary

Assuming a known model structure, the parameters of the model were identified as the main source of uncertainty. For process intensification it is shown that uncertainty in the parameters directly affecting the heat generation during the reaction have the largest influence on thermal stability prediction.

The effect of $\pm 5\%$ deviation within a 95% confidence interval on the enthalpy of reaction, the Arrhenius pre-exponential factor, the activation energy, as well as the heat transfer coefficient are shown. Uncertainty in the activation energy is found to have the largest effect due to its presence within the exponential of the Arrhenius rate equation.

Scenario-based MPC together with samples of the uncertain parameters are used to investigate how robust such an MPC framework is when criterion $\mathscr{K}$ and Lyapunov exponents are embedded. As the number of scenarios used within the MPC framework increases:

1. the number of thermal runaways decreases
2. the time to reach final conversion, t_{reac}, increases
3. the computational time per MPC step, $\bar{t}_{\text{comp}}$, increases

For scenario-based MPC with criterion $\mathscr{K}$ it is found that 5 scenarios result in 0% thermal runaway processes for the 100 simulations considered in this work for each case study. The processing times are half that of constant temperature set-point processes. Therefore process intensification is achieved with this robust MPC framework. The computational times are found to increase with the number of scenarios. Since there is limited computational time per MPC step, the number of scenarios used has to be chosen carefully. For the case studies considered in this thesis, using 5 scenarios leaves enough time to carry out other calculations, such as data processing. With increase in system size no significant increase in computational time for the same number of scenarios is found when criterion $\mathscr{K}$ is used. The results for computational time with respect to scenario-based MPC are summarised in Table 6.2.

Table 6.2 Summary of computational times $\bar{t}_{\text{comp}}$ in CPUs for scenario-based MPC embedded with criterion $\mathscr{K}$ and Lyapunov exponents.

Number of	Criterion $\mathscr{K}$			Lyapunov exponents		
scenarios S	P_1^1	P_4^2	nitration of toluene	P_1^1	P_4^2	nitration of toluene
1	2.5	1.1	3.4	2.5	2.4	7.8
2	3.4	1.6	3.6	3.8	3.5	9.3
3	3.9	2.4	3.8	4.5	4.5	11.4
5	6.5	6.5	5.3	6.2	5.3	13.5
8	9.5	7.7	7.8	8.3	7.8	15.1
10	12.3	10.2	11.3	11.2	9.4	19.6

Using Lyapunov exponents with scenario-based MPC also results in profound improvements of thermal stability. Once 3 scenarios are used it is found that no thermal runaways are observed for all simulations carried out in this work. Compared to the implementation using criterion $\mathscr{K}$ the processing times to reach final conversions are doubled when using Lyapunov exponents, *i.e.* less process intensification is achieved. Furthermore, as the number of Lyapunov exponents evaluated increases due to system size, the computational time increases significantly. For the nitration of toluene case study this becomes evident, because only 2 scenarios can be used whilst not exceeding the time limit of 10 s per MPC step, as is seen in Table 6.2.

Interesting to note is that criterion $\mathscr{K}$ can be used to quantify how unstable a process is initially. Process P_4^2 is found to be closest to thermal instability when compared to processes P_1^1 and the nitration of toluene. Hence, more thermal runaway simulations are observed for this process. The fewest thermal runaway simulations are observed for the nitration of toluene, which is in line with this process having the most negative value of criterion $\mathscr{K}$ initially. The initial value of criterion $\mathscr{K}$ for process P_1^1 is between those of the nitration of toluene and process P_4^2. This is also reflected by the number of thermal runaway simulations observed, which lies between those of process P_4^2 and the ntiration of toluene. In conclusion, as the initial potential of thermal runaway behaviour increases, uncertainty in the system parameters will have a larger effect on thermal stability.

Worst case MPC is applied to the same case studies with criterion $\mathscr{K}$ and Lyapunov exponents embedded. It is found that as the worst case considered in the model has a higher thermal runaway potential:

1. the number of thermal runaways decreases
2. the time to reach final conversion, t_{reac}, increases
3. the computational time per MPC step stays approximately constant, as the number of scenarios does not increase

The results shown above with respect to an increase in conservativeness are similar to those for scenario-based MPC. Important to note, however, is that worst case MPC only uses one single scenario which limits the computational time required per MPC step. Similar extents of process intensification can be achieved with criterion $\mathscr{K}$ and Lyapunov exponents as obtained for scenario-based MPC but at a fraction of the computational time. This is a major advantage of worst case MPC over scenario-based MPC with embedded stability criteria. For the system considered in this work, worst case MPC can be used because the parameter values causing higher thermal runaway potential can be evaluated easily. For highly nonlinear system dynamics, where the effect of changing the parameter on thermal runaway potential cannot be observed, this type of control scheme cannot be used. Therefore, for the special case of exothermic batch processes of the form considered in this work worst case MPC with Lyapunov exponents and criterion $\mathscr{K}$ outperforms scenario-based MPC.

Lyapunov exponents embedded in worst case MPC result in longer processing times for processes P_1^1 and P_4^2 compared to embedding criterion $\mathscr{K}$, whereas for the nitration of toluene the opposite is observed. For the nominal MPC cases embedding Lyapunov exponents as constraints resulted in shorter reaction times than criterion $\mathscr{K}$, too. Important to still consider is the computational time per MPC step: using Lyapunov exponents with worst case MPC requires 80% of the computational time available, whereas criterion $\mathscr{K}$ only requires 40%. As the number of variables increases the time required by the Lyapunov exponent approach will increase further. Therefore, the use of worst case MPC embedded with criterion $\mathscr{K}$ results in the most reliable and computationally efficient control scheme for the intensification of batch processes in this work.

Chapter 7

Conclusions and future work

7.1 Conclusions

The underlying goal of this work was to improve the efficiency of batch processes by continuously increasing the reactor temperature in a safe manner, hence intensifying the reaction. The solution found must predict thermal runaway behaviour reliably and has to be computationally efficient, such that implementation in industry is possible.

Advanced control systems are capable of using information about system stability to achieve such intensification. Model Predictive Control (MPC) is used for this purpose due to its ideal structure and common use in industry. The concept of embedding stability criteria within an MPC framework in the manner presented in this thesis has not been previously used for batch processes.

Stability criteria commonly used for CSTRs are found not to work reliably for batch processes. The Semënov and Routh-Hurwitz criteria, as well as all criteria based on the theory by Semënov, give unreliable predictions of thermal runaway behaviour for batch processes. Even though these criteria work well for CSTRs, process intensification of batch processes cannot be achieved using these criteria.

Two stability criteria specifically for batch processes are found in literature: Lyapunov exponents and the divergence criterion.

Lyapunov exponents are shown to predict thermal runaway behaviour of batch processes reliably after the initial perturbation δx_0 and the Lyapunov time frame t_{Lyap} are set optimally. This is dependent on the underlying system, but for the batch processes in this work one set of parameter values $\left(\delta x_0 = 10^{-3}, t_{\text{Lyap}} = 5000\,\text{s}\right)$ are found to work well. Process intensifi-

cation is achieved with the MPC framework embedding stability criteria, also showing that more stable and more efficient processes are obtained than is possible with standard MPC approaches subject to a limited amount of computational time available. The main advantage of using Lyapunov exponents is therefore its reliable stability predictions and its ease of implementation for a variety of systems. The major limitation of using Lyapunov exponents is the exponential increase in computational time as the model size increases.

The divergence criterion is found to over-predict the thermal runaway potential of batch processes. When embedded within an MPC framework no consistent process intensification is achieved. Qualitatively, the profiles of the divergence criterion do however follow that of the thermal runaway potential. Furthermore, the computational times obtained when implemented within an MPC framework are found not to increase with model size and complexity.

The computational limitation of Lyapunov exponents lead to the development of a thermal stability criterion based on the divergence criterion. If the conservativeness of the divergence criterion is corrected, a reliable and computationally efficient thermal stability criterion is obtained.

The new thermal stability criterion $\mathscr{K}$ is found by correcting the value of the divergence with function $\mathscr{E}$, which estimates the behaviour of the divergence at the boundary of stability. It is found that taking a full differential of the divergence leads to a linear extrapolation with constant gradient coefficients m_B, m_γ, $m_{\mathrm{Da}_{\mathrm{res}}}$ and m_{St}. These gradient coefficients are evaluated for a large variety of process parameters of single reaction processes. Their values are found not to vary significantly. Therefore, these values are applied to single reaction, as well as multiple reaction processes. Reliable prediction of thermal runaway behaviour is obtained for each reaction network in batch processes. The derivations shown are not applicable to fed-batch systems in their current form, as the system equations change with the inclusion of inflows into the reactor.

Criterion $\mathscr{K}$ embedded within MPC results in consistent process intensification, comparable to that with Lyapunov exponents, whilst retaining the computational cost of the divergence criterion. Hence, a computationally efficient and reliable control scheme is developed, which outperforms standard MPC frameworks for batch process intensification.

The industrial case study for the nitration of toluene shows that MPC embedded with Lyapunov exponents results in good process intensification, but the limit of computational time available is reached. For MPC embedded with criterion $\mathscr{K}$ a similar extent of intensification

is achieved, whilst there is still 80% of computational time available for other purposes, *e.g.* model re-fitting.

Process uncertainty is of great importance in industry, especially when dealing with systems prone to thermal runaway behaviour. The main source of uncertainty in the models used in this thesis are due to parametric uncertainty. The main parameters affecting thermal runaway prediction in case of uncertainty are identified as being the enthalpy of reaction, the Arrhenius pre-exponential factor, the activation energy, and the heat transfer coefficient. Of these, the activation energy is found to have the largest impact, due to its exponential impact on the heat generation of the batch processes in this work.

A scenario-based MPC framework, as is commonly found in literature, is implemented with the MPC concept embedding stability criterion $\mathscr{K}$ and Lyapunov exponents. As the number of scenarios is increased, the number of processes causing thermal runaway behaviour due to uncertain parameter values decreases significantly. An interesting feature observed is the percentage of processes resulting in thermal runaway behaviour and the initial value of criterion $\mathscr{K}$. As the potential of thermal runaway behaviour increases, uncertainty in parameters have larger effects on process safety. Therefore, if processes have a value of criterion $\mathscr{K}$ closer to zero and uncertain parameters are used for thermal stability prediction, a larger fraction of simulations will result in thermal runaway behaviour.

The scenario-based MPC approach embedding criterion $\mathscr{K}$ results in shorter processing times than embedding Lyapunov exponents. For the 100 simulations carried out in this work, scenario-based MPC with criterion $\mathscr{K}$ results in no thermal runaways once 5 or more scenarios are used, whereas with Lyapunov exponents only 3 scenarios are required. For the nitration of toluene, representing an industrial case study, larger computational times are obtained when embedding Lyapunov exponents. This is the case because the larger the number of Lyapunov exponents required, the larger the computational time.

Criterion $\mathscr{K}$ and Lyapunov exponents embedded within scenario-based MPC both result in significant process intensification whilst reducing the number of thermal runaway reactions considerably. Therefore the added conservativeness of the control scheme does not result in no process intensification.

Worst case MPC is shown to result in stable processes when using criterion $\mathscr{K}$ and Lyapunov exponents. Unlike the scenario-based approach, only one scenario is used throughout. Because the parameter values resulting in the highest thermal runaway potential can be easily calculated, the percentage deviation from the sampled mean values of each parameter can be used to tune the conservativeness of the control scheme.

For criterion $\mathscr{K}$ a percentage deviation of 8% or larger results in no thermal runaway reactions. The processing time is comparable to that of scenario-based MPC, whilst the computational time required does not increase with the conservativeness of the model used. Lyapunov exponents embedded within worst case MPC results in no thermal runaway reactions for percentage deviations of 5% or larger for the 100 simulations carried out in this thesis. Significant process intensification with respect to constant set-point temperature reactions is achieved. The computational time again does not increase with the extent of conservativeness, but as the underlying systems become more complex, the computational time increases.

The use of criterion $\mathscr{K}$ results in a computationally more efficient control system whilst achieving the same extent of process intensification and stability as the scenario-based approach with both stability criteria. Because the computational time required per MPC step does not depend on the complexity and size of the system, it is considered more efficient than the implementation with Lyapunov exponents for the batch processes simulated in this work. Therefore, worst case MPC with criterion $\mathscr{K}$ is considered the superior control scheme for the processes considered in this work.

7.2 Future work

Many requirements for implementing MPC with embedded stability criteria for batch process intensification were developed in this work. More work is still necessary for potential application of this technique in industry.

Industrial systems may contain many more reaction components, as well as control variables. Therefore more work on larger scale systems is required to understand how the MPC framework and stability criteria developed behaves for such systems. Furthermore, the inclusion of inflows into the reactor, resulting in a fed-batch process, needs to be investigated to extend the theory developed in this thesis.

First principles models might not be available for certain runaway systems. Therefore uncertainty in the model structure might be present. How uncertainty in the model affects the prediction of thermal runaway behaviour, and how this uncertainty can be dealt with in an MPC framework hence requires investigation. This includes estimation of process models with Bayesian processes, as well as machine learning techniques such as artificial neural networks.

The stability constraints within the MPC formulation for the nominal, scenario-based and worst case MPC currently have to be satisfied at every time step. The inclusion of soft constraints was attempted in this work but resulted in badly scaled problems. For the scenario-based approach it is nevertheless interesting to include the stability constraints as chance constraints, in which case a certain percentage of constraints have to be satisfied. Issues due to computational time will still be present, but significant improvements in process intensification are possible compared to scenario-based simulations shown in this work.

The optimisation algorithm used in this work requires the evaluation of finite differences to find the optimal control input. As the system size increases, finite differences can cause large computational overhead. The use of automatic differentiation could resolve this problem, hence reducing the computational time of optimisation significantly.

Once the methods developed in this work are applied to real laboratory-scale systems, it is for certain that many other issues will be observed. Measurement noise is expected to be one of these issues, since the evaluation of criterion $\mathscr{K}$ requires second order derivatives with respect to measured variables. Techniques such as Kalman filtering can potentially be used for this purpose, but more work in this area is required. Furthermore, if concentrations of certain reagents cannot be measured, estimation techniques will be required to obtain values for these.

Steam running through the cooling jacket, or a separate jacket around the batch reactor is often used to heat up the reactor contents in the beginning of the reaction. This represents an additional degree of freedom during batch processes, since the temperature can be actively increased by heating the reactor contents. This possibility has to be considered for potential application, since this would result in more significant process intensification.

After these challenges are considered and solved, batch process intensification with stability criteria embedded in MPC are ready to be applied in industry, hence improving operational safety, making batch processes more efficient, and reducing environmental impact.

Appendix A

Reaction data and physical properties

In this Appendix all of the data used for the batch reactor model are given.

A.1 Reaction Scheme 1

The process parameters for reaction scheme 1 are shown in Table A.1.

Table A.1 Reaction data for processes $P_1^1 - P_{15}^1$.

Process	k_0 $\left[\left(\mathrm{m^3\,kmol^{-1}}\right)^{n_{A-1}}\,\mathrm{s^{-1}}\right]$	n_A	ΔH_r $\left[\mathrm{kJ\,mol^{-1}}\right]$	$[A]_0$ $\left[\mathrm{kmol\,m^{-3}}\right]$	E_a/R [K]
P_1^1	2.76×10^6	1.0	−75.0	13.0	9525
P_2^1	7.65×10^5	1.5	−75.0	13.0	9525
P_3^1	2.12×10^5	2.0	−75.0	13.0	9525
P_4^1	5.89×10^4	2.5	−75.0	13.0	9525
P_5^1	3.06×10^4	3.0	−75.0	13.0	9525
P_6^1	2.76×10^6	1.0	−130.0	8.0	9525
P_7^1	9.76×10^5	1.5	−110.0	8.0	9525
P_8^1	3.45×10^5	2.0	−90.0	8.0	9525
P_9^1	1.22×10^5	2.5	−75.0	8.0	9525
P_{10}^1	4.31×10^4	3.0	−70.0	8.0	9525
P_{11}^1	2.76×10^6	1.0	−75.0	8.0	9525
P_{12}^1	2.76×10^6	1.0	−75.0	9.0	9525
P_{13}^1	2.76×10^6	1.0	−75.0	11.0	9525
P_{14}^1	2.76×10^6	1.0	−75.0	13.0	9525
P_{15}^1	2.76×10^6	1.0	−75.0	15.0	9525

A.2 Reaction Scheme 2

The process parameters for reaction scheme 2 are shown in Table A.2. The initial concentration of component B is set to 8 kmol m^3 for each process in reaction scheme 2.

Table A.2 Process parameters for processes $P_1^2 - P_{20}^2$.

Process	k_0 $\left[\frac{(\mathrm{m^3\,kmol^{-1}})^{(n_A+n_B-1)}}{\mathrm{s}}\right]$	ΔH_r $[\mathrm{kJ\,mol^{-1}}]$	n_A $[-]$	n_B $[-]$	$[A]_0$ $\left[\frac{\mathrm{kmol}}{\mathrm{m^3}}\right]$	ν_A $[-]$	ν_B $[-]$	E_a/R [K]
P_1^2	1.0×10^4	-150	1.0	1.0	10.0	1.0	1.0	9525
P_2^2	3.0×10^3	-110	2.0	2.0	10.0	1.0	1.0	9525
P_3^2	6.0×10^4	-110	1.5	1.0	10.0	1.0	1.0	9525
P_4^2	8.0×10^4	-110	1.0	1.5	10.0	1.0	1.5	9525
P_5^2	1.2×10^5	-150	1.0	1.0	8.0	1.0	1.0	9400
P_6^2	5.0×10^4	-150	1.5	1.0	8.0	1.0	1.0	9400
P_7^2	2.3×10^4	-130	1.5	1.5	8.0	1.0	1.0	9450
P_8^2	2.0×10^4	-140	2.0	1.0	8.0	1.0	1.0	9450
P_9^2	5.0×10^3	-110	2.0	2.0	8.0	1.0	1.0	9525
P_{10}^2	9.0×10^4	-130	1.5	1.0	8.0	2.0	1.0	9525
P_{11}^2	1.0×10^5	-130	1.5	1.0	8.0	2.0	1.5	9525
P_{12}^2	1.25×10^5	-150	1.5	1.0	6.0	1.5	1.5	9525
P_{13}^2	3.0×10^4	-150	2.5	1.0	6.0	1.0	2.0	9700
P_{14}^2	5.0×10^3	-180	3.5	1.0	6.0	1.5	2.5	9650
P_{15}^2	1.5×10^3	-280	4.0	1.0	6.0	2.5	2.5	9670
P_{16}^2	1.1×10^5	-150	1.0	1.5	5.0	1.0	1.0	9525
P_{17}^2	8.0×10^4	-150	1.0	1.5	5.0	1.0	1.0	9350
P_{18}^2	1.2×10^5	-150	1.0	1.5	5.0	1.0	1.0	9550
P_{19}^2	1.2×10^5	-140	1.0	1.5	5.0	1.0	1.0	9480
P_{20}^2	1.2×10^5	-140	1.0	1.5	5.0	1.0	1.0	9500

A.3 Reaction Scheme 3

For reactions 1 and 2, the data used for processes $P_1^3 - P_6^3$ are summarized in Table A.3.

Table A.3 Process parameters for reactions 1 and 2 for processes $P_1^3 - P_6^3$.

Process	$\nu_{A,1}$; $\nu_{B,1}$	$\nu_{A,2}$; $\nu_{C,2}$	$n_{A,1}$; $n_{B,1}$	$n_{A,2}$; $n_{C,2}$	$k_{0,1}; k_{0,2}$ $\left[\mathrm{m^3\,mol^{-1}\,s^{-1}}\right]$	$E_{a,1}; E_{a,2}$ $\left[\mathrm{kJ\,mol^{-1}}\right]$	$\Delta H_{r,1}; \Delta H_{r,2}$ $\left[\mathrm{kJ\,mol^{-1}}\right]$
P_1^3	1;2	2;1	1.5;1.5	1;1	100; 200	60; 70	-85; -75
P_2^3	1;3	3;1	1;2	2;1	3×10^4; 2×10^4	80; 90	-60; -55
P_3^3	1;2	3;2	2;2	1.5;1	1.1; 0.7	65; 75	-90; +35
P_4^3	1;3	1;1	1;2.5	1.5;1.5	2×10^4; 1.5×10^4	90; 92	-100; -95
P_5^3	1;1	2;1	3;1.5	2;2.5	2.1 ;3.2	58; 61	-40; -50
P_6^3	1;2	1;1	2;1.5	2;1.5	280; 170	82; 84	-55; -62

The reaction data for reactions 3 and 4 for processes $P_1^3 - P_6^3$ are given in Table A.4.

Table A.4 Process parameters for reaction 3 and 4 for processes $P_1^3 - P_6^3$.

Process	$\nu_{A,3}$; $\nu_{B,3}$	$\nu_{A,4}$; $\nu_{C,4}$	$n_{A,3}$; $n_{B,3}$	$n_{A,4}$; $n_{C,4}$	$k_{0,3}; k_{0,4}$ $\left[\mathrm{m^3\,mol^{-1}\,s^{-1}}\right]$	$E_{a,3}; E_{a,4}$ $\left[\mathrm{kJ\,mol^{-1}}\right]$	$\Delta H_{r,3}; \Delta H_{r,4}$ $\left[\mathrm{kJ\,mol^{-1}}\right]$
P_1^3	1;1	1;1	1.5;1	1.5;1	100; 300	83; 80	-35; -45
P_2^3	3;1	1;3	1;1	1;1	2×10^4; 3×10^4	71; 78	-66; -48
P_3^3	3;2	2;1	2;2.5	1.5;1.5	0.8; 1.9	63; 75	-120; -105
P_4^3	1;1	1;1	2;1.5	2;2.5	1.5×10^4; 2×10^4	90; 92	-95; -90
P_5^3	2;1	1;2	1.5;1	2;2	8700; 9200	73; 81	-155; -165
P_6^3	1;1	1;1	1.5;1.5	1.5;3	6×10^4; 4×10^4	87; 90	-105; -125

A.4 Reaction Scheme 4

The reaction data for reactions 5 and 6 for processes $P_1^4 - P_6^4$ are given in Table A.5.

Table A.5 Process parameters for the additional reactions 5 and 6 within reaction scheme 4 with processes $P_1^4 - P_6^4$.

Process	$\nu_{A,5}$; $\nu_{B,5}$	$\nu_{A,6}$; $\nu_{C,6}$	$n_{A,5}$; $n_{B,5}$	$n_{A,6}$; $n_{C,6}$	$k_{0,5}; k_{0,6} \times 10^{-5}$ $\left[\mathrm{m^3\,mol^{-1}\,s^{-1}}\right]$	$E_{a,5}; E_{a,6}$ $\left[\mathrm{kJ\,mol^{-1}}\right]$	$\Delta H_{r,5}; \Delta H_{r,6}$ $\left[\mathrm{kJ\,mol^{-1}}\right]$
P_1^4	2;1	1;1	1.5;1	1.5;1.5	150; 190	93; 90	-115; -90
P_2^4	2;1	1;3	1;1	1;2	1.1×10^4; 8000	91; 94	-92; +40
P_3^4	3;2	1;2	1.5;1.5	2;2	1.7; 1.3	89; 92	-125; -95
P_4^4	1;1	1;3	2;2.5	1;2.5	1400; 1500	87; 65	-100; -75
P_5^4	2;1	1;1	2.5;2.5	3;1.5	230; 810	93; 81	+45; -145
P_6^4	1;2	1;2	1.5;3	2;1.5	1.1×10^4; 3.9×10^4	90; 95	-88; -75

A.5 Physical properties of reagents and products

The physical properties for all liquid components in this thesis are shown in Tables A.6−A.9.

Table A.6 Density data with varying temperature for each component used in this thesis (Bohne *et al.*, 2010; Chen *et al.*, 2008; Crittenden *et al.*, 2012; Green and Perry, 2008*a*).

Temperature [K]	300	350	400	450	500
Component density $\left[\mathrm{kg\,m^{-3}}\right]$					
A	911	852	798	740	685
B	790	727	675	620	560
C	1200	1150	1095	1040	1000
D	1205	1150	1100	1042	1005
E	810	780	695	640	590
F	790	727	675	620	560
G	1000	945	890	840	778
H	1300	1245	1190	1140	1085
Toluene	870	815	763	705	636
Mono-nitrotoluene mixture*	1160	1110	1060	1005	951
$HNO_3/H_2SO_4/H_2O$ mixture**	1430	1370	1310	1230	1160

* The change in densities with temperature are assumed to be parallel to those of TNT (Green and Perry, 2008*a*) due to a lack of data available for mono-nitrotoluene.

** The change in densities with temperature are assumed to be parallel to those of water (Green and Perry, 2008*a*) due to a lack of data available for the acid mixture.

Table A.7 Viscosity data with varying temperature for each component used in this thesis (Bohne *et al.*, 2010; Chen *et al.*, 2008; Crittenden *et al.*, 2012; Green and Perry, 2008*a*).

Temperature [K]	300	350	400	450	500
Component viscosity $\times 10^{-4}$ [Pa s]					
A	1.00	0.50	0.30	0.17	0.10
B	3.00	1.70	0.80	0.20	0.15
C	9.00	6.00	3.00	2.00	1.50
D	2.00	1.00	0.60	0.40	0.20
E	1.00	0.45	0.30	0.20	0.15
F	3.00	1.70	0.80	0.20	0.15
G	10.0	7.00	4.00	2.50	2.20
H	2.00	1.00	0.60	0.40	0.20
Toluene	6.00	3.30	2.10	1.30	0.70
Mono-nitrotoluene mixture*	2.00	0.98	0.58	0.35	0.19
$HNO_3/H_2SO_4/H_2O$ mixture**	11.0	6.00	3.70	2.90	2.60

* The change in viscosities with temperature are assumed to be parallel to those of TNT (Green and Perry, 2008*a*) due to a lack of data available for mono-nitrotoluene.

** The change in visocosities with temperature are assumed to be parallel to those of water (Green and Perry, 2008*a*) due to a lack of data available for the acid mixture.

Table A.8 Specific heat capacity data with varying temperature for each component used in this thesis (Bohne *et al.*, 2010; Chen *et al.*, 2008; Crittenden *et al.*, 2012; Green and Perry, 2008*a*).

Temperature [K]	300	350	400	450	500
Component heat capacity $\left[\mathrm{J\,kg^{-1}\,K^{-1}}\right]$					
A	1100	1200	1300	1400	1500
B	950	1000	1050	1100	1150
C	850	920	980	1070	1130
D	4190	4190	4200	4230	4300
E	1250	1350	1460	1560	1670
F	950	1000	1050	1100	1150
G	750	900	1060	1210	1380
H	2250	2350	2440	2560	2680
Toluene	1700	1940	2210	2480	2730
Mono-nitrotoluene mixture*	1470	1600	1750	1890	2050
$HNO_3/H_2SO_4/H_2O$ mixture**	2600	2600	2620	2650	2700

* The change in heat capacities with temperature are assumed to be parallel to those of TNT (Green and Perry, 2008*a*) due to a lack of data available for mono-nitrotoluene.

** The change in heat capacities values with temperature are assumed to be parallel to those of water (Green and Perry, 2008*a*) due to a lack of data available for the acid mixture.

Table A.9 Thermal conductivity data with varying temperature for each component used in this thesis (Bohne *et al.*, 2010; Chen *et al.*, 2008; Crittenden *et al.*, 2012; Green and Perry, 2008*a*).

Temperature [K]	300	350	400	450	500
Component thermal conductivity $\left[\mathrm{W\,m^{-1}\,K^{-1}}\right]$					
A	0.300	0.295	0.290	0.286	0.282
B	0.250	0.247	0.244	0.240	0.236
C	0.150	0.140	0.130	0.120	0.110
D	0.685	0.667	0.652	0.635	0.618
E	0.400	0.388	0.375	0.362	0.348
F	0.250	0.247	0.244	0.240	0.236
G	0.100	0.097	0.094	0.091	0.088
H	0.850	0.837	0.826	0.812	0.800
Toluene	0.141	0.130	0.117	0.105	0.093
Mono-nitrotoluene mixture*	1.47	1.60	1.75	1.89	2.05
$HNO_3/H_2SO_4/H_2O$ mixture**	0.840	0.880	0.910	0.920	0.920

* The change in thermal conductivities with temperature are assumed to be parallel to those of TNT (Green and Perry, 2008*a*) due to a lack of data available for mono-nitrotoluene.

** The change in thermal conductivities with temperature are assumed to be parallel to those of water (Green and Perry, 2008*a*) due to a lack of data available for the acid mixture.

References

Akpan, V. A. and Hassapis, G. D. (2011), 'Nonlinear model identification and adaptive model predictive control using neural networks', *ISA Transactions* **50**, 177–194.

Albalawi, F., Alanqar, A., Durand, H. and Christofides, P. D. (2016), 'A feedback control framework for safe and economically-optimal operation of nonlinear processes', *American Institute of Chemical Engineers Journal* **62**(7), 2391–2409.

Albalawi, F., Durand, H. and Christofides, P. D. (2017), 'Process operational safety using model predictive control based on a process Safeness Index', *Computers and Chemical Engineering* **104**, 76–88.

Albalawi, F., Durand, H. and Christofides, P. D. (2018), 'Process operational safety via model predictive control: Recent results and future research directions', *Computers and Chemical Engineering* **114**, 171–190.

Ameur, H., Kamla, Y. and Sahel, D. (2018), 'Performance of Helical Ribbon and Screw Impellers for Mixing Viscous Fluids in Cylindrical Reactors', *Multidisciplinary Digital Publishing Institute* **26**, 1–9.

Anagnost, J. J. and Desoer, C. A. (1991), 'An elementary proof of the Routh-Hurwitz stability criterion', *Circuits Systems Signal Process* **10**.

Anucha, S., Chayavivatkul, V. and Banjerdpongchai, D. (2015), Comparison of PID Control and Linear Model Predictive Control Application to Regenerative Thermal Oxidizer System, *in* 'Control Conference (ASCC)'.

Arnold, V. I. (1973), *Ordinary differential equations*, MA: MIT Press, Cambridge, chapter 3, pp. 95–208.

Badwe, A. S., Patwadhan, R. S., Shah, S. L., Patwardhan, S. C. and Gudi, R. D. (2010), 'Quantifying the impact of model-plant mismatch on controller performance', *Journal of Process Control* .

Baerns, M. and Renken, A. (2004), *Chemische Reaktionstechnik*, Wiley-VCH, chapter 4.

Balakotaiah, V. (1989), 'Simple runaway criteria for cooled reactors', *American Institute of Chemical Engineers Journal* **35**, 1039–1043.

Barkelew, C. (1959), 'Stability of chemical reactors', *Chemical Engineering Progress Symposium Series* **25**, 37–46.

Bernadini, D. and Bemporad, A. (2009), Scenario-based model predictive control of stochastic constrained linear systems, *in* '48th IEEE Conference on Decision and Control', pp. 6333–6338.

Bertsekas, D. P. (1982), *Constrained Optimization and Lagrange Multiplier Methods*, Academic Press, chapter 3.

Bird, R. B., Stewart, W. E. and Lightfoot, E. N. (2007), *Transport phenomena*, John Wiley & Sons, Inc., chapter 9.

Bohne, D., Fischer, S. and Obermeier, E. (2010), 'Thermal Conductivity, Density, Viscosity, and Prandtl-Numbers of Ethylene Glycol-Water Mixtures', *Berichte der Bundesgesellschaft für physikalische Chemie* **88**(8), 739–742.

Bosch, J., Strozzi, F., Zbilut, J. and Zaldívar, J. M. (2004), 'On-line runaway detection in isoperibolic batch and semibatch reactors using the divergence criterion', *Computers and Chemical Engineering* **28**(4), 527–544.

Bradford, E., Schweidtmann, A. M. and Lapkin, A. (2018), 'Efficient multiobjective optimization employing Gaussian processes, spectral samplingand a genetic algorithm', *Journal of Global Optimization* **71**(2), 407—438.

Bryson, A. and Ho, Y.-C. (1975), *Applied Optimal Control*, Taylor & Francis Group, chapter 3, pp. 90–125.

Byrd, R. H., Schnabel, R. B. and Schultz, G. A. (1988), 'Approximate solution of the trust regions problem by minimization over two-dimensional subspaces', *Mathematical Programming* **40**, 247–263.

Campo, P. J. and Morari, M. (1987), Robust model predictive control, *in* 'Proceedins of the American control conference', pp. 1021–1026.

Çengel, Y. A. (2002), *Heat and Mass Transfer*, McGraw Hill, chapter 6.

Cellier, F. and Kofman, E. (2006), *Continuous system simulation*, Springer Science+Business Media.

Chang, S.-J. and Hung, B.-C. (2002), 'Optimization of Batch Polymerization Reactors Using Neural-Network Rate-Function Models', *Industrial & Engineering Chemistry Research* **41**(11), 2716–2727.

Chen, L.-P., Chen, W.-H., Liu, Y., Peng, J.-H. and Liu, R.-H. (2008), 'Toluene mono-nitration in a semi-batch reactor', *Central European Journal of Energetic Materials* **5**, 37–47.

Christofides, P. D., Liu, J. and Muñoz de la Peña, D. (2011), *Networked and Distributed Predictive Control*, Springer, London, chapter 2, pp. 13–45.

Chuong La, H., Potschka, A. and Bock, H. G. (2017), 'Partial stability for nonlinear model predictive control', *Automatica* **78**, 14–19.

Copelli, S., Torretta, V., Pasturenzi, C., Derudi, M., Cattaneo, C. and Rota, R. (2014), 'On the divergence criterion for runaway detection: Application to complex controlled systems', *Journal of Loss Prevention in the Process Industries* **28**, 92–100.

Courant, R. (1943), 'Variational methods for the solution of problems with equilibrium and vibration', *Bulletin of the American Mathematical Society* **49**, 1–23.

Crittenden, J. C., Trussell, R. R., Hand, D. W., Howe, K. J. and Tchobanoglous, G. (2012), *MWH's Water Treatment: Principles and Design*, third edn, John Wiley & Sons, chapter Appendix C, pp. 1861–1862.

Dantzig, G. B. (1963), *Linear Programming and Extensions*, Princeton University Press.

Davis, M. and Davis, R. (2003), *Fundamentals of Chemical Reaction Engineering*, McGraw-Hill, chapter 2, pp. 53–56.

Dochain, D. (2003), 'State and parameter estimation in chemical and biochemical processes: a tutorial', *Journal of Process Control* **13**, 801–818.

Frank-Kamenet͡skiĭ, D. (1969), *Diffusion and Heat Transfer in Chemical Kinetics*, Plenum Press.

Ge, M., Chiu, M.-S. and Wang, Q.-G. (2002), 'Robust PID controller design via LMI approach', *Journal of Process Control* **12**(1), 3–13.

Ghaffar, H. F. A., Hammad, S. A. and Yousef, A. H. (2014), 'Stability analysis of embedded nonlinear predictor neural generalized predictive controller', *Alexandria Engineering Journal* **53**(1), 41–60.
URL: *http://dx.doi.org/10.1016/j.aej.2013.11.008*

Goldfarb, D. (1980), 'Curvilinear path steplength algorithms for minimization which use directions of negative curvature', *Mathematical Programming* **18**, 31–40.

Green, D. W. and Perry, R. H. (2008*a*), *Perry's Chemical Engineers' Handbook*, eighth edn, The McGraw-Hill, chapter 2.

Green, D. W. and Perry, R. H. (2008*b*), *Perry's Chemical Engineers' Handbook*, eighth edn, The McGraw-Hill, chapter 5.

Griffith, D. W., Zavala, V. M. and Biegler, L. T. (2017), 'Robustly stable economic NMPC for non-dissipative stage costs', *Journal of Process Control* **57**, 116–126.

Haber, R., Bars, R. and Schmitz, U. (2011), *Predictive Control in Process Engineering*, Wiley-VCH Verlag GmbH & Co. KGaA, chapter 2, pp. 29–54.

Hagedorn, D. W. (1965), Prediction of batch heat transfer coefficients for pseudoplastic fluids in agitated vessels, PhD thesis, Newark College of Engineering.

Halder, R., Lawal, A. and Damavarapu, R. (2008), 'Nitration of toluene in a microreactor', *Catalysis Today* **125**, 74–80.

Hestens, S. P. (1969), 'Multiplier and gradient methods', *Journal of Optimization Theory and Applications* **4**, 303–320.

Hirschfelder, J. O., Curtiss, C. F. and Bird, R. B. (1955), 'Molecular theory of gases and liquids', *American Insitute of Chemical Engieers Journal* **1**(2), 272.

Hong, W., Lie, X. and Zhihuan, S. (2012), 'A review for model plant mismatch measures in process monitoring', *Chinese Journal of Chemical Engineering* **20**(6), 1039–1046.

Hosen, M. A., Hussain, M. A. and Mjalli, F. S. (2011), 'Control of polystyrene batch reactors using neural network based model predictive control (NNMPC): An experimental investigation', *Control Engineering Practice* **19**(5), 454–467.

Hurwitz, A. (1895), 'Über die Bedingungen, unter welchen eine Gleichung nur Wurzeln mit negativen reellen Theilen besitzt.', *Mathemathische Annalen* **46**(2), 273–284.

Jäschke, J., Yang, X. and Biegler, L. T. (2014), 'Fast economic model predictive control based on NLP-sensitivities', *Journal of Process Control* **24**(8), 1260–1272.

Jones, D. R., Schonlau, M. and Welch, W. J. (1998), 'Efficient global optimization of expensive black-box functions', *Journal of Global Optimization* **13**(4), 455–492.

Joseph, E. A. and Olaiya, O. O. (2018), 'Cohen-Coon PID Tuning Method: A Better Option to Ziegler Nichols-PID Tuning Method', *Computer Engineering and Intelligent Systems* **9**(5), 33–37.

Kalmuk, A., Tyushev, K., Granichin, O. and Yuchi, M. (2017), 'Online parameter estimation for MPC model uncertainties based on LSCR approach', *1st Annual IEEE Conference on Control Technology and Applications, CCTA 2017* pp. 1256–1261.

Kocijan, J., Murray-Smith, R., Rasmussen, C. E. and Girard, A. (2004), Gaussian process model based predictive control, *in* 'American Control Conference, 2004', pp. 2214—2219.

Krishnamoorthy, D., Thombre, M., Skogestad, S. and Jäschke, J. (2018), 'Data-driven Scenario Selection for Multistage Robust Model Predictive Control', *IFAC-PapersOnLine* **51**(20), 462–468.

Lee, J. H. (1994), 'State-space interpretation of model predictive control', *Automatica* **30**(4), 707–717.

Lee, J. H. (2011), 'Model predictive control: Review of the three decades of development', *Journal of Control, Automation, and Systems* **9**, 415–424.

Likar, B. and Kocijan, J. (2007), 'Predictive control of a gasliquid separation plant based on a Gaussian process model', *Computers & Chemical Engineering* **31**(3), 142—152.

Lucia, S., Andersson, J. A., Brandt, H., Bouaswaig, A., Diehl, M. and Engell, S. (2014), 'Efficient Robust Economic Nonlinear Model Predictive Control of an Industrial Batch Reactor', *IFAC Proceedings Volumes* **47**(3), 11093–11098.

Lucia, S., Finkler, T., Basak, D. and Engell, S. (2012), 'A new Robust NMPC Scheme and its Application to a Semi-batch Reactor Example', *IFAC Proceedings Volumes* **45**(15), 69–74.

Lucia, S., Finkler, T. and Engell, S. (2013), 'Multi-stage nonlinear model predictive control applied to a semi-batch polymerization reactor under uncertainty', *Journal of Process Control* **23**(9), 1306–1319.

Lucia, S. and Paulen, R. (2014), Robust Nonlinear Model Predictive Control with Reduction of Uncertainty via Robust Optimal Experiment Design, *in* 'IFAC Proceedings', Vol. 47, pp. 1904–1909.

Luo, K.-M. and Chang, J.-G. (1998), 'The stability of toluene mononitration in reaction calorimeter reactor', *Journal of Loss Prevention in the Process Industries* **11**, 81–87.

Maciejowski, J. M. and Yang, X. (2013), Fault tolerant control using Gaussian processes and model predictive control, *in* 'Conference on Control and Fault-Tolerant Systems (SysTol), IEEE', pp. 1–12.

Martí, R., Lucia, S., Sarabia, D., Paulen, R., Engell, S. and de Prada, C. (2015), 'Improving scenario decomposition algorithms for robust nonlinear model predictive control', *Computers and Chemical Engineering* **79**, 30–45.

Mawardi, M. (1982), 'The nitration of monoalkyl benzene and the separation of its isomers by gas chromatography', *Pertanika* **5**, 7–11.

Maxeiner, L. S. and Engell, S. (2017), 'Hierarchical MPC of batch reactors with shared resources', *IFAC-PapersOnLine* **50**(1), 12041–12046.

Mayne, D. Q. (2014), 'Model predictive control: Recent developments and future promise', *Automatica* **50**, 2967–2986.

Mayne, D., Seron, M. and Rakovic, S. (2005), 'Robust model predictive control of constrained linear systems with bounded disturbances', *Automatica* **41**, 219–224.

Melcher, A. (2003), Numerische Berechnung der Lyapunov-Exponenten bei gewöhnlichen Differentialgleichungen, PhD thesis, Universität Karlsruhe, Fakultät für Mathematik.

Muñoz-Carpintero, D., Kouvaritakis, B. and Cannon, M. (2016), 'Striped Parameterized Tube Model Predictive Control', *Automatica* **67**, 303–309.

Nocedal, J. and Wright, S. (2006), *Numerical Optimization*, Springer, chapter 18, pp. 526–572.

Osborne, M. R. (1976), 'Nonlinear least squares - the Levenberg algorithm revisited', *Journal of the Australian Mathematical Society, Series B* **19**, 343–357.

Padron, G. (2003), Measurement and Comparison of Power Draw in Batch Rotor-Stator Mixers, Master's thesis, University of Maryland, College Park, MD 20742, USA.

Paul, E., Atiemo-Obeng, V. and Kresta, S. (2004), *Handbook of industrial mixing : science and practice*, Wiley-Interscience.

Rajavathsavai, D., Khapre, A. and Munshi, B. (2014), 'Study of mixing behaviour of CSTR using CFD', *Brazilian Journal of Chemical Engineering* **31**, 119–129.

Rakovic, S., Kouvaritakis, B., Cannon, M., Panos, C. and Findeisen, R. (2011), Fully parameterized tube MPC, *in* 'Proceedins of the 18th IFAC World Congress', pp. 197–202.

Rasmussen, C. E. and Williams, C. K. I. (2006), *Gaussian Processes for Machine Learning*, MIT Press, chapter 2.

Rawlings, J. and Animit, R. (2009), *Nonlinear model predictive control*, Springer, chapter Optimizing process economic performance using model predictive control, pp. 119–138.

Rawlings, J. and Mayne, D. (2015), *Model Predictive Control: Theory and Design*, Nob Hill Publishing, chapter 1, pp. 1–60.

Routh, E. (1877), *A Treatise on the Stability of a Given State of Motion: Particularly Steady Motion.*, Macmillan and Co.

Rupp, M. (2015), Über die Ethoxylierung von Octanol im Mikrostrukturreaktor, PhD thesis, Universität Stuttgart, Fakultät für Energie-, Verfahrens- und Biotechnik.

Rupp, M., Ruback, W. and Klemm, E. (2013), 'Octanol ethoxylation in microchannels', *Chemical Engineering and Processing: Process Intensification* **74**, 19–26.

Russel, T. W., Robinson, A. S. and Wagner, N. (2008), *Mass and Heat Transfer*, Cambridge University Press, chapter 3, pp. 55–109.

Salmi, T. O., Mikkola, J.-P. and Wärnå, J. P. (2011), *Chemical Reaction Engineering and Reactor Technology*, CRC Press, chapter 3, pp. 27–92.

Schlichting, H. and Gersten, K. (2017), *Boundary-Layer Theory*, Springer, chapter 15, pp. 416–419.

Schultz, G. A., Schnabel, R. B. and Byrd, R. H. (1985), 'A family of trust-region-based algorithms for unconstrained minimization with strong global convergence properties', *SIAM Journal on Numerical Analysis* **22**, 47–67.

Scokaert, P. O. M. and Mayne, D. Q. (1998), 'Min-max feedback model predictive control for constrained linear systems', *IEEE Transactions on Automatic Control* **43**, 1136–1142.

Semënov, N. (1940), Thermal theory of combustion and explosion, *in* 'Progress of Physical Science (U.S.S.R)'.

Shampine, L., Reichelt, M. and Kierzenka, J. (1999), 'Solving Index-1 DAEs in MATLAB and Simulink', *SIAM Review* **41**, 538–552.

Sheats, G. and Strachan, A. (1978), 'Rates and activation energies of nitronium ion formation and reaction in the nitration of toluene in 78% sulphuric acid', *Canadian Journal of Chemistry* **56**, 1280–1283.

Sinnot, R. (2005), *Chemical Engineering Design*, Vol. 6, Elsevier Butterworth-Heinemann, chapter 12, pp. 634–638.

Sirohi, A. and Choi, K. Y. (1996), 'On-Line Parameter Estimation in a Continuous Polymerization Process', *Industrial and Engineering Chemistry Research* **35**, 1332–1343.

Štampar, S., Sokolič, S., Karer, G., Žnidaršič, A. and Škrjanc, I. (2011), 'Theoretical and fuzzy modelling of a pharmaceutical batch reactor', *Mathematical and Computer Modelling* **53**(5-6), 637–645.

Stephanopoulos, G. (1984), *Chemical Process Control*, PTR Prentice Hall, chapter 14, pp. 258–279.

Strozzi, F. and Zaldívar, J. (1994), 'A general method for assessing the thermal stability of batch chemical reactors by sensitivity calculation based on Lyapunov exponents', *Chemical Engineering Science* **49**(16), 2681–2688.

Strozzi, F. and Zaldívar, J. (1999), 'On-line runaway detection in batch reactors using chaos theory techniques', *American Institute of Chemical Engineers Journal* **45**(11), 2429–2443.

Teja, A. S. (1983), 'Simple method for the calculation of heat capacities of liquid mixtures', *Journal of Chemical Engineering Data* **28**, 83–85.

Thangavel, S., Lucia, S., Paulen, R. and Engell, S. (2018), 'Dual robust nonlinear model predictive control: A multi-stage approach', *Journal of Process Control* **72**, 39–51.

Theis, A. (2014), 'Case study: T2 Laboratories explosion', *Journal of Loss Prevention in the Process Industries* **30**, 296–300.

Till, Z., Molnár, B., Egedyl, A. and Vargal, T. (2019), 'CFD Based Qualification of Mixing Efficiency of Stirred Vessels', *Periodica Polytechnica Chemical Engineering* **63**, 226–238.

Torotwa, I. and Ji, C. (2018), 'A Study of the Mixing Performance of Different Impeller Designs in Stirred Vessels Using Computational Fluid Dynamics', *MDPI Design* **2**, 10–26.

Vanderbei, R. J. (2001), *Linear Programming: Foundations and Extensions*, Springer Verlag.

Wächter, A. and Biegler, L. T. (2006), 'On the implementation of an interior-point filter line-search algorithm for large-scale nonlinear programming', *Mathematical Programming* **106**, 25–57.

Wang, Y., Biegler, L. T., Patel, M. and Wassick, J. (2018), 'Parameters estimation and model discrimination for solid-liquid reactions in batch processes', *Chemical Engineering Science* **187**, 455–469.

Winde, M. (2009), Systematische Bewertung und Ertüchtigung von industriellen Regelkreisen in verfahrenstechnischen Komplexen, PhD thesis, Ruhr-Universität Bochum, Fakultät für Maschinenbau.

Wu, Z., Zhang, J., Zhang, Z., Albalawi, F., Durand, H., Mahmood, M., Mhaskar, P. and Christofides, P. D. (2018), 'Economic model predictive control of stochastic nonlinear systems', *American Institute of Chemical Engineers Journal* **64**(9), 3312–3322.

Yucelen, T., Kaymakci, S. and Kurtulan, S. (2006), Self-Tuning PID Controller Using Ziegler-Nichols Method for Programmable Logic Controllers, *in* 'IFAC Proceedings', Vol. 39.

Zhang, J. (2017), 'Design of a new PID controller using predictive functional control optimization for chamber pressure in a coke furnace', *ISA Transactions* **67**, 208–214.

Zhang, Z., Wu, Z., Durand, H., Albalawi, F. and Christofides, P. D. (2018), 'On integration of feedback control and safety systems: Analyzing two chemical process applications', *Chemical Engineering Research and Design* **132**, 616–626.

Zhou, K. and Doyle, J. C. (1998), *Essentials of robust control*, Prentice Hall, chapter 8.